UNIVERSITÀ
DEGLI STUDI
DI PADOVA

FRONT PAGE

Head Office: Università degli Studi di Padova

Department of Comparative Biomedicine and Food Science

Ph.D. COURSE IN: VETERINARY SCIENCES

SERIES XXXV

MULTIMODAL ASSESSMENT OF CETACEAN CENTRAL NERVOUS AUDITORY PATHWAYS, WITH EMPHASIS ON FORENSIC DIAGNOSTICS OF ACOUSTIC TRAUMA

Thesis written with the financial contribution of the ECCE AQUA project.

Coordinator: Prof. Mattia Cecchinato

Supervisor: Prof. Ranieri Verin

Co-Supervisor: Prof. Sandro Mazzariol

Ph.D. student: Ksenia Orekhova

Multimodal Assessment of Cetacean Central Nervous Auditory Pathways, with Emphasis on Forensic Diagnostics of Acoustic Trauma

PhD Dissertation

Ksenia Orekhova

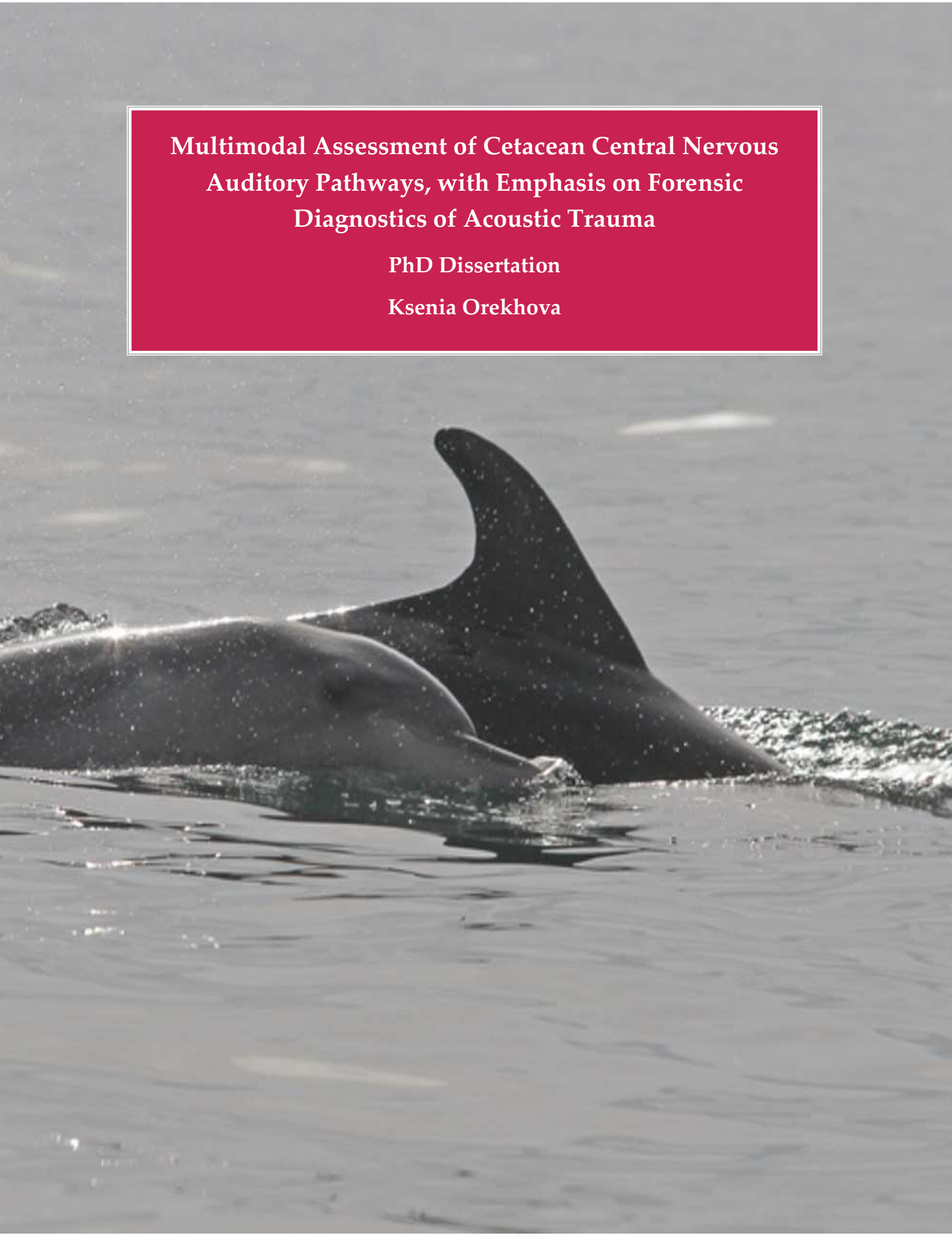

To Marco, my parents and all the animals that this might one day serve.

"We have become the impatient species, too busy to let nature replenish itself and too puffed up with our own sense of importance to acknowledge our utter dependence on its generosity."

- *David Suzuki*

Summary

Cetaceans encompass some of the world's most enigmatic species, with one of their greatest adaptations to the marine environment being the ability to "see" by hearing. Their anatomy and behavior are fine-tuned to emit and respond to underwater sounds, which is why anthropogenic noise pollution is likely to affect them negatively.

There are many effects of noise on living organisms, and while knowledge of their entire palette and interplay remain incomplete, evidence for insults ranging from acoustic trauma over behavioral changes, to masking and stress, is accumulating. Humans are subject to peak interest in terms of medical research on noise-induced hearing loss (NIHL). The World Health Organization estimates over 13% of the global population to be at risk from NIHL, via both occupational and recreational exposure. As major health concerns can be expected across species, addressing this problem in free-ranging cetacean populations will lead to a more sustainable management of marine ecosystems, more effective and balanced policies, and successes in conservation. While progress has been made in behavioral monitoring, electrophysiological hearing assessments and *post-mortem* examination of the inner ear of cetaceans, very little is known about the neurochemical baseline and neuropathology of their central auditory pathways.

In the present work, we focused on reviewing the known effects of sound on cetaceans in both wild and managed settings and explored the value of animal models of neurodegenerative disease. We began by evaluating a group of markers associated with neurodegeneration in a more readily available species, the dog (*Canis lupus familiaris*), where acute neurological insult could be derived from clinical history. Immunohistochemical assessment narrowed down the pathogenetic mechanisms responsible for the animals' deaths (Publication I).

We then set out to systematically validate a key panel of protein biomarkers for the assessment of similar neurodegenerative processes in the cetacean central nervous system (Publication II). For this, we developed protocols to adequately sample cetacean auditory nuclei, optimized the immunohistochemical workflow, and used Western blot and alignment of protein sequences between the antigen targeted by our antibodies and the bottlenose dolphin (*Tursiops truncatus*) proteome. A Histoscore was used to semi-quantitively categorize immunoreactivity patterns and dolphins by age and presence of pathology. First results indicated significant differences both between sick and healthy, and young and old animals.

Following this, we expanded our list of validated antibodies for use in the bottlenose dolphin and the techniques used to assess them in a multimodal, quantitative way. Stereology was implemented to assess the neuronal, axonal, and glial cell numbers in the inferior colliculus and ventral cochlear nucleus of a healthy bottlenose dolphin, which created a baseline understanding of protein expression in these structures. *In situ* volumes from 7-Tesla MRI scans were estimated to gauge the influence of tissue processing on neuronal density (Publication III). This data will make a valuable comparison for positive controls of acoustic trauma. Furthermore, we explored the connectome and neuronal morphology of auditory nuclei and experimented with probe designs and machine learning algorithms to quantify structures of interest (Addenda). Comparisons with pathological human brains revealed similarities in the configuration of extracellular matrix components to those of a healthy dolphin, in line with existing knowledge on the tolerance to hypoxia in diving mammals. This has implications for future investigation of the evolutionary development of marine mammal brains, as well as help diversify out-of-the-box approaches to researching human neurodegenerative disease, as is being done with hibernating species.

The data and methodologies described herein contribute to the knowledge on the neurochemical signature of the cetacean central nervous system. They are intended to facilitate understanding of auditory and non-auditory pathology and build an evidence-based backbone to future policies regarding noise and other forms of anthropogenic threats to the marine environment.

Table of Contents

List of Abbreviations

A1 – primary auditory cortex

A2 – secondary auditory cortex

Aβ – amyloid-β peptide

AD – Alzheimer's Disease

AEP – Auditory Evoked Potential

ALARP – As Low As Reasonably Practical

AN – Auditory Nerve

Apaf-1 – pro-apoptotic protease factor 1

APP – Amyloid Precursor Protein

ARHL – Age-Related Hearing Loss

Bcl-2 – B-Cell Lymphoma related protein 2

CE – Coefficient of Error

CEE – Controlled Exposure Experiment

CNS – Central Nervous System

CUBIC – Clear, Unobstructed Brain/Body Imaging Cocktails and Computational analysis

DGK-ζ – Diacylglycerolkinase-ζ

DTAG – Digital Acoustic Recording Tag

DTI – Diffusion Tensor Imaging

ECM – Extracellular Matrix

GAD^{67} – glutamate decarboxylase 67

GAP-43 – Growth Associated Protein 43

GFAP – Glial Fibrillary Acidic Protein

GlyR – Glycine Receptor

Iba1 – Allograft inflammatory factor

iDISCO – immunolabeling-enabled three-Dimensional Imaging of Solvent-Cleared Organs

IC – Inferior Colliculus

IC EC – External Cortex of the IC

IC CN – Central Nucleus of the IC

IL-6 – Interleukin-6

LL – Lateral Lemniscus

LOBE – Level of Onset of Adverse Biological Effects

MAP2 – Microtubule-Associated Protein 2

MDR1 – Multidrug Resistance gene 1

MGN – Medial Geniculate Nucleus

ML – Machine Learning

fMRI – functional Magnetic Resonance Imaging

7T-MRI – 7 Tesla-Magnetic Resonance Imaging

MRS – Magnetic Resonance Spectroscopy

MSE – Mass Stranding Event

NFT – Neurofibrillary Tangle

NIHL – Noise-induced Hearing Loss

NF200 – Neurofilament 200 (kDa)

PCB – Polychlorinated Biphenyls

PET – Positron Emission Tomography

POP – Persistent Organic Pollutant

p53 – Tumor Protein p53

PCB – Polychlorinated Biphenyls

PET – Positron Emission Tomography

PHF – Paired Helical Fragments

POP – Persistent Organic Pollutant

PTS – Permanent Threshold Shift

ROI – Region of Interest

RNS – Reactive Nitrogen Species

ROS – Reactive Oxygen Species

SELcum – cumulative Sound Exposure Level

SMI-32 – Sternberger-Meyer Immunochemicals catalog #32

SPL(peak) – (peak) Sound Pressure Level

SWITCH – System-Wide control of Interaction Time and kinetics of CHemicals

TBI – Traumatic Brain Injury

TDP-43 – TAR DNA-binding protein 43

TNFα – Tumor Necrosis Factor α

TTS – Temporary Threshold Shift

QKI – KH Domain Containing RNA Binding gene and encoded protein

VCN – Ventral Cochlear Nucleus

Introduction

Cetaceans and Sound

Cetaceans are a biodiverse group of mammals belonging to the order *Artiodactyla* (even-toed ungulates) that evolved to thrive in an aquatic environment. They inhabit every ocean in the world and can be divided into two sub-orders: *Mysticeti,* or baleen whales, and *Odontoceti,* or toothed whales. Species of both sub-orders show remarkable cognitive and social capabilities and rely heavily on their hearing and vocalizations for orientation, foraging and reproduction (Jefferson et al., 2011). Odontocetes have evolved a fine-tuned ability to use sonar-like signals to create a mental image of their prey, called echolocation. This is particularly advantageous for hunting in murky waters, or at night, and required the evolution of a highly sophisticated anatomical apparatus for the transmission, reception, and processing of sounds. Adaptations include structures such as the melon, the acoustic fats, and very large, complex brains (Au et al., 2000). As a result, the largest extant odontocete, the sperm whale (*Physeter macrocephalus*), possesses the largest and heaviest cerebrum known to humankind (Ridgway and Hanson, 2014).

Cetaceans are long-living K-strategists that nurse and nurture their young, with the oldest known individuals belonging to the bowhead whale species (*Balaena mysticetus*), estimated to live to about 200 years, and with the females of some odontocetes like orcas (*Orcinus orca*), short-finned pilot whales (*Globicephala macrorhynchus*), belugas (*Delphinapterus leucas*), narwhals (*Monodon monoceros*), false killer whales (*Pseudorca crassidens*), and potentially sperm whales surviving well beyond menopause up to 80-100 years of age (Marsh and Kasuya, 1968; Olesiuk et al., 1990; McAuliffe and Whitehead, 2005; Foote, 2008; Croft et al., 2017; Ellis et al., 2018; Photopoulou et al., 2017). Since they are apex predators in marine food chains, they bioaccumulate toxins to the extent that some fetuses are stillborn due to a phenomenon termed "maternal offloading" (Tanabe et al., 1994; Jepson et al., 1999). This is one of the ways that cetaceans represent sentinel and bioindicator species of marine ecosystems. Further indications of insufficient environmental status are increased deaths and strandings of individuals, sometimes resulting in mass stranding events (MSEs) due to epidemics of infectious disease, zoonotic parasitosis, oil spills and other contaminant overloads, entanglement in fishing gear and plastic, and poor body condition (Dierauf and Gulland, 2001).

Over the last several decades, another source of marine pollution—anthropogenic noise—has been proven to affect marine mammals, although guidelines protecting them against this stressor lack executive character (Bröker, 2019). A growing amount of evidence is elucidating the structural-functional mechanisms contributing to noise-induced hearing loss (NIHL), unravelling correlations between sound properties and severity of tissue damage down to the molecular level (Kujawa and Liberman, 2009; Morell et al., 2017; Erbe et al., 2018). This creates opportunities to clarify a possible causal relation between anthropogenic impulsive noise (e.g., air guns, pile driving, explosives, sonar) and its impacts on individuals from a veterinary-pathological perspective in the context of evidence-based medicine. Such knowledge is of paramount importance for marine species that depend on hearing integrity for survival. They are subject to a growing variety and intensity of man-made underwater noise, and considering the unpredictable nature of unmitigated impulsive noise, it has strong potential to induce functional and structural damage.

Sound Types and Properties

Impulsive sounds are described as "monopole energy source level in units of dB re 1 µPa2·s or zero to peak monopole source level in units of dB re 1 µPa·m, both over the frequency band 10 Hz to 10 kHz" (Commission Decision (EU) 2017/848) and imply an impulse duration of < 10 s whose repetition time is longer than four times the signal (Van der Graaf et al., 2012). The most relevant anthropogenic sources for marine conservation include seismic air guns, pile driving, explosives, mid-frequency active sonar and multibeam echosounders (Richardson et al., 1995; Hildebrand, 2004; Bröker, 2019). Their frequency ranges and peak sound pressure levels (SPLs) at 1 m range from the source are listed in Table 1.

Table 1. Properties of pertinent underwater impulsive sound sources.

Type of impulsive anthropogenic sounds	Peak SPL 1 m from the source (dB re 1 µPa)	Frequency range (Hz)	Reference
Seismic air guns	240-250	100-250	Richardson et al. (1995)
Pile driving	30-40	131-135	Richardson et al. (1995)
Underwater explosives	Dependent on weight and type of the explosive	10-1,000	Hildebrand (2004)
Mid-frequency active sonar	≥ 235	1,000-20,000	Hildebrand (2004)
Multibeam echosounders	235	12,000-500,000	Bröker (2019)

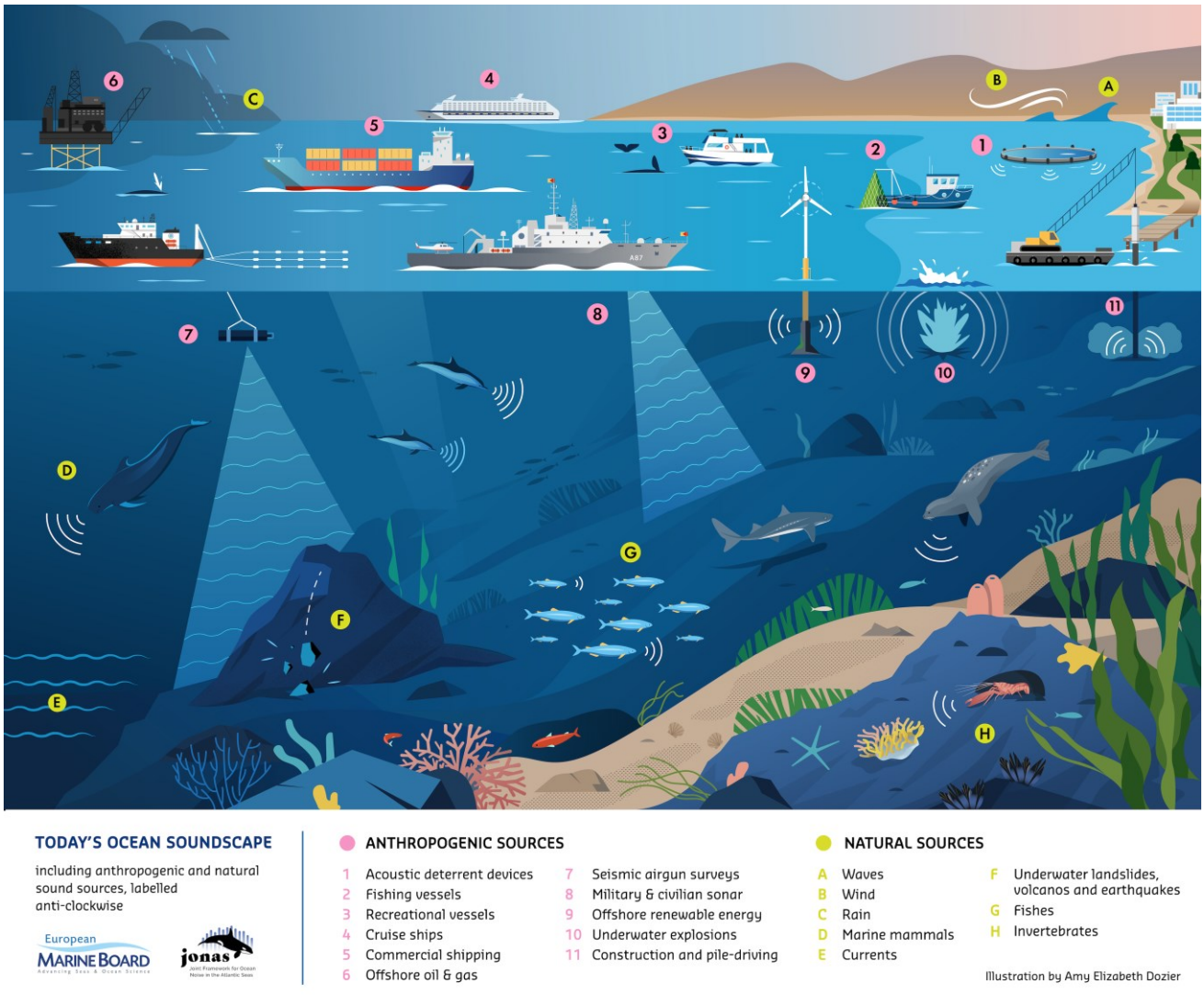

Figure 1. Infographic on the ocean soundscape (with kind permission from Amy Dozier, who illustrated it for the JONAS Project, European Marine Board, 2021).

A large portion of these sounds (up to 83% between 2015 – 2017; Merchant et al., 2020) can be attributed to the hydrocarbon exploration and production industry, with air gun arrays operable at depths over 300 m. A habitat overlap with pelagic cetacean species and deeper-diving seals is therefore probable. The OSPAR Convention (Oslo/Paris convention for the Protection of the Marine Environment of the North-East Atlantic) initiated the establishment of the "Impulsive Noise Indicator" calculated in "pulse block days" to quantify and coordinate international impulsive noise emissions within the Northeast Atlantic region. Similar developments are ongoing for the Mediterranean Sea (Maglio et al., 2018) and US waters (Hatch et al., 2016). After a large gap in the frequency of use, pile driving, sonar and other noise sources become significant, with the former being especially common in the North Sea and increasingly implemented throughout the OSPAR area (Merchant et al., 2020). International noise registries are the first step to understanding spatiotemporal impulsive noise distribution (Dekeling et al., 2014). Meanwhile, risk assessment frameworks concerning impacts on marine fauna are being developed (Drira et al. 2018; Merchant et al. 2018).

The effects of sounds on an organism depend on many factors. Apart from the sound's frequency, intensity and directionality at the source, the abiotic and biotic components of the propagation medium and the state of the receiver may greatly influence its impact. Abiotic factors include the composition and movement of both the water and the sea floor, the depth, background sounds of waves, and wind and seismic activity. Some of the biotic factors of the aquatic environment are the presence and acoustic properties of marine flora and fauna, which may to some extent absorb or mask or reflect the signal of interest (Erbe et al., 2018).

The SPL that reaches the animal is referred to as the received level, and its effects can range from lethal blast to those of acoustic overexposure (AOE), behavioral changes (with or without perceived disturbance), stress response, and masking of other sounds that are biologically relevant to the receiver (such as echolocation clicks or intra- and interspecific vocalizations) (Stevens et al., 2021). The elevation in SPL necessary to evoke the action potential of the acoustically overexposed auditory nerve fibers compared to before the AOE is called a threshold shift, and it can be permanent (PTS) or temporary (TTS) (Liberman, 2016; Southall et al., 2019).

The received level does not necessarily correspond to the sensation level of the incoming sound, which depends on the subjective experience of the individual animal based on its experience, position relative to the sound, potential habituation or sensitization to that sound based on its predictability and similarity to those of predators, capacity to self-mitigate, behavioral state, group composition, and overall health of the animal (Stevens et al., 2021). Dose-response relationships can act as a proxy for the perception of the sound but are prone to all the confounders inherent to a dynamic, live system mentioned above (Erbe et al., 2018; Bolle et al., 2016; NRC, 2005). Per definition, sound is only named "noise" once it has the potential to affect a receiver negatively (Bradley and Stern, 2008).

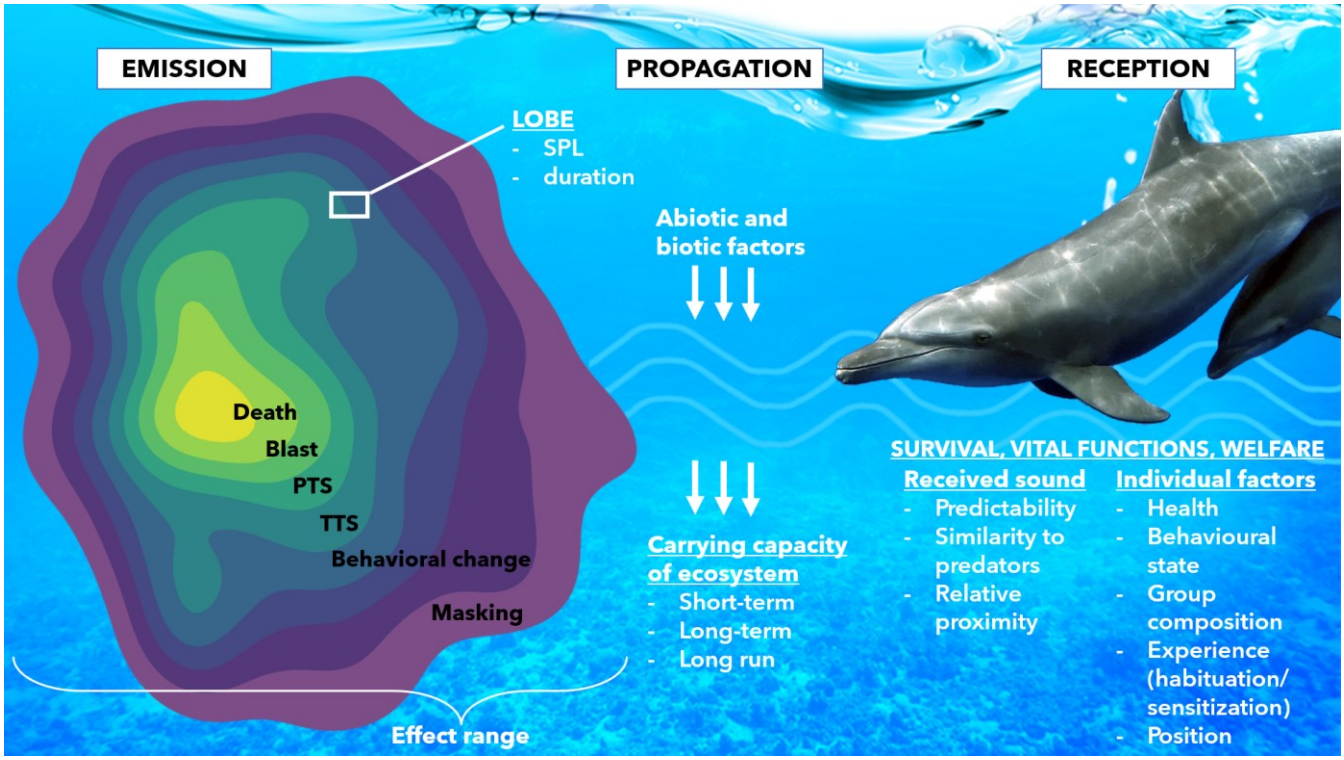

Figure 2. Overview of the potential effects of noise as a function of the distance from its source and considering the influencing factors at the point of its emission, propagation through the marine environment, and reception by the animal. The LOBE—Level of Onset of Adverse Biological Effects—is visualized on the theoretical border between behavioral change and TTS, since the margins of interpretation of the sensation level of the animal are quite broad. SPL—Sound Pressure Level.

Legal Framework of Underwater Noise

Cetaceans are protected in many countries via regulatory frameworks (e.g., the U.S. Marine Mammal Protection Act, 1972; the E.U. Marine Strategy Framework Directive, MSFD, 2008/56/EC), and non-binding guidelines regarding underwater noise pollution have emerged globally over the last 14 years (Southall et al., 2007; Southall et al., 2019; NMFS, 2016; NMFS, 2018; Commission Decision (EU) 2017/848). It has become of increasing concern that all branches of terrestrial and marine fauna can be negatively affected by an overexposure to anthropogenic impulsive noise (Richardson et al., 1995; André et al., 2009; Hastings, 2008; Popper and Hastings, 2009; Southall et al., 2019). However, a legally binding set of acceptable SPLs i.e., thresholds to acoustic injury, remains elusive for numerous reasons.

With the gradual recognition of adverse effects as a consequence of AOE in humans, domestic, zoo, and wild animals (Weeks et al., 2009; Coppola et al., 2006; Jakob-Hoff et al., 2019; Ketten et al., 1993), guidelines have been developed that delineate thresholds to acoustic damage in the form of TTS and PTS in marine mammals (Southall et al, 2007; Southall et al., 2019; NMFS, 2016; NMFS 2018). Due to lack of data, most of the estimated SPLs (peak, or accumulated over 24 hours—SELcum) had to be extrapolated from examined species such as bottlenose dolphins (*Tursiops truncatus*) and porpoises. Southall et al. (2019) defined a 6 dB threshold shift as significant in the context of AOE. However, even with a behavioral/digital acoustic recording tag (DTAG)-detected alteration in the exposed animal, there is no way of ascertaining the causal correlation

(versus spatiotemporal association) of exposure to the noise sources mentioned above. Baleen whale species' audiograms are almost entirely unavailable, but estimations of TTS levels have nevertheless been attempted (Gedamke et al., 2011). These guidelines are meant to serve as interim foundations for national and Union-wide regulations, but due to several limitations, are not legally binding (e.g., NMFS 2018) or are incomplete and actively underline the need to establish regulatory thresholds (Commission Decision (EU) 2017/848). In fact, the only case where empirical evidence led to a change in the legal framework was the creation of a military sonar exclusion zone along the Canary coastline after the description of gas and fat embolism in mass-stranded beaked whales (*Ziphiidae*) associated to the use of mid-frequency sonar by Fernández and colleagues in 2005.

It must be considered that a "one number fits all" approach, as often found in guidelines, may be inappropriate in the context of underwater noise. Reasons for this include the lack of empirical knowledge in the measurement of received levels and the difficulties in developing accurate underwater particle motion sensors (Popper et al., 2019), as well as potential imprecision of source level estimation through back-propagation (Martin et al., 2017; Bröker, 2019). Despite this, international regulations are necessary due to the global nature of underwater noise. Sound may easily travel across national borders, a fact contrasted by the lack of regulations pertaining to international waters (Hildebrand, 2004). The International Ocean Noise Coalition is a conglomerate of NGOs working towards a coordination of global efforts to regulate underwater noise pollution since 2005, and to include a clause on it in the United Nations Convention on the Law of the Sea (UNCLOS, 1982). In the current phrasing, noise falls under "pollution" that needs to be controlled and reduced. The EU's MFSD explicitly included ocean noise as criteria to be addressed to achieve Good Environmental Status (Annex I [11]) by 2020, which complements the "Ecosystem Approach" (EcAp) from the Barcelona Convention (UNEP/MAP) consistent with the objectives of the Marine Spatial Planning Directive (MSPD 2014/89/EU). Commission Decision 2010/477/EU(2) pinpoints low- and mid-frequency (10 Hz–10 kHz) impulsive sound and continuous low-frequency sound as potentially impactful.

Since 2009, research on ocean noise has been deemed a priority issue by the International Whaling Commission, and multinational regulatory expert panels born of the ASCOBANS (Agreement on the Conservation of Small Cetaceans of the Baltic, North East Atlantic, Irish and North Seas) and ACCOBAMS (Agreement for the Conservation of Cetaceans in the Mediterranean, in the Black Sea and in the contiguous Atlantic areas) agreements have passed several resolutions regarding different aspects of underwater noise impacts (ASCOBANS resolutions 2003, 2006, 2009; ACCOBAMS resolutions 2004, 2007, 2010). The ACCOBAMS agreement was ratified by Italy in 2005 (GU 53, 2005). The JNCC—Joint Nature Conservation Committee—assessed mitigation measures in 2010 and developed one of most widespread cross-boundary guidelines used by operators of marine geophysical surveys (JNCC, 2010).

Since then, further actions (ACCOBAMS 2013; 2019a) have focused on management of marine anthropogenic noise including the certification of marine mammal observers aboard seismic vessels (ACCOBAMS; 2016a, b), the development of a methodological guide to underwater noise mitigation measures (ACCOBAMS, 2019b), and a Mediterranean strategy for underwater noise monitoring (ACCOBAMS, 2021). The most recent development born out of the MFSD, in line with the Zero Pollution Action Plan, has been the definition of limits for underwater noise: "to be in tolerable status, no more than 20% of a given marine area, can be exposed to continuous

underwater noise over a year […] no more than 20% of a marine habitat can be exposed to impulsive noise over a given day, and no more than 10% over a year", endorsed by EU marine directors on November 29, 2022 (MSFD Common Implementation Strategy, 2022). The LOBE (Level of Onset of Biological adverse Effects) is proposed as a parameter for assessing the impact level of noise on marine organisms, dividing the temporal scale into short-term (one day), long-term (one year) and long-run (more than one year) to assess the disturbance of different species considering potential protracted effects on their biological cycles.

This guideline lacks a legally binding character and focuses on displacement of marine organisms. TTS, injury, and death are addressed by the Habitats Directive (Council Directive 92/43/EEC) and the Environmental Impact Assessment Directive (Directive 2011/92/EU).

Legally binding frameworks, once matured, will provide only minimum requirements for presumably safe source SPLs, as is the case with noise regulations for pig farms (Directive 2008/120/EC). They must then be applied critically under consideration of the local geophysical landscape, fauna, and economic activity.

The efficacy of current mitigation measures (e.g., ramp-up, bubble-curtains [Dähne et al., 2017; Kastelein et al., 2019c], spatiotemporal avoidance of critical habitats, pre-survey marine mammal search by trained observers, shut-downs) in the context of seismic exploration and underwater construction is under continuous scrutiny (Malme et al., 1986; Yazvenko et al., 2007, Bröker et al., 2015; Martin et al., 2019; Austin et al., 2018; Stone, 2015a; 2015b), since in several behavioral studies, cetacean responses were ambiguous (Weir, 2008; Dunlop et al., 2016; Wensveen et al., 2017). Behavioral response to continuous versus pulsed active sonar in sperm whales revealed that the ratio of sound energy to sound amplitude over time, rather than the impulsive or continuous nature of underwater sound, accounted for changes in foraging behavior (Isojunno et al., 2020). Consequently, more recent guidelines focus increasingly on the impact of sound rather than its pulsed or continuous source (Southall et al., 2021). Development of more advanced forensic protocols could allow an evidence-based correlation between AOE and physiopathological consequences for the exposed animals and help reduce the gap between spatiotemporal association and the vacuum for reasonable and risk-oriented legislation in an integrative, multidisciplinary manner. In this way, the "ALARP" ("As Low as Reasonably Practical") principle, as conceived by the International Association of Oil and Gas Producers (IOGP) and employed by exploration and production companies (Petersen & Valeur, 2013), could be better aligned to the various regulatory guidelines they adhere to (e.g., Weir and Dolman, 2007; Australian Government Department of the Environment, Water, Heritage and the Arts [DEWHA], 2008; Department of Conservation [DOC] Te Papa Atawhai, 2013; van Beest et al., 2015; Fisheries and Oceans Canada, 2016; NMFS, 2016; 2018). Thus, it may help strike a better balance between over- and under-regulation, reducing cost and unnecessary procedures.

Effects of Sound on Cetaceans

Due to the variable nature of sound effects on live animals in a dynamic system such as the ocean, an artificial structure is helpful to assess the range of adverse effects reported in marine mammals. When sound impacts are categorized as a function of distance from the noise source, their negative effects decrease, ranging from lethal and blast injury, to AOE with the potential

consequence of PTS, TTS, tinnitus, stress (primary, secondary, and tertiary), behavioral changes, and masking of relevant biological information. In the case of marine mammals, an important challenge is to establish the causality from a spatiotemporal association of animals in the vicinity of an intense sound (or blast) source. Relevant literature reporting on cases where such associations were apparent is summarized below.

Blast Effects - Lethal

Strong blast overpressures and effects of particle motion at closer range may induce whole-body lesions like lung hemorrhage, tissue ripping, and bone fractures (Ketten et al., 1993). The latter case with severe, systemic mechanical trauma was recorded in two humpback whales that died in close range of a 5000 kg underwater explosive. Reports from harvested minke whales (*Balaenoptera acutorostrata*) killed with 30 g penthrite harpoons include blast-induced neurotrauma that led to the animals' immediate loss of consciousness and death. Harpoons that hit closer to the head resulted in severe traumatic brain injury (brain laceration, as well as hemorrhages in the meninges, brainstem, ventricles, and the white matter of the cerebellum), and those hitting body parts further from the head triggered acceleration-induced diffuse traumatic brain injury (subarachnoid and petechial hemorrhages, diffuse vacuolation of brain tissue, and enlargement of perivascular spaces) (Knudsen et al., 2003; Øen et al., 1995a, b, c,; 1999). More recent reports include harbor porpoises (*Phocoena phocoena*) likely exposed to detonations that stranded with hemorrhages in auditory—acoustic fats, ear, peribullar sinuses—and non-auditory tissues, microfractures, and dislocation of the ear bones (Siebert et al., 2022). Similar findings are reported for long-beaked common dolphins (*Delphinus capensis*) and bottlenose dolphins by Danil and colleagues (2011, 2021). Anderson and colleagues (1954) estimated that over 19,000 harbor seals (*Phoca vitulina*) were killed by blast in Alaska between 1951-1954.

Blast Effects - Sublethal

With a sublethal exposure to blast waves, mechanical injury plays an important role. Next to sensory hair cell loss and oxidative damage, the spiral organ may become entirely separated from its basilar membrane, while the tympanic membrane may show hemorrhagic infiltration or rupture (Roberto et al., 1989).

At these pressure levels, blast-induced neurotrauma commonly appears in the form of mild traumatic brain injury (TBI) (Pun et al., 2011). Within the brain of humans and rodents, mild traumatic blast injury may cause increased vascular permeability and neuroinflammation (Readnower et al., 2010), white matter damage including glial edema, and myelin rupture (associated with upregulation of amyloid-β peptide—Aβ—and amyloid precursor protein—APP). It also causes changes in neuronal structure (Cernak et al., 2001a; b) with transient shrinkage and proteolysis of cytoskeletal proteins (e.g., spectrin-IIα and phosphorylated and non-phosphorylated neurofilaments) (Pun et al., 2011; Park et al, 2011). To date, few unequivocal reports of sublethal blast trauma are available for cetaceans, since the blast-associated lesions could often not be reliably differentiated as an ultimate versus proximate cause of death (Koschinski, 2011). The theoretical effects thereof have been summarized (Ketten et al., 1995), and severity on this level may vary as a function of the same physical, biotic, and abiotic factors (Danil et al., 2021; von Benda-Beckmann et al., 2015; Soloway, 2018), as is the case for noise (see chapter "Sound Types and Properties").

In pinnipeds, Bohne et al. (1985; 1986) deemed NIHL owing to exposure to explosives of free-ranging Weddell seals in Antarctica likely, but shooting the seals to acquire the inner ear may have greatly confounded the findings with blast-induced damage.

Permanent Threshold Shift

With more distance from the acoustic source or lower received noise levels, PTS and TTS become the principal concerns for marine mammal hearing. Southall and colleagues (2007, 2019) categorized cetaceans into high-, middle-, and low-frequency groups derived from psychoacoustic i.e., auditory evoked potential (AEP) data, and made inferences for unavailable species. Tables 2 and 3 visualize the cetacean species grouped into the different hearing groups and their TTS and PTS thresholds in terms of SELcum and SPLpeak.

Table 2. Marine mammal hearing groups proposed by Southall et al. (2019), applicable auditory weighting functions, genera, and species within each proposed group.

Marine mammal hearing group	Auditory weighting function	Genera (or species) included
Low-frequency cetaceans	LF	Balaenidae (*Balaena*, Eubalaenidae spp.); Balaenopteridae (*Balaenoptera physalus*, *B. musculus*)
		Balaenopteridae (*Balaenoptera acutorostrata*, *B. bonaerensis*, *B. borealis*, *B. edeni*, *B. omurai*; *Megaptera novaeangliae*); Neobalenidae (*Caperea*); Eschrichtiidae (*Eschrichtius*)
High-frequency cetaceans	HF	Physeteridae (*Physeter*); Ziphiidae (*Berardius* spp., *Hyperoodon* spp., *Indopacetus*, *Mesoplodon* spp., *Tasmacetus*, *Ziphius*); Delphinidae (*Orcinus*)
		Delphinidae (*Delphinus*, *Feresa*, *Globicephala* spp., *Grampus*, *Lagenodelphis*, *Lagenorhynchus acutus*, *L. albirostris*, *L. obliquidens*, *L. obscurus*, *Lissodelphis* spp., *Orcaella* spp., *Peponocephala*, *Pseudorca*, *Sotalia* spp., *Sousa* spp., *Stenella* spp., *Steno*, *Tursiops* spp.); Mon odontidae (*Delphinapterus*, *Monodon*); Plantanistidae (*Plantanista*)
Very high-frequency cetaceans	VHF	Delphinidae (*Cephalorhynchus* spp.; *Lagenorhynchus cruciger*, *L. australis*); Phocoenidae (*Neophocaena* spp., *Phocoena* spp., *Phocoenoides*); Iniidae (*Inia*); Kogiidae (*Kogia*); Lipotidae (*Lipotes*); Pontoporiidae (*Pontoporia*)
Sirenians	SI	Trichechidae (*Trichechus* spp.); Dugongidae (*Dugong*)
Phocid carnivores in water Phocid carnivores in air	PCW PCA	Phocidae (*Cystophora*, *Erignathus*, *Halichoerus*, *Histriophoca*, *Hydrurga*, *Leptonychotes*, *Lobodon*, *Mirounga* spp., *Monachus*, *Neomonachus*, *Ommatophoca*, *Pagophilus*, *Phoca* spp., *Pusa* spp.)
Other marine carnivores in water Other marine carnivores in air	OCW OCA	Odobenidae (*Odobenus*); Otariidae (*Arctocephalus* spp., *Callorhinus*, *Eumetopias*, *Neophoca*, *Otaria*, *Phocarctos*, *Zalophus* spp.); Ursidae (*Ursus maritimus*); Mustelidae (*Enhydra*, *Lontra feline*)

Table 3. Summary of the predicted PTS and TTS thresholds for these groups from Finneran et al. (2016) and Southall et al., 2019 (as adapted by Guan and Brookens, 2021). SELcum—cumulative sound exposure level is weighted, SPLpeak—peak sound pressure level is unweighted. LF—low-frequency cetaceans; MF—mid-frequency cetaceans; HF—high-frequency cetaceans; SI—sirenians; OW—otariids in water (also includes odobenids, mustelids, and ursids); PW—phocids in water.

Functional Hearing Group	Impulsive				Non-Impulsive	
	TTS		PTS		TTS	PTS
	SEL_{cum}	SPL_{peak}	SEL_{cum}	SPL_{peak}	SEL_{cum}	SEL_{cum}
LF	168	213	183	219	179	199
MF	170	224	185	230	178	198
HF	140	196	155	202	153	173
SI	175	220	190	226	186	206
OW	188	226	203	232	199	219
PW	170	212	185	218	181	201

While TTS onset could be measured in controlled exposure experiments (CEEs) and behavioral trials (Finneran et al., 2015a, b; Kastelein et al., 2017), PTS thresholds are mostly predicted from TTS growth rates. Bottlenose dolphins, belugas, and harbor and finless porpoises (*Neophocaena phocaenoides*) have undergone multiple psychoacoustic tests, yet data is lacking particularly in the upper limits of sensitivity of the very-high-frequency group (Stevens et al., 2021) and mysticetes. The Minke Whale Hearing Project is currently underway to assess the latter (Norwegian Defense Research Establishment, 2021).

AEP data from stranded cetaceans revealed a pervasive incidence of profound hearing loss in bottlenose and rough-toothed dolphins (*Steno bredanensis*), and in a short-finned pilot whale, however, the mechanism behind these findings is unclear. Hearing loss was found even in subadult animals, which led the authors to consider genetic or developmental hearing impairment linked to chemical contamination, as might be the case with polychlorinated biphenyls (PCBs) (Mann et al., 2010). Similar findings are reported from a melon-headed whale (*Peponocephala electra*), although the paucity of available baseline data restricts their interpretation (Wang et al., 2021).

A study on the PTS of an amphibious harbor seal highlighted in-air and underwater ambiguity in AOE-induced threshold shifts. The shifts were induced by a sonar-like, octave-band sound (Kastak et al., 2008; Reichmuth et al., 2019), resulting in varying threshold amplitudes between the two media and a differential 3-phase recovery (TTS for 2 days at the cochlear segment corresponding to the noise's characteristic frequency versus long-term recovery at one octave above it and PTS a half-octave above it). This finding is paradoxical to other studies in the same species (Kastelein, 2013; 2019a; Kastak and Schusterman, 1998), and in odontocetes (Finneran et al., 2015b), but closer to those described in terrestrial mammals (Salvi and Boettcher, 2008). Interestingly, the abruptness and unpredictability of threshold shift onset parallels those observed in voluntary human tests using impulsive noise, as summarized by Price (2007). This stresses the high individual variability and the difficulty of establishing "one fits all" thresholds according to an impact hierarchy using traditional behavioral and AEP methods in amphibious species (Bröker, 2019).

To date, the only potential morphological evidence of PTS in a free-ranging cetacean was in one juvenile long-finned pilot whale (*Globicephala melas*), which presented missing outer hair cells at the cochlear apex, a finding consistent with low-frequency acoustic impact (Morell et al, 2017). This was one of the animals involved in two MSEs with a spatiotemporal association to anthropogenic noise. The subsequent work of Morell and colleagues (2020a) on belugas in managed care settings has helped align psychoacoustic profound hearing loss with corresponding loss of inner ear sensory hair cells and innervation. They also assessed the expression of proteins such as prestin in several cetacean species to facilitate future inner ear analyses in MSE cases (Morell et al., 2020b, 2022).

Temporary Threshold Shift

TTS studies consist primarily of CEEs recording AEP-measured audiogram and behavioral changes (or lack thereof), with bottlenose dolphins and harbor porpoises representing the most studied species (Finneran et al., 2002; 2007; 2015a; Nachtigall et al., 2004; Lucke et al., 2009). They are reviewed comprehensively for the period between 1996-2015 by Finneran and colleagues (2015b), who also established that results of behavioral and electrophysiological methods are comparable (Houser and Finneran, 2006). Since then, efforts have continued to assess TTS onset, recovery, and attenuation in relation to different pulsed and non-pulsed sources (Kastelein et al., 2017, 2019b, c) in both cetaceans and pinnipeds (Kastelein et al, 2019a; Reichmuth et al., 2016, Kastak 1998, 2008), even under consideration of mitigation measures such as bubble-curtains (Kastelein et al., 2019c).

Behavioral Changes

Many behavioral studies on both wild cetaceans (e.g., using DTAGS; Johnson, 2003) and aquarium odontocetes (Finneran et al., 2015b) have been conducted in the last decades, but despite cases of spatiotemporal association (Hildebrand, 2005; Gray and Van Waerebeek, 2011), no conclusive evidence for AOE-triggered stranding exists (Gordon et al., 2004; Bröker. 2019). Many of those studies have recorded alteration in behavior (e.g., displacement, changes in vocalization patterns) with regards to seismic surveys in bottlenose dolphins, harbor porpoises, sperm whales, common and Atlantic spotted dolphins (*Stenella frontalis*), orcas, humpback (*Megaptera novaeangliae*), bowhead, blue (*Balaenoptera musculus*), and fin whales (*Balaenoptera physalus*) (Evans et al., 1993; Bain and Williams, 2006; Rankin & Evans, 1998; Madsen et al., 2002; Goold & Fish, 1998; McCauley et al., 1999; Ljungbald et al., 1988; McDonald et al., 1995; IWC 2007—reviewed in André et al., 2009 and Weilgart, 2013), whilst other studies noted the lack of a significant response in harbor porpoises and sperm whales (van Beest et al., 2015; Sarnocińska et al., 2020; Gordon et al., 2006; Winsor and Mate, 2006; Madsen et al., 2000; Miller et al., 2009).

However, following unusual mortality events and MSEs that took place in spatiotemporal proximity to anthropogenic underwater noise, such as that of melon-headed whales after exposure to multibeam echosounders in Madagascar in 2008 (Southall et al., 2013), and the beaked whale MSEs associated with exposure to mid-frequency active navy sonar (Jepson et al., 2003, Fernández et al., 2005), drawing a causal link between an anthropogenic acoustic source and stranding events remains challenging. Lesions in the ears, as well as cerebral and cranial hemorrhage in the sonar-associated beaked whale MSEs (Balcomb and Claridge, 2001; Rowles et al., 2001) were frequently recorded within peripheral—and likely affecting central nervous—auditory system components.

However, these findings were often complemented by systemic changes (gas bubble formation) both within and outside auditory tissues that were hypothetically associated with a behavioral change and decompression sickness-like condition or formation of gas nuclei due to direct acoustic impact of sonar, though there is no objective method to confirm the latter. Some reasons for this include the multifactorial nature of such events, technical and logistical difficulties, and lack of forensic tools and expertise to recognize noise-induced lesions in marine species. Nevertheless, the lack of mass strandings in the Canary Islands following a moratorium on the use of mid-frequency sonar strengthens the hypothesis of its initial involvement (Fernández et al., 2013; Bernaldo de Quirós et al., 2019).

Effects such as altered habitat use, redistribution and changes in foraging, social, reproductive, and resting behaviors may lead to important long-term effects on population health, leading them to be emphasized in more recent guidelines in scoring noise impact on wild cetaceans (Southall et al., 2021).

In pinnipeds, CEEs using impulsive sounds, like those of acoustic deterrent devices and pile-driving, have often caused avoidance or aversive behavior without significant elevations in auditory thresholds (Finneran et al., 2003a; Götz and Janik, 2010). Exposure of their wild counterparts has shown similar trends of short-term alteration (Richardson, 1999; Blackwell et al., 2004; Edrén et al., 2004), although assessments often remain restricted to models and estimations (Jacobs & Terhune, 2002; Tougaard et al., 2009; Madsen et al., 2006).

Masking

Masking is the drowning out of biologically relevant sounds by anthropogenic noise, and its consequences have been summarized to affect cetaceans in mainly two ways: 1) the Lombard effect or 2) modification of the species' own signals (Stevens et al., 2021). The Lombard effect involves the animals raising the intensity of their sound emissions above the elevated background noise— "shouting" to be heard—and is a common response recorded for several species (e.g., bottlenose dolphins: Kragh et al., 2019; orcas: Holt et al., 2019; De Clerk et al., 2019). Modifications to the cetacean signals include raising or lowering their frequencies (e.g., right whales [North—*Eubalena glacialis* and South Atlantic—*Eubalena australis*]: Parks et al., 2007; fin whales: Castellote et al., 2012; gray whales: Dahlheim et al., 2016), changing the duration (bottlenose dolphins: Buckstaff, 2004; orcas: Foote et al., 2004) or ceasing to signal completely for a given period of time (Luis et al., 2014).

While some of these modifications could represent short-term solutions for intraspecies communication and foraging, they may also result in long-term impacts on the animals' energy budgets. Nieukirk and colleagues (2012) reported that in some areas of the Mid-Atlantic Ridge, seismic air guns were heard at distances of 4,000 km from survey vessels and for 80-95% of the days/month for more than 12 consecutive months, sometimes entirely drowning out whale calls. This could result in reduced ability to find mates, or even in mother-calf separation. Both direct and indirect effects on foraging success (by affecting prey species) are conceivable and may also affect the likelihood of ending up as prey. Relaxation of acoustic crypsis— modification of acoustic signals by prey species to use a higher or lower frequency than detectable by predators— in species such as Heaviside's dolphins (*Cephalorhynchus heavisidii*) and beaked whales may lead to higher depredation effects on vulnerable populations (Martin et al., 2018). A similar adaptation is used by dolphins with high-frequency hearing loss: they lower the frequency of echolocation clicks

to one that they can still hear, potentially exposing themselves to prey and predators (*Strahan et al., 2020*).

Stress

In terms of stress associated with AOE, serologic markers like interleukins, interferon-ɣ, and stress hormones were significantly elevated in aquarium bottlenose dolphins exposed to air gun noise playback (Chen et al., 2018; Romano et al., 2004). It is possible to differentiate stress effects as primary, secondary, and tertiary. Primary stress involves the acute reaction to a stressor via increased stress hormone levels in the blood (e.g., glucocorticoids, catecholamines). A recent study recorded increases in cortisol and interleukin-10 gene expression in captive bottlenose dolphins without significant behavioral response to playback of pile-driving sounds (Yang et al., 2021). Further methods to assess stress using easier accessible matrices (skin, blubber, feces) are available for several cetacean species (Southern, 2000; Unal and Romano, 2021).

Secondary effects appear at a cellular level (e.g., changes in expression of heat shock proteins) and provoke changes in plasma metabolites and immune function, while tertiary response includes changes in behavioral patterns and impaired reproduction (Wright et al., 2007; 2021), and shares many detrimental health effects with chronic stress (Barton, 2002). Multiple publications focus on the latter (Rolland et al., 2012; Graham et al., 2021), even recording potential adrenal failure in a humpback whale (Lowe et al., 2021). The pause in human activity during the COVID-19 pandemic provided unique opportunities to assess the reduction in baseline underwater noise levels (Ryan et al., 2020; Thomson et al., 2020).

Regarding stranded wild marine mammals, when blood samples are inaccessible it is important to obtain as much information reflecting their general health as possible. Routine sampling of peripheral and central auditory pathway components may provide a more complete picture of the pre-mortem condition of the animal, its energetic resources, and anthropogenic effects on its essential sensory systems.

Cetacean Brains in Health and Disease

As an organ with remarkable sensory, cognitive, and metabolic capabilities and thus presumptive high energy consumption, the cetacean brain is a good candidate indicator of deficits in cetacean health and welfare. There are abundant hints as to its alternative cytoarchitectural and molecular wiring in comparison to terrestrial artiodactyls. For instance, the neocortex is largely agranular (lacking a consistent layer IV), thalamic afferents likely connect mostly to layer II instead of the typical layers III and IV in terrestrials (Hof et al., 2005; Furutani et al., 2008; Kesarev, 1970; Hof et al., 1992; Glezer et al., 1998), and the brainstem and midbrain auditory nuclei of odontocetes are deemed "hypertrophic" in comparison to other mammals (Bullock and Gurevich, 1979). The neurochemical signature underlines adaptations to frequent exposures to hypoxemia and hypoxia in the context of diving (Krüger et al., 2020), similar to the situation in seals (Geβner et al., 2022), and of unihemispheric sleep (Ridgway et al., 2006), although the extent of these adaptations is unclear.

Several infectious agents such as *Cetacean morbillivirus* (*CeMV*), *Herpesvirus* (α and ϒ), *Brucella ceti*, and *Toxoplasma gondii* (*T. gondii*) are well-characterized with respect to

neuropathology (Giorda et al., 2022; Sierra et al., 2020; Van Bressem et al., 2014; Kennedy et al.,1992; Van Elk et al., 2016; Di Guardo et al., 2010; Grattarola et al., 2016, Pintore et al., 2018). While these diseases manifest themselves systemically in the acute and subacute stages, brain-only forms of chronic *CeMV* have been described (Domingo et al., 1995; Soto et al., 2011; Di Guardo et al., 2013; Sierra et al., 2014). *Nasitrema* spp. have been linked to lesions of both the ears and brain (Ridgway et al., 1972; O'Shea et al., 1991; Sierra et al., 2020), with evidence suggesting a migration of the parasites along the VIIIth cranial nerve (Morimitsu et al., 1987; 1992), and nematodes have been recorded to cause granulomatous and necrotizing encephalitis (Martin et al., 1970; Perrin and Powers, 1980).

Nevertheless, many questions regarding the pathogenesis of these and other diseases remain open, including the extent of the tropism to different neuronal, glial and vascular components (Lucá et al., 2017; Sacchini et al., 2022), chronicity staging, the comparative resilience of different age groups, sexes, subpopulations, and species, and the differentiation in pathogenesis between pathogens of the same type (e.g., between different viral agents, and other *Brucella spp*.; Garofolo et al., 2014). Dynamics of co-infections are largely unexplored, and very few studies consider comorbidities such as baseline overexposure to contaminants and natural toxins (Davis et al., 2021). While histopathological findings largely overlap between etiologies and vary between individuals, including non-suppurative meningoencephalitis marked by perivascular lymphoplasmacytic cuffing, neuronal necrosis, malacia, astro-microgliosis, hemorrhages, vasculitis, and edema, immunohistochemical, and molecular examination could reveal differences in the nature of the cellular insult triggering them.

Neoplasms in cetacean brains have been recorded to have a very low incidence and it is unclear to what extent they lead to mortality (Pilleri, 1966; 1968; Ridgway et al., 2002; Newman and Smith, 2006; Miclard et al., 2006; Baily et al., 2013; Arbelo et al., 2014; Díaz-Delgado et al., 2015; Pintore et al., 2018). Other pathological findings in cetaceans include spongy myelinopathy (Díaz-Delgado et al., 2015), astro-microgliosis, neuronal degeneration, and neuronophagia in the gray matter (satellitosis) and are categorized as nonspecific lesions without evidence of etiological agents (Pintore et al., 2018).

There is increasing evidence of the presence of Aβ deposition and tau pathology in cetacean brains, which is suggested to be correlated to the species longevity and long postfertility life span (Gunn-Moore et al., 2018; Stylianaki et al., 2019; Vacher et al., 2022). This renders cetaceans unique, unconventional models for human neurodegenerative disease (Di Guardo et al., 2018; Ackermans et al., 2021). The occasional appearance of Aβ in neuronal nuclei as a potential neuroprotective mechanism against hypoxia (Sacchini et al., 2020) raises the question of whether tau phosphorylation is another adaptation for this condition, and thus whether a cognitive decline can be measured in cetaceans using these typical Alzheimer's disease (AD) associated proteins. Another consideration is the apparent lack of adult neurogenesis in the areas where it is commonly detected in humans and rodents: the hippocampus and subventricular zone (Parolisi et al., 2018).

Cetacean brains are one of the most susceptible organs to contaminant and biotoxin exposure. Bioaccumulated methylmercury levels well above laboratory toxicity thresholds have been recorded in the brains of beluga whales (Dietz et al., 2013; Lemes et al., 2011; Krey et al., 2015; Ostertag et al., 2014) and short-beaked common dolphins (Davis et al., 2019). However, no associated neuropathology was observed in bottlenose dolphins with high mercury measurements in their liver and lymph nodes, which led to the current assumption that cetaceans may counteract

high mercury with high selenium concentrations (Turnbull et al., 1998). Nevertheless, synergistic effects between methylmercury and additional algal biotoxins result in distinct neuropathological central nervous system (CNS) changes (Davis et al., 2021). There are no equivalent studies in cetaceans to those reported in California sea lions (*Zalophus californianus*) on the loss of hippocampal neurons related to harmful algal bloom toxicity (Buckmaster et al., 2014; Silvagni et al., 2005).

In summary, cetacean neuroanatomy and pathology has progressed with large steps towards a greater knowledge of the most important organ to assess cognitive capacity of free-ranging cetaceans, yet large knowledge gaps persist.

Knowledge Gaps

While the predominance of the acoustic sense in cetaceans is unchallenged, many gaps regarding the functional anatomy of the acoustic pathways remain (Cozzi et al., 2016; De Vreese et al., 2020). Electrophysiological division of the bottlenose dolphin and harbor porpoise neocortex into primary (A1) and secondary (A2) auditory areas from the 1960s (Bullock et al., 1968; Sokolov et al., 1972; Ladygina and Supin, 1977; reviewed by Ridgway 1980; 1983; Popov et al., 1986, 1992; Popov and Supin, 1990) remains unparalleled and would be unethical to reproduce. Transcutaneous AEPs do not allow for exact localization of nervous activity, nor are calibrated for repeatable results (Finneran, 2020), and so are functional near infrared spectroscopy systems (Williams & Ponganis, 2013; Mc Knight et al., 2019). Functional MRI (fMRI) in live animals is yet to be achieved, although *post-mortem* MRI studies do exist (e.g., Montie et al., 2007, 2008; Oelschläger et al., 2010; Wright et al., 2017; Kot et al., 2020; Ridgway et al., 2002; Marino et al., 2003; Marino et al., 2004 a,b) and *post-mortem* perfusion is greatly complicated by the presence of cervical rete mirabilia, tremendously dampening the blood flow of the brain (Lillie et al., 2022).

Even if these hurdles can be overcome, the cytoarchitectonic structure of the primary auditory cortex in cetaceans, despite having been studied for decades (Kesarev, 1970; Hof et al., 1992; Glezer et al., 1998; Furutani, 2008), still perplexes anatomists due to its remarkable uniformity when compared to the animals' obvious capacities (Evans and Powell, 1967; Titov 1972; Murchison 1980; Au and Turl 1983; Turl 1991; Au and Pawloski, 1992). In seals, the location of the auditory cortex is known (Alderson et al., 1960). Although their hearing system is not deemed as essential for survival as it is for cetaceans, the nature of the mammalian auditory apparatus is necessarily sensitive to lesions potentially occurring during a dive.

Even in CEEs, correlation between psychophysical and AEP-recorded threshold shifts is problematic (Finneran et al., 2007; Finneran, 2015a; Kujawa and Liberman, 2009), with the former being a more astute indicator of reduction in hearing sensitivity. Most studies enacted hitherto using seismic air gun noise in odontocetes and seals (in bottlenose dolphins: Finneran et al., 2015a; harbor porpoise: Kastelein et al., 2017; spotted—*Phoca largha*—and ringed—*Pusa hispida*—seals: Reichmuth et al., 2016) appeared to cause very slight to no TTS, while Sarnocińska et al. (2020) concluded that pile-driving has a stronger effect on harbor porpoise echolocation patterns than air guns do. The first in-air, unilateral acoustic stimulation of bottlenose dolphins was performed by Finneran (2020) and re-demonstrated the odontocete ability of conditioned self-mitigation as had previously been recorded by Nachtigall and Supin (2013, 2014, 2015) and Nachtigall et al. (2016a, b;

2018), although many knowledge gaps regarding the cellular processes behind this remain. Considering potential parallels in conditioning mechanisms in rodents like elevation of calbindin concentration (Canlon et al., 1988), imbalance between expression of anti-apoptotic and apoptotic proteins (Yamashita, 2004) and induction of heat shock proteins (Altschuler et al., 1996; Samson et al., 2007; Soares et al., 2019; Helfert et al., 2002), such mechanisms that play a protective role long-term may, in the short term, serve as evidence for recent AOE.

The acoustic resonance of air-filled organs like the ventral sinus complex associated with the ears, ear sinuses, and inflated lungs was deemed unlikely to lead to noise-induced pathology in a NOAA report (2002), which is in line with a later study by Finneran et al. (2003b) using *post-mortem* cetacean lungs. In the reports of beaked whale mass-stranded in association with military exercises using mid-frequency sonar (Balcomb and Claridge, 2001; Rowles et al., 2001, Fernández et al., 2005) findings included cranial hemorrhage in the acoustic fatty tissues, the subarachnoid spaces, and cerebral ventricles, as well as within the cochlea. In the study of Fernández and colleagues (2005), white froth was found within the peribullar and pterygoid sinuses, and next to the hemorrhages in the subarachnoid spaces. Marked congestion and the presence of gas bubbles in cerebral vessels were noted. Hemorrhages were most severe around the vasculature of the brainstem and proximal spinal cord and were often surrounded by spongiotic parenchyma. In these cases, a causal link to the sonar signal is likely, due to the consistency in multi-species MSEs and their spatiotemporal association to sonar exercises, but it is not unequivocally demonstrated.

The lesions were not exclusive to auditory tissue and could theoretically arise from behavioral changes leading to decompression sickness-like symptoms. In some cases (Balcomb and Claridge, 2001), the heads of the animals were frozen prior to transportation to other laboratories, precluding reliable histopathological findings. Furthermore, due to the high-intensity nature of sonar, the method of looking only at the presence of gas and fat embolism and widespread hemorrhage is arguably not sensitive or specific enough to identify anthropogenic noise of comparatively lower SPLs (such as those associated with air guns and pile driving) as the agents triggering cumulative detrimental effects within cetaceans, despite these noise sources being used more commonly than military sonar.

Owing to the necessity of having impromptu guidelines for noise emissions underwater, Southall et al. (2007, 2019) summarized hitherto available AEP-elicited audiograms for several cetacean species and carefully extrapolated audiograms for the species that lack baseline data. They used a specially derived M-weighting paradigm (comparable to A-weighting applied in human otolaryngology) to account for presumed maximum sensitivity in the three cetacean hearing groups: low-, high-, and very-high-frequency cetaceans. The empirical audiograms originated from very few individuals per species. Therefore, their validity remains to be determined by systematically conducting electrophysiological measurements on a high number of specimens belonging to the same species, followed by routine *post-mortem* analysis of their acoustic pathways (Bröker, 2019). Until such practices are adopted, attempts at predicting cochlear frequency maps for cetaceans are being explored as a proxy (Morell et al., 2020b), using machine-learning algorithms to correlate cochlear morphology to specific cochleotopic regions in species with known audiograms (like bats, rats, mice, and gerbils).

For now, several questions on cetacean auditory perception are beginning to be addressed, such as the upper limit of high-frequency hearing in the very-high-frequency group (Southall et al., 2019), the effects of directionality of the incoming sound (Accomando et al., 2020), and the

development of adequate assessment frameworks for acoustic disturbance in wild and aquarium cetaceans (Southall et al., 2021). Nonetheless, even with the ability to assess lesions in the inner ear, we are not yet able to account for a phenomenon termed "hidden hearing loss"— "the condition where an individual experiences common symptoms associated with noise-related auditory damage, such as difficulty in hearing in noise, and that is undetectable on pure-tone audiometry" (WHO, 2021)—and where inner ear sensory hair cells often lack visible lesions (Kujawa and Liberman, 2009). Several mechanisms are presumed to contribute to this inability to distinguish significant signals amongst background noise (the "cocktail-party effect"; Cherry, 1953): cochlear synaptopathy, auditory nerve demyelination, elevated central gain, and neural maladaptation in the auditory pathways (Valderrama et al., 2022). In the marine environment of the Anthropocene, this kind of deficit could range from debilitating to deleterious in many species, and merits further research.

Other CNS changes could include tinnitus and lead to chronic changes of behavioral states, a condition described as "pessimistic biases" (Bateson et al., 2007; Stevens et al., 2021), negatively affecting cetacean ability to process ambiguous cues and potentially increasing stranding probability. It is strongly suspected that chronic stress leads to morphological and structural changes in cetacean brains, but compelling evidence has yet to be presented (Jacobs et al., 2022). To assess this, more information is needed on the mechanisms affecting the CNS of cetaceans in acute and chronic noise exposure. To the best of our knowledge, only one study reported a significant morphological change in the brain in association to a dolphin with confirmed hearing loss (without blast injury). The striped dolphin (*Stenella coeruleoalba*) female presented a Hydrocephalus internus (André et al., 2007), possibly causing the compression of auditory nuclei due to elevated intraventricular pressure and leading to severe hearing loss.

To acquire more specific information on the potential AOE, fresh, intact samples of the auditory pathways are essential. This stands in stark contrast to the difficulty of obtaining fresh *post-mortem* samples of cetaceans and pinnipeds, the ethical crux of the perfusion method in wild animals, the ongoing development of best practice protocols in sampling (e.g., joint ACCOBAMS/ASCOBANS protocol, IJsseldijk et al., 2019), and scarcity of expertise on processing and interpreting the results. Since Ketten and colleagues' morphological and functional analyses of dolphin and whale ears (e.g., Ketten et al., 1994; 1997, 2000), relatively few morphofunctional studies of the cetacean auditory pathway have been published (e.g., Ridgway, 2000; Cranford et al., 2008; 2010; Zook and DiCaprio, 1990). Comparative morphology of the cetacean external ear canal was performed by De Vreese and colleagues (2020), Hemilä and colleagues (1995, 1999) examined the cetacean middle ear, and a few research groups worldwide have meticulously described the ultrastructure of the odontocete inner ear using scanning and transmission electron microscopy (Morell, 2012, 2020a, 2022; Girdlestone, 2017). The anatomy and physiology of baleen whale auditory pathways still largely present a puzzle, despite a minke whale being included in the auditory brainstem study by De Graaf (1967).

Post-mortem MRI scans of varying resolution have sporadically been applied to cetacean brains (Marino et al., 2003; Ketten and Montie, 2008). Imaging techniques (e.g., diffusion tensor imaging—DTI) applied to *post-mortem* cetacean brain scans revealed a marked asymmetry of both auditory and non-auditory nuclei and connectome within the CNS (Wright et al., 2018). Berns et al. (2015) noted a connection between the medial geniculate nucleus and the temporal lobe,

complementing the 1960s electrophysiological data that highlights the parietal lobe as the location of A1 and A2. It is generally accepted that A1 and A2 in the bottlenose dolphin and harbor porpoise correspond to the primary (and perhaps secondary) auditory areas. However, there is a total absence of knowledge regarding association areas pertaining to more subtle functions such as echolocation, as well as little data on volumes of specific brain nuclei (Montie et al., 2008; Hall, 1967) and their connections across species. Only single MRI scans have been published for mysticetes (e.g., Raghanti et al., 2019). This forces a heavy reliance on historical manuscripts such as De Graaf (1967) that are restricted to a handful of species and rely on simple histochemical stains. As such, the situation can be improved greatly by being updated using modern approaches.

Virtopsy techniques (Kot et al., 2020; Ketten et al., 2008; Montie et al., 2010; Hamel et al., 2020; Granados-Zapata et al., 2022) complement electrophysiological methods and may serve to detect macroscopic pathology regarding grey and white matter volume changes in auditory and associated CNS centers (as measured in human studies [Mühlau et al., 2006; Schneider et al., 2009; Ha et al., 2020; Tuladhar and de Leeuw, 2020] and associated to somatosensory pain [Schmidt-Wilcke et al., 2006; Moller, 2000]). First protocols for the fMRI of sea lion brains to evaluate domoic acid toxicosis have been shared, facilitated by the animals' amphibious nature, and further work intends to assess *in-utero* development of affected pups (Cook et al., 2018; 2021). Cetacean functional imaging is in its infancy, with only single, highly trained dolphins having been scanned using SPECT and PET techniques (Ridgway et al., 2006). Berns (2015b) discusses the technical hurdles of dolphin fMRI but concludes that it is achievable given the right resources.

At the same time, ultra-high-resolution techniques (e.g., 7 – 9 Tesla MRI; µCT; SR-PCI; SLOT; CLARITY, AbScales), and multimodal imaging (Costantini et al., 2021, 2022; Scardigli et al., 2021) of *post-mortem* tissues may allow for a better correlation with histological data. These techniques hold promise for reducing the number of artifacts associated with thin sectioning for conventional histopathology and allow for telediagnostics involving international experts. This is an important development, because worldwide, there are very few experts qualified both in veterinary pathology and marine mammal biology.

Effects of Sound on Laboratory Animals and Humans

In terms of knowledge of the pathophysiological effects of AOE on mammals, the research on humans and rodents is by far the most advanced. In these species, a functional assessment of the auditory pathway subparts under physiological and pathological conditions can be ascertained using numerous *in-vivo* and *post-mortem* techniques. *In-vivo*: CEEs, fMRI (e.g., Manganese enhanced), electroencephalography, psychophysical audiograms, and evoked potentials recorded from central nervous auditory nuclei allow for a functional assessment of the auditory pathway subparts under physiological and pathological conditions (Watanabe et al., 2008; Elgoyhen et al., 2015; Brozoski et al., 2002). *Post-mortem*: availability of fresh samples, long-standing, standardized, but also emerging techniques for dissection and tissue processing (Nolte et al., 2017; Pende et al., 2020), established anatomical knowledge, and the existence of reference labs enable exemplary advances in the understanding of biomolecular auditory pathophysiology.

Humans are a long-lived species with the ability to communicate our perception of (phantom or real) sound, which enables long-term studies on a demographic and genomic scale (Liu et al., 2010; Moser and Starr, 2016) that benefit from in-vivo imaging using PET, MEG, MRS, MRI, voxel-based morphometry, repetitive transcranial magnetic stimulation, and DTI with ever higher resolution (Lobarinas et al., 2008; Elgoyhen et al., 2015; Gröhn et al., 2019; Mühlau et al., 2006). Both hydrophobic and hydrophilic clearing methods have been applied in investigating neuropathology related to autism, AD, and Parkinson's Disease, which share common neurodegenerative mechanisms with central repercussions of AOE. Whole-organ and whole-body tissue clearing techniques such as hydrophobic iDISCO, hydrophilic CUBIC, and hydrogel-based protocols like SWITCH (for an extensive review, see Ueda et al., 2020) enable mapping of the entire rodent brain (e.g., Allen Brain Atlas, 2020) including its white matter connectome in subcellular resolution. This builds the foundation for 3D-visualization of central nervous physiopathology. Differences in cell density, limited tissue penetration, autofluorescence associated with neuropigment content, variable and often prolonged formalin-fixation, and issues with preservation of antigenicity currently limit whole-organ approaches in larger brains (Scardigli et al., 2021). The ongoing development of these, and even label-free advanced microscopy applications (Axer et al., 2016; Wang et al., 2018; Menzel et al., 2021), will lead to better validation of imaging techniques like DTI (Costantini et al., 2021).

Laboratory animals hold the key to seeing noise-induced metabolic changes in very fresh and perfused *post-mortem* auditory tissues, so that psychophysically or electrophysiologically detected TTS or PTS can be correlated to protein and gene expression changes using immunohistochemical and immunofluorescence methods (e.g., anti-apoptotic Bcl2-family proteins; Yamashita et al., 2008). They generally display a balance between a detrimental and reparative process, such as apoptotic and anti-apoptotic, inflammatory and anti-inflammatory, and degenerative and plastic (Figure 3).

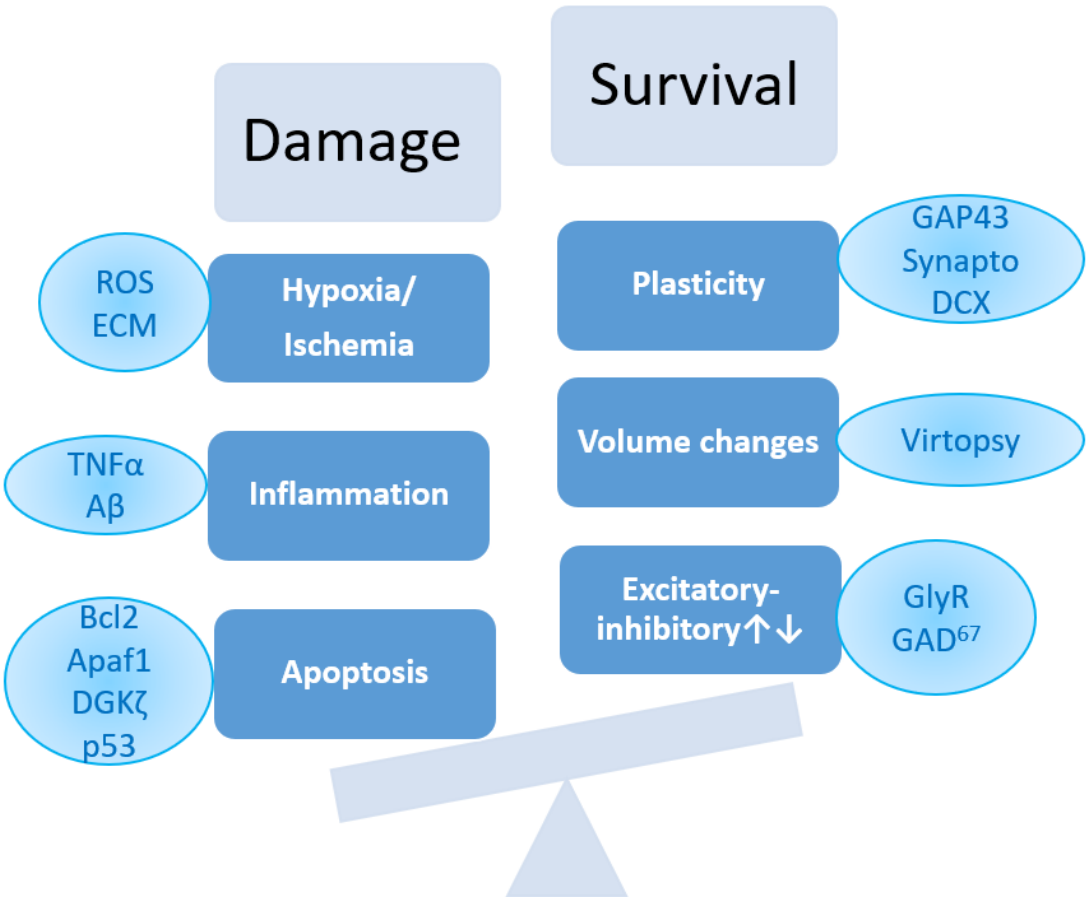

Figure 3. Balance between damaging and protective/reparative mechanisms in the CNS, and some examples of protein or morphological biomarkers associated with each process. ROS—reactive oxygen species; ECM—extracellular matrix with components such as fibronectin. TNFα—tumor necrosis factor α; Aβ—amyloid-β peptide; Bcl-2—B-cell lymphoma related protein 2; Apaf-1—pro-apoptotic protease factor 1; DGK-ζ—diacylglycerolkinase-ζ; p53—tumor protein p53; GAP-43—growth associated protein 43; DCX—doublecortin; GlyR—glycine receptors; GAD^{67}—glutamate decarboxylase 67.

From that point on, the cell could lean towards one or the other extreme once it reaches a tipping point between survival and death. For instance, DGK-ζ is a molecule that has been seen to translocate from the nucleus into the cytoplasm in cochlear hair cells undergoing subsequent noise-induced apoptosis in guinea pigs, potentially visualizing the "point of no return" for the cell (Shinkawa et al., 2019). To retain proteostasis, the protein and genomic expression profiles are often inverse to each other i.e., the gene expression is commonly upregulated following the increased use or depletion of a given protein. An example for this relation is the anti-apoptotic Bcl2A1A, a marker found to be decreased after AOE on a proteomic level, parallel with an increase in mRNA-expression (Gröschel et al. 2018) along the central auditory pathway. Plasticity following distinct contra- and ipsilateral distribution patterns was demonstrated within the auditory brainstem weeks to years after unilateral impulsive AOE (Michler et al., 2002), and shown to occur after neuroinflammation-mediated synaptic destruction and reorganization (Di Filippo et al. 2008).

Keeping in mind the combination, location, and timing of these basic mechanisms, one can attempt to visualize a "fingerprint" of a potential AOE event in very fresh or freshly fixed tissues. This multimodal and multi-marker approach is necessary because there is no pathognomonic mechanism exclusive to NIHL. Metabolic changes parallel those in age-related hearing loss (ARHL), such as increased radical oxygen species (ROS) concentration and reduced integrity of the stria vascularis within the cochlea (Wu et al., 2019, Fetoni et al. 2011). Changes in the auditory midbrain include reduced expression of potassium channels, neurotransmitters and their receptors (Wong and Ryan, 2015). These changes in aged individuals can be independent of those in the auditory periphery, but nevertheless contribute to altered sound perception through diminished neural firing rates and synchrony (Caspary et al., 2008). Structural damage may arise from such subtle changes as genetic mutations in exons encoding inner hair cell or stereociliar proteins (Jain et al., 2018), or neural changes from physiological plastic—or pathological neoplastic—reorganization (Miranda et al., 2014; May et al., 2011).

Nevertheless, the temporal progression of the processes tends to reflect the time point of the AOE, the first of which is the accumulation of ROS appearing within minutes to hours after exposure to the noise (Du et al., 2011; Shi and Nuttall, 2003) and triggering inflammatory processes (marked by cytokine upregulation, like IL-6, Wakabayashi et al., 2010; and TNF-α, Wang et al., 2019), and phagocytosis of damaged hair cells. Apoptosis (Yamashita et al., 2004) and necrosis subsequently affect first outer, then inner hair cells. This degeneration is reversed by regeneration in birds, reptiles, and fish (Warchol et al., 2011), which takes days to weeks, whereas mammals predominantly revert to compensatory plastic mechanisms further up the auditory pathway (Gil-Loyzaga et al., 2010). In rodents, there appears to be a rough 8-week time frame in which plastic neuronal changes take place after acoustic deafferentation (Kim et al., 2018), with different chronicity-indicating inflammatory, apoptotic, metabolic, and structural markers peaking most significantly at various time-points within those weeks. Some examples of the protein and biomolecular changes on a temporal scale can be seen in Figure 4.

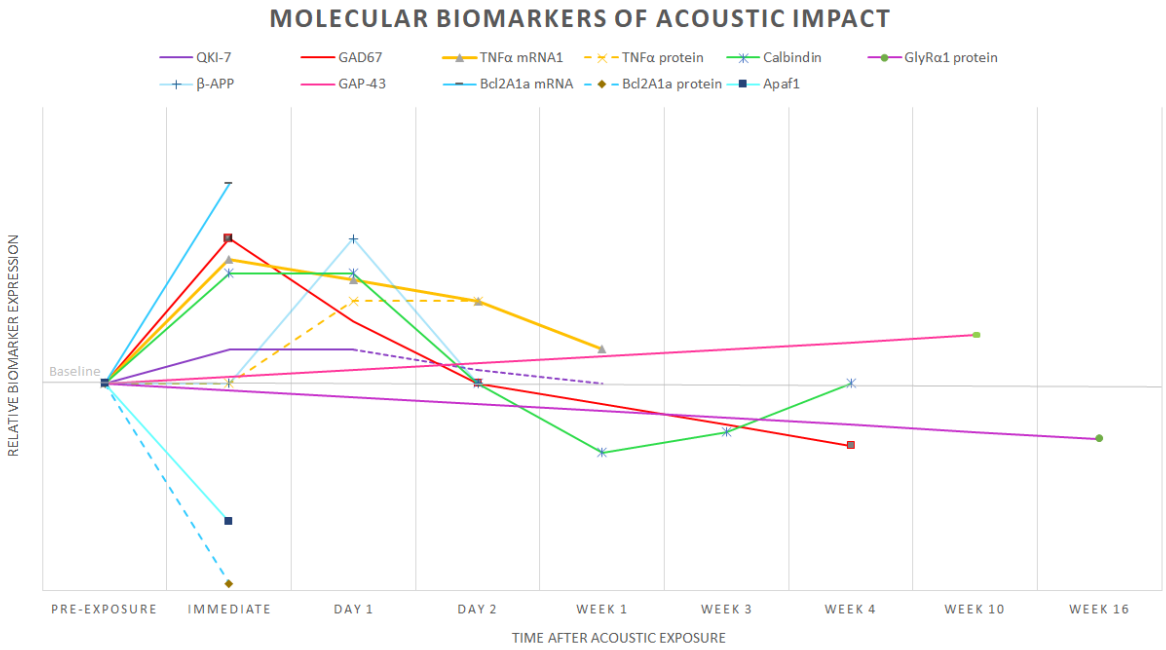

Figure 4. The line graph shows the relative expression changes of proteins, and Bcl2A1A, TNFα and QKI mRNA, against the time after an AOE. Publication references can be found in the Supplementary Materials. Upregulation of inflammatory (TNFα) and acute-damage (amyloid precursor protein—APP) markers was detected immediately to one day post-AOE. TNFα also serves as an example of temporally differentiated expression, with an upregulation first on the proteomic, then genomic levels, which correlates to a morphological change and activation of microglia. Together, these changes presumably underlie excitatory-inhibitory imbalance within the brain. The anti-apoptotic Bcl2A1A mRNA expression is inverse to significant immediate protein upregulation. Calbindin, GlyRα1 and GAD^{67} reflect changes in neuronal firing rates, with the latter two showing decreased inhibitory regulation with time after an AOE—a condition consistent with tinnitus. QKI reflects remyelination dynamics, while GAP-43 marks the steady increase in plastic processes in the brain within the post-AOE months. Markers were measured at different levels of the auditory pathway (in alphabetical order): Apaf-1 (cochlear nucleus—CN, inferior colliculus—IC, auditory cortex—AC); Bcl2A1a protein (CN, IC, AC); Bcl2A1a mRNA (CN, IC); β-APP (AC); Calbindin (trapezoid body, lateral superior olive); GAD^{67} (IC); GAP-43 (ventral CN); GlyRα1 (dorsal cochlear nucleus); TNFα protein and mRNA (AC); QKI mRNA (auditory nerve).

The lesion location also varies with the severity and time following the AOE. Cochlear damage is tonotopic, with the greatest damage at the cochleotopic region corresponding to the noxious noise's characteristic frequency and a half-octave above it i.e., more basal on the basilar membrane (Reichmuth et al., 2019; Morell et al., 2017). It is an acute change, beginning immediately with the influence of the AOE, and persisting over the following days. As displayed in the diagram below (Figure 5), the 2-peak upregulated expression of malondialdehyde reflects transient intense ROS production immediately after AOE, correlating to the early-onset mechanical damage of hair cells, and later rise in the two-week period of gradually continuing hair cell loss (Yamashita et al., 2004; Du et al., 2011).

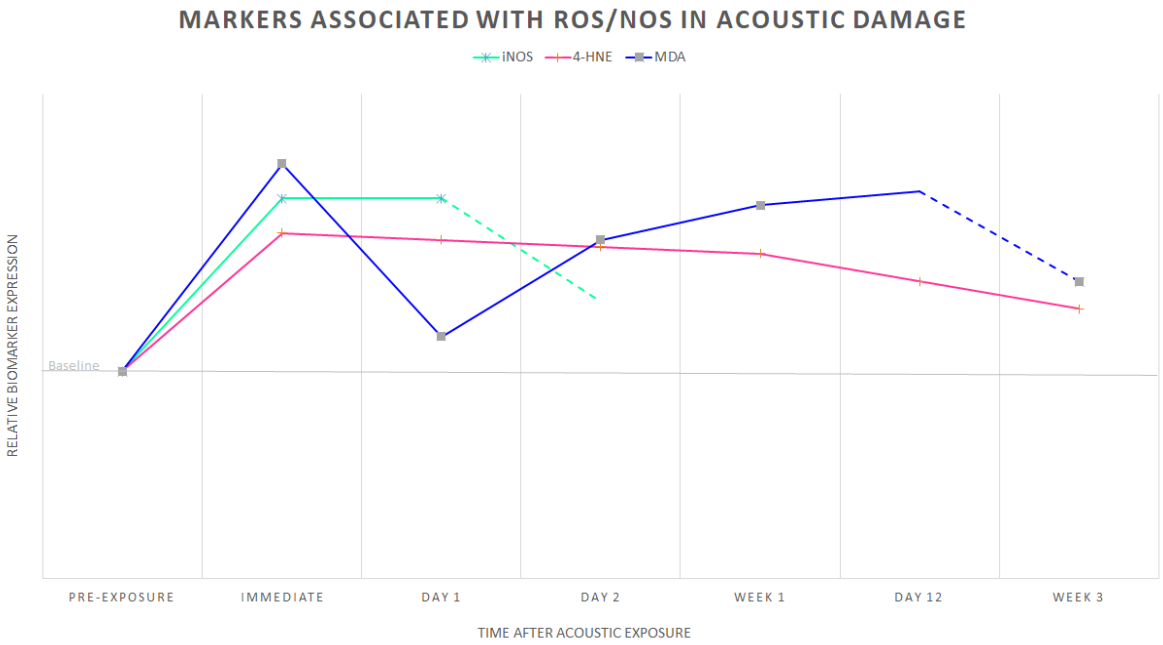

Figure 5. The line graph shows the relative expression changes of protein markers of ROS production against the time after an AOE. Publication references can be found in the Supplementary Materials. Almost all the ROS markers show a marked upregulation immediately after AOE. With time, some appear to persist at high concentrations within cochlear tissue (4-Hydroxynonenal—4-HNE), whilst others present a 2-peak course within the first two weeks after AOE (malondialdehyde—MDA). These concentrations are consistent with high initial auditory hair cell loss and more gradual apoptotic processes that diminish approximately two weeks post-AOE. Markers were measured at different levels of the auditory pathway (in alphabetical order): 4-HNE (inner hair cells and supporting cells); inducible nitric oxide synthase—iNOS (cochlea, hippocampus, thalamic reticular formation); MDA (cochlear tissue).

With time (weeks to years), the peripheral damage leads to more central changes like auditory nerve fiber degeneration and progressive reorganization of synaptic connections in auditory relay stations like the ventral cochlear nucleus (VCN) and inferior colliculus (IC) (Abbott et al., 1999). However, this is not a strictly linear timeline, as myelin disorganization in centripetal nerve fibers (Coyat et al., 2019), central shrinkage of brain stem nuclei after AOE, and shrinkage and darkening of cortical neurons with mild traumatic blast injury were recently found as acute changes (Kraus et al., 2011; Pun et al., 2011). Interestingly, microarray analysis of myelination genes of the QKI family and immunohistochemistry of proteins involved in the organization of the first heminodes at the habenula perforata revealed active processes that paralleled developmental myelination after TTS-inducing AOE (Panganiban et al., 2018; Wan and Corfas, 2017). This remyelination was, however, incomplete, as reflected in electrophysiological auditory threshold elevations and upon transmission electron microscopic analysis. Wang and colleagues (2019) reported persisting neuroinflammation up to 10 days (peak at 12 h) after the AOE in murine central nervous tissue, pointing out the potential of investigating changes within the brain. Provided the sample is collected fresh, processed adequately, and interpreted critically, changes could be detected at almost every level of the auditory pathway (see Table 4 for examples).

Table 4. Overview of most frequently seen changes of auditory pathway morphology and molecule expression after AOE in laboratory animals. CN—cochlear nucleus; IC—inferior colliculus; AC—auditory cortex, CNS—central nervous system; HSP—heat shock protein; ROS—reactive oxygen species; RNS—reactive nitrogen species; SPL—Sound pressure level.

Affected tissue	Pathophysiological changes	Chronology	Species	Reference
AC, CN, IC	Intrinsic apoptosis	Immediate	Mice	Gröschel et al. (2018), Yamashita et al. (2008)
AC, anteroventral CN, cochlea	Upregulated TNFα expression	Peaks between day 1-10 after AOE, diminishing gradually by day 30	Rats	Fuentes-Santamaria et al. (2017)
Cortical and cochlear vessels	Vasospasm	For ≥ 4 days after blast overexposure and AOE	Rats	Pun et al. (2011), Shin et al. (2019)
Cortical neurons, ipsilateral ventral CN	Shrinking with and without darkening of neurons	1 day after mild TBI-inducing blast overexposure. Recovery after 4-7 days	Rats	Pun et al. (2011), Kraus et al. (2011)
CNS glia	Increased amyloid precursor protein expression	1 day after blast overexposure	Rats	Pun et al. (2011)
White matter axons	Decrease in myelin-associated protein expression	≤ 3 days after blast overexposure	Rats	Park et al. (2011)
IC	Changes in expression of major inhibitory neurotransmitter GAD[67]	Increases immediately post-AOE. Drops below baseline levels 30 days post-AOE	Rats	Abbott et al. (1999)
Auditory midbrain, superior olivary complex, CN	Decrease in inhibitory glycine uptake	≤ 145 days post-AOE	Guinea pigs	Suneja et al. (1998)
Dorsal CN	Spontaneous neuronal hyperactivity. Decrease in inhibitory glycine receptor expression and glycine uptake. Increase in somatosensory input	Begins ~1 week post-trauma. Increases gradually over the next 3-4 weeks	Rat, chinchilla, hamster	Kaltenbach and Afman (2000), Kaltenbach et al. (1998), Wang et al. (2009), Zeng et al. (2009)
IC, lateral superior olivary complex, medioventral CN, auditory nerve fibers	Upregulated GAP-43 expression	Starting ≥ 10 post-exposure* and lasting up to ≤ 1.5 years post-exposure**	Rats, chinchilla	*Kraus et al. (2011), Kraus et al. (2013), **Michler et al. (2002)
Auditory nerve fibers	Reduction in myelin thickness and organization. Insufficient transcription of remyelination-associated genes	3-5 days post-exposure. Still evident 1 year post-exposure	Rats	Panganiban et al (2018), Coyat et al., (2019), Pilati et al. (2012)
Auditory nerve fibers and cochlea	Elevation in reactive oxygen and nitrogen species (ROS, RNS)	ROS: cause acute damage and may persist 7-10 days post-exposure, displaying a basal-to apical gradient in severity. RNS: peak 6 days post-exposure iNOS: peaks immediately post-AOE	Rats, guinea pigs	Yamashita et al. (2004), Karlidağ et al. (2002), Du et al. (2011), Shi and Nuttall (2003)
Cochlea	Increase in lipid peroxidation products	Peak ~3 days post-AOE Decrease over following 7 days	Guinea pigs	Maulucci et al. (2014)
Cochlear hair cells	Upregulated structural protein prestin expression	Immediate	Rats	Fuentes-Santamaria et al. (2017)

Cochlear hair cells	Decrease in Ca^{2+}-buffering protein calbindin expression. Potential conditioning	Immediately post-exposure, even to non-traumatic SPLs. Recovery to baseline 2-4 weeks post-exposure	Guinea pigs	Canlon et al. (1988)
Cochlear hair cells	Cytoplasmic expression of heat shock proteins (HSP) 27 and 72 in outer hair cells and stria vascularis. Modulation of constitutive HSP90	HSP27: peak 5 hours post-AOE HSP72: peak 6 hours post-AOE	Rats	Altschuler et al. (1996)

Parallels between NIHL and ARHL have repeatedly been drawn. Research has shown that in asymptomatic humans over 60 years old, neural degeneration outweighs that of the OHCs by up to three times (Wu et al., 2019). Building upon Kujawa and Liberman's (2009) paradigm of noise-induced synaptopathy, this fact could potentially be attributed to accumulated "hidden hearing loss" owing to repeated TTS over the subject's lifetime.

Despite extensive study of laboratory animals and humans, many gaps in our understanding of central auditory pathway health and disease, such as the topography of the acoustic radiation in humans (Maffei et al., 2019) or the relationship between NIHL, ARHL, excitotoxic synaptic CNS damage, and cognitive decline (Moser and Starr, 2016) await research and could profit from unconventional translational models including cetaceans.

Animal Brains as Models for Human Neurodegenerative Diseases

Historically, the use of laboratory animal (foremostly rodents and primates as mammals and zebrafish and insects as non-mammals) models to experiment and expand on the knowledge of human neurodegenerative conditions is well established. However, many of the species used are not long-lived species with a considerable postfertility lifespan (and thus likely different aging dynamics), having highly convoluted brains and sophisticated emotional development. Moreover, rodents often fail to manifest the typical lesions seen in corresponding neurodegenerative conditions in humans (Yin et al. 2022).

Cetacean brains face all the same logistical problems as humans: variable and sometimes very long fixation times and storage, large dimensions complicating optimal diffusion of the fixative, irregular geometry, presence of intravascular blood, resistance to perfusion, and autofluorescence from lipofuscin-type pigments that accumulate with age. This, together with the dense composition of the tissue, often results in inconsistent immunohistochemical labeling of the tissue due to either loss of antigenicity or mechanical hindrances for the binding of the antibody (Costantini et al., 2022). By bringing a considerable contribution to the health of their ecosystems (e.g., the circulation of nutrients in the context of the "whale pump", Roman and McCarthy, 2010), they merit the monitoring of their welfare as individuals. However, being at the top of their respective food chains, they can also provide unique insight into the detrimental effects of bioaccumulation over a lifetime (Hayes et al., 2022)—a perspective large, domestic animal models (e.g., pigs or sheep) cannot yield.

Dogs are another increasingly recognized animal model for several neurodegenerative diseases like AD, amyotrophic lateral sclerosis, and neuronal ceroid lipofuscinosis (Story et al., 2020). Up to 60% of geriatric dogs present canine cognitive dysfunction (Fast et al., 2013), and accumulate Aβ in a similar way to humans (Cummings et al., 1996; Näslund et al., 2000). They are widely accessible, have relatively large brains and present several known mutations responsible for hereditary diseases and drug toxicity (Donner et al., 2016). However, comparatively little is known about the pathogenesis of many central nervous afflictions, such as the role of hypoxia in brain insults.

Under the roof of the One Health principle, both dogs and cetaceans can help understand pathological processes in mammalian brains, show adaptations to their respective environments and serve as unconventional translational models for human neurodegenerative disease.

Publication I: Immunohistochemical Markers of Apoptotic and Hypoxic Damage Facilitate Evidence-based Assessment in Pups with Neurological Disorders

Several neuropathological phenomena have been described in literature, such as canine cognitive dysfunction and Old Dog Encephalitis, however information on the dynamics of neuronal damage in more acute insults, such as seizures, is spurious. Particularly in cases where multiple etiologies of neuronal damage are possible, immunohistochemistry against peri-apoptotic proteins can indicate the phase of neurodegeneration and contextualize clinical and necropsy findings, which are sometimes scant. Puppies present a demanding diagnostic challenge, since their organs are still maturing and metabolization of toxins from both infectious agents, and the drugs to treat them, may be insufficient. These complications are often exacerbated in dogs with mutations of the *MDR1* gene, resulting in neurotoxicity.

In this study, we compared the clinical progression and *post-mortem* findings of two 5 week-old Australian Shepherd puppies that succumbed to convulsions and dyspnea following deworming with milbemycin oxime at an appropriate dosage for the treatment of a severe intestinal helminth infection. They differed in the duration of clinical symptoms, access to supportive therapy, and *post-mortem* interval, although the symptomatology was similar, and necropsy findings were inconclusive. Immunohistochemistry against the following peri-apoptotic proteins were performed: diacylglycerolkinase-ζ (DGK-ζ), apoptotic protease activating factor 1 (Apaf1), and B-cell lymphoma related protein 2 (Bcl-2). Amyloid precursor protein (APP) expression was evaluated as a means to assess hypoxic damage. Three control dog brains were used to compare the results with patients without neurological symptoms.

The results corresponded to the stage and duration of the puppies' clinical history, reflecting a more severe and extensive neuronal insult in the animal with a longer duration of symptoms (Puppy-1) without access to supportive therapy, and a degree of damage consistent with acute to sub-acute hypoxia that was incompatible with survival in both puppies. The consideration of APP and the peri-apoptotic proteins were instrumental in the assessment of the severity, distribution and abundance of neuronal apoptosis and degeneration before the appearance of their morphological features, indicating that they are useful tools in assessing the chronicity of the damage even within an acute timeframe. Their immunohistochemical signature differed qualitatively both between the two sibling puppies, as well as to the control canine brains. Integrated evaluation of these puppies' and their siblings' *MDR1* status revealed that, while Puppy-1 presented a mutation, it was likely a contributing, but not the sole, cause of the observed symptoms. Instead, a multifactorial hypoxic syndrome was deemed the cause of acute neuronal degeneration and ensuing death. This approach demonstrated that immunohistochemical markers hold great potential as an ancillary diagnostic tool in the assessment of neuropathological insults in canines and other domestic and wild animals.

veterinary sciences

IMPACT FACTOR 2.518

Indexed in: PubMed

Case Report

Immunohistochemical Markers of Apoptotic and Hypoxic Damage Facilitate Evidence-Based Assessment in Pups with Neurological Disorders

Ksenia Orekhova, Sandro Mazzariol, Beatrice Sussan, Massimo Bucci, Federico Bonsembiante, Ranieri Verin and Cinzia Centelleghe

MDPI

https://doi.org/10.3390/vetsci8100203

veterinary sciences

MDPI

Case Report

Immunohistochemical Markers of Apoptotic and Hypoxic Damage Facilitate Evidence-Based Assessment in Pups with Neurological Disorders

Ksenia Orekhova [1,*], Sandro Mazzariol [1], Beatrice Sussan [2], Massimo Bucci [2], Federico Bonsembiante [1,2], Ranieri Verin [1] and Cinzia Centelleghe [1]

[1] Department of Comparative Biomedicine and Food Science, University of Padova AGRIPOLIS, viale dell'Università 16, 35020 Legnaro, Italy; sandro.mazzariol@unipd.it (S.M.); federico.bonsembiante@unipd.it (F.B.); ranieri.verin@unipd.it (R.V.); cinzia.centelleghe@unipd.it (C.C.)

[2] Department of Animal Medicine, Production and Health, University of Padova AGRIPOLIS, viale dell'Università 16, 35020 Legnaro, Italy; Beatrice.sussan@unipd.it (B.S.); Massimo.bucci@unipd.it (M.B.)

* Correspondence: ksenia.orekhova@phd.unipd.it

Abstract: Seizures in puppies often present a diagnostic challenge in terms of identifying and treating the underlying cause. Dog breeds with mutations of the *MDR1*-gene are known to show adverse reactions to certain drugs, yet metabolic imbalance exacerbated by physiologically immature organs and other contributing pathologies require consideration before arriving at a diagnosis. This study analysed the brains of two male, 5-week-old Australian Shepherd siblings that died after displaying severe neurological symptoms upon administration of MilproVet® to treat severe intestinal helminth infection. Despite the initial symptoms being similar, their case histories varied in terms of the symptom duration, access to supportive therapy and post-mortem interval. Histopathology and immunohistochemistry were used to obtain more information about the phase of the pathological processes in the brain, employing protein markers associated with acute hypoxic damage (β-amyloid precursor protein/APP) and apoptosis (diacylglycerolkinase-ζ/DGK-ζ, apoptotic protease activating factor 1/Apaf1, and B-cell lymphoma related protein 2/Bcl-2). The results seem to reflect the course of the animals' clinical deterioration, implicating that the hypoxic damage to the brains was incompatible with life, and suggesting the usefulness of the mentioned immunohistochemical markers in clarifying the cause of death in animals with acute neurological deficits.

Keywords: seizures; hypoxic brain injury; canine diacylglycerolkinase zeta; beta-amyloid precursor protein; Apaf1 protein; Bcl-2 protein; MDR1 mutation

Citation: Orekhova, K.; Mazzariol, S.; Sussan, B.; Bucci, M.; Bonsembiante, F.; Verin, R.; Centelleghe, C. Immunohistochemical Markers of Apoptotic and Hypoxic Damage Facilitate Evidence-Based Assessment in Pups with Neurological Disorders. *Vet. Sci.* **2021**, *8*, 203. https://doi.org/10.3390/vetsci8100203

Academic Editor: Mark L. Weiss

Received: 16 July 2021
Accepted: 18 September 2021
Published: 22 September 2021

1. Introduction

Puppies with seizures are challenging veterinary patients, with ongoing post-natal organ maturation predisposing them to metabolic crises such as hypoglycemia [1] and inability to adequately metabolize certain drugs [2]. Clinical parameters vary individually and daily during development, and breed-associated *MDR1* status may contribute significantly to arising neurological deficits [3]. This fragile physiological balance limits therapeutic options, commonly resulting in death. However, integrative evidence-based assessment may help in understanding the underlying neuropathogenesis. Neurotoxicity is often associated with brain hypoxia, neurodegenerative and apoptotic changes [4]. In this study, immunohistochemistry (IHC) of cell stress-indicator proteins was employed to visualize biochemical imbalance prior to its morphological manifestation [5] in seizuring puppies, comparing them to control brains of three dogs of varying PMI intervals and without neurological symptoms at the time of death.

A litter (n = 8) of 5-week-old Australian Shepherd puppies presented severe neurological symptoms (videos thereof may be found in the Supplementary Materials) following

deworming with one pill of Milprovet® each (containing 2.5 mg milbemycin oxime/25 mg praziquantel): owners refer seizures, tremors and ataxia with manifestation of severe abdominal pain 12–24 h after its administration. One male (Puppy-1) died before arrival to the Veterinary Teaching Hospital of the University of Padova. A second male (Puppy-2) succumbed about an hour after initiation of supportive therapy. Their littermates recovered within 1.5 h of flow-by oxygen administration, intravenous ringer-lactate (4 mL/kg/h) and Intralipid® 20% (1 mL/kg; Fresenius Kabi) infusion. Puppy-3 suffered two convulsive crises 3 h upon initiation of supportive care, recovering after repeated diazepam administration. Supplementary Table S1 summarizes the anamnestic, clinical and post-mortem findings in the Australian Shepherd puppies.

2. Materials and Methods

Post-mortem analyses were performed 24 h and 20 min after death in Puppy-1 and Puppy-2, respectively, and samples processed for routine histology and IHC with haematoxylin counterstain, using the same equipment and protocols as previously described [6], and antibody-specific positive, negative and blank controls. Formalin-fixed, paraffin-embedded archived brain cortex tissues from three control dogs without neurological symptoms (Control-1, -2, and -3) were cut and IHC-stained in the same way to assess for qualitative differences in the IHC-patterns dependent on three increasing post-mortem intervals (PMI). Pertinent demographic and forensic information on the control dogs is displayed in Table 1. Their *MDR1* phenotype is unknown.

Table 1. Pertinent demographic and forensic information on the five dog brains included in this study. M: male; F: female.

Control Dog (M/F)	Breed	Age	Cause of Death	Pertinent Pathological Findings	Post-Mortem Interval
Puppy-1 (M)	Australian Shepherd	5 weeks	To be determined	Hepatic, enteric, respiratory and central nervous system damage (described in "Results")	24 h
Puppy-2 (M)	Australian Shepherd	5 weeks	To be determined	Hepatic, enteric, respiratory and central nervous system damage (describe in "Results")	20 min
Control-1 (F)	Toy Poodle	12 years	Cardiovascular insufficiency	Aortic aneurism; monolateral inner ear infection	24 h
Control-2 (F)	Shitzu	1 week	Neonatal immaturity and pneumonia potentially resulting in septicemic shock	Diffuse atelectasis; diffuse severe pleuropneumonia; moderate multifocal tubular necrosis, mild diffuse gastroenteritis	48 h
Control-3 (M)	Dogue de Bordeaux	1 week	Neonatal immaturity and cardiorespiratory insufficiency	Diffuse atelectasis; ascites (serosanguinous); perihepatic vascular mineralisations	72 h

Images were scanned with a D-sight scanning microscope at ×400 magnification (A. Menarini Diagnostics). A board-certified pathologist (R.V.) checked all the slides to assess histological and IHC findings.

Primary polyclonal antibodies used for IHC included anti-amyloid precursor protein (Abcam, #ab15272, diluted 1:50), rabbit anti-diacylglycerolkinase-ζ (DGK-ζ; MyBiosourse, #MBS2026991, 1:100), anti-apoptotic protease activating factor-1 (Apaf1; Enzo, #ADI-905-179-100, 1:500), and anti-B-cell lymphoma related protein (Bcl-2; Abcam, # ab196495, 1:150). The whole litter of Australian Shepherd puppies was tested for *MDR1*-gene mutation via allelic discrimination [7].

3. Results

Gross findings in the Australian Shepherd puppies were scant, with both livers appearing mildly enlarged, with fragile consistency, light-red coloration and rounded edges. Additionally, Puppy-2 displayed multifocal to coalescing pulmonary consolidation.

Histopathology confirmed the mild to moderate edema and congestion observed in all examined internal organs, and further revealed multifocal cortical laminar necrosis, superficial spongiosis and meningeal congestion of mild and mild to moderate severity in Puppy-2 and Puppy-1, respectively. Multifocal Purkinje cell degeneration was observed in the cerebellum, with perivascular edema of the molecular and Purkinje cell layers and the white matter (WM). These changes were mild and multifocal in Puppy-2, but moderate and multifocal to coalescing in Puppy-1, with additional Purkinje single cell necrosis. Both animals had mild to moderate, diffuse, micro- and macro-vesicular hepatic steatosis, and mild multifocal subacute lymphohistiocytic enteritis with reactive GALT. Both lungs displayed mild to moderate, multifocal, subacute, histiocytic interstitial pneumonia. Multifocal atelectasis, severe perivascular edema, interstitial hemorrhages, and a focal eosinophilic granuloma were observed in Puppy-2, while Puppy-1 presented mild emphysema at the lobe tip, multifocal interstitial and alveolar hemorrhages, and agonal edema. Heterozygous *MDR1*-gene mutations were present only in Puppy-1 and Puppy-4—the rest presented the wild-type phenotype.

IHC results for the brain and the markers used are summarized in Table 2. In general, immunoreactivity was more intense and diffuse in Puppy-1. The specific IHC findings are depicted in Figure 1.

Control brain tissues were included for comparison to a dog that did not have any neurological symptoms at time of death (Control-1; PMI: 24 h), likely having endured only mild agonal hypoxia. Two control puppies presenting neonatal immaturity and additional inflammatory symptoms in the lungs (Control-2; PMI: 48 h) and metabolic imbalance as evidenced by perihepatic mineralizations (Control-3; PMI: 72 h) were included to assess potential changes of IHC-signal deriving from post-mortem protein degradation.

APP-reactivity of Control-1 was limited to a very mild, arborized or granular signal around single cortical neurons. Controls-2 and -3 both presented a background in the neuropil that was lighter than in both Australian Shepherd puppies, with multifocal cytoplasmic and synaptic neuronal immunoreactivity (+/++), with a mildly enhanced signal in the capillary vessel walls and meninges of Control-2. Control-2 and Control-3 were negative for Bcl-2, while Control-1, being mostly negative, presented findings more subtle, but reminiscent of those in Puppy-2, with a few foci of mild, cytoplasmic immunoreactivity (+) in neurons and neuropil. DGK-ζ was detected only in neuronal nuclei of Control-1 (+/++), while alternating between nuclear and cytoplasmic compartments in Control-2 (++/+++) and appearing exclusively in the cytoplasm in Control-3 (+). Apaf1-signal was most prominent as a radiating pattern from the superficial cortical layers and choroid plexus-adjoining regions in Control-2, and as a multifocal to coalescing immunoreactivity of endothelial cells and meninges (+++) in Control-3. No Apaf1 signal was observed in Control-1.

Table 2. Summary of qualitative immunohistochemical assessment of the neocortices and cerebella of the two tested puppies. Immunoreactivity with **—/+**: very light; **+**: light; **++**: moderate and **+++**: strong intensity. **-**: no immunoreactivity. PMI: post-mortem interval. WM: white matter.

Antibody	Puppy	Puppy-1			Puppy-2		
	PMI	24 h			20 min		
	Cell Type	Neurons	Glia	Meninges/ Endothelia	Neurons	Glia	Meninges/ Endothelia
APP	Cortex	+++ Synaptic membranes Diffuse	++ Light background + Multifocal coalescing axons in WM	-	++ Synaptic membranes in sulci	+ Light background	-
	Cerebellum	++ Cytoplasmic	+ Light background	-	+++ Cytoplasmic	++ Light-moderate background	-
Bcl-2	Cortex	+++ Cytoplasmic Multifocal in gyri	+/++ Granular Diffuse	+++ Leptomeninx Multifocal ++ Cytoplasmic, choroid plexus endothelia Diffuse	-	+ Granular Diffuse, mild pericapillary emphasis	++ Leptomeninx Few foci
	Cerebellum	++ Cytoplasmic Multifocal in gyri	-	-	—/+ very light cytoplasm, Single foci	-	-
DGK-ζ	Cortex	+ Cytoplasmic Diffuse	+ Light background ++ Astrocyte cytoplasm Multifocal	+ Leptomeninx Multifocal	+++ Cytoplasmic Diffuse	++ Moderate background +++ Astrocyte nuclear Multifocal	+++ Endothelia Diffuse
	Cerebellum	++/+++ Cytoplasmic Diffuse, with multifocal shrunken, deformed cells	+	—/+ Leptomeninx Single foci	+++ Cytoplasmic, Diffuse; Nuclear, Multifocal	—/+	++ Endothelial Multifocal
Apaf1	Cortex	-	+++ Cytoplasmic and nuclear Multifocal in WM	+++ Leptomeninx Multifocal	-	-	++ Small/mid-caliber vessels Multifocal
	Cerebellum	- Cytoplasmic +++ Diffuse in molecular layer axons	+ Light background	+++ Leptomeninx Diffuse	++ cytoplasmic Multifocal in gyri ++/+++ Multifocal-coalescing in sulci	+ Light background	+/++ Leptomeninx Multifocal-coalescing

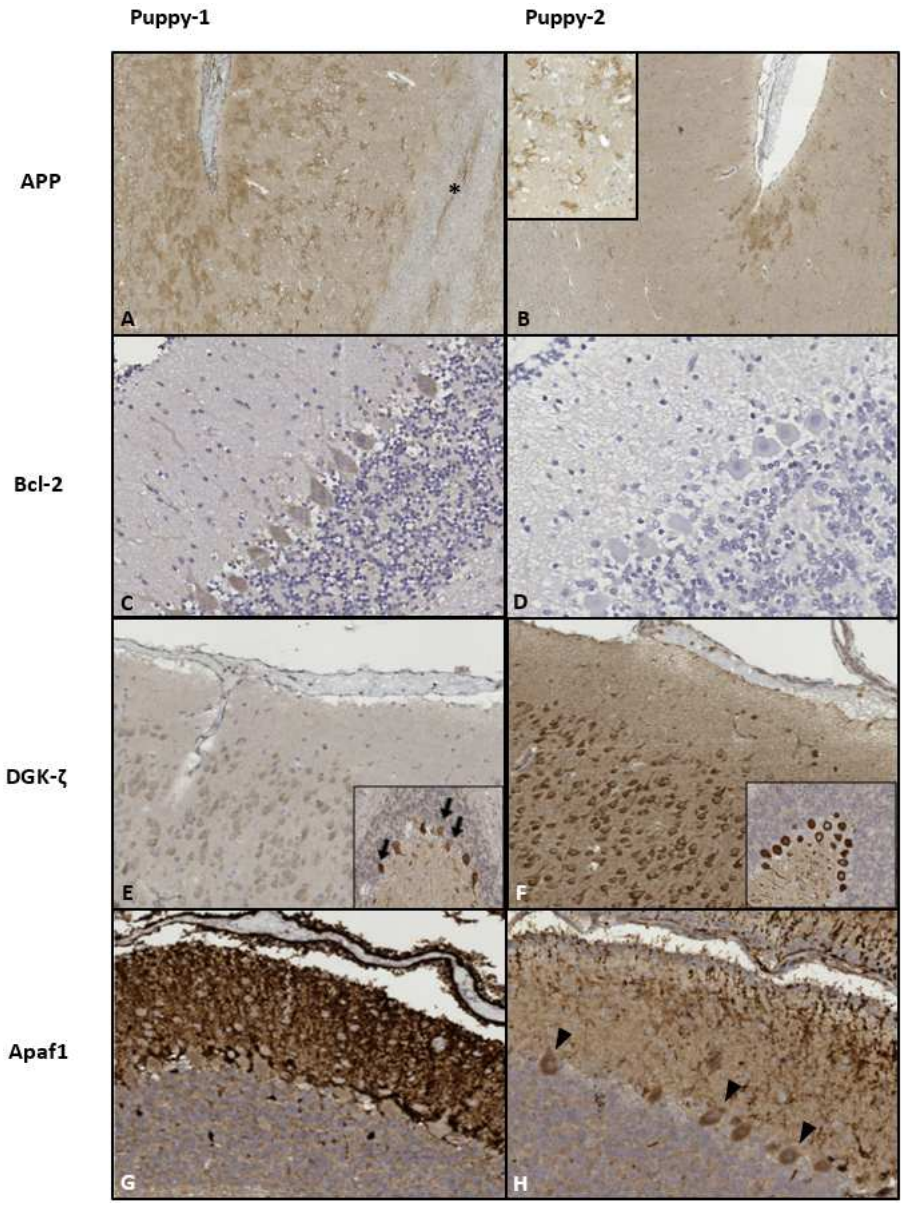

Figure 1. Immunohistochemicalpatterns of the implemented protein markers. (**A**,**B**): Neocortex. β-amyloid precursor protein/APP localized to neuronal synaptic membranes, multifocally enhanced against a light background in the superficial cortical layers. Intense staining was diffuse in Puppy-1, with affected white matteraxons (*). In Puppy-2, strong intensity was limited to the sulci; magnification ×50. Inset in (**B**) (×200): detail of arborized synaptic pattern. (**C**–**H**): apoptotic markers. (**C**,**D**): Moderate diffuse Purkinje cell cytoplasmic B-cell lymphoma related protein 2/Bcl-2-signal (with slight emphasis on gyral crowns; not shown) in Puppy-1 vs. predominantly negative cerebellum in Puppy-2. Magnification ×400. (**E**,**F**): Neocortex: "faded" appearance in Puppy-1 vs. strong cytoplasmic diacylglycerolkinase-ζ/DGK-ζ-signal in neurons and neuropil in Puppy-2; magnification ×100. Insets depict the puppies' cerebella, whereby Puppy-1 displays more neuronal loss (arrows). In both animals, immunoreactivity was more pronounced in the gyral crowns, as opposed to the sulci (not shown). (**G**): Cerebellum of Puppy-1 shows intense and diffuse, predominantly axonal apoptotic protease activating factor 1/Apaf1 immunoreactivity in the molecular layer of cerebellar folia, while in Puppy-2, intensity is moderate and the pattern is multifocal to coalescing (**H**). The neuronal cytoplasm is negative in Puppy-1, yet there are multiple gyral foci of moderate immunoreactivity in Puppy-2 (arrowheads in (**H**)); Magnification ×200.

4. Discussion

Despite few macroscopic changes, histopathology revealed that the puppies were compromised under several aspects. Severe intestinal parasitic infection could have led to deficits in energy uptake and protein absorption in a challenging period such as weaning, inflicting initial damage to a physiologically immature liver [8]. Large breeds are more resistant to hypoglycemia than toy breeds [9], yet all dehydrated and anorectic puppies <4 months of age are highly susceptible [10]. While steatosis is a common finding in sudden pediatric death, it is not usually the sole cause [11]. Acute liver failure leads to hepatic encephalopathy displaying corticocerebral necrosis, edema and meningitis [12]. Due to the severity of parasitic infestation, additional complications of deworming, i.e., systemic resorption of parasitic endotoxin-like substances not only could have damaged the liver, but directly lead to a hypersensitivity reaction with symptoms similar to those of septic shock [13]. Systemic edema may have resulted from this, contributing to hypo-oxygenation of blood in the lungs. Mild to moderate interstitial pneumonia, subsequent to helminthic larval migration, likely impeded gas exchange further. In this case, evidence is insufficient to establish direct nematode-induced neurotoxicity.

Lesions caused by hypoxia were evident in the brains of both Australian Shepherd puppies. Cerebellar Purkinje cells are notoriously sensitive to acute hypoxic stress [14], and their degeneration may have explained some of the motor control deficits. Furthermore, IHC of the brains allowed a detailed look into the phase of neuronal degeneration, and a comparison with available controls without neurological findings.

APP is a synaptic membrane protein that plays a role in various physiological functions like axonal outgrowth and neuronal adhesion. It is expected in moderate concentrations in the developing brain [15]. Under pathological conditions like traumatic [16] and hypoxic-ischemic brain injury [5], APP may accumulate in damaged axons within minutes after exposure to the stressor [17]. No trauma pre-existed in this case. Therefore, we could reasonably state that the strong immunoreactivity of the dendritic synapses indicates acute hypoxic damage of cortical neurons and their axons in the WM. A more widespread distribution of the immunoreactivity in Puppy-1 suggests a more severe progression of the hypoxic-ischemic injury that led to its earlier death. Non-neurological controls presented overall lighter immunoreactivity, consistent with Control-1 experiencing the shortest duration of hypoxia coinciding with a short agonal period, comparing with Control-2 and -3 puppies that presented evidence of lung atelectasis, and therefore a longer ante-mortem hypoxic condition. Despite this, Controls-2 and -3 had a lighter and mostly background or vascular APP reactivity, and so differed to the stronger background and more pronounced synaptic and axonal reactivity of Puppy-1 and -2, implying that seizures induce a stronger degenerative and apoptotic stimulus in an acute timeframe compared to predominantly hypoxic conditions.

The DGK-ζ isoform physiologically localizes in the nucleus of neurons, but has been shown to acutely and irreversibly translocate into the cytoplasm of hippocampal neurons following ischemic injury, before gradually disappearing [18]. Its absence putatively indicates a "point-of-no-return", anticipating apoptosis [19]. The intense immunoreactivity of the neuronal cytoplasm in Puppy-2 could match the acute respiratory distress leading to hypoxia and death, as mirrored by Control-2 and to a lesser extent, Control-1, while the faded appearance of Puppy-1's cortex may reflect a later phase of widespread neurodegeneration incompatible with life. Furthermore, Control-1 displayed exclusively intranuclear neuronal DGK-ζ, implying a largely physiological neurochemical profile affected mildly by the agonal process.

Bcl-2 is an anti-apoptotic protein [20], yet according to Shinoura and colleagues [21], it can be pro-apoptotic in higher concentrations. Its multifocal appearance in Puppy-1's neuronal cytoplasm in the context of a lack of nuclear DGK-ζ -expression and overlapping with Apaf1-immunoreactive neurons of the gyri could therefore imply a pro-apoptotic or ineffective compensatory mechanism preceding widespread neuronal apoptosis. Lack of Bcl-2-immunoreactivity in Puppy-2's neurons could suggest the predominance of acute,

pro-apoptotic mechanisms, with a milder expression in astrocytes highlighting their greater resilience to hypoxia compared to neurons. Controls were mostly negative apart from the focal mild granular neuropil reactivity in Control-1 (displaying similarity to Puppy-2), thereby implying that Bcl-2 protein upregulation as visualized by the herein employed IHC-antibody is detectable in animals that experienced a comparatively stronger apoptotic stimulus surpassing that expected during acute agonal hypoxia, such as in the seizuring Puppy-1.

Apaf1 reflects intrinsic apoptosis upstream of executioner caspase-activating caspase 9 [22]. Multifocal to coalescing axonal and WM-glial immunoreactivity in Puppy-1 may therefore indicate an advanced stage of neurodegeneration, since glia generally succumb to hypoxia later than neurons [23]. A similar pattern was observed in the Control-2 and -3 puppies, with Control-2 presenting the most disseminated axonal granular immunoreactivity, and an additional multifocal to coalescing endothelial signal, potentially indicative of vascoconstriction-induced apoptosis [24]. It represents evidence that early apoptotic mechanisms, next to acute necrosis observed in the hematoxylin-eosin sections, played a role in the neuronal degeneration of both the control and the Australian Shepherd puppies, but not in the adult Control-1.

Relevant IHC-findings in Puppy-1 include widespread APP-, faded DGK-ζ- and multifocal Bcl-2-immunoreactivity in cortical neurons simultaneous to necrotic shrinkage, diffuse cerebellar early-apoptotic Apaf1-reactivity and severe necrosis as evidenced by complete multifocal disintegration of Purkinje-neurons. This pattern matches advanced necrotic and progressive apoptotic changes. Puppy-2's central nervous system rather reflects acute necrosis and pre- to early apoptosis with intense cortical DGK-ζ-, multifocal cerebellar Apaf1- and lack of Bcl-2-expression, and multifocally shrunken, but mostly intact neurons. Though apoptosis is more prominent in immature brains if compared to adults [25], necrotic emphasis putatively indicates more severe hypoxic-ischemic insults, with delayed apoptosis, by itself, associated with milder damage [26]. Thus, Puppy-1 conceivably experienced more severe and longer-lasting brain injury than Puppy-2. Compared with available control puppies with evidence of severe ante-mortem hypoxia, the findings in Puppy-1 in particular, and Puppy-2 to a lesser extent, indicate that a slightly different, or stronger noxious stimulus led to the neurochemical imbalance visualized by the employed IHC markers in the Australian Shepherd siblings. The hepatoencephalic toxicity exacerbated by parasitic die-off induced by macrocyclic lactone administration could have represented such a stimulus. The stronger differences between all the puppies and the adult Control-1 with no neuropathological findings, especially in the case of the intranuclear vs cytoplasmic DGK-ζ distribution and intensity, and the low APP and lack of Bcl-2 and Apaf1 signal, appear to underline this.

Single reports describe dogs with heterozygous *MDR1*-gene mutations responding to macrocyclic lactones with mild depression and ataxia, or more severe, transient (<48 h) neurotoxicosis preceding full recovery [27]. Furthermore, milbemycin oxime at dosages < 2.5 mg/kg is postulated as a safe macrocyclic lactone, even in sensitive dogs [28]. Compromised by dyspnea and an injured liver, however, even a mildly reduced function of the blood-brain-barrier P-gp channel protein, responsible for the efflux of macrocyclic lactones from the brain cells to prevent neurotoxicity [29,30], may have contributed to the faster progression of brain injury and earlier death in Puppy-1. Atelectasis and severe perivascular edema probably triggered the terminal respiratory distress in Puppy-2, resulting in more acute hypoxia-induced necrosis and apoptosis.

Puppy-4, also being a heterozygous *MDR1* mutant, responded well to the supportive care. Meanwhile, *MDR1*-wild-type Puppy-3 suffered further seizures but responded well to diazepam, unlike dogs with moxidectin toxicity [31]. These facts underline the significant contribution of severe metabolic imbalance and parasite-associated dyspnea to the two fatalities.

This study is based on diagnostic cases, and therefore contains inevitable limitations. In particular, the selection of control animals without neurological changes is problematic,

thus our knowledge on a healthy profile for the dog brain is limited. Ideally, controls would be healthy experimental, age-, sex-, and breed-matched dogs that had little to no hypoxic changes within the brain tissues at the time of death. In reality, every animal, whether dying of natural causes or euthanasia, experiences some extent of agonal hypoxia [32], therefore some overlap between the results of Puppies-1 and -2 and the controls is not surprising. In our case, the controls had to be selected from archived tissues from animals submitted to the University Veterinary Necropsy Service, thus limiting the possibility of an age-matched control without respiratory distress. Controls-2 and -3 were more appropriate in age, but some vascular changes were noticed. Therefore, they could only serve as a preliminary comparison for the confounder of a longer PMI.

In this respect, consistency between clinical state and IHC findings, as well as similar IHC-patterns seen in animals with a PMI of up to about 72 h, render it unlikely that the longer post-mortem interval of Puppy-1 significantly compromised IHC results. The robustness of some protein markers in human post-mortem neuronal tissue is postulated to be conserved at a PMI of up to 50 h, though this varies by marker [33]. Changes in Bcl-2-expression have previously been suggested as reliable markers correlating negatively to increasing PMI [34], yet in our case, Puppy-2 with the shortest PMI of 20 min displayed the least Bcl-2-expression, while dogs with a PMI of 24 h (Puppy- and Control-1) yielded a slightly stronger IHC signal. Thus, further research employing a larger number of experimental animals is required before asserting a reliable PMI threshold for IHC evaluation in canines. Nevertheless, results obtained in the context of this diagnostic case suggest that above-mentioned IHC markers could merit systematic validation using orthogonal proteomic methods such as Western blot [35].

5. Conclusions

Considered together, the anamnestic, clinical, histological and immunohistochemical findings point to a multifactorial hypoxic syndrome as the cause of acute neuronal degeneration, contributing significantly to the disruption of vital functions and resulting in the puppies' deaths. Direct drug toxicity is unlikely but cannot be excluded, since single-gene approaches to pharmacogenetics leave considerable individual variation to be explored with pharmacogenomics [36]. The recovery of 6/8 littermates with supportive care emphasizes the greater likelihood of a metabolic imbalance and liver damage exacerbated by parasitic die-off. Evaluation of IHC markers in the context of the case helped interpret severity and pathogenesis of brain lesions before morphological changes became evident, implying that while general neurodegenerative and apoptotic processes are common, the nature of the noxious stimulus may allow neurochemical differentiation between agonal or perinatal hypoxia and seizures owing to (e.g., hepatoencephalic) toxicity. To our knowledge, this is the first report of nucleocytoplasmic translocation of DGK-ζ in cortical neurons. While results are preliminary and the influence of PMI on protein expression needs further research, they demonstrate that appropriate validation of IHC-markers holds great potential as an ancillary forensic tool for patients presenting neurological deficits without a clear etiology.

Supplementary Materials: The following are available online at https://www.mdpi.com/article/10.3390/vetsci8100203/s1, Table S1: Case summary for the two Australian Shepherd puppies that died following Milprovet® administration, Video S1: Neurological symptoms of Puppy-1 (~12 h after Milprovet® administration), Video S2: Neurological symptoms of Puppy-1 (~14 h after Milprovet® administration). The videos show Puppy-1 is displaying apathy, ataxia, tremors, incoordination and dyspnea that all got progressively worse over a period of several hours prior to a comatose state followed by death.

Author Contributions: Conceptualization, S.M.; methodology, K.O., S.M., B.S., M.B., F.B. and C.C.; writing—original draft preparation, K.O.; writing—review and editing, S.M., B.S., M.B., F.B., R.V., C.C. and R.V.; supervision, S.M. and C.C. All authors have read and agreed to the published version of the manuscript.

Funding: This research received no external funding.

Institutional Review Board Statement: Ethical review and approval were waived in this study, since it does not involve the use of experimental animals, only archived tissues of diagnostic cases.

Informed Consent Statement: Informed consent for the use of sampled tissues for research purposes was obtained from all the dog owners involved in the study, upon submitting the dog carcasses to the facilities of the Veterinary Necropsy Service of the Department of Comparative Biomedicine and Food Science of the University of Padova.

Acknowledgments: The authors would like to thank the laboratory technicians Rossella Zanetti and Davide Trez for their practical support for the immunohistochemistry.

Conflicts of Interest: The authors declare no conflict of interest.

References

1. Idowu, O.; Heading, K. Hypoglycemia in dogs: Causes, management, and diagnosis. *Can. Vet. J.* **2018**, *59*, 642.
2. Grijalva, J.; Vakili, K. Seminars in Pediatric Surgery Neonatal liver physiology. *Semin. Pediatr. Surg.* **2013**, *22*, 185–189. [CrossRef]
3. Mealey, K.L.; Meurs, K.M. Breed distribution of the ABCB1-1Δ (multidrug sensitivity) polymorphism among dogs undergoing ABCB1 genotyping. *J. Am. Vet. Med. Assoc.* **2008**, *233*, 921–924. [CrossRef]
4. Oechmichen, M.; Meissner, C. Cerebral Hypoxia and Ischemia: The Forensic Point of View: A Review. *J. Forensic Sci.* **2006**, *51*, 880–887. [CrossRef]
5. Rahaman, P.; Del Bigio, M.R. Histology of Brain Trauma and Hypoxia-Ischemia. *Acad. Forensic Pathol.* **2018**, *8*, 539–554. [CrossRef] [PubMed]
6. Mazzariol, S.; Centelleghe, C.; Petrella, A.; Marcer, F.; Beverelli, M.; Di Francesco, C.E.; Di Francesco, G.; Di Renzo, L.; Di Guardo, G.; Audino, T.; et al. Atypical Toxoplasmosis in a Mediterranean Monk Seal (Monachus monachus) Pup. *J. Comput. Pathol.* **2021**, *184*, 65–71. [CrossRef] [PubMed]
7. Klintzsch, S.; Meerkamp, K.; Döring, B.; Geyer, J. Detection of the nt230 [del4] MDR1 mutation in dogs by a fluorogenic 5′ nuclease TaqMan allelic discrimination method. *Vet. J.* **2010**, *185*, 272–277. [CrossRef] [PubMed]
8. Hoskins, J.D. The Liver and Pancreas. In *Veterinary Pediatrics: Dogs and Cats from Birth to Six Months*, 2nd ed.; Hoskins, J.D., Ed.; WB Saunders: Philadelphia, PA, USA, 1995; pp. 200–224. [CrossRef]
9. de Bruijne, J.J.; Altszuler, N.; Hampshire, J.; Visser, T.J.; Hackeng, W.H.L. Fat mobilization and plasma hormone levels in fasted dogs. *Metabolism* **1981**, *30*, 190–194. [CrossRef]
10. Okkens, A.C. Canine pediatrics. *Vet. Q.* **1994**, *16*, 19–20. [CrossRef]
11. Milroy, C.M. Fatty Liver and the Forensic Pathologist. *Acad. Forensic Pathol.* **2018**, *8*, 296–310. [CrossRef] [PubMed]
12. Van der Linde-Sipman, J.S.; van den Ingh, T.V.D.; van Toor, A.J. Fatty Liver Syndome in Puppies. *J. Am. Anim. Hosp. Assoc.* **1990**, *26*, 9–12.
13. Van Amersfoort, E.S.; Van Berkel, T.J.C.; Kuiper, J. Receptors, Mediators, and Mechanisms Involved in Bacterial Sepsis and Septic Shock. *Clin. Microbiol. Rev.* **2003**, *16*, 379–414. [CrossRef]
14. Hausmann, R.; Seidl, S.; Betz, P. Hypoxic changes in Purkinje cells of the human cerebellum. *Int. J. Leg. Med.* **2007**, *121*, 175–183. [CrossRef] [PubMed]
15. Plummer, S.; Van Den Heuvel, C.; Thornton, E.; Corrigan, F.; Cappai, R. The neuroprotective properties of the amyloid precursor protein following traumatic brain injury. *Aging Dis.* **2016**, *7*, 163–179. [CrossRef]
16. Reichard, R.R.; Smith, C.; Graham, D.I. The significance of APP immunoreactivity in forensic practice. *Neuropathol. Appl. Neurobiol.* **2005**, *31*, 304–313. [CrossRef] [PubMed]
17. Morrison, C.; Mackenzie, J.M. Axonal injury in head injuries with very short survival times. *Neuropathol. Appl. Neurobiol.* **2008**, *34*, 124–125. [CrossRef]
18. Ali, H.; Nakano, T.; Saino-Saito, S.; Hozumi, Y.; Katagiri, Y.; Kamii, H.; Sato, S.; Kayama, T.; Kondo, H.; Goto, K. Selective translocation of diacylglycerol kinase ζ in hippocampal neurons under transient forebrain ischemia. *Neurosci. Lett.* **2004**, *372*, 190–195. [CrossRef] [PubMed]
19. Goto, K.; Tanaka, T.; Nakano, T.; Okada, M.; Hozumi, Y.; Topham, M.K.; Martelli, A.M. DGKζ under stress conditions: "To be nuclear or cytoplasmic, that is the question". *Adv. Biol. Regul.* **2014**, *54*, 242–253. [CrossRef] [PubMed]
20. Siddiqui, W.A.; Ahad, A.; Ahsan, H. The mystery of BCL-2 family: Bcl-2 proteins and apoptosis: An update. *Arch. Toxicol.* **2015**, *89*, 289–317. [CrossRef]
21. Shinoura, N.; Yoshida, Y.; Nishimura, M.; Muramatsu, Y.; Asai, A.; Kirino, T.; Hamada, H. Expression level of Bcl-2 determines anti- or proapoptotic function. *Cancer Res.* **1999**, *59*, 4119–4128.
22. Mishra, O.P.; Delivoria-Papadopoulos, M. Mechanism of Tyrosine Phosphorylation of procaspase-9 and Apaf1 in Cytosolic Fractions of the Cerebral Cortex of Newborn Piglets during Hypoxia. *Neurosci. Lett.* **2010**, *480*, 35–39. [CrossRef] [PubMed]
23. Zachary, J. The Nervous System. In *Pathologic Basis of Veterinary Disease*, 4th ed.; McGavin, M.D., Zachary, J., Eds.; Elsevier Limited: St. Louis, MO, USA, 2007.

24. Intengan, H.D.; Schiffrin, E.L. Vascular remodeling in hypertension: Roles of apoptosis, inflammation, and fibrosis. *Hypertension* **2001**, *38*, 581–587. [CrossRef] [PubMed]
25. Zhu, C.; Wang, X.; Xu, F.; Bahr, B.A.; Shibata, M.; Uchiyama, Y.; Hagberg, H.; Blomgren, K. The influence of age on apoptotic and other mechanisms of cell death after cerebral hypoxia-ischemia. *Cell Death Differ.* **2005**, *12*, 162–176. [CrossRef]
26. Stroemer, R.P.; Rothwell, N.J. Exacerbation of Ischemic Brain Damage by Localized Striatal Injection of Interleukin-1β in the Rat. *J. Cereb. Blood Flow Metabolism.* **1998**, *18*, 833–839. [CrossRef] [PubMed]
27. Geyer, J.; Janko, C. Treatment of MDR1 Mutant Dogs with Macrocyclic Lactones. *Curr. Pharm. Biotechnol.* **2012**, *13*, 969–986. [CrossRef] [PubMed]
28. Tranquilli, W.J.; Paul, A.J.; Todd, K.S. Assessment of toxicosis induced by high-dose administration of milbemycin oxime in Collies. *Am. J. Vet. Res.* **1991**, *52*, 1170–1172.
29. Noack, S.; Harrington, J.; Carithers, D.S.; Kaminsky, R.; Selzer, P.M. Heartworm disease–Overview, intervention, and industry perspective. *Int. J. Parasitol. Drugs Drug Resistance.* **2021**. [CrossRef]
30. Merola, V.M.; Eubig, P.A. Toxicology of avermectins and milbemycins (macrocyclic lactones) and the role of P-glycoprotein in dogs and cats. *Vet. Clin. Small Anim. Pract.* **2018**, *48*, 991–1012. [CrossRef]
31. Snowden, N.J.; Helyar, C.V.; Platt, S.R.; Penderis, J. Clinical presentation and management of moxidectin toxicity in two dogs. *J. Small Anim. Pract.* **2006**, *47*, 620–624. [CrossRef]
32. Parish, D.C.; Goyal, H.; Dane, F.C. Mechanism of death: There's more to it than sudden cardiac arrest. *J. Thorac. Dis.* **2018**, *10*, 3081. [CrossRef] [PubMed]
33. Blair, J.A.; Wang, C.; Hernandez, D.; Siedlak, S.L.; Rodgers, M.S.; Achar, R.K.; Fahmy, L.M.; Torres, S.L.; Petersen, R.B.; Zhu, X.; et al. Individual case analysis of postmortem interval time on brain tissue preservation. *PLoS ONE* **2016**, *11*, e015161.
34. Mohamed, A.A.R.; Elbohi, K.M.; El Sharkawy, N.I.; Hassan, M.A. Biochemical and apoptotic biomarkers of experimentally induced traumatic brain injury: In relation to time since death. *Beni-Suef Univ. J. Basic Appl. Sci.* **2018**. Available online: https://www.sciencedirect.com/science/article/pii/S2314853517301579 (accessed on 8 September 2021). [CrossRef]
35. Ramos-Vara, J.A.; Kiupel, M.; Baszler, T.; Bliven, L.; Brodersen, B.; Chelack, B.; Czub, S.; Del Piero, F.; Dial, S.; Ehrhart, E.J.; et al. Suggested guidelines for immunohistochemical techniques in veterinary diagnostic laboratories. *J. Vet. Diagn. Investig.* **2008**, *20*, 393–413. [CrossRef] [PubMed]
36. Mealey, K.L.; Martinez, S.E.; Villarino, N.F.; Court, M.H. Personalized medicine: Going to the dogs? *Hum. Genet.* **2019**, *138*, 467–481. [CrossRef] [PubMed]

Methodology of Working with Cetacean Tissues

Auditory Pathway Sampling Protocol

To assess the histopathology and immunohistochemical expression of the above, and further, protein markers within the auditory pathways of the cetacean brain, we selected one of the most studied odontocetes species—bottlenose dolphin—and elaborated a sampling protocol encompassing representative areas from the auditory nerve, brainstem, midbrain, and neocortex.

AUDITORY PATHWAY SAMPLING PROTOCOL

Introduction

The brain is an important organ to assess in stranded cetaceans. It may reflect pathological processes owing to infectious or degenerative processes, as well as anthropogenic pressures, such as underwater noise. Using immunohistochemistry and molecular methods, we are attempting to build a baseline for the expression of proteins involved in apoptotic, inflammatory and vascular changes. For this, brains of very fresh cetaceans with a **decomposition code** (DCC) of **1** and **2** are necessary.

Particular targets are *Tursiops truncatus* and *Phocoena phocoena* specimens. To obtain the highest probability of observing potential pathology associated with underwater anthropogenic noise exposure, we are focusing on structures of the auditory brain stem and mid-brain.

The samples of the brain's right side should be placed in 10% neutral-buffered formalin with a **tissue to fixative** ratio of at least **1:10**. The samples of the brain's left side should be frozen. Liquid nitrogen would be the golden standard for freezing, followed by dry ice, and finally "traditional" freezing to at least -20 °C. We believe that any of these methods should be sufficient for the purposes of our study, but would encourage you to use the highest quality freezing method available to you.

Please fill out the checklist of necessary samples below, adding any relevant comments below:

Structure	**Left side – Frozen (≤ -20° Celsius)**	**Right side – Formalin-fixed (10% neutral buffered)**	**Label acronym after: Animal ID, DCC, date, stranding location**
Auditory Nerve	*		L/R AN (distal/proximal)
Cochlear nuclei	*		L/R CN
Inferior colliculi	*		L/R IC
Comments:			

*If RNA*later*® or a comparable fixative for mRNA/DNA is available to you, please contact us and consider the *Addendum* below.

Where to send the samples:

Please call us as soon as there is a sampling candidate:
Ksenia Orekhova: **+39 351 9667099** / Dr. Sandro Mazzariol: **+39 347 5705311**.

Please send frozen samples on dry ice, and the formalin samples in leak-proof containers, via **DHL** at the earliest opportunity to:

Ksenia Orekhova, DVM
Laboratorio di Anatomia Patologica, Edificio 'Museo'
Università di Padova - Campus di Agripolis
Viale dell'Università, 16, 35020 Legnaro PD

If you have any further questions or concerns, please feel free to contact me via call or email: **ksenia.orekhova@phd.unipd.it**

THANK YOU FOR YOUR COOPERATION ☺

SAMPLING:

1. Carefully extract the brain, trying to leave the cranial nerves attached as long as possible. Please refer to the attached "Brain sampling protocol" by Jean-Marie Graïc, Cinzia Centelleghe and Bruno Cozzi. Please record the weight of the fresh brain.
2. **COCHLEAR/VIII CRANIAL NERVE**
   - Place the brain with the ventral side facing you (Fig.1)
   - Using flat-tipped forceps and a scalpel, carefully detach the meninges in order to obtain a clear view of the brain stem (Fig.2).

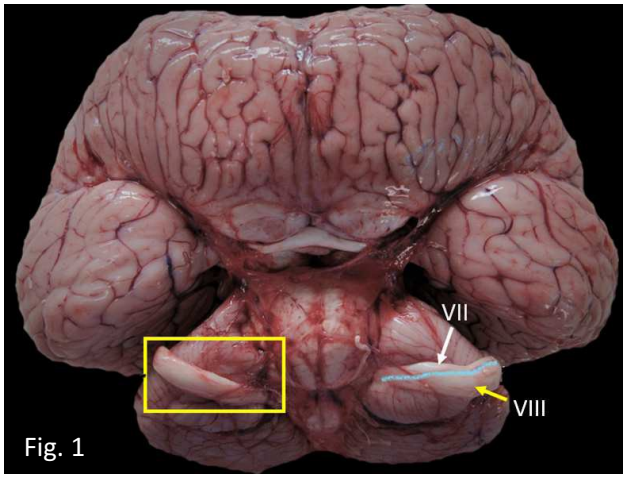

Fig. 1


Fig. 2

- Once the vestibulocochlear nerve and the cerebellopontine angle are clearly visible, make a transverse cut to separate the distal 3 cm of the right cochlear nerve. The smaller, facial (VII) nerve is normally adhered to the cochlear nerve. Leave the distal end of the facial nerve longer for later orientation. Alternatively, place the fresh nerve on a piece of cardboard, writing a D (for distal) and a P (for proximal) next to the respective ends (Fig.4). After ~30 seconds, place the cardboard with the adhered nerve in 10% neutral-buffered formalin.

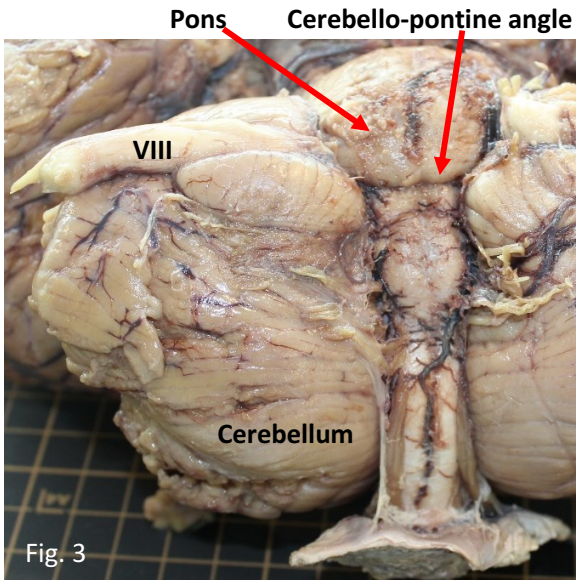

Fig. 3

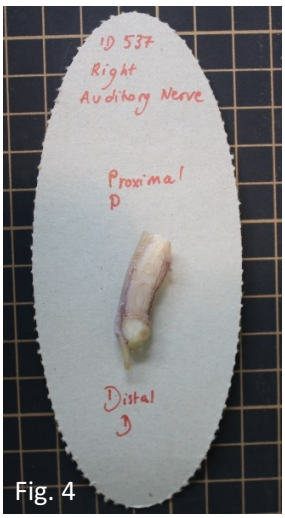

Fig. 4

- Repeat the procedure for the left cochlear nerve. This time, detach the thinner facial from the thicker cochlear nerve, and place only the cochlear nerve into a container for freezing.

3. COCHLEAR NUCLEI

- Orienting yourself by the insertion of the cochlear nerves into the brain stem, make incisions of ~3 cm depth 2 cm rostral to the cerebellopontine angle, 1 cm caudal to it, and encompassing the stumps of the cochlear nerves laterally (Fig. 5).
- Carefully cut through the deep end of the tissue block at the height of the **4th ventricle**, and lever out the tissue block, gently holding it with your fingers (Fig. 6, 7).


Fig. 5

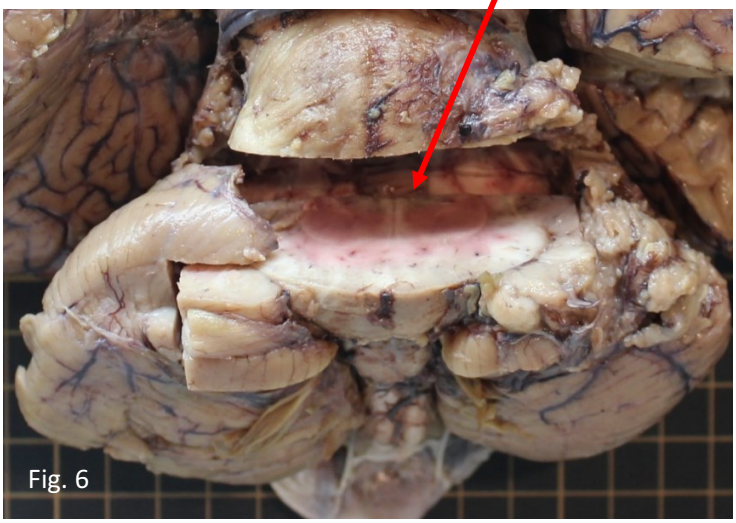
Fig. 6

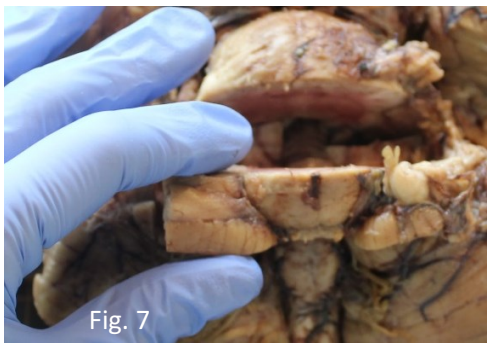
Fig. 7

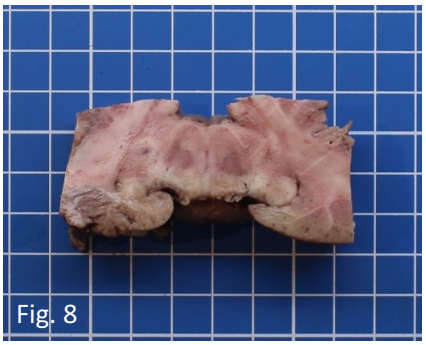
Fig. 8

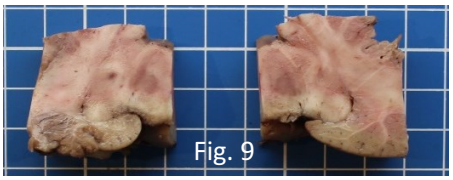
Fig. 9

- Placing the tissue block with the caudal aspect facing you (Fig. 8), make a clean cut down the midline (Fig. 9). Place the right cochlear nucleus in 10% neutral-buffered formalin. Place the left cochlear nucleus in a container for freezing.

4. INFERIOR COLLICULI:

4a) If your protocols are compatible with detaching the brain stem:

- Make a transverse cut at the rostral border of the inferior colliculi, cleanly detaching the brain stem from the rest of the brain. Placing the brain stem so that the rostral aspect is facing you, make incisions caudal to the caudal border of the inferior colliculus (Fig. 10). The incision should be deep enough to encompass the nucleus of the lateral lemniscus (Fig. 11).
- Place the right inferior colliculus in 10% neutral-buffered formalin. Place the left inferior colliculus in a container for freezing.

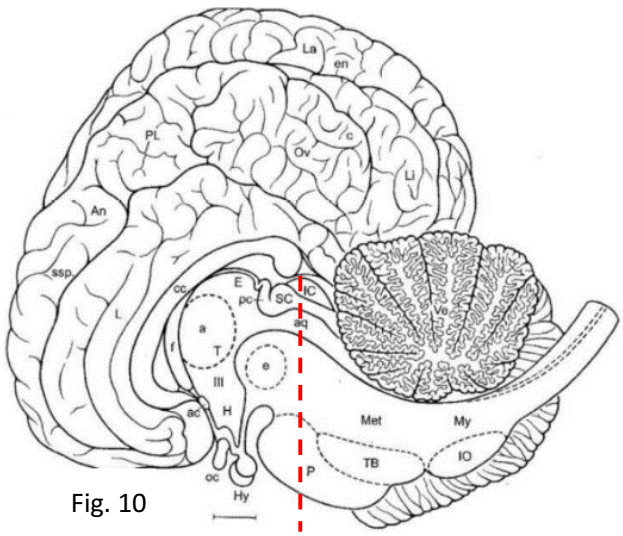

Fig. 10

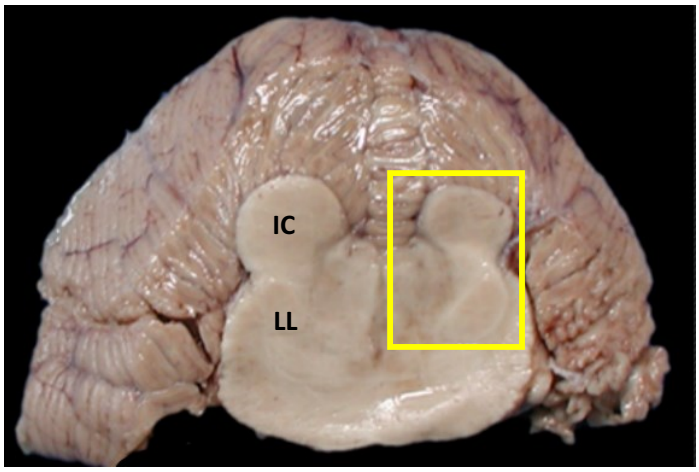

Fig. 11

4b) If you require your brain to remain more intact:

- Place the brain ventral side down and gently hold apart the cerebral hemispheres to visualize the large inferior colliculi (Fig. 12):

Fig. 12

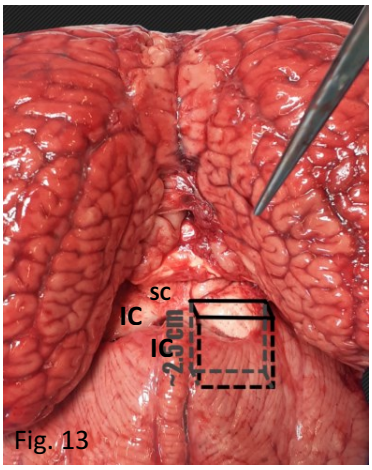

Fig. 13

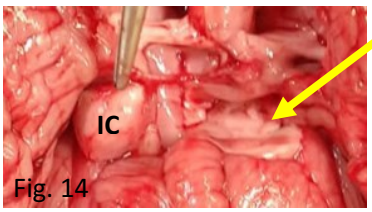

Fig. 14

- Make incisions encompassing the entire colliculus rostrally and caudally, cutting at least 2.5 cm deep (Fig. 13) from the base of the colliculus. From lateral, make the ventral cut and lever out the tissue block, carefully supporting the colliculus with your fingers. It is easier to take out one side at a time (Fig. 14).
- Place the right inferior colliculus in 10% neutral-buffered formalin. Place the left inferior colliculus in a container for freezing.

***ADDENDUM*:**

In case RNA*later*® (Sigma-Aldrich) is available to you, please contact us. In this case, the 3 structures on the **left** side should be sampled fresh, and immersed into the RNA*later*® solution with a **tissue:fixative ratio of at least 1:10** in a leak-free container.

CAVE:

The immersed tissues must remain in the **refrigerator** (2-8° C) for the **first 24 hours**,

then frozen at ≤ 20°C.

Optimization of Immunohistochemical Protocols

Following the initial acquisition of cetacean samples, we optimized the immunohistochemical protocols by selecting adequate positive control tissues for each antibody and making pilot runs with the Ventana Benchmark® semi-automatic immunostaining machine using the decision tree presented in Figure 6.

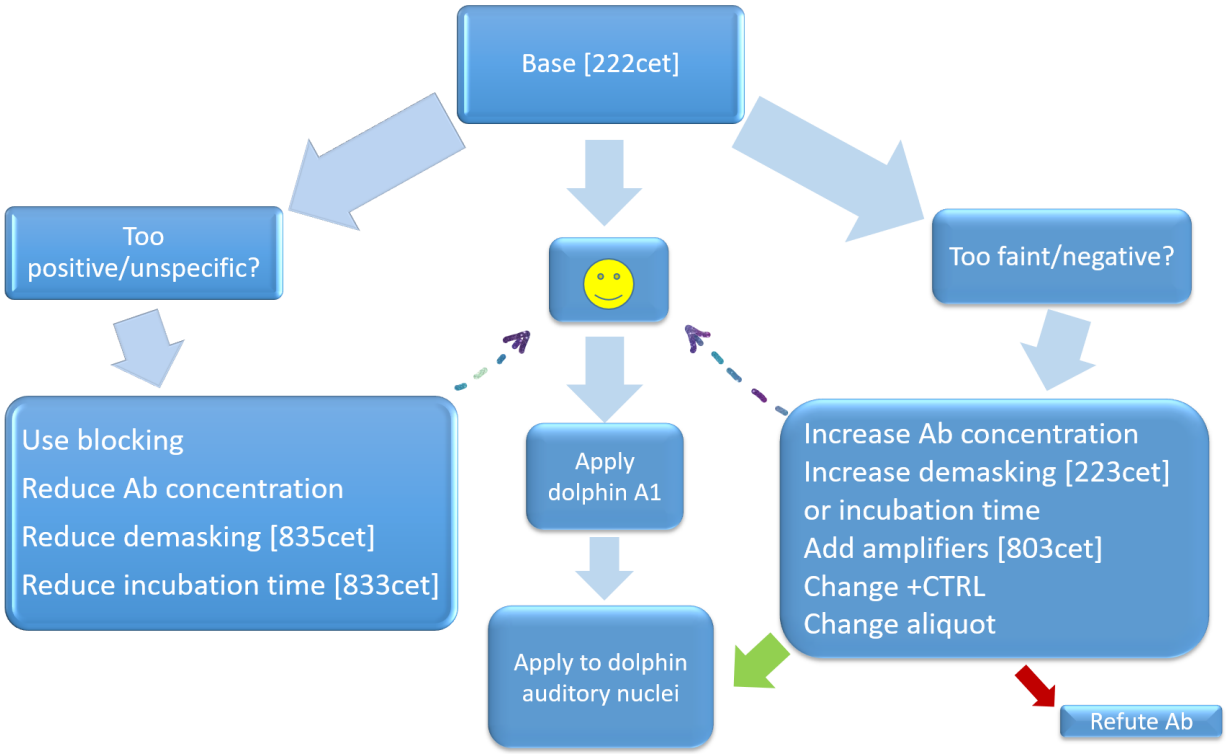

Figure 6. Decision tree for optimizing immunohistochemical results in the pilot runs using positive control tissues for antibodies implemented in the studies presented in this dissertation. Protocols 222cet, 223cet, 803cet, 833cet and 835cet are for internal reference for the Ventana Benchmark® immunostaining machine. A1 refers to the primary auditory cortex tissue of three bottlenose dolphins used in the pilot immunohistochemistry study of the respective antibodies in this species: a calf, a healthy adult, and an adult with presence of brain pathology.

After initial immunohistochemical successes with the antibodies, a validation procedure in bottlenose dolphins was initiated, oriented on the steps summarized by MacNeil and colleagues (2020), visualized in Figure 7. The steps of the most often used protocols, 222cet and 223cet, are attached in Annex I of this dissertation. Results of these preliminary tests are displayed in Annex II.

Steps of antibody validation	Summary	Common pitfalls	Significance
Step 1. Architectural or subcellular localization of expression	Illustration of the expected biologic localization of signal for the target of interest Includes tissue type, histologic subtype, cellular and subcellular compartments	Nonspecific staining patterns due to suboptimal antibody concentration	Provides early proof of antibody specificity Justifies further validation efforts
Step 2. Antibody optimization	Optimization of assay conditions Includes optimization of antigen retrieval buffer, antibody concentration and incubation conditions	Proper assay conditions often not indicated by the vendor	Ensures that all subsequent validation steps will be conducted under optimal assay conditions
Step 3. *Uhlen pillar 2* Orthogonal methods of validation and/or	Utilization of independent methods to prove antibody specificity. Includes western blot, mass spectrometry etc.	Positive band in a western blot for nonspecific antibodies; multiple bands in a western blot for specific antibodies	Provides additional proof of antibody specificity by one or more independent methods
Step 3. *Uhlen pillar 1* Genetic methods of validation and/or	Genetic manipulation of the expression of the target of interest to generate positive and/or negative controls	Overexpression or underexpression of the target of interest in wild-type cell lines	Links the genetic basis of the target of interest with the corresponding protein product
Step 3. *Uhlen pillar 3* Independent epitope validation	Correlation of multiple antibodies with nonoverlapping epitopes for the target of interest	Identification of a second antibody for the target of interest	Provides substantial proof for the specificity of both antibodies
Step 4. Antibody reproducibility	Demonstration of antibody sensitivity and specificity across different runs, operators, manual vs automated staining methods and lots	Inherent heterogeneity of the target of interest; vendor lot variability	Proves that assay is robust and ready to use

Figure 7. Good laboratory practice in the procedure of antibody validation (from MacNeil et al., 2020).

Addenda

Throughout the PhD research, smaller side projects were conducted using the same biomarkers and methodologies as presented in Publications I-III. These results of these side projects are interspersed throughout this dissertation as Addenda, matched thematically to the topics of the publication that precede them. The figures and tables appearing therein are numbered continuously from the introduction.

Publication II: Systematic Validation and Assessment of Immunohistochemical Markers for Central Nervous System Pathology in Cetaceans, with Emphasis on Auditory Pathways

Cetacean neuroanatomy has long occupied scientific attention as an example of unusual convergent evolution with non-human primates, but many aspects of its varied pathology lack systematic scrutiny. Neurodegenerative, infectious, and traumatic processes are known to affect the cetacean brain, leading to increased risk of stranding. While some of them cause characteristic lesions, such as *Cetacean morbillivirus*, more subtle changes potentially occurring following biotoxin, contaminant and noise exposure may not result in clear morphological changes. Immunohistochemical markers that target proteins involved in the homeostasis of neuronal, glial, and vascular integrity can help visualize neurochemical imbalance before the ensuing morphological damage. While several studies have employed these techniques in the past, the approach of systematically validating the antibodies, which are generally repurposed from human and laboratory animal research, is not standard practice.

In this study, we underlined the use of two or more orthogonal techniques—immunohistochemistry, Western blot, and the basic linear alignment search tool—to validate five out of twelve investigated antibodies associated with hypoxic-ischemic, inflammatory, plastic and excitatory-inhibitory changes involved in AOE. The inferior colliculi and ventral cochlear nuclei of 20 Mediterranean bottlenose dolphins were used, which allowed semi-quantitative and preliminary statistical analyses of the observed immunoreactivity.

Biomarkers of apoptosis (Apaf-1, DGK-ζ, Bcl-2), neuroinflammation (Aβ) and cytoskeletal integrity (NF200) displayed specific patterns of immunoreactivity consistent with those reported in other mammals and provided additional diagnostic information on early apoptotic, neurodegenerative, inflammatory, and vascular changes. Apaf-1 was useful in the qualitative assessment of neurochemical dysregulation and was expressed more consistently in adult dolphins with CNS-lesions. DGK-ζ was more often observed in neuronal cytoplasm than in the nucleolus in older animals. The variable immunoreactivity of Aβ requires further investigation regarding its function and reflection of evolutionary adaptations in cetaceans.

These results encourage the integration of the implemented antibodies into a key panel of immunohistochemical biomarkers of pathological processes in the cetacean brain. Therefore, the antibodies tested in this study may support existing diagnostic methods, increasing the transparency, reliability, and comparability in the assessment of cases of neurological diseases and establishing systematic validation as a standard practice in cetacean research.

PLOS ONE

RESEARCH ARTICLE

Systematic validation and assessment of immunohistochemical markers for central nervous system pathology in cetaceans, with emphasis on auditory pathways

Ksenia Orekhova[1]*, Cinzia Centelleghe[1], Giovanni Di Guardo[2], Jean-Marie Graïc[1], Bruno Cozzi[1], Davide Trez[1], Ranieri Verin[1], Sandro Mazzariol[1]

1 Department of Comparative Biomedicine and Food Science, University of Padova, Legnaro, Padova, Italy, **2** Faculty of Veterinary Medicine, University of Teramo, Località Piano d'Accio, Teramo, Italy

* ksenia.orekhova@phd.unipd.it

Citation: Orekhova K, Centelleghe C, Di Guardo G, Graïc J-M, Cozzi B, Trez D, et al. (2022) Systematic validation and assessment of immunohistochemical markers for central nervous system pathology in cetaceans, with emphasis on auditory pathways. PLoS ONE 17(6): e0269090. https://doi.org/10.1371/journal.pone.0269090

Editor: Stephen Raverty, Animal Health Centre, CANADA

Received: March 28, 2022

Accepted: May 14, 2022

Published: June 1, 2022

Data Availability Statement: All relevant data are within the paper and its Supporting information files.

Funding: S.M. ECCE AQUA Project [Ministero dell'Istruzione, dell'Università e della Ricerca, CUP C26C18000030004] The funders had no role in study design, data collection and analysis, decision to publish, or preparation of the manuscript.

Competing interests: The authors have declared that no competing interests exist.

Abstract

Cetacean neuropathology is a developing field that aims to assess structural and neurochemical changes involved in neurodegenerative, infectious and traumatic processes, however markers used previously in cetaceans have rarely undergone systematic validation. This is a prerequisite to investigating the potential damage inflicted on the cetacean auditory system by anthropogenic noise. In order to assess apoptotic, neuroinflammatory and structural aberrations on a protein level, the baseline expression of biomarker proteins has to be characterized, implementing a systematic approach to validate the use of anti-human and anti-laboratory animal antibodies in dolphin tissues. This approach was taken to study 12 different antibodies associated with hypoxic-ischemic, inflammatory, plastic and excitatory-inhibitory changes implicated in acoustic trauma within the ventral cochlear nuclei and inferior colliculi of 20 bottlenose dolphins (*Tursiops truncatus*). Out of the 12 tested antibodies, pro-apoptotic protease factor 1 (Apaf-1), diacylglycerolkinase-ζ (DGK-ζ), B-cell lymphoma related protein 2 (Bcl-2), amyloid-β peptide (Aβ) and neurofilament 200 (NF200) were validated employing Western blot analyses and immunohistochemistry (IHC). The results of the validation process indicate specific patterns of immunoreactivity that are comparable to those reported in other mammals, thus suggesting a key panel of IHC biomarkers of pathological processes in the cetacean brain. As a consequence, the antibodies tested in this study may constitute a valid tool for supporting existing diagnostic methods in neurological diseases. The approach of systematic validation of IHC markers in cetaceans is proposed as a standard practice, in order for results to be transparent, reliable and comparable.

Introduction

The pathogenesis of the most common pathological changes of the central nervous system (CNS) of whales and dolphins lacks systematic characterization. Detailed and complete studies

on protein dynamics describing changes in protein properties as drivers and responses to pathophysiological mechanisms, including changes in subcellular location (e.g. shift from nucleus to cytoplasm), depletion and up- or down-regulation, are often missing. A better understanding of brain pathology holds potential to investigate the causative role of natural threats, such as infectious agents [1] and algal biotoxins [2], but also anthropogenic disturbances including noise [3] and various environmental contaminants [4], particularly after mass stranding events.

The brain is extracted during routine necropsy procedures [5] and sampling from six to eight well defined areas for subsequent microscopic examination in all well-conserved carcasses is strongly recommended [6]. In addition to the above mentioned protocol, the examination of two to three central auditory pathway components using IHC, as proposed for laboratory and terrestrial species [7], could facilitate comparisons between both individuals and species, and visualizing pathological processes before the appearance of morphological lesions could reveal significant changes associated with auditory and non-auditory pathology.

The most common pathological conditions of the CNS often do not produce relevant grossly visible changes, and histopathological examination could reveal different forms of damage including apoptosis [8, 9], inflammation associated to relevant pathogens [1, 10], and neoplasia [11]. These and other changes such as vascular pathology related to free radical accumulation, myelinopathy and synaptic remodeling [12–14] are not pathognomonic of a single cause but they are differentially associated with some of them. Examples include inflammation marked by encephalitis and vasculitis triggered by infections (e.g. DMV [10]), blast or acoustic trauma [15, 16] and neurodegeneration involving deposits of misfolded proteins resulting from biotoxin accumulation (e.g. β-N-methylamino-L-alanine) [4]. By providing stronger evidence for a specific source of damage and anticipating morphological evaluation, IHC allows for a deeper insight into pathological mechanisms and represents considerable support in the microscopic examination of the CNS. IHC markers have previously been assessed in cetacean brains for both homeostatic mechanisms (e.g. calcium-binding proteins [17–19]), as well as neurodegenerative changes, e.g. Aβ [20–23], NFT, TDP-43 [4] and caspases [24]. However, systematic validation involving at least two orthogonal methods and the consistent use of positive control tissues is found in relatively few of those studies [4, 19].

This is particularly relevant for markers of noise exposure, since the auditory sense predominates cetacean perception [25]. In fact, while methods to investigate harmful effects of underwater acoustic sources already exist for the inner ear of cetaceans [3, 26], they are limited by carcass decomposition (i.e. they can be applied only a few hours from the death of the animals) and they may not provide conclusive information on other changes, such as tinnitus and non-auditory CNS pathology.

In the biomedical literature on humans and laboratory animals, numerous selected biomarkers reflect the above-mentioned mechanisms, and have previously proven useful in the assessment of acute to chronic noise-induced pathology in laboratory animals. Inducible nitric oxide synthase (iNOS) and malondialdehyde (MDA) [27] indicate peracute, free radical build-up in perivascular tissues inducing vasoconstriction and ischemia/reperfusion damage [12]. Glutamate decarboxylase^{67} (GAD^{67}) may mark the disequilibrium of excitatory/inhibitory transmission due to build-up of excitotoxic glutamate [28]. Extracellular Aβ-accumulation [29] may exacerbate dysregulation of vascular tone via both vasoconstriction [30] and vasodilation [31], and induce neuroinflammation through interactions with tumor necrosis factor α (TNFα) [16]. Apaf-1 [8], DGK-ζ [9] and Bcl-2 [7] are all involved in programmed cell death as apoptotic and anti-apoptotic signal molecules. NF200 is an integral cytoskeletal protein, and may undergo proteolysis as a consequence of neurodegeneration [32] and focal ischemia [33].

This cycle of deterioration leads to further cell death on one hand [29], but may also contribute to limited tissue repair by reducing the resulting cellular debris. This may enable the formation of new synaptic connections [13], or neuroplasticity, where synaptic sprouting induces an increased expression of growth associated protein 43 (GAP43) [34] and focally decreases synaptophysin expression [27]. Quaking protein-7 (QKI-7) is one of the proteins upregulated during developmental myelination that may be reactivated in the course of a myelinopathy as a form of attempted repair [14]. The effects of these and further changes may compromise tissue function for up to years after their occurrence [35], hence their detection could characterize pathological processes in dolphins, including acoustic trauma.

In order to implement existing protocols [5, 23] by increasing the numbers of systematically validated antibodies, in the present study we tested two crucial central auditory processing centers—the ventral cochlear nuclei (VCN) and inferior colliculi (IC)—of 20 bottlenose dolphins (*Tursiops truncatus*). Thereby, we could integrate the requirements of representative brain sampling with the possibility to detect auditory pathology using structures that are easy to identify and sample. The timing, severity and distribution of the lesions, combined with an investigation of a key panel of biomarkers in the central auditory pathways, may help derive the cause of a pathology that cannot otherwise be ascertained.

The aim of this study is to establish a baseline for comparison in the characterization of cetacean CNS pathology. This could help create an IHC "fingerprint" of specific diseases and, eventually corroborate morphopathological findings associated with noise-related damage.

Materials and methods

Animals and tissue processing

Brain tissues were sampled from 20 bottlenose dolphins archived in the Mediterranean Marine Mammals Tissue Bank of the University of Padova. The brains originated from both stranded and captive cetaceans with a decomposition and conservation code (DCC) of 1 and 2, according to the available guidelines for cetacean *post mortem* investigation [5]. Table 1 summarizes pertinent information on the investigated dolphins, with additional information on their sex, body length, full histopathological findings of the CNS, and the most probable cause of death provided in the supplementary materials. Brains had been extracted within 24 hours after death, cut into 1 cm-thick coronal sections, fixed in 10% neutral-buffered formalin and washed in phosphate buffer (0.1 M, pH: 7.4) prior to paraffin embedding [36, 37]. When available, the right VCN (n = 11) and IC (n = 17) of each animal were sampled according to the protocol in Supplementary Materials, and routinely processed for histological and IHC analyses as previously reported [38]. In the case that the selected brain nuclei were not intact on the right side (ID114 VCN, ID142 VCN, ID145 VCN and IC, ID192 IC, ID196 VCN, ID319 VCN), the left side was sampled. In few animals, some nuclei were no longer available bilaterally (VCN of ID20, ID133, ID139 and ID159; IC of ID343) and could not be included in this study.

Four μm-sections were cut and mounted onto TOMO® Adhesion Microscope Slides (Matsunami Glass). A semi-automatic HE-staining using a Leica Autostainer XL (Leica Biosystems Nussloch GmbH) was performed and the slides were then coverslipped using a mixture of Eukitt® (ORSAtec GmbH) and xylene, and checked for CNS lesions by a blinded board-certified pathologist using a light microscope. An overview of the significant histopathological findings is visualized in the supplementary files.

Antibody validation process

Systematic validation of the selected antibodies for bottlenose dolphin species followed published approaches [39, 40]. Besides testing the IHC immunoreactivity (IR) on bottlenose

Table 1. Summary of the ID, age group, predominant pathological process detected histologically the CNS, and pooled histoscore averages of the protein marker immunoreactivity for the VCN and IC of the dolphins of this study (0—No immunoreactivity; 3—Very intense immunoreactivity).

ID	Age/ age group	Categories			Predominant pathological proccess	Histoscore averages for the VCN and IC				
		A	B	C		Apaf-1	DGK-ζ	Bcl-2	Aβ	NF200
146	Adult	N	N	Y	Cell death and degeneration	1.42^{nc}; 1.71^{ac}	2.63^{nnl}; 0^{nc}	0^{all}	1.5^{nn}; 2.15^{nc}	2.69^{nc}
20	30 y	N	N	O	Cell death and degeneration	0.43^{nc}; 0.88^{ac}	1.01^{nnl}; 0.7^{nc}	1.09^{n}c; 0.6^{ac}	0.9^{nn}; 1.07^{nc}; 2.0^{ac}	2.39^{nc}
89	5 y	N	N	Y	Cell death and degeneration	0.7^{nc}; 1.57^{ac}	2.16^{nnl}; 0.47^{nc}	0.6^{nc}; 0.55^{ac}	2.4^{nn}; 1.08^{nc}; 1.55^{ac}	2.69^{nc}
139	30 y	N	N	O	Cell death and degeneration	0.65^{nc}; 0.9^{ac}	1.45^{nnl}; 0.68^{nc}	0^{all}	0.93^{nn}; 0.8^{nc}; 2.1^{ac}	2.98^{nc}
159	40 y	N	N	O	Inflammation; Cell death and degeneration	1.0^{nc}; 1.46^{ac}	0.3^{nnl}; 0.84^{nc}	0^{all}	0.6^{nn}; 1.0^{nc}, 2.0^{ac}	2.94^{nc}
319	Old	N	N	O	Inflammation; Hypoxia	1.45^{nc}; 2.13^{ac}	0.15^{nnl}; 0.72^{nc}	0.1^{nc}; 0.59^{ac}	1.92^{nn}; 1.22^{nc}; 1.7^{ac}	2.61^{nc}
344	Sub-adult	N	P	Y	Hemodynamic disorder	0.95^{nc}; 1.76^{ac}	0.99^{nnl}; 0.74^{nc}	0^{all}	2.17^{nn}; 1.0^{nc}; 1.9^{ac}	2.78^{nc}
192	Adult	N	N	Y	None detected	0.8^{nc}; 1.64^{ac}	1.79^{nnl}; 0.52^{nc}	0^{nc}; 0.75^{ac}	1.63^{nn}; 1.48^{nc}; 1.9^{ac}	2.69^{nc}
196	Old	P	P	O	Inflammation (associated with T. gondii)	0.92^{nc}; 1.75^{ac}	1.5^{nnl}; 0.62^{nc}	0.6^{nc}; 0.6^{ac}	1.39^{nn}; 1.48^{nc}; 1.85^{ac}	2.85^{nc}
95	Adult	P	P	O	Hemodynamic disorder; Inflammation	0.87^{nc}; 1.98^{ac}	1.3^{nnl}; 0.89^{nc}	1.0^{nc}; 0.4^{ac}	1.9^{nn};1.23^{nc}; 2.05^{ac}	2.59^{nc}
107	9 y	P	N	Y	Inflammation; Cell death	1.04^{nc}; 1.89^{ac}	2.38^{nnl}; 0.41^{nc}	0^{all}	1.78^{nn}; 1.4^{nc}; 1.85^{ac}	2.7^{nc}
133	>30 y	P	P	O	Inflammation; Cell death	0.8^{nc}; 1.79^{ac}	1.72^{nnl}; 0.9^{nc}	0^{all}	1.77^{nn}; 1.13^{nc}; 2.0^{ac}	2.91^{nc}
142	Old	P	P	O	Inflammation (associated with T. gondii)	0.6^{nc}; 1.32^{ac}	0.48^{nnl}; 0.27^{nc}	0^{all}	0.8^{nn}; 0.67^{nc}; 2.0^{ac}	2.47^{nc}
165	Old	P	P	O	Inflammation (associated with T. gondii)	0.37^{nc}; 1.99^{ac}	0.34^{nnl}; 0.94^{nc}	0^{all}	2.05^{nn}; 1.12^{nc}; 1.8^{ac}	2.81^{nc}
201	Old	P	P	O	Inflammation (associated with DMV)	0.86^{nc}; 2.05^{ac}	0.9^{nnl}; 1.01^{nc}	0^{all}	1.77^{nn}; 1.1^{nc}; 2.02^{ac}	2.96^{nc}
203	Old	N	P	O	Cell death and degeneration; Hypoxia	1.11^{nc}; 1.03^{ac}	0.05^{nnl}; 1.21^{nc}	0^{all}	0.0^{nn}; 1.38^{nc}; 1.75^{ac}	1.78^{nc}
114	9 d	C	C	C	Cell death and degeneration	1.59^{nc}; 1.88^{ac}	2.07^{nnl}; 0.72^{nc}	1.09^{nc}; 0.82^{ac}	2.34^{nn}; 1.3^{nc}; 1.45^{ac}	2.27^{nc}
144	9 d	C	C	C	Cell death	1.8^{nc}; 1.84^{ac}	1.53^{nnl}; 0.99^{nc}	0.95^{nc}; 0.2^{ac}	2.76^{nn}; 1.32^{nc}; 1.65^{ac}	2.71^{nc}
145	9 d	C	C	C	Cell death	1.54^{nc}; 1.73^{ac}	2.62^{nnl}; 0.02^{nc}	1.17^{nc}; 0.42^{ac}	2.7^{nn}; 1.31^{nc}; 1.6^{ac}	2.79^{nc}
343	Calf	C	C	C	Cell death	1.79^{nc}; 1.4^{ac}	0.97^{nnl}; 1.05^{nc}	0^{all}	2.78^{nn}; 1.0^{nc}; 1.4^{ac}	2.92^{nc}

Columns A, B and C apply to the grouping of the animals according to microscopic changes in hematoxylin-eosin (HE)-stained slides (A), independent IHC slide analysis (B), and age (C). N—adults without visible lesions in HE-slides or observed aberration in the IHC slides; P—adults with observed microscopic lesions/aberrant IHC-patterns, Y—young (<30 y.o.) adult, O—old (≥30 y.o.) adult. C—cal. M—male; F—female. Subcellular compartments: ac—astrocyte cytoplasm; all—all cell types and compartments; an—astrocyte nuclei; nc—neuronal cytoplasm; nn—neuronal nuclei; nnl—neuronal nucleoli.

https://doi.org/10.1371/journal.pone.0269090.t001

dolphin tissues, selecting adequate positive and negative control tissues and including sections not treated with the primary antibody (blank sections), orthogonal Western blot (WB) or BLAST analyses were performed to confirm the presence and specificity of the antigen. Antibodies were then selected when a clear IR was detected by IHC and when the antigen specificity was confirmed in the examined tissues by at least one of the two orthogonal techniques.

Western blot analysis

Protein extraction for WB analysis was performed as reported by De Vreese and colleagues (2019) [38], using frozen brain tissue from bottlenose dolphin, fin whale, Cuvier's beaked whale, striped dolphin and sperm whale specimens. Overnight incubation at 4˚C followed, using polyclonal rabbit Apaf-1 (Enzo, #ADI-905-179-100, 1:1000), anti-DGK-ζ (MyBiosourse, #MBS2026991, 1:500), anti-Bcl-2 (Abcam, #ab196495, 1:1000), anti-MDA (Abcam, #ab6463, 1:1000) and anti-iNOS (Abcam, #ab15323, 1:250); a monoclonal recombinant rabbit anti-Aβ (ThermoFisher Scientific, #700254, 1:500); and monoclonal mouse anti-NF200 (Sigma-Aldrich, #N0142), anti-GAD^{67} (Sigma-Aldrich, #MAB5406, 1:2000), anti-GAP43 (Sigma-Aldrich, #MAB347, 1:1000), anti-TNFα (Santa Cruz, #sc-52746, 1:200), anti-QKI-7 (Antibodies-online, #ABIN1304925, 1:1000) and anti-synaptophysin (Dako; #M7315, 1:1000). After several washes in TBS-T, the membrane was incubated with an anti-rabbit peroxidase-

conjugated secondary antibody (ThermoFisher Scientific, #32260) for 1 hour at room temperature. In order to visualize immunoreactive bands, a chemiluminescent detection kit (SuperSignal West Pico Chemiluminescent Substrate, ThermoFisher Scientific) and the iBright machine (ThermoFisher Scientific) were employed.

BLAST analysis

In the case of inconclusive WB results, target proteins of employed antibodies were additionally tested against the predicted *T*. *truncatus* proteome made available by the NCBI (https://blast.ncbi.nlm.nih.gov/Blast.cgi?PAGE_TYPE=BlastSearch&PROG_DEFAULTS=on&PAGE=Proteins&PROGRAM=blastp&BLAST_SPEC=OGP__9739__20365&DATABASE=RefseqProteins/Refseq_Protein_9739). The NCBI amino acid sequences were selected according to their similarity to the proteins targeted by the antibodies utilized in this study. Dolphin protein isoforms with the closest molecular weight and sequence homology to the requested sequence were ranked in terms of degree of identity (in percent) and E-Value.

IHC analysis

In order to validate the use of the primary antibodies for bottlenose dolphin, validated positive control tissues were first selected for each antibody. IHC protocols were adjusted using a Ventana Benchmark® GX semi-automatic immunostainer containing a kit of automatically dispensed reagents including the secondary antibody and HRP-conjugated polymer (UltraView Universal DAB; Ventana Medical Systems).

Primary antibodies included the same ones tested in the WB procedures, with dilutions optimized for IHC: polyclonal rabbit anti-Apaf-1 (dilution: 1:500), anti-DGK-ζ (1:100), anti-Bcl-2 (1:150), anti-MDA (1:100) and anti-iNOS (1:100); monoclonal recombinant rabbit anti-Aβ (1:1000); monoclonal mouse anti-NF200 (1:400), anti-GAD^{67} (1:500), anti-GAP43 (1:1000), anti-TNFα (1:50), anti-QKI-7 (1:100) and anti-synaptophysin (1:50).

In each IHC run, a positive control, as well as blank sections of the same tissues were included to exclude unspecific binding of the secondary antibody and of the HRP-conjugated polymer. Internal negative controls were evaluated in each slide according to the specific cell type reactivity as described by the antibody producer and existing biomedical literature.

Additionally, a polyclonal rabbit anti-human *T*. *gondii* antibody (MyBioSource; # MBS373041; 1:80), was used on the brain tissue of animals in which molecular analyses had confirmed the presence of the protozoa [41] in order to investigate the localization of *T*. *gondii* itself in relation to the IR patterns of selected antibodies in neuroinflammatory foci.

Animal categorization and semi-quantitative scoring

Adult animals were grouped into pathological (*P*)/non-pathological (*N*) categories according to the presence or absence of microscopic changes (Table 1, column A) including 1) neuronal degeneration and necrosis as marked by cell hypereosinophilia, loss of subcellular detail, darkened or shrunken appearance, and satellitosis; 2) cerebral edema recognizable by spongiotic foci and widened perivascular spaces; 3) (meningo-)encephalitis evidenced by infiltrates of inflammatory cells, perivascular cuffing, astrocytosis and/or presence of parasitic agents, glial nodes and/or gemistocytes. Previously established molecular positivity to *T*. *gondii* (ID142, ID165, ID196) [41] and *Dolphin Morbillivirus* (ID201) [10] were also considered in the classification of the animals, particularly when associated to the aforementioned CNS lesions.

In order to evaluate the potential of IHC to deliver information on the health status of brain tissue, the animals were then categorized independently into adult dolphins with evident CNS pathology/adult dolphins without evident CNS pathology/calf (*P*, *N*, *C*, respectively) categories

according to qualitative assessment of only the IHC IR patterns considering the extent, localization and distribution of the IR (Table 1, column B).

Lastly, the animals were again independently grouped into the following categories (Table 1, column C): young adults (≈<30 years old) (Y), old adults (≈≥30 y.o.) (O) and calves (C) to account for age-related changes in expression profiles.

Since the ages of the adult animals were not always known, 5 individuals of known ages (9 days, 3.5 years, 9 years, 30 years, 40 years) were used as references for a scatterplot-based correlation of total length (from tip of the rostrum to the notch of the fluke) to approximate age according to age-length reference ranges for Mediterranean bottlenose dolphin specimens [42] and necropsy findings including tooth wear, body condition, gonad weight and presence of ovarian scars. An age-length estimation curve for the animals with known total body lengths is depicted in S1 Fig, and represents a logarithmic trend line automatically calculated in Microsoft Powerpoint® from a scatterplot of the available length measurements. Adult dolphins with a total length superior to that of ID139 (30 y.o.) were estimated to be ≥ 30 y.o., regardless of their sex.

For each marker, the IR intensity was recorded subjectively for each relevant cell type and subcellular compartment (SC) of each animal and auditory nucleus. A value of *1* (mild), *2* (moderate) or *3* (intense) was assigned on IHC staining by evaluating five high power fields (400x magnification) for each auditory nucleus and animal. In order to assess the relative number of observed SCs of each intensity level, the histoscore (H = (1 * % of intensity score "*1*" SCs) + (2 * % of intensity score "*2*" SCs) + (3 * % of intensity score "*3*" SCs) was calculated. The H-average value for the five fields was then used for the database used for statistical assessment of the various animal groups.

Statistical analysis

In order to properly evaluate the potential of IHC to deliver information on the health status of brain tissue going beyond routine morphological assessment, three analyses based on the aforementioned categorization of the animals were performed in RStudio®. Scores of the semi-quantitative manual scoring for relevant subcellular compartments were tested for normality visually (histograms can be found in S2 Fig) and using the Shapiro-Wilk test. Due to the relatively small sample size, homogeneity of variance was additionally tested using Levene's test in cases where the Shapiro-Wilks implied normality. Results were considered statistically significant at a p-value < 0.05. Animal groups independently categorized into three health categories: adult brains with lesions; adult brains without lesions; and neonate brains according to A) microscopic findings in HE sections B) IHC-patterns and C) age. One-way ANOVAs were used to compare normally distributed marker scores, whereas the Kruskal-Wallis test was implemented on non-normally distributed scores (Bcl-2—neuronal cytoplasm in IC and VCN; DGK-ζ—neuronal cytoplasm, VCN; Apaf-1—astrocyte cytoplasm, VCN; Aβ—neuronal nucleus, VCN; NF200—neuronal cytoskeleton, IC).

The statistically significant results were then compared using the Tukey HSD and Wilcoxon signed-rank test for parametric and non-parametric data, respectively, in order to assess which animal categories displayed relevant differences. Due to the small sample size, three levels of adjustment with increasing restriction for α-error of the Wilcoxon test were used: None, Benjamini-Hochberg and Bonferroni.

Results

Antibody validation process

The selected antibodies were developed against human or laboratory animal antigens, so their specificity in cetacean tissues required validation through a well-defined procedure aimed at

confirming their IR. WB analyses confirmed reactivity with antigens of adequate molecular weight; alternatively, a basic local alignment search tool (BLAST) allowed to compare protein sequences to sequence databases calculating the statistical significance [39]. Finally, IHC validation in 20 bottlenose dolphins was performed detecting any cross-reactivity of the selected antibodies with unrelated antigens, and cross-reactivity among different species [39]. Antibodies were only selected for further analyses if IHC and at least one of the orthogonal methods (WB/BLAST) confirmed their specificity [40]. Out of the 12 antibodies listed in the methodology, only four encompassed the criteria of contemporary positive IHC reaction and WB (DGK-ζ, Bcl-2, Aβ and NF200). While Apaf-1 was negative in the WB, BLAST analysis and specificity of its IHC-IR in selected positive control tissues, verified its suitability for systematic IHC analysis.

Western blot analysis

Among all the tested antibodies, WB analysis (see Fig 1) established the specificity of primary antibodies against Bcl-2 (≈26 kDa) and Aβ (≈87 kDa) for brain tissue in bottlenose and striped dolphin (*Stenella coeruleoalba*), as well as for fin whale (*Balaenoptera physalus*), Cuvier's beaked whale (*Ziphius cavirostris*; henceforth: BW) and sperm whale (*Physeter macrocephalus*). For NF200, IR-bands were detected for fin, beaked and sperm whales at approximately 200 kDa, while for DGK-ζ, a weak signal was observed for BW, sperm whale and striped dolphin at around 100 kDa, which corresponds to the length of human and rat isoforms (≈104 kDa). The antibodies against Apaf-1, MDA iNOS, GAD^{67}, GAP43, TNFα, QKI-7 and synaptophysin did not yield detectable results. Unprocessed images of the blots of the successful markers are included in S3 Fig.

BLAST analysis

WB signal against bottlenose dolphin tissue was not detected for Apaf-1, NF200 and DGK-ζ. However, BLAST analysis against the estimated *T. truncatus* proteome showed that proteins

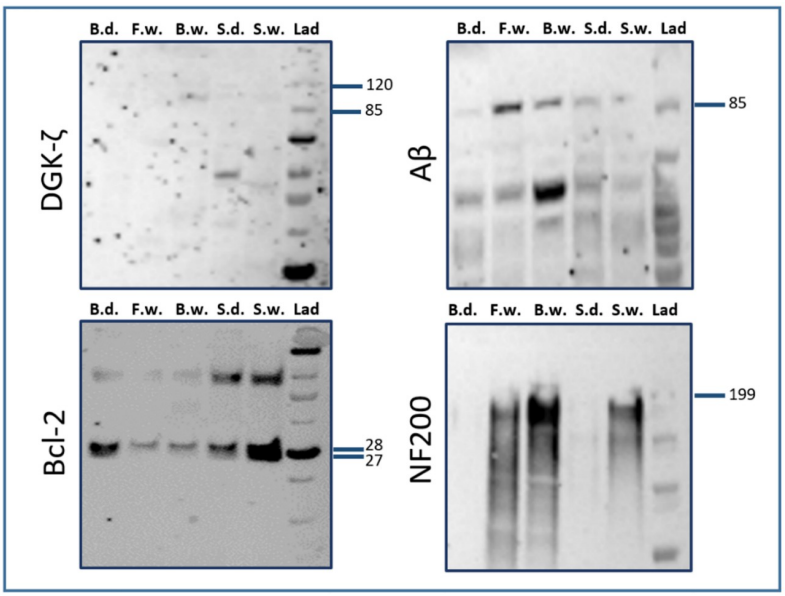

Fig 1. Results of WB analyses for antibodies against DGK-ζ, Bcl-2, Aβ, and NF200. B.d.: Bottlenose dolphin; F.w.: Fin whale; B.w.: Beaked whale; S.d.: Striped dolphin; S.w.: Sperm whale; Lad: Ladder. Labels on the right of each panel signify molecular weight in kDa.

https://doi.org/10.1371/journal.pone.0269090.g001

with a comparable amino acid sequence are present in this species. Therefore, the IHC patterns were deemed reliable. For DGK-ζ, the homology degree between the mouse (NP_612179.2) and dolphin isoforms X7 and X8 equaled 94.4% (E-value: 0). An 85.83% homology level (E-value: 0) was found between the human Apaf-1-isoform c protein (NP_863651.1) and the dolphin Apaf-1-isoform X5 (XP_019773955.1—the closest protein in terms of molecular weight). For NF200, the homology degree between the mouse (NP_035034.2) and the dolphin neurofilament heavy polypeptide (XP_019805688.2) equaled 79.69% (E-Value: 0).

IHC analysis

Positive control tissues, antibody concentration, and expected immunoreactive cell types for the antibodies that passed the selection criteria (a clear IHC-pattern in combination with the positivity of at least one of the orthogonal validation methods), as well as reported significance of the cellular pattern are summarized in Table 2.

Apaf-1. Cytoplasmic IR was detected in different cell types including astrocytes (ranging in intensity score from *1* to *3*), oligodendrocytes (*3*) and neurons (*1*), the latter showing a stronger immunostaining (*2*) in calves compared to adults. Disseminated glial IR was apparent in all the studied specimens, making a clear differentiation between oligodendrocytes and astrocytes challenging. Apaf-1-IR appeared to be reduced in glial nodules surrounding *Toxoplasma gondii* cysts (Fig 3e).

The VCN neuropil displayed a mild background signal, with a mild to moderate (*1–2*) perisomatic IR surrounding the large neurons of the VCN of three dolphins (ID145, ID319, ID343). VCN neurons of the older dolphins ID319 and ID142—the latter also presenting *T. gondii* cysts—additionally displayed a moderate nuclear IR (Fig 2a). In a few large neurons of the VCN, Apaf-1 preferentially localized to the Nissl substance (S4 Fig).

Table 2. Summary of IHC parameters of the herein utilized antibodies, and their roles in the body depending on subcellular location.

Antibody	Dilution	+ CTRL	CNS cell type	Significance of cellular pattern
polyclonal rabbit anti-Apaf-1	1:500	Lung with lymphoma, rat	• Neurons	Cytoplasmic—up-regulated in the process of intrinsic apoptosis (including that in the developing brain);
			• Glia (incl. pericytes)	Nuclear—associated to acute hypoxic conditions;
			• Endothelia	Acellular perivascular leakage—mild hypoxia (likely a common phenomenon in diving mammals) may result in transient, physiological reduction of BBB integrity
polyclonal rabbit anti-DGK-ζ	1:100	Cerebellum, rat	• Neurons	Nuclear—common in morphologically healthy neurons;
			• Glia	Nucleolar—potential interaction with Mdm2 and p53 proteins, which are implicated in nucleolar stress;
				Cytoplasmic—association with pre-apoptotic state following ischemic-hypoxic episodes and auditory insults, may be neuroprotective and can also be associated with neuroplasticity
polyclonal rabbit anti-Bcl-2	1:150	Lymphonode, Canine	• Neurons	Cytoplasmic—low amounts expected in neonatal neurons and as an anti-apoptotic response to cell injury
			• Glia	
monoclonal recombinant rabbit anti-Aβ	1:1000	Neocortex, canine neonate	• Neurons	Cytoplasmic—neurotoxic effect through disruption of calcium homeostasis, organelle and synaptic function;
			• Glia	Nuclear—presumed regulation of apoptosis and potential indicator of neuroprotection against neurodegeneration;
			• Endothelia	Extracellular plaques—presence positively correlated with cognitive decline in Alzheimer's disease
Monoclonal mouse anti-NF200	1:400	Cerebellum, rat	• Neurons	Cytoskeletal—reduced in cases of traumatic brain injury and hypoxia

+CTRL: Positive control tissue. BBB: Blood-brain barrier.

https://doi.org/10.1371/journal.pone.0269090.t002

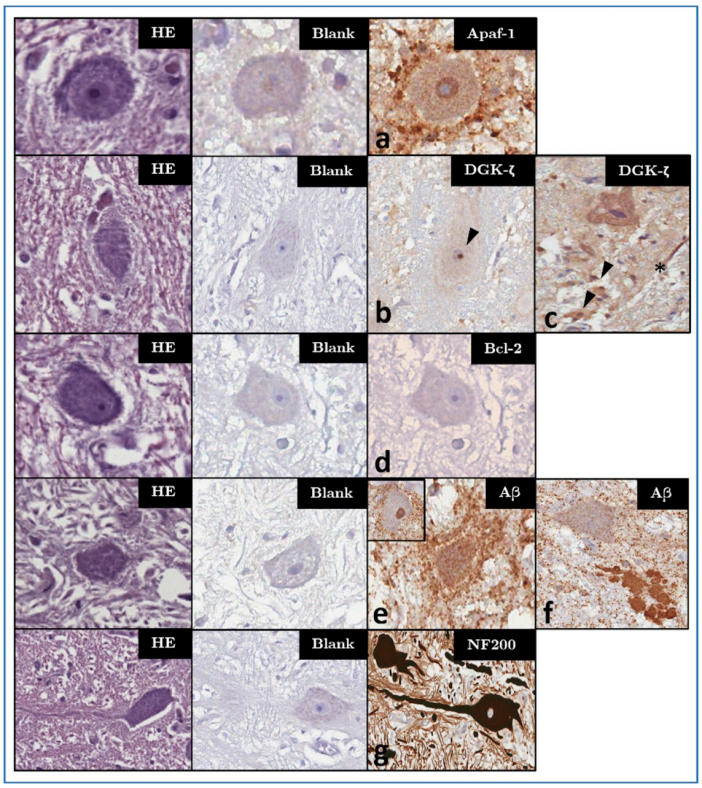

Fig 2. Haematoxylin-eosin/HE (left column), blank control/CTRL (middle column) and IHC patterns (right columns) for the investigated markers—magnification: 400x. Panels marked a-f represent characteristic IHC patterns for each marker: (a) Apaf-1-IR in both neuronal cytoplasm and, unlike in most other examined animals, in the nucleus of ID319. (b) Nucleolar DGK-ζ-IR (arrowhead) in the VCN of a younger adult dolphin without brain lesions (ID146) as compared to (c) its cytoplasmic appearance in the VCN of a bycaught, older adult (ID203). In this animal, multifocal cytoplasmic IR in glial cells (arrowheads), as well as streaks of IR in the neuropil (asterisk) are apparent. (d) Lack of Bcl-2-IR in the VCN of a younger adult dolphin (ID89), representative of most adults. (e) Perineuronal enhancement of glial Aβ-IR in the VCN of a bycaught, hypoxic dolphin (ID203). (f) Aβ-IR marking a coalescing extracellular plaque between the VCN and superior olivary complex of older adult (ID319). An adjacent neuron shows light disseminated granular IR in its cytoplasm, but not in the nucleus, as in the VCN of most investigated adult dolphins <30 y.o. (inset in e). (g) Intense NF200-IR of the dendritosomatic and axonal cytoskeleton of VCN neurons (ID89, representative of all investigated animals).

https://doi.org/10.1371/journal.pone.0269090.g002

Perivascular IR was prominent in the IC of three of the examined dolphins (ID107, ID201, ID344), variably associated to pericytes (Fig 4c-4d) or to acellular perivascular deposits (S5 Fig). The neuropil also appeared to have a homogeneous, light background.

DGK-ζ. DGK-ζ-IR was mainly localized to two different compartments: neuronal nucleoli (intensity: *3*; Fig 2b) and cytoplasm (intensity: *1–2*; Fig 2c). In four adult dolphins and one calf, a clear predominance for the nucleolar pattern emerged in the qualitative assessment. In the others, an overlapping pattern of variable cytoplasmic IR with or without simultaneous nucleolar IR was apparent. In the IC of four adults, and the VCN of 5 adults and one calf, cytoplasmic IR predominated over a weak/undetectable nucleolar staining. No IR was observed in either auditory nucleus of ID142.

Some immunoreactive glial cells were also detected (Fig 2c), at times displaying a more focal labeling where tissue appeared to be spongiotic, although it was difficult to attribute it to a certain cell type due to the mild signal (*1*) and light haematoxylin counterstaining.

No particular deviations from the abovementioned IHC pattern were observed for the VCN. On the other hand, multifocal foci of pericapillary IR (intensity *2–3*; inset in Fig 4b) were apparent in the IC of two old dolphins (ID133, ID95) with evidence of mild microscopic pathology (Table 1). In four animals, a nucleolar IR was particularly evident in the IC external cortex (ID89, ID107, ID145, ID146).

Bcl-2. Cytoplasmic IR was scant, and most often detected multifocally in glial cell cytoplasm (*1–3*). In all adults, at least one of the nuclei had negative neuronal cytoplasm (Fig 2d), while all the calves but one (ID 343) displayed mild IR (*1*) in both nuclei.

Aβ. In general, Aβ-IR could variably be observed in both the nucleus (*1–3*) and cytoplasm (*1*) of neurons (Fig 2e). A disseminated granular IR (*1–2*) characterized the neuropil and reduced within white matter tracts. Prominent nuclear IR (*3*) appeared multifocally in oligodendrocytes, and a mild astrocytic IR (*1–2*) was evident around the vessels and in spongiotic areas.

With the exceptions of ID142 and ID203, 14 out of the 16 dolphins in which the VCN was available displayed an intense intranuclear IR (*3*) in VCN neurons (inset in Fig 2e). A mildly augmented perineuronal IR was observed in the VCN of putatively older dolphins ID142, ID203 and ID319 (Fig 2e). Additionally, one coalescing plaque (Fig 2f) was detected between the cochlear and superior olivary nuclei of ID319, in whose brain multifocal neuronal lipofuscin deposits were also apparent.

In the IC, nuclear IR was more heterogeneous between the external cortex and core of the structure, with the former displaying stronger intranuclear IR. Neuronal cytoplasmic IR (*1*) was generally weaker compared to that of glial cells.

NF 200. A prominent IR (*2–3*) against the cytoskeletal NF200 protein was detected in all visible myelinated axons and perikarya of all tested auditory and non-auditory nuclei (Fig 2g). No qualitative differences were visible between specimens.

The most remarkable observed IHC patterns are summarized in Fig 2, while patterns associated with specific inflammatory and vascular phenomena are depicted in Figs 3 and 4, respectively.

Fig 5 provides a visual overview of the biological roles of the implemented biomarkers.

Even in the heterogeneous sample population available for this study, qualitative combinations of cellular patterns corresponding to certain pathological processes appeared to emerge, although the differences in the patterns of single markers overlapped between these processes.

Inflammation. Dolphins with inflammatory lesions (e.g. ID142, ID319, ID165) tended to have stronger cytoplasmic Apaf-1-IR in the astrocytes and surrounding the vasculature, perineuronal Aβ appeared augmented, while intranuclear neuronal Aβ was reduced.

Hypoxia. Dolphin ID203, presumed to have asphyxiated in a net, displayed increased cytoplasmic neuronal Apaf-1-IR, a higher ratio of cytoplasmic:nucleolar DGK-ζ-IR, no intranuclear neuronal Aβ and no sign of Bcl-2-IR.

Aging. The clearest pattern for old dolphins was the consistent presence of cytoplasmic DGK-ζ-IR in the neurons. In the calves, neuronal Bcl-2 was more frequently observed in the cytoplasm compared to adults.

Statistical analysis

When the animals were grouped according to microscopic pathological changes in the CNS, significantly higher H-averages (ANOVA; $p = 0.0068$) were observed for cytoplasmic Apaf-1 in astrocytes of the IC in adults with evident ongoing CNS pathology (*P*), as opposed to adult animals without visible lesions (*N*). No significant differences emerged between these two groups for the VCN.

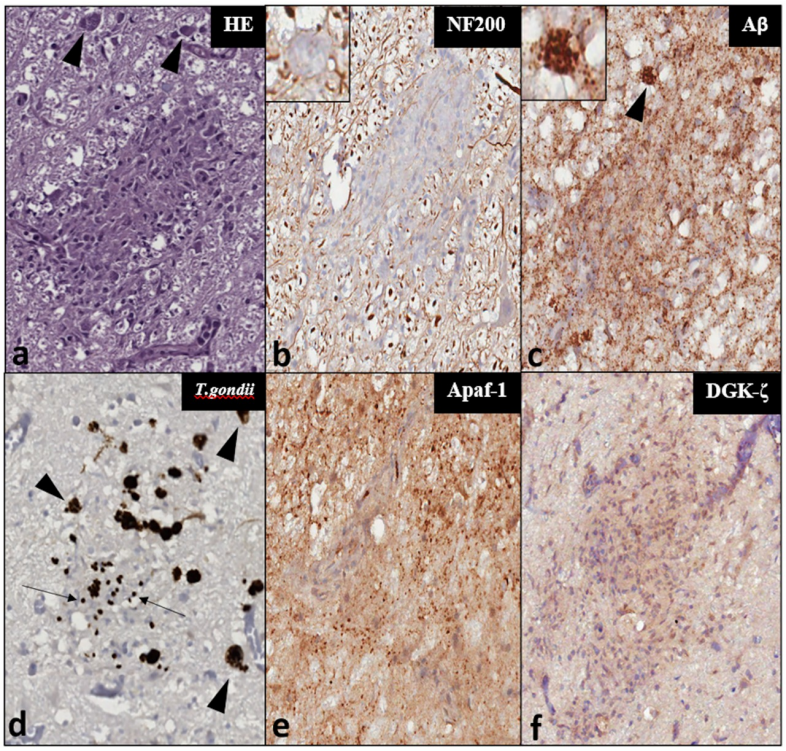

Fig 3. Comparison between histochemical and IHC staining results for a glial node surrounding *T. gondii* cysts (arrowheads) in the IC of ID142—Magnification: 200x. Insets display detail of cysts at a magnification of 400x. (a) HE-stain. (b) NF200-IR within the glial node tissue (c) Aβ-IR which also localizes to the *T. gondii* cysts (inset); (d) *T. gondii* cysts and zoites recognized by a specific anti-*T. gondii* antibody; (e) Apaf-1-IR appears attenuated within the cell-rich microglial nodule in comparison to the granular IR and high background of the surrounding neuropil; (f) DGK-ζ-IR is mildly stronger within the glial cells of the parasitic nodule compared to the surrounding neuropil.

https://doi.org/10.1371/journal.pone.0269090.g003

Following qualitative IHC assessment of the implemented biomarkers in each dolphin, adults were regrouped according to qualitative deviations from the expected IHC-pattern for a lesion-free brain. In this case, cytoplasmic Apaf-1-IR was significantly higher (ANOVA; $p = 0.0067$) in the astrocytes of animals with deviating IHC-patterns (e.g. perivascular IR in Fig 4c–4d).

In the comparison between young (*Y*) and old (*O*) dolphins, a significantly higher nucleolar DGK-ζ-IR was apparent in the IC of young adults (ANOVA; $p = 0.0018$), with a similar tendency ($p = 0.0786$) apparent for the VCN in the parametric tests, while cytoplasmic DGK-ζ-IR was significantly higher in older adults (ANOVA; $p = 0.0330$).

In all three analytical scenarios, statistically significant differences between calves (*C*) and adults resulted from both parametric and non-parametric tests (S1 Table). The most prominent differences were evident for the neuronal cytoplasm in the IC, with the calves yielding relatively higher H-averages for Bcl-2-IR than adults with lesions. A stronger Apaf-1-IR occurred as well in the neuronal cytoplasm compared to both adults with and without CNS pathology in both IC and VCN. Intranuclear neuronal Aβ-IR was significantly more intense and widespread in calves *vs*. both young/old animals, and *vs*. adults with/without evident CNS pathology. Averages of absolute numbers of NF200-IR neurons were higher in calves compared to both adult groups for most analyses.

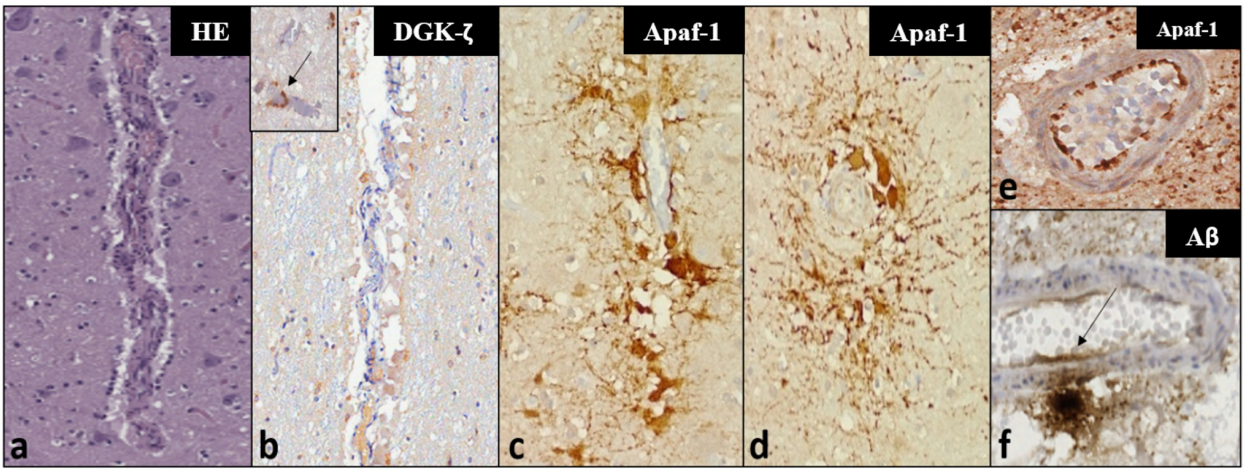

Fig 4. Histochemical (a) and IHC (b-f) findings in vascular and perivascular tissues in the investigated dolphins—Magnification: 100x. Panels a-c represent the same vessel in consecutive sections. (a) Microscopic appearance of a mid-caliber vessel in the IC of ID344 using a haematoxylin-eosin staining, with a mild perivascular infiltrate characterized by mononuclear inflammatory cells. (b) very mild cytoplasmic DGK-ζ-IR in few foci of perivascular glia. Inset: Moderate, multifocal IR in pericapillary neuropil of ID133 (arrow)—magnification: 200x. (c) The same vessel of ID344 displays intense Apaf-1-IR, mostly in the cytoplasm of pericytes, showing perivascular distribution and radiating cellular processes, visible also in transverse sections of the IC vessels of ID344 (d). (e) Clearly demarcated endothelial Apaf-1-IR in a VCN vessel of ID142. (f) Aβ-IR deposit in neuropil adjacent to a mid-caliber VCN vessel—the IR appears to extend into the vessel wall and endothelial lining (arrow).

https://doi.org/10.1371/journal.pone.0269090.g004

Discussion

Understanding the baseline expression of biomarkers within the cetacean CNS is key to future evaluation of animals affected by various insults, including those deriving from suspected overexposure to anthropogenic underwater noise. In the latter case, IHC should be performed on the acoustic pathways, as proposed in the cited literature [7, 26, 43, 44].

Recent protocols attempt to optimize the fixation of cetacean brains for histopathological analyses [23]. Our suggested addition to the CNS sampling protocol (Supplementary Materials) underlines the sampling method for the VCN and IC, which could easily be collected during standard necropsy [5], while also suggesting that one side of the bilateral structures be frozen fresh for future molecular studies going beyond routine pathogen detection (e.g. for Morbillivirus, *Brucella ceti* or *T. gondii*). Alternatively, as suggested by Ijsseldijk and colleagues [5], a midline sagittal cut between the two hemispheres and sides of the brainstem could preserve the structural integrity of the hemispheres while allowing fixative to penetrate into the tissue from the ventricles, which would allow potential imaging studies to corroborate microstructural findings. One of the hemispheres could be frozen after taking fresh samples for ancillary diagnostics—serving as a reserve for molecular correlation of histopathological and IHC findings of the fixed half.

The validation process identified the specificity of the IR of five biomarkers of apoptotic (Apaf-1, DGK-ζ, Bcl-2), neurodegenerative (Aβ) and structural (NF200) changes of the neuropil and vasculature, and found them consistent with biomedical literature [7, 26, 33, 43, 44]. These markers were subsequently compared in adult dolphins with and without pathological changes assessed during microscopic examination, and in four calves to account for age-related changes in protein expression.

Apaf-1

In our study, several markers identifying apoptotic processes have been investigated. Among these, Apaf-1 is the only marker that yielded statistically significant differences for the

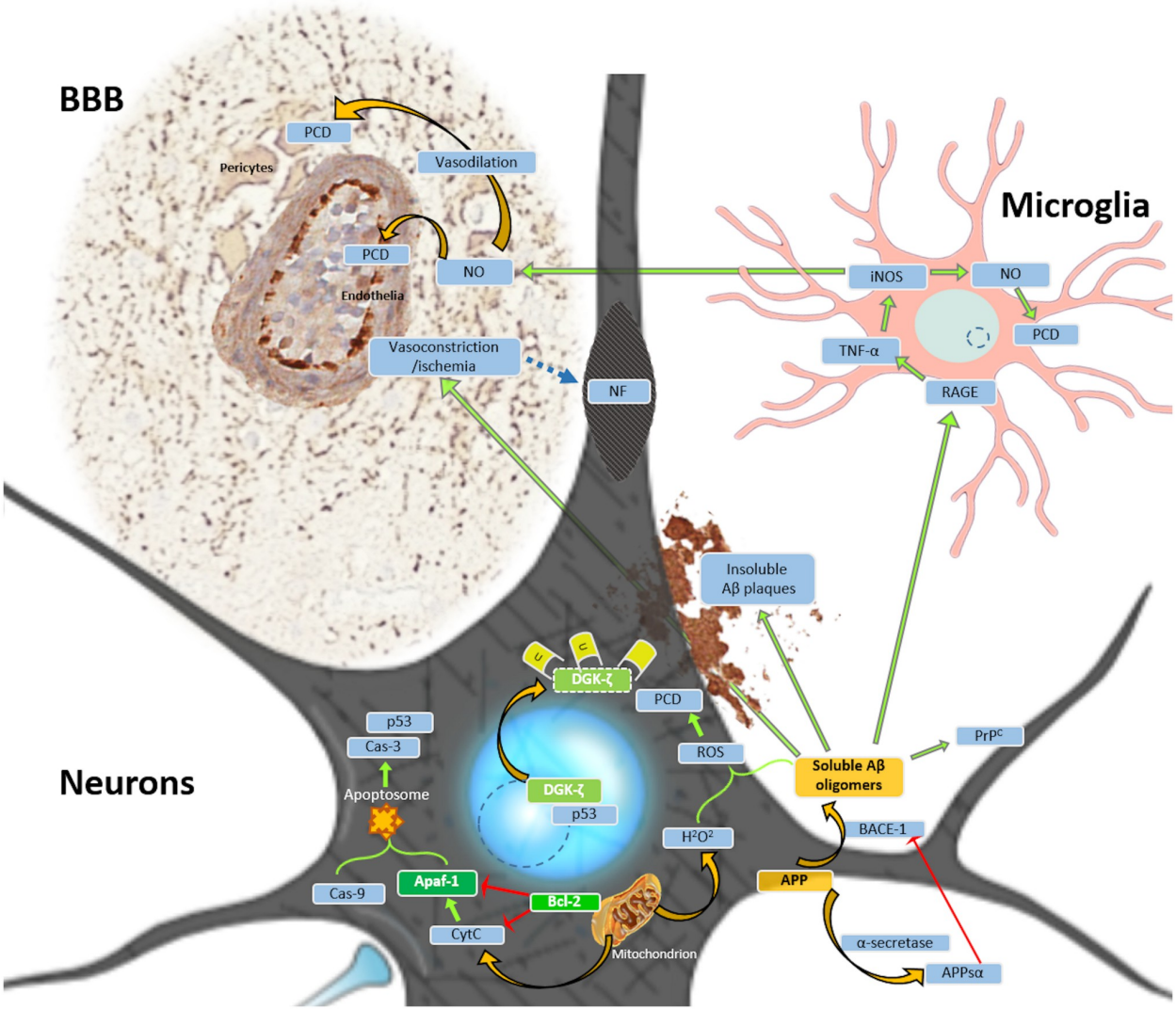

Fig 5. Relevant biological roles of the implemented biomarkers protein in programmed cell death PCD (PCD; green highlight) and Aβ-associated toxicity (orange highlight) as referred to in the main text. Light blue circles—nuclei. Dashed line circles—nucleoli. Orange arrows—translocation and transformation of molecules/processes. Green arrows—activation or induction of molecules. Red arrows—inhibition of molecules. Blue highlight—interacting molecules. Blue dashed arrow: Association between focal ischemia and proteolysis of cytoskeletal neurofilaments (NF), leading to the development of spheroids. Abbreviations: APPsα—soluble APP α; BACE-1—Beta-site APP Cleaving Enzyme 1; BBB—blood brain barrier; Cas—caspase; iNOS—inducible nitric oxide synthase/NOS II; NO—nitric oxide; p53—(tumor) protein 53; Prp^{C}—cellular prion protein; RAGE—Receptor for Advanced Glycation End Products; U—ubiquitin (degrades cytoplasmic DGK-ζ). Astrocytes are omitted from this figure for simplification, though they closely interact with both neurons and microglia under both physiological and pathological conditions.

https://doi.org/10.1371/journal.pone.0269090.g005

cytoplasmic astrocyte IR in the IC between dolphins with and without brain lesions in analyses based on pathological and IHC findings. In the literature, Apaf-1 has been shown to activate during early intrinsic apoptosis of various cell types including neuronal [8], glial [45] and endothelial cells [46], inducing apoptosome formation by cleaving initiator caspases [8]. Distinct glial cell types show different sensitivity to Apaf-1-associated PCD [46], and assessment of its expression may enhance our understanding of cetacean CNS pathogenesis.

Apaf-1-IR was more widespread in the cytoplasm of astrocytes of adult dolphins affected by pathologies of the CNS. An increased expression of Apaf-1 in perivascular astrocytes in some

dolphins appeared to conflict with the inconspicuous findings of routine histopathology (Fig 4a and 4c). However, the suspected involvement of bacterial toxins in the death of those animals could explain damage spreading from the vasculature [46, 47]. At the same time, Apaf-1-IR appeared to be reduced around glial nodules neighbouring *T. gondii* cysts. Therefore, this marker could help evaluate perivascular and glial pathology potentially corresponding to vasoconstriction [48] and toxin exposure [47], without marking the presence or protozoan parasites.

In neurons, a diffuse intranuclear neuronal IR, seen in two older dolphins in this study, could correspond to early apoptotic changes preceding any morphological evidence: it should be noted that intranuclear Apaf-1 concentration has previously been reported to rise significantly in hypoxic laboratory animals [8]. Neuronal cytoplasmic IR was notably less indicative: in fact, the IR in calves was significantly more intense, though how developmental phenomena or hypoxia may influence this remains unclear [49]. It should be noted that all the 9-day-old calves investigated herein died of respiratory distress following meconium aspiration syndrome, likely leading to hypoxic conditions.

Statistically significant differences were absent when comparing neuronal cytoplasmic IR between young (<30 y.o.) and old (≥30 y.o.) adult dolphins. These results imply that Apaf-1 identifies cells affected by noxious stimuli, but does not specifically mark aging cells. Although degenerating neurons are suspected to re-express Apaf-1 in physiological aging, convincing evidence is lacking [50]. It is therefore advisable to consider neonate specimens separately, and to conduct further studies to acquire reliable baseline data for this age group.

DGK-ζ

DGK-ζ has been reported to undergo irreversible nucleocytoplasmic translocation prior to the cell's apoptosis in both the cochlear hair cells and various populations of cerebral neurons in mammalian species like guinea pigs and mice [43, 51]. In the present study, statistical analyses for this marker showed significantly higher cytoplasmic- and lower nucleolar IR in older compared to younger adults, implying a higher prevalence of neuronal degeneration in putatively older, stranded animals. Furthermore, It is remarkable that a non-parametric analysis yielded a higher nucleolar DGK-ζ expression bordering on statistical significance in lesion-free dolphins compared to those with microscopically evident brain pathology (S6 Fig).

Bcl-2

Bcl-2—an established anti-apoptotic marker—is the only one for which neuronal H-averages were unevenly distributed in both IC and VCN. Bcl-2-protein expression has been shown to diminish 15 minutes after acoustic overexposure in mice [7], but there are contradictory reports on its up-/down-regulation [52, 53] under other cellular stress events. Furthermore, quantitative expression was previously reported with molecular techniques like WB, and the present IHC results do not clearly indicate its specificity in the assessment of CNS lesions in bottlenose dolphins.

Aβ

We next considered a classic indicator of neurodegeneration in brain tissues: Aβ [54–56]. Although it has previously been successfully employed in at least 3 cetacean species [21, 22], to the best of our knowledge, the obtained results were not supported by a validation including WB. Aβ is claimed to target amyloid-β oligomer 1–42, which is found in cytotoxic extracellular plaques in human Alzheimer's disease (AD) [56]. In our study, WB analyses yielded clear IR bands for all examined cetacean species at 87 kDa—a molecular weight corresponding to one of the APP isoforms [55].

In our study, the diffuse granular IR in the neuropil of the majority of the investigated dolphins could be justified, considering that APP yields a variety of cleavage products. Examples range from cytoprotective APPsα to Aβ1–42. The latter, generated via the amyloidogenic pathway, induces neurotoxicity through metabolic disruption and induction of apoptosis [56]. Intranuclear neuronal localization of this Aβ isoform has previously been reported in the brains of 2 out of 9 animals belonging to two cetacean species (pantropical spotted dolphin, *Stenella frontalis*, and BW) [22]. Despite using a higher antibody dilution in our study (1:1000 *vs*. 1:200), intranuclear neuronal IR was evident in at least one of the two auditory nuclei in all investigated specimens. The reasons could include species-specific functional specializations [57], and the higher intensity of the heat-induced antigen retrieval method used by the semi-automatic immunostainer used in our study. A higher initial demasking may have exposed more of the antigen, making it more available for the antibody, even at a higher dilution of the latter. The intranuclear location-associated role of this protein is under debate, with several neurodegenerative diseases associated with intranuclear Aβ aggregates [58]. Other studies suggest a neuroprotective role, such as against hypoxia [22, 56]. Aβ 1–42 is known to inhibit Apaf-1-induced intrinsic apoptosis, albeit to a limited degree [59]. The light IR observed in the cytoplasm of both glial and neuronal cells could therefore also represent an adaptation of an organism evolved to buffer the consequences of hypoxia in all its tissues including the CNS, as documented by comparatively higher anti-oxidant protein levels in cetacean brains [60], and a higher degree of myelination in deeper diving species [57].

As with DGK-ζ, if one does not assume normal distribution, young adults and calves display more intranuclear Aβ than older adults. Investigating a larger sample population and employing antibodies against Aβ-interactors, such as PrP^{c} [61], would be recommended to understand the meaning of this diminution in aged individuals.

The presence of a coalescing extracellular amyloid plaque in the white matter between the VCN and the superior olivary complex of an older bottlenose dolphin is arguably the most interesting finding of the herein reported microscopic investigations. Amyloid plaques have previously been reported in the human central auditory system [62]. In this study, the authors reasoned that impaired connectivity in major integration centers, such as the IC, could well contribute to the auditory impairment seen in many AD-affected patients. Our evidence does not support or suggest that amyloid plaques may impact the sensory abilities of the dolphin. However, connections between AD-associated neurovascular pathology and age-related hearing loss are consistently reported in the human literature [63]. Neurodegenerative diseases may also impact cetaceans because of the extended life span of these aquatic mammals. In this sense, dolphins and whales may hold potential as comparative translational models for the onset, development and evolution of human AD [20]. Perivascular Aβ-IR enhancement is also important to consider for the regulation of blood vessel caliber. The downstream interactions with TNFα [16], released by microglial cells interacting with Aβ through their RAGE (*Receptor for Advanced Glycation End Products*) receptors [64], may further promote iNOS biosynthesis, with subsequent production of nitric oxide (NO), a powerful vasodilator [31]. Conversely, Aβ has also been reported to cause a marked vasoconstriction [30]. In large quantities, NO may induce apoptosis [31]. Thus, comparing perivascular Aβ- and Apaf-1-IR may facilitate assessment of vascular pathology.

NF 200

Concerning structural changes, NF200 is considered to be a reliable cytoskeletal marker to visualize neuronal structure. Our preliminary density estimates did not yield significant differences between dolphins with/without evident CNS pathology, although NF200 has been

reported to be downregulated in studies on hypoxic-ischemic and traumatic brain injury, with the presence of spheroids marking the loss of structural integrity [32, 33]. Nevertheless, further studies (e.g. using co-labeling) are needed before making inferences on the pathological effects on NF200 expression. Finally, the lack of significant differences among adult animals, coupled with the simultaneous presence of statistically significant differences in the expression of pro-apoptotic/apoptotic biomarkers, underline the importance of IHC-based investigations on these biomarkers to assess tissue damage before microscopic lesions become apparent.

Despite these encouraging results, several limitations were identified and considered. Some of the investigated biomarkers were negative according to one of the orthogonal methods of validation, such as Apaf-1 in the WB analysis. While its specificity in the presently reported IHC staining was convincing, the percentage of amino acid sequence homology for the protein targeted by the tested antibody was moderate (85.83%). Moreover, the protein sequence was predicted from the genomic level via automated computational analysis, which may harbor errors by not considering species-specific post-transcriptional modifications. Further studies including independent epitope validation [64] should be performed to corroborate these results. NF200-IR in the WB was very weak for bottlenose and striped dolphins, but very pronounced for fin, BW and sperm whales. However, clear-cut IHC specificity of this biomarker for the cytoskeleton of perikarya and axons was found in this and in previous studies [65].

Due to the extremely delicate nature of the CNS, differentiating *post mortem* changes from *ante mortem* lesions is crucial. The examined brains were sampled from DCC 1–2 animals and the fixation procedure was aimed at preserving the tissue for cytoarchitectural studies [36, 37], being consistent through the entire study. Furthermore, where clear evidence of *post mortem* changes (gas bubbles, enlargement of Virchow-Robin spaces, bacterial presence etc.) was apparent, no IR enhancement for any of the five studied biomarkers could be detected. In a previous study, we established that using the same protocols in canine brains with *post mortem* intervals ranging up to 72 hours, these biomarkers did not show significant IR pattern/intensity changes [66]. However, the blubber layer of cetaceans tends to induce a stronger increase in *post mortem* temperature, accelerating autolysis. It remains vital to examine only very well preserved carcasses.

Calves were also included in our study to account for the likelihood of protein expression differences secondary to developmental processes occurring in neonatal brains. Although the stronger Bcl-2-IR in the neuronal cytoplasm and the more consistent DGK-ζ-IR in neuronal nucleoli could be indicative of tissues more resistant to apoptosis [67], this does not imply that a significant neuroprotective mechanism in animals at this developmental stage represents the only explanation.

Conclusion

The biomarkers validated in this study promise additional diagnostic information for microscopic analysis of the CNS, particularly for pre- to early-apoptotic (Apaf-1, DGK-ζ), but also neurodegenerative, inflammatory, and even reversible vascular changes (Aβ) [30]. Apaf-1-IR yielded additional qualitative evidence of neurochemical dysregulation, a feature elusive in routine microscopic analysis, differing significantly between adult dolphins with and without CNS-lesions. DGK-ζ-IR appeared more shifted to neuronal cytoplasm than to the nucleolus in older adults. Aβ, due to its variable IR, requires further investigation regarding its function and reflection of evolutionary adaptations in cetaceans. Structural changes (NF200) were not observed, but further studies implementing 3-dimensional advanced microscopy may provide different insights. The fact that these antibodies helped visualize cellular processes evasive in a purely morphological analysis implies their particular usefulness in cases of suspected noise

overexposure in marine mammals, especially for subtle cases that might exhibit cumulative damage rather than extreme cases where decompression sickness-like symptoms prevail and inner ear lesions are evident.

It is noteworthy that only 5 out of the 12 tested markers actually passed the hurdles of systematic validation, which underlines that we cannot rely only on IHC results of antibodies that were not custom-made for dolphins. Future analyses must justify their use of antibodies with rigorous scrutiny of the markers they use.

Laboratory animal studies imply temporally differentiated expression profiles of the investigated biomarkers in auditory structures after acoustic overexposure. Systematically validating and applying IHC biomarkers in the VCN and IC of cetacean brains could therefore help answer the question of how much time passed between a potentially anthropogenic acoustic trauma and a mass stranding of cetaceans.

Exposure to environmental pollutants may result in the occurrence of central neuropathies in other marine mammals, as in domoic acid-intoxicated California sea lions (*Zalophus californianus*) [2], or methylmercury and cyanotoxin-exposed short-beaked common dolphins (*Delphinus delphis*) [4] thus other forms of pollution can also be characterized. Additionally, long-lived marine mammals could serve as comparative pathology models for human neurological diseases [20].

Finally, understanding *in situ* protein expression is a vital step in bridging the gap between currently available research techniques and future establishment of organoid models for various types of pathology [68]. Therefore, expanding the preliminary baseline reference data reported herein and understanding interactions between the markers, but also applying quantifiable biomolecular techniques will be crucial to understand pathophysiological processes in cetaceans.

Supporting information

S1 Fig. Age-length estimation curve for the tested bottlenose dolphins.
(TIF)

S2 Fig. Shapiro-Wilks tests for normality.
(TIF)

S3 Fig. Raw images of the Western blot membranes for DGK-ζ, Bcl-2, Aβ and NF200 antibodies, captured with the iBright machine (ThermoFisherScientific) and used in Fig 1. The blue "X" marks the lanes and rows that are not included in the final image. Nota bene: The 9 left lanes of these blots correspond to species not included in this study.
(ZIP)

S4 Fig. Apaf-1-IR localizes to Nissl-substance in large pyramidal neurons of ID343. Other neurons display an agranularcytoplasmic IR (intensity score 2). Magnification 400x.
(TIF)

S5 Fig. Acellular perivascular Apaf-1 positivity in IC of ID201. Magnification 400x.
(TIF)

S6 Fig. Box-plot demonstrating the difference in the histo score average between dolphins brains classified according to their IHC patterns.
(TIF)

S7 Fig. Overview of histopathological CNS-lesions visible in hematoxylin-eosin slides of the dolphins in this study.
(ZIP)

S1 Table. Results of the statistical comparisons of groups made according to A) morphopathological findings in haematoxylin-eosin stained sections, B) immunohistochemical findings C) age. In gray—results that do not fit into the parametric/non-parametric category according to results of the Shapiro-Wilks and/or Levene's tests. If the group differences persist in post-hoc analyses, level of adjustment for α-error are documented. Bf—Bonferroni adjustment for α-error.
(PDF)

S2 Table. Summary of the ID, sex, body length, full histopathological findings of the CNS, and the most probable cause of death of the dolphins included in this study.
(PDF)

Acknowledgments

The authors would like to thank Dr. Enrico Orvieto and Dr. Valentina Zappulli for their helpful collaboration in the scanning of the immunohistochemical slides, Dr. Elisa Giaretta for her assistance in the statistical analysis and to Enna Selmanovic for her proofreading of the edited document.

Author Contributions

Conceptualization: Sandro Mazzariol.

Funding acquisition: Sandro Mazzariol.

Methodology: Ksenia Orekhova, Cinzia Centelleghe, Davide Trez, Sandro Mazzariol.

Resources: Sandro Mazzariol.

Supervision: Cinzia Centelleghe, Sandro Mazzariol.

Validation: Cinzia Centelleghe.

Writing – original draft: Ksenia Orekhova.

Writing – review & editing: Cinzia Centelleghe, Giovanni Di Guardo, Jean-Marie Graïc, Bruno Cozzi, Ranieri Verin, Sandro Mazzariol.

References

1. Sierra E, Fernández A, Felipe-Jiménez I, Zucca D, Di Francesco G, Díaz-Delgado J, et al. Neurobrucellosis in a common bottlenose dolphin (Tursiops truncatus) stranded in the Canary Islands. BMC Vet Res. 2019; 15: 1–8.
2. Silvagni PA, Lowenstine LJ, Spraker T, Lipscomb TP, Gulland FMD. Pathology of domoic acid toxicity in California sea lions (Zalophus californianus). Vet Pathol. 2005; 42: 184–191. https://doi.org/10.1354/vp.42-2-184 PMID: 15753472
3. Morell M, Brownlow A, McGovern B, Raverty SA, Shadwick RE, André M. Implementation of a method to visualize noise-induced hearing loss in mass stranded cetaceans. Sci Rep. 2017; 7: 1–8.
4. Davis DA, Garamszegi SP, Banack SA, Dooley PD, Coyne TM, McLean DW, et al. Bmaa, methylmercury, and mechanisms of neurodegeneration in dolphins: A natural model of toxin exposure. Toxins. 2021. https://doi.org/10.3390/toxins13100697 PMID: 34678990
5. Ijsseldijk LL, Brownlow AC, Mazzariol S. Best practice on cetacean post mortem investigation and tissue sampling. 2019.
6. Summers B. Veterinary neuropathology. St. Louis Mo.: Mosby; 1995.
7. Gröschel M, Basta D, Ernst A, Mazurek B, Szczepek AJ. Acute noise exposure is associated with intrinsic apoptosis in murine central auditory pathway. Front Neurosci. 2018; 12: 1–14.
8. Ashraf QM, Mishra OP, Delivoria-Papadopoulos M. Mechanisms of expression of apoptotic protease activating factor-1 (Apaf-1) in nuclear, mitochondrial and cytosolic fractions of the cerebral cortex of

newborn piglets. Neurosci Lett. 2007; 415: 253–258. https://doi.org/10.1016/j.neulet.2007.01.023 PMID: 17275190

9. Goto K, Tanaka T, Nakano T, Okada M, Hozumi Y, Topham MK, et al. DGKζ under stress conditions: "To be nuclear or cytoplasmic, that is the question". Adv Biol Regul. 2014; 54: 242–253. https://doi.org/10.1016/j.jbior.2013.08.007 PMID: 24119575
10. Di Guardo G, Di Francesco CE, Eleni C, Cocumelli C, Scholl F, Casalone C, et al. Morbillivirus infection in cetaceans stranded along the Italian coastline: Pathological, immunohistochemical and biomolecular findings. Res Vet Sci. 2013; 94: 132–137. https://doi.org/10.1016/j.rvsc.2012.07.030 PMID: 22921372
11. Díaz-Delgado J, Fernández A, Sierra E, Sacchini S, Andrada M, Vela AI, et al. Pathologic findings and causes of death of stranded cetaceans in the Canary Islands (2006–2012). PLoS ONE. 2018. https://doi.org/10.1371/journal.pone.0204444 PMID: 30289951
12. Henderson D, Bielefeld EC, Harris KC, Hu BH. The role of oxidative stress in noise-induced hearing loss. Ear and Hearing. 2006. pp. 1–19. https://doi.org/10.1097/01.aud.0000191942.36672.f3 PMID: 16446561
13. Di Filippo M, Sarchielli P, Picconi B, Calabresi P. Neuroinflammation and synaptic plasticity: theoretical basis for a novel, immune-centred, therapeutic approach to neurological disorders. Trends in Pharmacological Sciences. Elsevier Current Trends; 2008. pp. 402–412. https://doi.org/10.1016/j.tips.2008.06.005 PMID: 18617277
14. Panganiban CH, Barth JL, Darbelli L, Xing Y, Zhang J, Li H, et al. Noise-induced dysregulation of Quaking RNA binding proteins contributes to auditory nerve demyelination and hearing loss. J Neurosci. 2018; 38: 2551–2568. https://doi.org/10.1523/JNEUROSCI.2487-17.2018 PMID: 29437856
15. Gama Sosa MA, De Gasperi R, Pryor D, Perez Garcia GS, Perez GM, Abutarboush R, et al. Low-level blast exposure induces chronic vascular remodeling, perivascular astrocytic degeneration and vascular-associated neuroinflammation. Acta Neuropathol Commun. 2021; 9: 1–27.
16. Wang W, Zhang LS, Zinsmaier AK, Patterson G, Leptich EJ, Shoemaker SL, et al. Neuroinflammation mediates noise-induced synaptic imbalance and tinnitus in rodent models. PLoS Biol. 2019; 17: e3000307. https://doi.org/10.1371/journal.pbio.3000307 PMID: 31211773
17. Glezer II, Hof PR, Morgane PJ. Comparative analysis of calcium-binding protein-immunoreactive neuronal populations in the auditory and visual systems of the bottlenose dolphin (Tursiops truncatus) and the macaque monkey (Macaca fascicularis). 1998; 15: 203–237.
18. Hof PR, Glezer II, Condé F, Flagg RA, Rubin MB, Nimchinsky EA, et al. Cellular distribution of the calcium-binding proteins parvalbumin, calbindin, and calretinin in the neocortex of mammals: Phylogenetic and developmental patterns. J Chem Neuroanat. 1999; 16: 77–116. https://doi.org/10.1016/s0891-0618(98)00065-9 PMID: 10223310
19. Cozzi B, Roncon G, Granato A, Giurisato M, Castagna M, Peruffo A, et al. The claustrum of the bottlenose dolphin Tursiops truncatus (Montagu 1821). Front Syst Neurosci. 2014; 8: 1–8.
20. Gunn-Moore D, Kaidanovich-Beilin O, Gallego Iradi MC, Gunn-Moore F, Lovestone S. Alzheimer's disease in humans and other animals: A consequence of postreproductive life span and longevity rather than aging. Alzheimer's Dement. 2018; 14: 195–204.
21. Stylianaki I, Komnenou AT, Posantzis D, Nikolaou K, Papaioannou N. Alzheimer's disease-like pathological lesions in an aged bottlenose dolphin (Tursiops truncatus). Vet Rec Case Reports. 2019; 7: 1–5. https://doi.org/10.1136/vetreccr-2018-000700
22. Simona S, Antonio EDLM, Yania P. Amyloid-beta peptide and phosphorylated tau in the frontopolar cerebral cortex and in the cerebellum of toothed whales: aging vs hypoxia Summary Statement: Biology Open • Accepted manuscript.
23. Sacchini S, Herráez P, Arbelo M, Espinosa de los Monteros A, Sierra E, Rivero M, et al. Methodology and Neuromarkers for Cetaceans' Brains. Vet Sci. 2022; 9: 1–19. https://doi.org/10.3390/vetsci9020038 PMID: 35202291
24. Mazzariol S, Centelleghe C, Cozzi B, Povinelli M, Marcer F, Ferri N, et al. Multidisciplinary studies on a sick-leader syndrome-associated mass stranding of sperm whales (Physeter macrocephalus) along the Adriatic coast of Italy. Sci Rep. 2018; 8: 1–18.
25. Ridgway SH. The Auditory Central Nervous System of Dolphins. Springer, New York, NY; 2000. pp. 273–293.
26. Morell M, IJsseldijk LL, Piscitelli-Doshkov M, Ostertag S, Estrade V, Haulena M, et al. Cochlear apical morphology in toothed whales: Using the pairing hair cell—Deiters' cell as a marker to detect lesions. Anat Rec. 2021 [cited 1 Jul 2021]. https://doi.org/10.1002/ar.24680 PMID: 34096183
27. Choi SH, Choi CH. Noise-induced neural degeneration and therapeutic effect of antioxidant drugs. Korean J Audiol. 2015; 19: 111–119. https://doi.org/10.7874/jao.2015.19.3.111 PMID: 26771008

28. Abbott SD, Hughes LF, Bauer CA, Salvi R, Caspary DM. Detection of glutamate decarboxylase isoforms in rat inferior colliculus following acoustic exposure. Neuroscience. 1999; 93: 1375–1381. https://doi.org/10.1016/s0306-4522(99)00300-0 PMID: 10501462

29. Tamagno E, Parola M, Guglielmotto M, Santoro G, Bardini P, Marra L, et al. Multiple signaling events in amyloid β-induced, oxidative stress-dependent neuronal apoptosis. Free Radic Biol Med. 2003; 35: 45–58. https://doi.org/10.1016/s0891-5849(03)00244-2 PMID: 12826255

30. Nortley R, Korte N, Izquierdo P, Hirunpattarasilp C, Mishra A, Jaunmuktane Z, et al. Amyloid b oligomers constrict human capillaries in Alzheimer's disease via signaling to pericytes. Science (80-). 2019; 365. https://doi.org/10.1126/science.aav9518 PMID: 31221773

31. Fabrizi C, Silei V, Menegazzi M, Salmona M, Bugiani O, Tagliavini F, et al. The Stimulation of Inducible Nitric-oxide Synthase by the Prion Protein Fragment 106–126 in Human Microglia is Tumor Necrosis Factor-α-dependent and Involves p38 Mitogen-activated Protein Kinase. J Biol Chem. 2001; 276: 25692–25696. https://doi.org/10.1074/jbc.M100133200 PMID: 11316802

32. Posmantur R, Hayes RL, Dixon CE, Taft WC. Neurofilament 68 and Neurofilament 200 Protein Levels Decrease After Traumatic Brain Injury. J Neurotrauma. 1994; 11: 533–545. https://doi.org/10.1089/neu.1994.11.533 PMID: 7861446

33. Mages B, Aleithe S, Altmann S, Blietz A, Nitzsche B, Barthel H, et al. Impaired neurofilament integrity and neuronal morphology in different models of focal cerebral ischemia and human stroke tissue. Front Cell Neurosci. 2018; 12: 1–15.

34. Kraus KS, Ding D, Jiang H, Lobarinas E, Sun W, Salvi RJ. Relationship between noise-induced hearing-loss, persistent tinnitus and growth-associated protein-43 expression in the rat cochlear nucleus: Does synaptic plasticity in ventral cochlear nucleus suppress tinnitus? Neuroscience. 2011; 194: 309–325. https://doi.org/10.1016/j.neuroscience.2011.07.056 PMID: 21821100

35. K SG, L MC. Acceleration of age-related hearing loss by early noise exposure: evidence of a misspent youth. J Neurosci. 2006; 26: 2115–2123. https://doi.org/10.1523/JNEUROSCI.4985-05.2006 PMID: 16481444

36. Ballarin C, Papini L, Bortolotto A, Butti C, Peruffo A, Mazzariol S. An on-line tissue bank for marine mammals of the Mediterranean sea and adjacent waters. Hystrix—Ital J Mammal. 2006; 16. https://doi.org/10.4404/hystrix-16.2-4350

37. Graïc JM, Peruffo A, Grandis A, Cozzi B. Topographical and structural characterization of the V1–V2 transition zone in the visual cortex of the long-finned pilot whale Globicephala melas (Traill, 1809). Anat Rec. 2021; 304: 1105–1118. https://doi.org/10.1002/AR.24558 PMID: 33119932

38. De Vreese S, André M, Cozzi B, Centelleghe C, Van Der Schaar M, Mazzariol S. Morphological Evidence for the Sensitivity of the Ear Canal of Odontocetes as shown by Immunohistochemistry and Transmission Electron Microscopy. 2020; 1–17. https://doi.org/10.1038/s41598-020-61170-4 PMID: 32144309

39. Ramos-Vara J, Kiupel M, Baszler T, Bliven L, Brodersen B, Chelack B, et al. Suggested guidelines for immunohistochemical techniques in veterinary diagnostic laboratories. 2008; 413: 393–413.

40. MacNeil T, Vathiotis IA, Martinez-Morilla S, Yaghoobi V, Zugazagoitia J, Liu Y, et al. Antibody validation for protein expression on tissue slides: A protocol for immunohistochemistry. BioTechniques. Future Science Ltd; 2020. pp. 461–468. https://doi.org/10.2144/btn-2020-0095 PMID: 32852223

41. Mazzariol S, Centelleghe C, Petrella A, Marcer F, Beverelli M, Di Francesco CE, et al. Atypical Toxoplasmosis in a Mediterranean Monk Seal (Monachus monachus) Pup. J Comp Pathol. 2021; 184: 65–71. https://doi.org/10.1016/j.jcpa.2021.02.005 PMID: 33894880

42. Mazzariol S, Cozzi B, Centelleghe C. Handbook for Cetaceans' Strandings. 2015; 240.

43. Shinkawa C, Ito T, Hozumi Y, Chiba M, Matsui H, Goto K, et al. Expression and localization of diacylglycerol kinase ζ in guinea pig cochlea and its functional implication under noise-exposure stress conditions. Histochem Cell Biol. 2019; 151: 461–474. https://doi.org/10.1007/s00418-019-01781-9 PMID: 30963236

44. Pun PBL, Kan EM, Salim A, Li Z, Ng KC, Moochhala SM, et al. Low level primary blast injury in rodent brain. Front Neurol. 2011;APR: 1–15.

45. Rose J, Brian C, Woods J, Pappa A, Panayiotidis MI, Powers R, et al. Mitochondrial dysfunction in glial cells: Implications for neuronal homeostasis and survival. Toxicology. 2017; 391: 109–115. https://doi.org/10.1016/j.tox.2017.06.011 PMID: 28655545

46. Chong ZZ, Kang JQ, Maiese K. Apaf-1, Bcl-xL, cytochrome c, and caspase-9 form the critical elements for cerebral vascular protection by erythropoietin. J Cereb Blood Flow Metab. 2003; 23: 320–330. https://doi.org/10.1097/01.WCB.0000050061.57184.AE PMID: 12621307

47. Berrich M, Boulouis H- J, Monteil M, Kieda C, Haddad N. Vascular Endothelium and Vector Borne Pathogen Interactions. Curr Immunol Rev. 2012; 8: 227–247. https://doi.org/10.2174/157339512800672010

48. Intengan HD, Schiffrin EL. Vascular remodeling in hypertension. Hypertens Princ Pract. 2001;Hypertensi: 581–587. https://doi.org/10.1161/hy09t1.096249 PMID: 11566935

49. Yoshida H, Kong Y, Yoshida R, Elia AJ, Hakem A, Hakem R, et al. Apaf1 Is Required for Mitochondrial Pathways of Apoptosis and Brain Development. 1998; 94: 739–750.

50. Kole AJ, Annis RP, Deshmukh M. Mature neurons: equipped for survival. Cell Death Dis. 2013; 4: 1–8. https://doi.org/10.1038/cddis.2013.220 PMID: 23807218

51. Okada M, Hozumi Y, Tanaka T, Suzuki Y, Yanagida M, Araki Y, et al. DGK ζ is degraded through the cytoplasmic ubiquitin—proteasome system under excitotoxic conditions, which causes neuronal apoptosis because of aberrant cell cycle reentry. Cell Signal. 2012; 24: 1573–1582. https://doi.org/10.1016/j.cellsig.2012.03.021 PMID: 22516102

52. Siddiqui WA, Ahad A, Ahsan H. The mystery of BCL2 family: Bcl-2 proteins and apoptosis: an update. Arch Toxicol. 2015; 89: 289–317. https://doi.org/10.1007/s00204-014-1448-7 PMID: 25618543

53. Shinoura N, Yoshida Y, Nishimura M, Muramatsu Y, Asai A, Kirino T, et al. Expression level of Bcl-2 determines anti- or proapoptotic function. Cancer Res. 1999; 59: 4119–4128. PMID: 10463617

54. Querfurth HW, Laferla FM. Alzheimer's Disease. 2010; 329–344.

55. Bros P, Delatour V, Vialaret J, Lalere B, Barthelemy N, Gabelle A, et al. Quantitative detection of amyloid-β peptides by mass spectrometry: State of the art and clinical applications. Clinical Chemistry and Laboratory Medicine. Walter de Gruyter GmbH; 2015. pp. 1483–1493. https://doi.org/10.1515/cclm-2014-1048 PMID: 25719328

56. Hefter D, Draguhn A. APP as a protective factor in acute neuronal insults. Frontiers in Molecular Neuroscience. Frontiers Media S.A.; 2017. p. 22. https://doi.org/10.3389/fnmol.2017.00022 PMID: 28210211

57. Ridgway SH, Brownson RH, van Alstyne KR, Hauser RA. Higher neuron densities in the cerebral cortex and larger cerebellums may limit dive times of delphinids compared to deep-diving toothed whales. PLoS One. 2019; 14: e0226206. https://doi.org/10.1371/journal.pone.0226206 PMID: 31841529

58. von Mikecz A. Pathology and function of nuclear amyloid: Protein homeostasis matters. Nucleus (United States). Landes Bioscience; 2014. https://doi.org/10.4161/nucl.29404 PMID: 25482120

59. Sharoar MG, Islam MI, Shahnawaz M, Shin SY, Park IS. Amyloid β binds procaspase-9 to inhibit assembly of Apaf-1 apoptosome and intrinsic apoptosis pathway. Biochim Biophys Acta—Mol Cell Res. 2014; 1843: 685–693. https://doi.org/10.1016/j.bbamcr.2014.01.008 PMID: 24424093

60. Cantú-Medellín N, Byrd B, Hohn A, Vázquez-Medina JP, Zenteno-Savín T. Differential antioxidant protection in tissues from marine mammals with distinct diving capacities. Shallow/short vs. deep/long divers. Comp Biochem Physiol—A Mol Integr Physiol. 2011; 158: 438–443. https://doi.org/10.1016/j.cbpa.2010.11.029 PMID: 21147244

61. Di Guardo G. Cetaceans, models for human disease? Research in Veterinary Science. Elsevier B.V.; 2018. pp. 43–44. https://doi.org/10.1016/j.rvsc.2018.05.012 PMID: 29804053

62. Ohm TG, Braak H. Auditory brainstem nuclei in Alzheimer's disease. Neurosci Lett. 1989; 96: 60–63. https://doi.org/10.1016/0304-3940(89)90243-7 PMID: 2648201

63. Shityakov S, Hayashi K, Störk S, Scheper V, Lenarz T, Förster CY. The conspicuous link between ear, brain and heart–could neurotrophin-treatment of age-related hearing loss help prevent alzheimer's disease and associated amyloid cardiomyopathy? Biomolecules. 2021; 11. https://doi.org/10.3390/biom11060900 PMID: 34204299

64. Laurén J, Gimbel DA, Nygaard HB, Gilbert JW, Strittmatter SM. Cellular prion protein mediates impairment of synaptic plasticity by amyloid-B oligomers. Nature. 2009; 457: 1128–1132. https://doi.org/10.1038/nature07761 PMID: 19242475

65. Morell M, Raverty SA, Mulsow J, Haulena M, Barrett-Lennard L, Nordstrom CA, et al. Combining Cochlear Analysis and Auditory Evoked Potentials in a Beluga Whale With High-Frequency Hearing Loss. Front Vet Sci. 2020; 7: 534917. https://doi.org/10.3389/fvets.2020.534917 PMID: 33330679

66. Orekhova K, Mazzariol S, Sussan B, Bucci M, Bonsembiante F, Verin R, et al. Immunohistochemical Markers of Apoptotic and Hypoxic Damage Facilitate Evidence-Based Assessment in Pups with Neurological Disorders. Vet Sci 2021, Vol 8, Page 203. 2021; 8: 203. https://doi.org/10.3390/vetsci8100203 PMID: 34679033

67. Bernier PJ, Parent A. Bcl-2 protein as a marker of neuronal immaturity in postnatal primate brain. J Neurosci. 1998; 18: 2486–2497. https://doi.org/10.1523/JNEUROSCI.18-07-02486.1998 PMID: 9502809

68. Sun AX, Ng HH, Tan EK. Translational potential of human brain organoids. Ann Clin Transl Neurol. 2018; 5: 226–235. https://doi.org/10.1002/acn3.505 PMID: 29468184

Addendum I: Using Machine Learning to Count Vestibulocochlear Nerve Fibers in Bottlenose Dolphins

While examination of the inner ear is an accepted practice (Guofu and Kaiya, 1992; Morell et al., 2022), few studies have reported fiber densities of the vestibulocochlear nerve for the bottlenose dolphin, and the number of examined specimens was limited. This study examined nerve fiber densities in transversal sections of the auditory nerves of 10 decomposition code 1 and 2 bottlenose dolphins using ilastik® machine learning (ML) algorithms. This may be a first step to determining noise-induced hearing loss that could be traced within a timeframe of weeks to months (Hurley et al., 2007) as opposed to hours to days (Raphael and Altschuler, 1991; Lim and Melnick, 1971).

Transverse, 4 μm-sections from formalin-fixed, paraffin embedded extracochlear auditory nerve segments of 10 bottlenose dolphins of varying ages from the European Marine Mammal Tissue Bank were immunostained using NF200, an antibody against heavy neurofilaments (Sigma-Aldrich, St. Louis, MO, USA: N0142, diluted 1:400). The slides were scanned (D-Sight®, Menarini Diagnostics, Florence, Italy), and each image analyzed to obtain three random regions of interest (ROI) corresponding to 1 mm^2 to measure the nerve fiber density. Three ROIs per dolphin were exported to ilastik®, where the cell counting algorithm was applied at three increasing levels of discrimination (Figure 8). This was done by increasing manual input of foreground (red dots) and background (green lines) reference points for 3 of the 30 images.

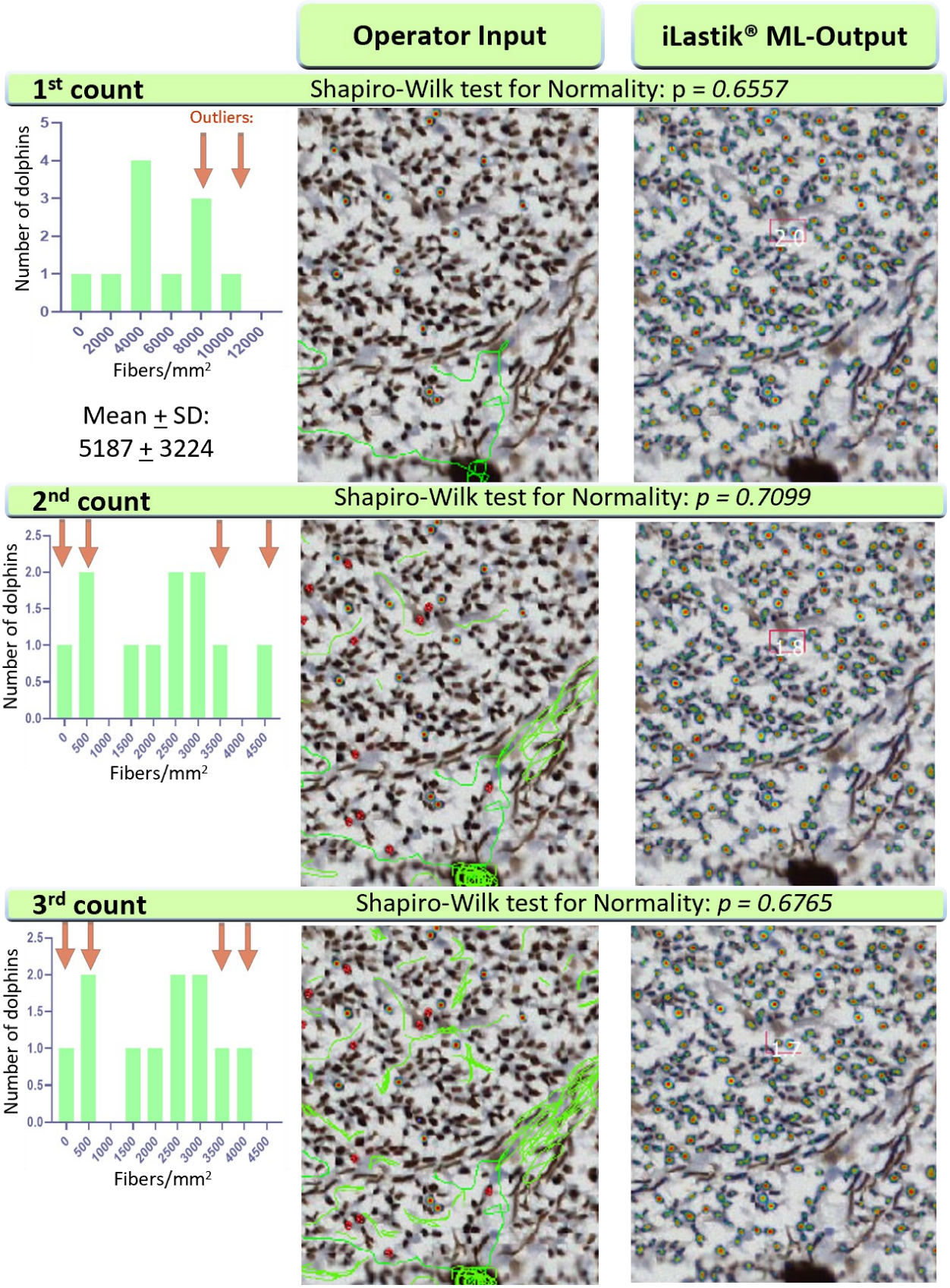

Figure 8. Example of ML training algorithm using increasing amount of operator input from the 1st count (top) to 3rd count (bottom).

Red dots – single transverse nerve fibers and green lines – background as "taught" by the operator (left) and inferred by the ML-algorithm (right). Graphs on the left display the distribution of the fiber counts in the three separate scenarios. Red arrows indicate the outliers.

Means of the fiber counts were obtained for each animal and are displayed in Table 5.

Table 5. Fiber density estimates at three increasing levels of discrimination with the ilastik® Cell Count algorithm. In italics: outliers.

Dolphin	VIII Nerve Fiber Density / mm²		
	1st count	2nd count	3rd count
ID 20	5382	2976	2904
ID 89	7340	*3674*	*3467*
ID 146	4466	2449	2345
ID 196	3067	1815	1759
ID 319	*8532*	3169	3007
ID 344	8251	*4449*	*4131*
ID 133	2801	*430*	*430*
ID 203	3105	1496	1455
ID 123	3195	*319*	*318*
ID 144	*10912*	2643	2389

The use of NF200 marker for visualizing transverse myelinated VIIIth nerve fibers was successful, but as expected, the results of the fiber counts may vary according to the amount of operator input when "teaching" the cell-counting algorithm of the ilastik® interface. Mean densities of auditory nerve fibers were normally distributed and within the same order of magnitude as those previously reported (3710 4188 and for the left and right VIIIth nerve, respectively, Guofu and Kaiya, 1992). Neither the present nor the referenced study corrected for tissue shrinkage.

In this case, the algorithm applied for the 2nd count could represent the real nerve fiber density in bottlenose dolphins. Any baseline values must be comprised of tissues that were sampled, processed, and counted in the same way, but standardized sampling and algorithms could help assess auditory nerve physiopathology in a wide range of cetacean species.

Publication III: Multimodal Assessment of Bottlenose Dolphin Auditory Nuclei Using 7-Tesla MRI, Immunohistochemistry and Stereology

Good cognitive health and acoustic perception are essential for the survival and welfare of cetaceans, yet few quantitative techniques are available to monitor them. Both natural and man-made threats can affect the health of the cetacean CNS, including infectious diseases, toxins from harmful algal blooms, contaminants from agricultural and industrial run-off, and noise from anthropogenic sources such as air guns and sonar. While qualitative pathological assessments are valuable in the assessment of neuropathology, quantitative approaches such as stereology (Kern et al., 2011; Mortensen et al., 2014; Nieder et al., 2022) help contextualize subjective evaluations, and multimodal investigation reduces the effect of artifacts.

In this study, we combined the use of 7-Tesla (7T) MRI and stereology in the *post-mortem* assessment of the IC and VCN of two bottlenose dolphins, using human brain tissue as a control. Protein expression of Aβ, fibronectin, TAR DNA-binding protein 43 (TDP-43), phosphorylated neurofilament protein, GFAP and Iba1 was quantified using customized systematic random sampling probes. The numbers and densities of immunoreactive neurons, axons and glia were assessed in relation to tissue volumes before and after processing, and the connectivity of the auditory brainstem and midbrain nuclei was visualized using DTI.

The results yielded reliable cell counts with coefficients of error <10% for most of the tested markers. Neuronal counts averaged at 6.13 million neurons in the IC and 316,379 in the VCN. Immunoreactivity patterns of fibronectin in the dolphin resembled those of a human chronic encephalopathy brain. In conjunction with presence of intranuclear Aβ and TDP-43, this suggests that neuroprotective protein expression to offset insults like hypoxia may constitute a noxious response in humans, while representing a physiological baseline in dolphins.

Systematic biomarker validation and quantification enables an evidence-based approach to monitoring cetacean CNS health, assessing potential acoustic trauma, and translational modeling of human neurodegenerative disease. This work expands our knowledge of the baseline neurochemical signature and connectivity of the cetacean auditory nuclei. It can be valuable in future comparisons with other individuals, cases with inconclusive pathological findings, and more species to deepen our understanding of cetacean CNS anatomy, physiology, and pathology in the context of a human-dominated environment.

veterinary sciences

IMPACT FACTOR 2.518

Indexed in: PubMed

Article

Multimodal Assessment of Bottlenose Dolphin Auditory Nuclei Using 7-Tesla MRI, Immunohistochemistry and Stereology

Ksenia Orekhova, Enna Selmanovic, Rita De Gasperi, Miguel A. Gama Sosa, Bridget Wicinski, Brigid Maloney, Alan Seifert, Akbar Alipour, Priti Balchandani, Tommaso Gerussi et al.

Special Issue

Neurodegenerative Diseases: What Can We Find Out in the Animal Brain?

Edited by

Prof. Dr. Simona Sacchini

MDPI

https://doi.org/10.3390/vetsci9120692

veterinary sciences

MDPI

Article

Multimodal Assessment of Bottlenose Dolphin Auditory Nuclei Using 7-Tesla MRI, Immunohistochemistry and Stereology

Ksenia Orekhova [1,*], Enna Selmanovic [2], Rita De Gasperi [3,4,5], Miguel A. Gama Sosa [3,4,6], Bridget Wicinski [2], Brigid Maloney [7], Alan Seifert [8], Akbar Alipour [8], Priti Balchandani [8], Tommaso Gerussi [1], Jean-Marie Graïc [1], Cinzia Centelleghe [1], Giovanni Di Guardo [9,†], Sandro Mazzariol [1] and Patrick R. Hof [2]

1 Department of Comparative Biomedicine and Food Science, University of Padova AGRIPOLIS, Viale dell'Università 16, 35020 Legnaro, Italy
2 Nash Family Department of Neuroscience, Friedman Brain Institute, Icahn School of Medicine at Mount Sinai, New York, NY 10029, USA
3 Department of Psychiatry, Icahn School of Medicine at Mount Sinai, New York, NY 10029, USA
4 Friedman Brain Institute, Icahn School of Medicine at Mount Sinai, New York, NY 10029, USA
5 Research and Development Service, James J. Peters Department of Veterans Affairs Medical Center, Bronx, New York, NY 10468, USA
6 General Medical Research Service, James J. Peters Department of Veterans Affairs Medical Center, Bronx, New York, NY 10468, USA
7 Laboratory of Neurogenetics of Vocal Learning, Rockefeller University, New York, NY 10065, USA
8 Department of Radiology, BioMedical Engineering and Imaging Institute (BMEII), Graduate School of Biomedical Sciences, Icahn School of Medicine at Mount Sinai, New York, NY 10029, USA
9 Faculty of Veterinary Medicine, University of Teramo, 64100 Teramo, Italy
* Correspondence: ksenia.orekhova@phd.unipd.it
† Retired.

Simple Summary: Monitoring cetacean health is important considering the high strain from both natural and human-related threats. Most of these, such as *Cetacean morbillivirus* and man-made pollution in form of toxins and noise, affect nervous tissues and brain function. Neuropathological research in cetaceans has been qualitative or semiquantitative. Here, we use stereology to quantify protein expression in neurons, axons, and glial cells in the auditory nuclei of a bottlenose dolphin and correlate the values to their pre-processed volumes from MRI scans. This multimodal approach is aims to avoid artifacts that may arise using either methodology. Similarities in protein expression between a healthy dolphin and a human with brain trauma implies that dolphins might have a baseline neurochemical buffer against low oxygen (hypoxia). This study will help expand our quantitative understanding of health and disease in cetacean brains.

Abstract: The importance of assessing neurochemical processes in the cetacean brain as a tool for monitoring their cognitive health and to indirectly model human neurodegenerative conditions is increasingly evident, although available data are largely semiquantitative. High-resolution MRI for post-mortem brains and stereology allow for quantitative assessments of the cetacean brain. In this study, we scanned two brains of bottlenose dolphins in a 7-Tesla (7T) MR scanner and assessed the connectivity of the inferior colliculi and ventral cochlear nuclei using diffusion tensor imaging (DTI). Serial thick sections were investigated stereologically in one of the dolphins to generate rigorous quantitative estimates of identifiable cell types according to their morphology and expression of molecular markers, yielding reliable cell counts with most coefficients of error <10%. Fibronectin immunoreactivity in the dolphin resembled the pattern in a human chronic traumatic encephalopathy brain, suggesting that neurochemical compensation for insults such as hypoxia may constitute a noxious response in humans, while being physiological in dolphins. These data contribute to a growing body of knowledge on the morphological and neurochemical properties of the dolphin brain and highlight a stereological and neuroimaging workflow that may enable quantitative and translational assessment of pathological processes in the dolphin brain in the future.

Keywords: cetaceans; animals; stereology; MRI; immunohistochemistry; human; neurodegeneration; chronic traumatic encephalopathy; hypoxia; amyloid β; fibronectin; microglia; astrocytes

Citation: Orekhova, K.; Selmanovic, E.; De Gasperi, R.; Gama Sosa, M.A.; Wicinski, B.; Maloney, B.; Seifert, A.; Alipour, A.; Balchandani, P.; Gerussi, T.; et al. Multimodal Assessment of Bottlenose Dolphin Auditory Nuclei Using 7-Tesla MRI, Immunohistochemistry and Stereology. *Vet. Sci.* **2022**, *9*, 692. https://doi.org/10.3390/vetsci9120692

Academic Editor: Simona Sacchini

Received: 22 November 2022
Accepted: 9 December 2022
Published: 13 December 2022

1. Introduction

The dolphin brain is subject to a lot of scientific interest for several reasons, although many aspects of its neurochemical functions and connectivity remain unexplored. It is an example of convergent evolution between artiodactyls and humans in terms of their large brain size and extensive gyrification [1], the longevity of their individuals, the development of age-related degenerative conditions, and similar pathological reactions following exposure to infections, toxins, and certain intensities and frequencies of sound [2–6].

Under baseline conditions, the dolphin brain is exposed to variable and prolonged periods of limited oxygen during diving. It could therefore display characteristics of human brains that have been exposed to chronic trauma and neurochemical changes consistent with hypoxia, as in the case of patients with chronic traumatic encephalopathy (CTE) [7].

Several lines of research hint at morphological and molecular adaptations of the cetacean nervous tissues to buffer the strain of deep diving in a cool aquatic environment under high pressure, including the evolution of cervical rete mirabilia that ensure steady blood flow [8], higher levels of myelination [9], and antioxidant proteins [10] in deeper- versus shallow-diving cetacean species. Comparatively high levels of uncoupling proteins are hypothesized to aid in non-shivering thermogenesis to preserve brain function under cold ambient temperatures [11], although this hypothesis has been disputed [12].

Our recent work focused on validating proteins as indices of the health status of bottlenose dolphin (*Tursiops truncatus*) brains, particularly in the dubious cases of potential anthropogenic acoustic trauma [5]. However, only a semiquantitative approach was available at the time. In the current study, we focused on stereological estimates of validated neuronal and glial proteins in the inferior colliculus (IC) and ventral cochlear nucleus (VCN) of a bottlenose dolphin and outline a workflow that could be used in further studies of these and other brain areas. A similar approach was taken by Nieder and colleagues (2022) [13] when examining neuronal numbers in the lateral superior olivary nucleus of short-beaked common dolphins (*Delphinus delphis*).

We refer to 7T-MRI and DTI data to assess the volumes and connectivity of the auditory nuclei of two bottlenose dolphins, one of which was used for quantitative immunohistochemical assessment. This multimodal approach may help to circumvent artifacts due to the opportunistic nature of cetacean brain recovery and sampling, particularly with respect to effects of processing-induced tissue shrinkage.

Neuronal proteins, such as amyloid-β (Aβ) protein, associated with human neurodegenerative diseases, such as Alzheimer's disease (AD), have already been used in previous cetacean brain studies. They are conversely linked to tolerance to hypoxia [5,14], and are quantified herein alongside TAR DNA-binding protein 43 (TDP-43)—another protein aggregating in diseases such as amyotrophic lateral sclerosis, Parkinson's disease, and frontotemporal dementia [15]—and the extracellular matrix protein fibronectin. TDP-43 was previously observed in the brains of seven common dolphins with known methylmercury and cyanotoxin intoxication [4]. Fibronectin was primarily intended to visualize vascular and capillary networks, as it is an important constituent of the extracellular matrix of the vascular basal membrane [16,17], and capillary length and density are known to change under metabolic stress conditions such as hypoxia [18,19]. Fibronectin also plays a role in the extracellular matrix surrounding neurons and facilitates repair following injury [20].

SMI-312, an antibody targeting phosphorylated medium and heavy neurofilament fibers, was used to quantify axon length and density, while Iba-1 and GFAP were used to quantify microglial and astrocytic cells, respectively. Furthermore, qualitative trends between fibronectin expression in human CTE are observed in comparison to dolphin and healthy human tissues.

The aim of this study was to provide the first quantitative estimates of neuronal, axonal, and glial cell populations within the dolphin IC and VCN, outlining a protocol for stereological probe design and limitations that could serve as a platform for standardized quantitative comparisons between different individual animals and species.

2. Materials and Methods

2.1. Specimens

The brains from bottlenose dolphins used in this study were obtained from the Peter J. Morgane Collection on the Cetacean Brain. Marine 0116 was a 15-year-old female from an aquarium whose death in 1995 was associated with liver disease and pancreatitis. Its brain consisted of both hemispheres cut mid-sagittally and was stored in 4% paraformaldehyde solution at 4 °C. The left hemisphere was available from another animal, Marine 0142, and was stored in 10% neutral-buffered formalin at 4 °C. No further information was available on Marine 0142′s history, but the size of the brain was somewhat larger than that of Marine 0116, implying that it was extracted from an adult dolphin. A separate bottlenose dolphin brain (Dolphin 2) was studied using archived coronal Nissl-stained and celloidin-embedded sections (for more information, refer to Hof and Van der Gucht, 2006 [21]). Neuronal morphology was assessed using Nissl-stained sections in all three dolphins, and in Marine 0116 and 0142 the MRI scans were assessed, yielding no obvious pathology. No animals were euthanized for this study.

Archived tissues from three human brains were used for comparisons and as controls: one healthy male individual (74 years, 5 h post-mortem interval, Clinical Dementia Score 0 (=control), Braak NFT stage I), one with AD and severe cognitive impairment (male, 85 years old, 11 h post-mortem interval, Clinical Dementia Rating 3, Mini-Mental State Exam 11, Thal amyloid stage 4, Braak tangle stage V), and one with advanced CTE and moderate hypoxic-ischemic encephalopathy (male, 69 years old, 9 h post-mortem interval, moderate cerebrovascular disease and athero-arteriolosclerosis; severe post-mortem autolysis). Further information on these specimens is detailed in Ackermans and colleagues (2022) [22].

2.2. MRI and DTI

Image acquisition was performed using a whole-body 7T MRI scanner (Magnetom, Siemens Healthineers, Erlangen, Germany) and a 1-channel-transmit 32-channel-receive radiofrequency head coil (Nova Medical, Wilmington, MA, USA).

The fixed hemispheres, while still immersed in formalin, were exposed to a vacuum of −1 bar and agitated for 30 min. The hemispheres were then removed from formalin and placed together into a custom-built 7T ex vivo brain-imaging vessel [23]. The vessel was filled with Fluorinert (FC-770, TMC industries, Waconia, MN, USA), the vessel lid was secured with machine screws and Kapton tape, two vent ports in the lid were opened, and the container was again exposed to a vacuum of −1 bar and agitated for 10 min. Following this, residual formalin was drained off, the Fluorinert level was topped off, and the vent ports were closed and sealed with Kapton tape. The specimen container was placed into the radiofrequency coil with the brain in an orientation consistent with head-first supine orientation in a human, and inserted into the scanner. Localizer images were acquired, and iterative magnetic field shimming was performed by 3D phase mapping.

High-resolution anatomical images were acquired with 3D phase-cycled balanced steady-state free precession (PC-bSSFP) and 3D multi-echo gradient echo (ME-GRE) with root-sum-of-squares echo recombination. The PC-bSSFP acquisition parameters were: field of view (FOV) = 196 × 156 × 128 mm, voxel resolution = 250 μm^3 isotropic, repetition time (TR) = 8.01 ms, echo time (TE) = 4.01 ms, flip angle (FA) = 30°, bandwidth (BW) = 277 Hz/pixel, parallel imaging acceleration by generalized autocalibrating partially parallel acquisition (GRAPPA) [24] with acceleration factor R = 2, 2 acquisitions per phase increment, phase increment cycle = {0°, 180°, 90°, 270°}, scan time = 67 min, and recombination of individual phase increment images by root-sum-of-squares. ME-GRE acquisition parameters were: field of view = 192 × 156 × 134 mm, voxel resolution = 380 µm isotropic, TR = 38 ms, TE = {5, 10, 15, 20, 25, 30} ms with bipolar readouts, FA = 18°, BW = 260 Hz/pixel, GRAPPA R = 2, 1 signal average, scan time = 47 min 56 s, and recombination of individual echo images by coregistration using FSL FLIRT [25,26] followed by root-sum-of-squares.

Diffusion-weighted imaging was performed using diffusion-weighted 3D steady-state free precession (DW-SSFP) [27] with the following acquisition parameters: field of view = 204 × 179 × 150 mm, voxel resolution = 850 µm isotropic, TR = 29 ms, TE = 21 ms, FA = 24°, BW = 393 Hz/pixel, echo-planar imaging factor = 3, echo spacing = 3.09 ms, diffusion encoding gradient amplitude = 52 mT/m and duration 13.56 ms for a q-value of 300 cm^{-1} (corresponding to an estimated b-value of 3594 s/mm^2), 120 diffusion encoding directions, six eddy-current-matched b = 0 acquisitions with diffusion encoding gradient amplitude = 52 mT/m and duration = 0.92 ms for a q-value of 20 cm^{-1}, and scan time = 12 h 36 min. Eddy-current correction was performed using FSL eddy [28], and preliminary diffusion-tensor analysis was performed using FSL dtifit.

Diffusion tractography was performed using DSI Studio (http://dsi-studio.labsolver.org, accessed on 22 May 2022). A deterministic fiber-tracking algorithm [29] was used. Seeding, ending, and regions of interest (ROIs) were placed in the vestibulocochlear nerve (AN), VCN, IC central nucleus and external cortex, IC brachium, and the medial geniculate nucleus (MGN) using imported, manually segmented regions from the ITK-Snap software (www.itksnap.org), which automatically calculated their volumes [30]. Seed-to-end, seed-to-terminative and end-to-end connections were evaluated for each nucleus of the brainstem and mesencephalic auditory pathway. The anisotropy threshold was 0.1. The angular threshold was 60°. The step size was randomly selected from 0.5 voxel to 1.5 voxels. Tracks with a length shorter than 20 or longer than 300 mm were discarded. A total of 1,000,000 seeds were placed for each tract calculation.

2.3. Western Blot and BLAST

Brain tissue (about 30 mg) was homogenized in 0.1 M Tris HCl buffer pH 7.4, containing 0.15 M NaCl, 5 mM EDTA, 1% Triton × 100/0.1% SDS and Halt protease and phosphatase inhibitor cocktail (Pierce, Rockford, IL, USA). Protein concentration was determined with BCA reagent (Pierce). Protein samples (50 µg) were separated by SDS-PAGE and blotted onto polyvinylidene difluoride (PVDF) membranes (Millipore-Sigma, Burlington, MA, USA). Blots were blocked with 25 mM Tris HCl, pH 7.5, 0.15 M NaCl, 0.1% Tween-20 (TBST), 5% nonfat dry milk and probed overnight with the relevant primary antibody diluted in blocking solution. Primary antibodies used for Western blots were the same as those for immunohistochemistry and are listed in Table 1. Blots were then incubated for 1.5 h with the appropriate horseradish peroxidase (HRP) conjugated secondary antibody (Cytiva, Marlborough, MA, USA: anti-rabbit NA934 and anti-mouse NA 931, and ThermoFisher Scientific, Waltham, MA, USA: anti-rat A18749 antibodies, respectively) diluted in blocking solution (1:7500). The bands were visualized by ECL Prime (Cytiva, RPN 2232) and imaged with an ImageQuant 800 imaging station (Cytiva), with a Precision Plus Protein All Blue prestained protein standard ladder (Biorad 1610373) on either side of the samples. In case of inconclusive results with Western blot, the basic linear alignment search tool (BLAST) was implemented as previously reported [5] to confirm antibody specificity.

2.4. Immunohistochemistry

Tissue blocks comprising the entire right (Marine 0116) and left (Marine 0142) IC and VCN were sampled from the formalin-fixed brains. Only the left hemisphere was available for Marine 0142, and the caudal part (about one-third) was missing. Brain sections from Marine 0116 were discarded following the pilot studies due to tissue deformation when drying on the slide. Following several washes in phosphate-buffered saline (PBS, pH 7.0), the blocks were cut coronally into 50 µm-thick sections using a vibratome (Leica VT1000S) and stored in solution with 0.1% sodium azide. Every 30th serial section of the LIC and every 20th section of the VCN was used for testing different antibodies that had elicited an immunoreactivity in pilot immunohistochemistry runs, which included dolphin primary auditory cortex sections. Antibodies that were initially tested but then excluded due to lack of reactivity can be found in Annex 1, Table A1. The antibodies chosen for stereology included anti-Aβ (ThermoFisher Scientific, #700254, diluted 1:500), anti-fibronectin (Sigma-

Aldrich, St. Louis, MO, USA: #F3648, 1:200), anti-TDP-43 (Biolegend, San Diego, CA, USA: #829901, 1:200) for neurons, antibody SMI-312 (Biolegend, #837904, 1:1000) against medium- and heavy-chain phosphorylated neurofilament proteins (pNFP) in axons, anti-Iba-1 (Wako, Neuss, Germany: #019-19741, 1:500) for microglia, and anti-GFAP (Dako, Düsseldorf, Germany: #Z0334, 1:500) for astrocytes. Appropriate secondary antibodies—biotinylated goat anti-rabbit (Vector Laboratories, Newark, CA, USA: #BA-1000-1.5) for Aβ, fibronectin, GFAP and Iba-1, biotinylated goat anti-rat (Vector Laboratories; #BA-9400-1.5) for TDP-43 and biotinylated donkey anti-mouse (Jackson ImmunoResesarch, West Grove, PA, USA: #715-065-150) for pNFP, respectively—were applied. Primary antibodies were omitted in concomitant negative control sections.

Table 1. Antibodies validated for bottlenose dolphin brains using immunohistochemistry (IHC) and Western blotting (WB) in this study.

Antibody	Host	Reactivity	Clonality	RRID	Catalogue Number	Dilution IHC	Dilution WB
Aβ	rabbit	rat, human, mouse, bottlenose dolphin	monoclonal	AB_2532306	700254	1:500	1:500 [1]
fibronectin	rabbit	human	polyclonal	AB_476976	F3648	1:200	1:1000
TDP-43	rat	human, Rat	monoclonal	AB_2750118	829901	1:200	1:1000
SMI-312	mouse	human, mouse, rat	monoclonal	AB_2566782	837904	1:1000	1:1000
Iba-1	rabbit	human, mouse, rat, other	polyclonal	AB_839504	019-1974	1:500	NA
GFAP	rabbit	cat, cow, dog, human, mouse, rat, sheep	polyclonal	AB_10013382	Z0334	1:500	1:1000

[1] Aβ-concentration in WB is derived from published work [5].

2.5. Microscopy and Stereology

Brightfield microscopy images and scans were taken on an Axiophot brightfield microscope (Carl Zeiss Microscopy, Jena, Germany), with a 20×/0.8 Plan-Apochromat and 40×/1.3 Oil Plan-Neofluar objective for immunohistochemical sections, and a 40×/0.6 Korr Plan-Neofluar objective for the archived Nissl sections using StereoInvestigator (version 11.03, MBF Bioscience, Williston, VT, USA).

Contours were traced around the whole of the left IC, and separate contours marked the neuron-dense, putative central IC nucleus (CN) and the surrounding tectosomes or external cortex (EC). The VCN was contoured in its entirety. The same procedure was followed for the right IC and VCN of Dolphin 2, whose Nissl-stained, serial, 35 µm-thick and celloidin-embedded coronal brain sections were assessed for differences in cell counts and densities arising from alternative tissue processing.

The volume of each subnucleus was calculated using the Cavalieri probe as recently reported by Nieder and colleagues (2022) [13], and the coefficient of error [31] calculated for each subnucleus was less than 0.09. Obtained volumes from processed tissue and from the MRI scans of the available brain hemispheres (left and right in Marine 0116; only left in Marine 0142) is represented in Table 2.

Image stacks in a systematic random sampling grid were acquired with a Z-step of 2 µm. The top of every sampling site was focused on manually. The optical fractionator workflow probe in StereoInvestigator (grid size 2000 × 2000 µm for the IC and 1000 × 1000 µm for the VCN, SRS grid layout at 100% of the region of interest, optical disector height 18 µm with 1-µm top and bottom guard zones, manual focus) was used on a series of 30 sections for IC and 20 sections for VCN, each separated by 1500 µm in the IC and 1000 µm in the VCN. For amyloid beta, TDP-43 and fibronectin, a counting frame of 150 × 150 µm was used, and neurons with nuclear, cytoplasmic, both, or no immunoreactivity were counted using different markers in StereoInvestigator. For Iba-1 and GFAP, a counting frame of 30 × 30 µm was used and cytoplasmic immunoreactivity

of microglia and astrocytes, respectively, was counted. In the case of pNFP, the axonal immunoreactivity and length density of the axons was recorded using a Spaceball probe with a radius of 18 µm.

Table 2. Comparison of IC and VCN volumes available from three bottlenose dolphin specimens.

Specimen	Auditory Nucleus	Volume MRI (mm^3)	Volume Cavalieri (mm^3)
Marine 0142	LIC	1775	1362
	LVCN	435	129 *
Marine 0116	LIC	1345	-
	LVCN	387	-
	RIC	1451	921
	RVCN	378	285
Dolphin 2 **	RIC	-	571
	LVCN	-	199

* This volume corresponds to the intact rostral two-thirds of the VCN. ** Dolphin 2 processed and embedded in a different way from Marine 0142 and 0116. L and R indicate the nuclei from the left and right hemisphere, respectively.

2.6. Data Analysis

Data analysis was performed using Microsoft Excel (from the Microsoft 365 apps package) and R version 4.2.1. Bar charts were created using GraphPad Prism 8. Heatmaps of 3-dimensional immunohistochemical marker distribution were generated following an R-script from Ackermans and colleagues (2022) [22], publicly available on GitHub (https://github.com/NLAckermans/Ackermans2022BovidTBI/blob/main/Muskox_heatmaps_220314.Rmd, accessed on 18 June 2022).

3. Results

3.1. MRI

The 7T-MRI scans enabled the identification and in situ volume estimate of unprocessed, formalin-fixed dolphin brain nuclei. Deterministic unihemispheric fiber tracking revealed strong connectivity between the auditory nuclei (VCN and lateral lemniscus and the cerebellum; Figure 1a), and the afferent auditory lemniscal pathway up to the IC, IC tectosomes, collicular brachium, and medial geniculate nucleus. The IC and its brachium were particularly rich in putative synaptic endings, corresponding to the former's role as a central integrative hub for sensory input processing, while the latter and the medial geniculate nucleus stood out in terms of the number of passing tracts (Figure 2). Overall, the cetacean auditory pathways described in historic works were recreated on the brainstem and mesencephalic levels [32–34]. More fiber tracts were calculated when the nucleus in question was considered as a region of interest (ROI) rather than as an ending point (Figure 1b,d). End-to-end connections revealed the intricate wiring between the different nuclei, such as the numerous tracts between the lateral lemniscus and the IC tectosomes (Figure 1c) and within different regions of the same nucleus, such as between the IC central nucleus and its tectosomes (Figure 1d).

3.2. Western Blot and BLAST

Western blots resulted in clear immunoreactivity against bottlenose and common dolphin and human control brains for fibronectin (~200 kDa) and GFAP (~40–50 kDa). SMI-312 revealed labeling against pNFP in all three tested species as well, showing a band at ~200 kDa and a weaker one at ~150 kDa in the human, and several intense bands between 150 and 200 kDa in bottlenose and common dolphins, corresponding to the weight of the medium and heavy neurofilament chains this antibody targets. Membrane images are provided in Appendix A, Figure A1.

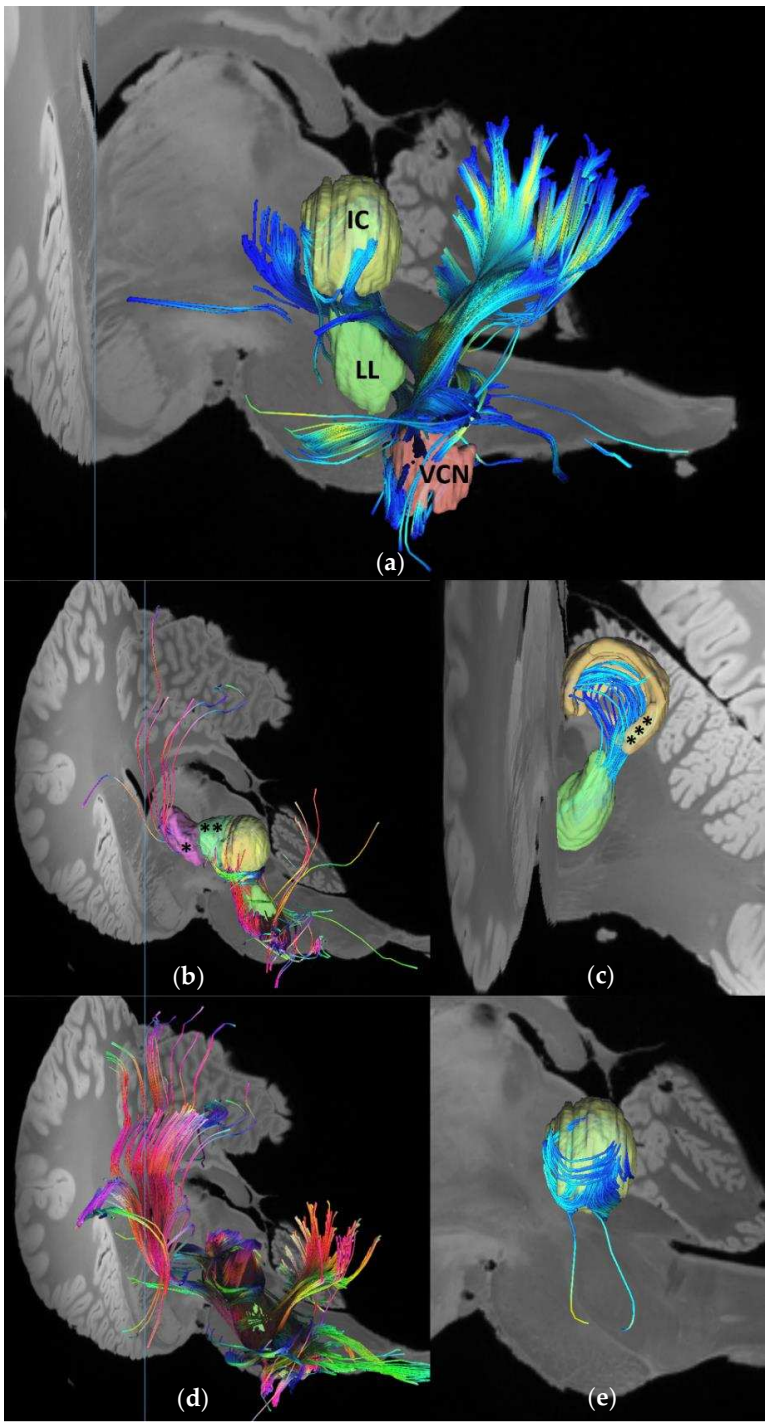

Figure 1. Fiber tracts between the brainstem and midbrain auditory nuclei using a deterministic tracking algorithm [29]. Number of seeds was limited to 1,000,000 in each calculation. (**a**) End-to-end connectivity between the left VCN and IC central nucleus. Total number of tracts: $n = 63$. The lateral lemniscus to accentuate the lemniscal pathway. Lateral perspective; (**b**) Fibers ($n = 1652$) calculated to end in the lateral lemniscus, with the whole brain considered as a seeding region. Caudolateral perspective. MGN (*) and IC brachium (**) are visualized for reference; (**c**) End-to-end fibers ($n = 46$) between the lateral lemniscus and the IC external cortex (***). Caudal perspective; (**d**) Fibers ($n = 7456$) calculated to pass through or end in the lateral lemniscus as a ROI, with the whole brain considered as a seeding region. A higher number of tracts is calculated in comparison with (**b**). Caudolateral perspective; (**e**) End-to-end fibers ($n = 362$) between the IC central nucleus and its external cortex (not shown to better visualize fibers). Lateral perspective.

SEED to END							
Nucleus	**L_AN**	**L_VCN**	**L_LL**	**L_IC CN**	**L_IC EC**	**L_Brachium**	**L_MGN**
L_AN	NA	10,275	1,458	2,023	636	224	6
L_VCN	3,990	NA	2,255	9,382	545	257	2
L_LL	41	21,553	NA	209,522	13,062	5,839	438
L_IC CN	1	3,801	102,948	NA	73,043	53,266	3,310
L_IC EC	1	3,379	36,366	256,602	NA	46,687	3,015
L_Brachium	0	44	2,570	157,946	98,229	NA	10,013
L_MGN	0	0	0	107,473	23,863	170,078	NA
SEED to TERMINATIVE							
Nucleus	**L_AN**	**L_VCN**	**L_LL**	**L_IC CN**	**L_IC EC**	**L_Brachium**	**L_MGN**
L_AN	NA	5,790	43	526,077	526,077	526,077	526,077
L_VCN	423,519	NA	458,304	471,679	471,679	471,679	471,679
L_LL	578,322	556,501	NA	485,482	531,809	576,179	578,325
L_IC CN	453,041	453,041	374,458	NA	253,621	352,316	440,863
L_IC EC	369,924	369,924	364,115	174,086	NA	276,873	354,561
L_Brachium	719,650	719,650	718,951	619,578	661,183	NA	516,932
L_MGN	972,942	972,942	972,942	971,207	972,420	920,253	NA
END to END							
Nucleus	**L_AN**	**L_VCN**	**L_LL**	**L_IC CN**	**L_IC EC**	**L_Brachium**	**L_MGN**
L_AN	NA	0	0	0	0	0	0
L_VCN	0	NA	12	63	11	1	0
L_LL	0	12	NA	988	46	32	0
L_IC CN	0	63	988	NA	362	380	37
L_IC EC	0	11	46	362	NA	56	17
L_Brachium	0	1	32	380	56	NA	3
L_MGN	0	0	0	37	17	3	NA

Figure 2. Calculated fiber tracts for seed-to-end, seed-to-terminative (ends all tracts regardless of their anatomical endings), and end-to-end connectivity of brainstem and midbrain auditory nuclei. The number of tracts is less indicative than their relative differences between the different nuclei, as their number does not correspond to the number of axons and synaptic connections.

TDP-43 did not show any immunoreactivity in any of the tested species with the antibodies used in this essay, and Iba-1 was not suitable for WB. A BLAST search confirmed that proteins of very similar amino acid sequence are encoded in the dolphin genome. Human TDP-43 (ABO32290.1) showed 97.83% identity with bottlenose dolphin TAR DNA-binding protein 43 (XP_019786443.1, E-Value: 0), while human Iba-1 (BAA13088.1) showed a 94.56% (E-Value: 1×10^{-96}) homology with the dolphin allograft inflammatory factor 1 (XP_004311265.1). The Aβ antibody was tested by WB in our previous study [5] and was considered validated in bottlenose dolphins.

3.3. Immunohistochemistry and Stereology

The six tested antibodies all showed clear immunoreactivity in the human control and bottlenose dolphin IC and VCN tissue. Pre-and post-processing IC and VCN volumes estimated from 7T-MRI scans and the Cavalieri probe from serial sections are reported in Table 2. Cell densities below are reported in reference to the Cavalieri volumes in Marine 0142.

Since the optical dissector probes for Aβ, fibronectin, and TDP-43 all considered non-immunoreactive (ir) neurons and therefore yielded independent estimates of total neuronal numbers and densities for the same nuclei, their results were averaged to obtain an estimate of 6.13 million neurons with 3313 neurons/mm^3 in the IC (4.85 million ± 754.58 thousand

in the CN with a density of 3561/mm^3; 1.28 million ± 159.71 thousand in the EC, with 2621/mm^3), and 3.16 million ± 102.19 thousand neurons with 2455/mm^3 in the VCN. The calculations of the percentages and densities of neurons with different types of immunoreactivity (nuclear/cytoplasmic/both nuclear and cytoplasmic) are reported in full in Supplementary Table S1, and all number estimates from StereoInvestigator probes are summarized in Table A2. Neuronal numbers and densities according to the observed types of immunoreactivity are visualized in Figure 3.

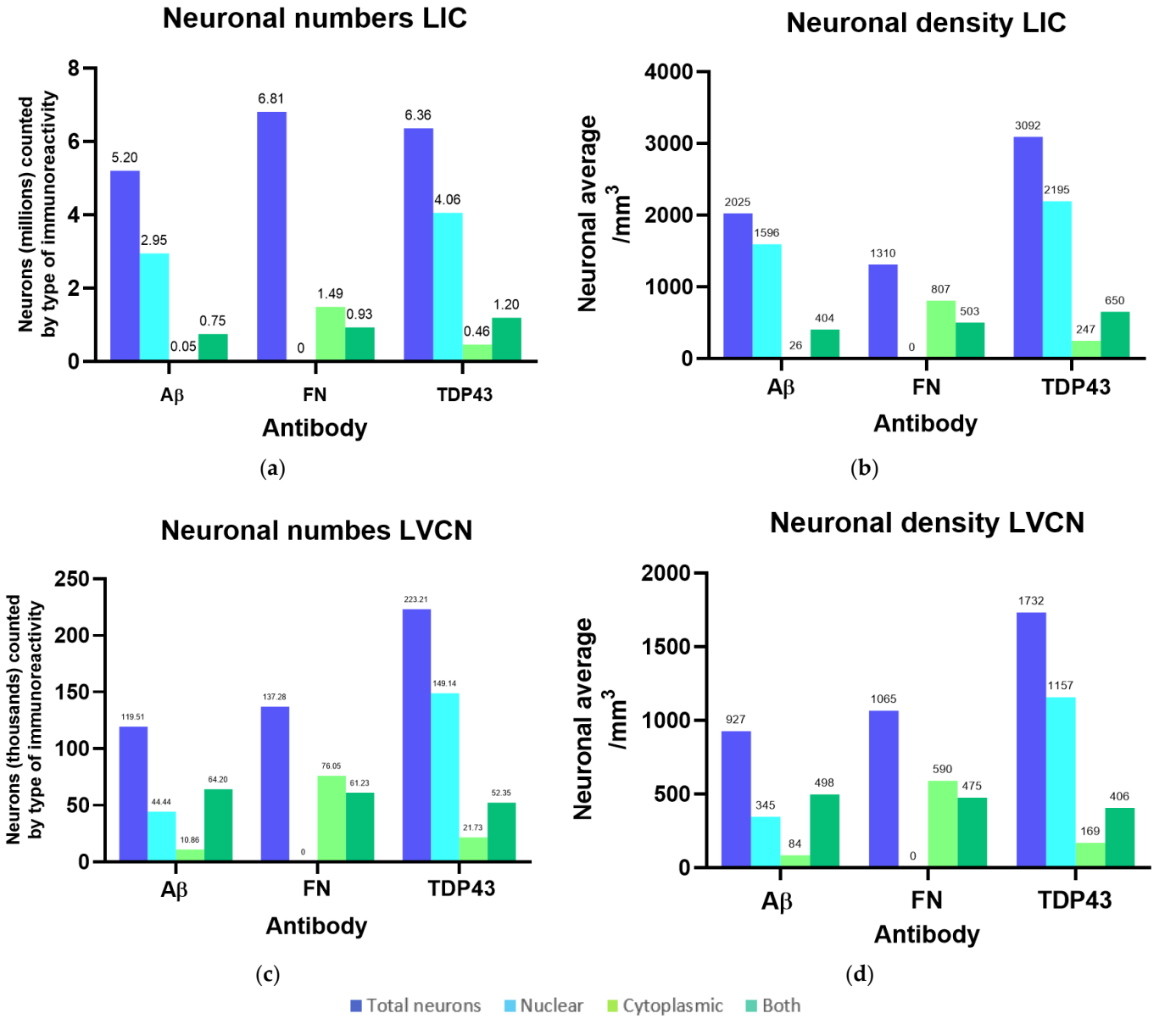

Figure 3. Neuronal numbers and their densities for the left IC and VCN considering different immunoreactivity patterns for Aβ, fibronectin (FN), and TDP-43. (**a**) Total number of neurons counted in each IC probe compared to nuclear, cytoplasmic, or both nuclear and cytoplasmic immunoreactivity; (**b**) Total density of neurons counted in each IC probe compared to nuclear, cytoplasmic, or both nuclear and cytoplasmic immunoreactivity referring to the IC Cavalieri volume; (**c**) Total number of neurons counted in each VCN probe compared to nuclear, cytoplasmic, or both nuclear and cytoplasmic immunoreactivity; (**d**) Total density of neurons counted in each VCN probe compared to nuclear, cytoplasmic, or both nuclear and cytoplasmic immunoreactivity referring to the VCN Cavalieri volume.

The main types of immunoreactivity observed in the tested dolphin tissues are displayed in Figure 4.

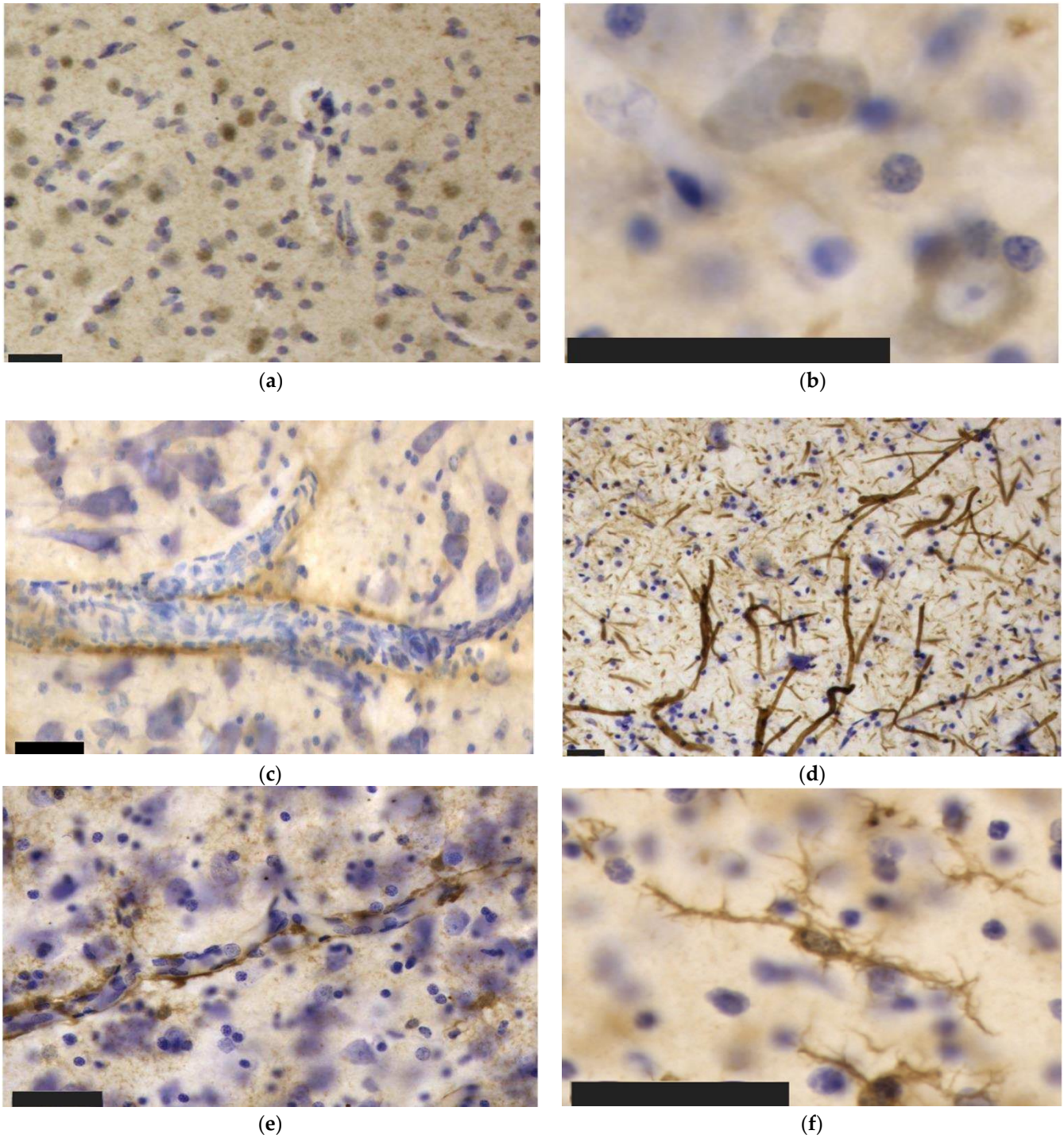

Figure 4. Immunohistochemical patterns of the antibodies tested in this study in the bottlenose dolphin brain. Scale bar: 50 µm. (**a**) Aβ reactivity in neuronal nuclei and in the neuropil of the IC; (**b**) Nuclear (top left) versus cytoplasmic (bottom right) neuronal immunoreactivity to TDP-43 in IC neurons; (**c**) Perivascular immunoreactivity TDP-43 in the IC; (**d**) pNFP-immunolabeled thinner axonal fibers of the IC central nucleus alternating with much thicker external cortex axons; (**e**) Perivascular and intraparenchymal GFAP-expressing astrocytes in the IC; (**f**) Though the ramified morphology prevailed, few rod-shaped Iba-1-ir microglia were present in the VCN.

3.3.1. Aβ

Aβ was observed in 71% of the neuronal nuclei of the IC central nucleus (Figure 4a) and in 7% of its external cortex neurons, where most of its immunoreactivity was present simultaneously in the nucleus and cytoplasm (48%). In total, 56% of all IC neurons displayed immunoreactivity in the nucleus, 14% in both nucleus and cytoplasm, and 0.9% only in the cytoplasm. In the VCN, only 18% of neurons showed only nuclear immunoreactivity, 26% nuclear and cytoplasmic, and 4% cytoplasmic alone. Mild diffuse pericapillary immunoreactivity was too faint to be quantified. A few glial cells also appeared IR, although without confocal microscopy, it was not possible to define whether these were micro- or macroglia.

3.3.2. Fibronectin

Fibronectin appeared only in the cytoplasmic or nuclear and cytoplasmic compartments simultaneously in the examined dolphin. The former pattern was seen in 23%, 17%, and 18%, and the latter in 14%, 13%, and 14% of the IC central nucleus, its external cortex, and the VCN, respectively. A total of 36% of IC and 32% of VCN neurons showed fibronectin immunoreactivity. Some glial cell nuclei were also fibronectin-ir. A human cortical section (Brodmann area 11) from a control case was used as a positive control for fibronectin (Figure 5a). Fibronectin coated the capillary walls and could be observed in most glial and a few neuronal cell nuclei. Unexpectedly, a comparable immunohistochemical pattern was observed in cortical samples from the bottlenose dolphin (Figure 5b; primary auditory cortex) and a human with CTE (Figure 5; superior frontal cortex) revealing very weak capillary immunoreactivity, little (bottlenose dolphin) or no (human with CTE) glial immunoreactivity, and mostly neuronal cytoplasmic and nuclear signal.

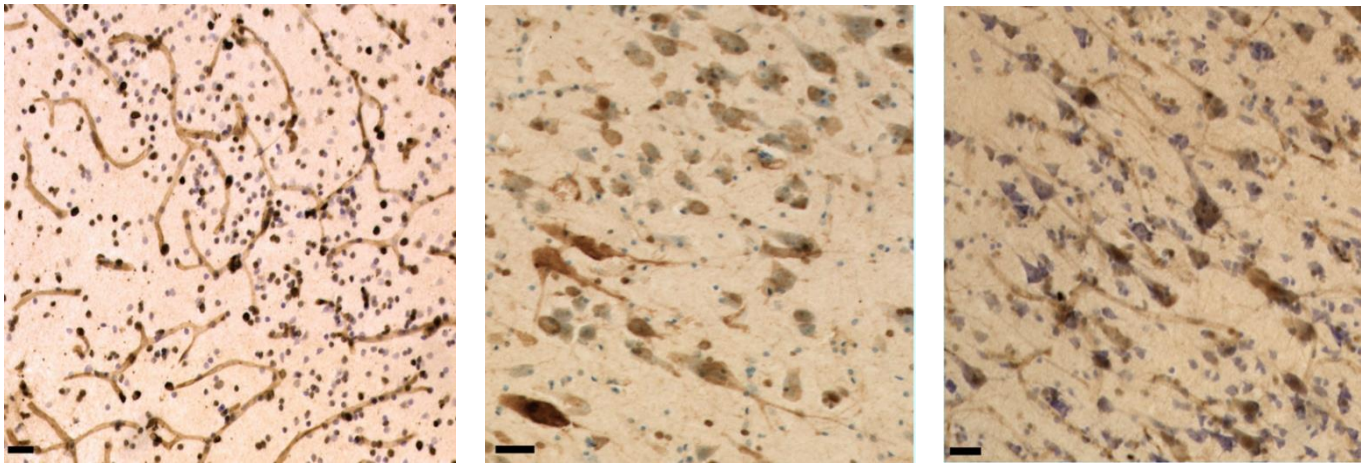

(**a**) (**b**) (**c**)

Figure 5. Fibronectin immunoreactivity in dolphin and human brain cortex. (**a**) Vascular and glial immunoreactivity in a healthy human brain; (**b**) Neuronal cytoplasmic and nuclear immunoreactivity in the primary auditory cortex of a healthy bottlenose dolphin brain; (**c**) Predominantly neuronal and very little vascular immunoreactivity in the blood vessels of a human brain with CTE.

3.3.3. TDP-43

As with Aβ, TDP-43 immunoreactivity was observed in neuronal nuclei or cytoplasm alone (Figure 4b), or in both compartments simultaneously. Predominant nuclear immunoreactivity was observed in the IC central nucleus (67%), external cortex (53%), and VCN (55%), followed by simultaneous nuclear and cytoplasmic immunoreactivity at 17%, 26%, and 19% and a cytoplasmic pattern in 7%, 7%, and 8% of the cells, respectively. Few vessels displayed mild perivascular immunoreactivity (Figure 4c).

3.3.4. pNFP

The axons of the VCN and IC external cortex appeared as very thick, pNFP-ir filamentous structures (Figure 4d). The IC central nucleus mostly consisted of thinner and shorter filaments. Axonal length was estimated to be 2299.47 m in the IC central nucleus, 1058.09 m in its external cortex and 195.31 m in the VCN, corresponding to the structures' different volumes (Figure 6a). Axonal length density was, respectively, 1.69 m/mm^3, 2.17 m/mm^3, and 1.52 m/mm^3 in the IC central nucleus, external cortex, and VCN (Figure 6b). The higher length density of the IC external cortex corresponds to the assumption that many afferent fibers reach the IC from here [33,35].

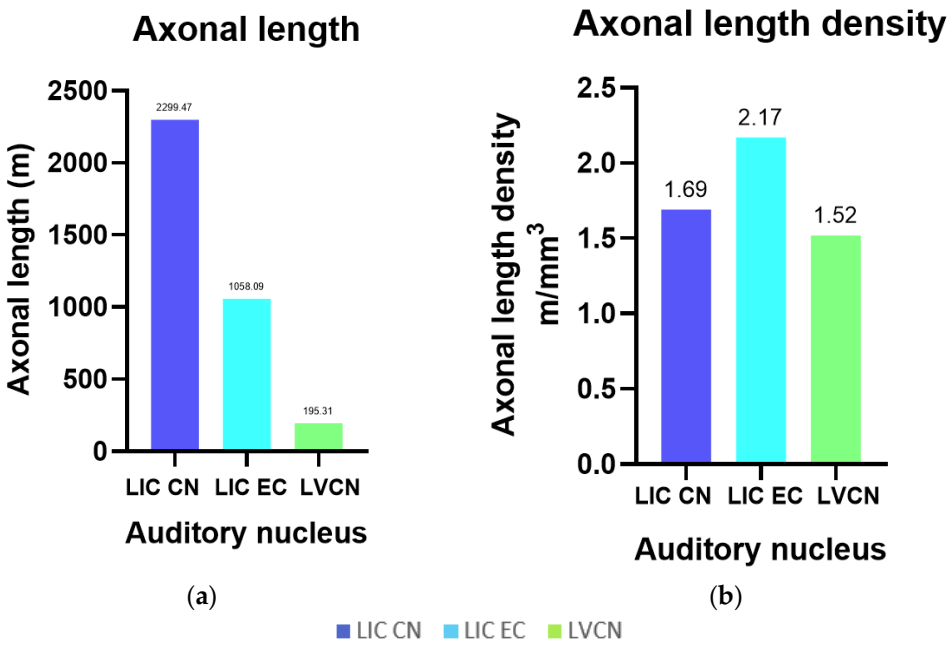

Figure 6. Axonal length and their densities for the left IC central nucleus (CN) and external cortex (EC) and VCN. (**a**) Total axonal length in the LIC CN and EC, and in the VCN; (**b**) Total length density of axons counted in the LIC CN and EC, and in the VCN, referring to the IC Cavalieri volume.

3.3.5. Iba-1

Iba-1 was localized in all parenchymal microglia (intravascular monocytes were not counted). The numbers counted in the IC central nucleus, external cortex and VCN totaled 405.63 million, 316.30 million, and 39.36 million, with their respective densities calculated at 297.85 thousand, 648.62 thousand, and 305.44 thousand microglia/mm^3 (Figure 7a). On average, the total microglial density in the IC is 390.33 thousand/mm^3. As such, it is in the same order of magnitude as that of the VCN (Figure 7b). Most of the observed microglia displayed a filamentous to dendritic morphology, suggesting that the animal did not display evident neuropathology, although few rod-shaped microglia were present in both IC and VCN (Figure 4f).

3.3.6. GFAP

GFAP-expressing astrocytes made up a population of 717.04 million (IC central nucleus), 394.37 million (IC external cortex), and 77.23 million (VCN) cells (Figure 7a). Their density in the three regions amounted to 526.51 thousand, 808.72 thousand, and 599.39 thousand astrocytes/mm^3, respectively, and as with Iba-1, the averaged IC density (600.92 thousand/mm^3) was comparable to that of the VCN (Figure 7b).

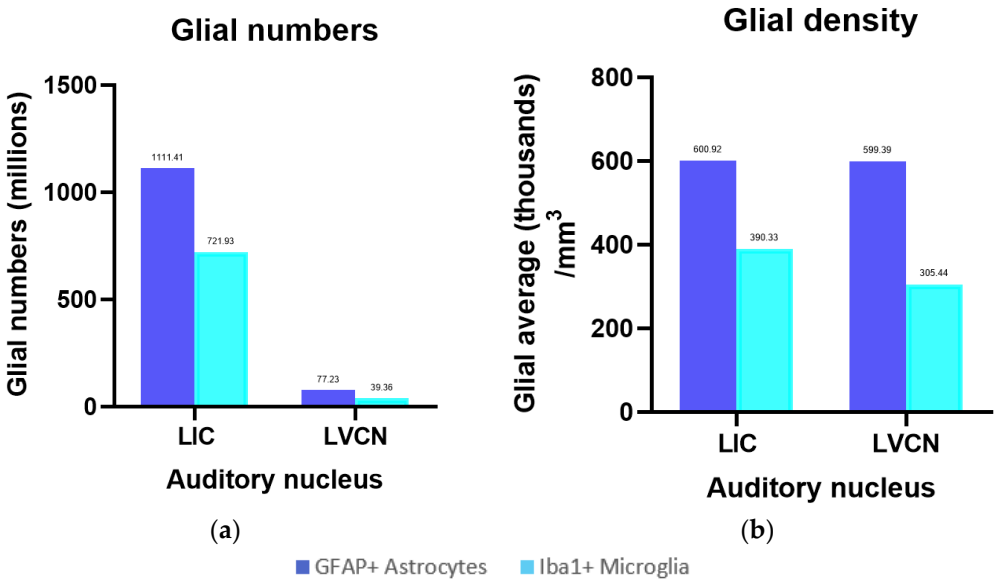

Figure 7. Glial numbers and their densities for the left IC and VCN. (**a**) Total number of GFAP-containing astrocytes and Iba-1-ir microglia in the left IC and VCN; (**b**) Total density of GFAP-expressing astrocytes and Iba-1-ir microglia in the left IC and VCN referring to the IC Cavalieri volume.

3.4. Marker Distributions

With the use of stereological data, it was possible to create heatmaps from 3-dimensional data to visualize the distribution of the immunolabeled neurons, axons, and glia in Marine 0142 (Figure 8 for the IC, Figure 9 for the VCN).

Most of the IC neurons were concentrated in the dorsomedial segment of the IC central nucleus, and this was reflected in the distribution of the neuron-associated markers (Figure 8a,c,e). In the VCN, this distribution was somewhat more homogeneous (Figure 9a,e) for Aβ and TDP-43, and reflected the glove-like morphology of the VCN surrounding the incoming cochlear nerve fibers. Fibronectin appeared to be concentrated in the dorsomedial VCN segment (Figure 9c).

Regarding the different immunoreactivity patterns, intranuclear Aβ was mostly restricted to the IC central nucleus, and less abundant in the external cortex and the VCN. Fibronectin immunoreactivity was observed mostly in the IC central nucleus, particularly with regards to its cytoplasmic expression. VCN distribution was homogenous.

TDP-43, on the other hand, was equally distributed between the central nucleus and external cortex of the IC and the VCN, with comparable nuclear and cytoplasmic immunoreactivity between the three subnuclei (58% nuclear; 21% nuclear and cytoplasmic; 7% cytoplasmic out of all the counted neurons).

pNFP appeared concentrated in the dorsomedial and ventrolateral regions of the IC central nucleus (Figure 8b), but also in the dorsal and lateral segments of the tectosomes, likely reflecting the main afferent and efferent fibers of the IC, which corresponds to the fiber tracks observed in the DTI data (Figure 1d,e). In the VCN, pNFP-ir fibers appeared interspersed with the neuronal somata, although it must be kept in mind that this nucleus was not complete in the examined specimen.

Glial distributions (Figure 8d,f and Figure 9d,f) lacked large concentration gradients, being somewhat denser in the dorsomedial segments of both auditory nuclei.

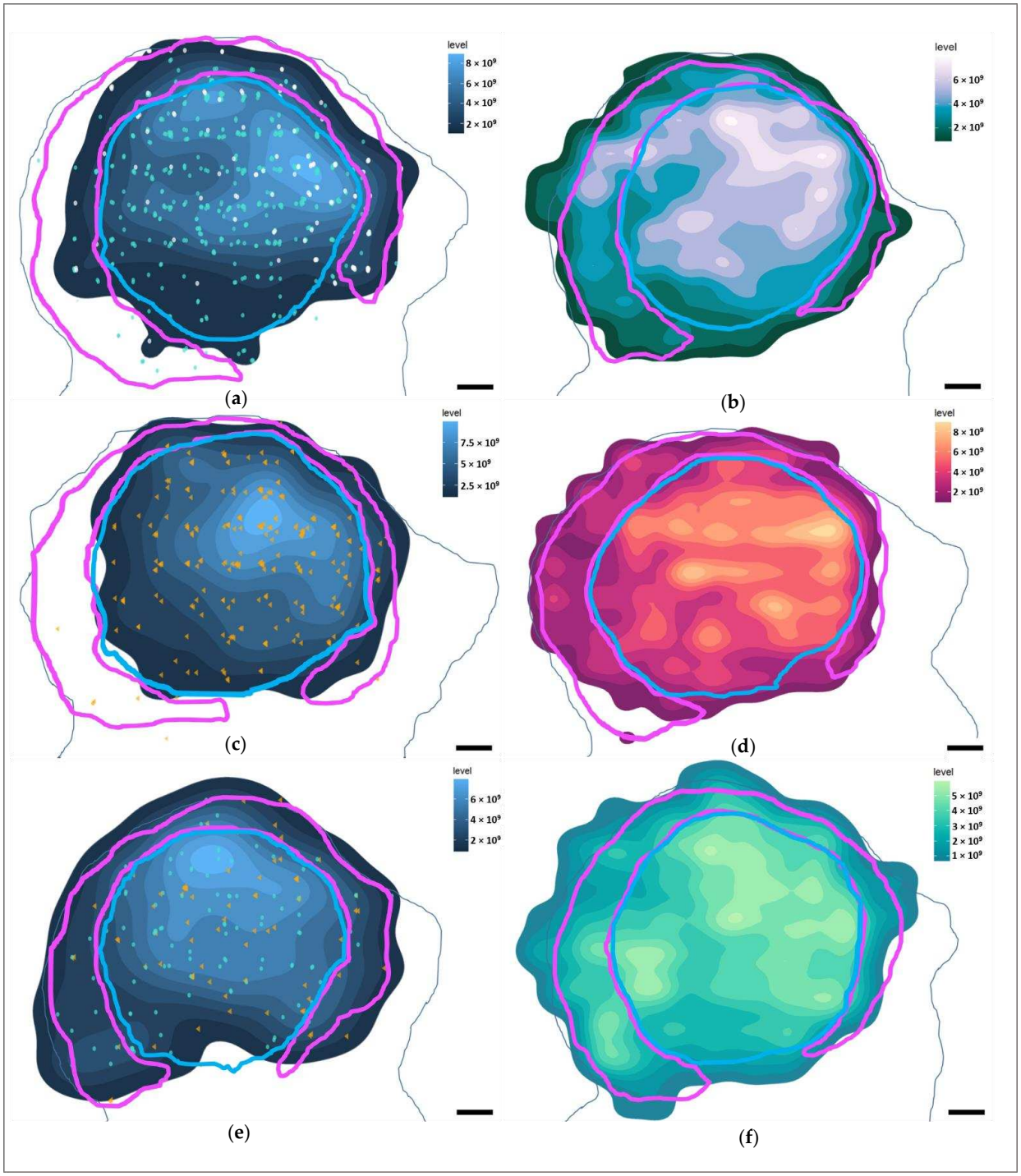

Figure 8. Heatmaps of marker distributions in the left IC of Marine 0142 in the coronal plane (caudal perspective). In light blue—the average contour surrounding the putative IC central nucleus area every 30th serial section, while the light pink contour represents the putative IC external cortex. Lighter colors of the heatmaps represent a higher marker density. Scale bar: 2 mm (**a**) Heatmap of all Aβ-containing neurons. Turquoise points—neurons with nuclear immunoreactivity. White points—neurons with simultaneous cytoplasmic and nuclear immunoreactivity. (**b**) Heatmap of pNFP-ir axons. (**c**) Heatmap of all fibronectin-ir neurons. Orange points—neurons with cytoplasmic immunoreactivity pattern. (**d**) Heatmap of GFAP-expressing astrocytes. (**e**) Heatmap of all TDP-43-containing neurons. Points as in (**a**,**c**). (**f**) Heatmap of Iba-1-expressing microglia.

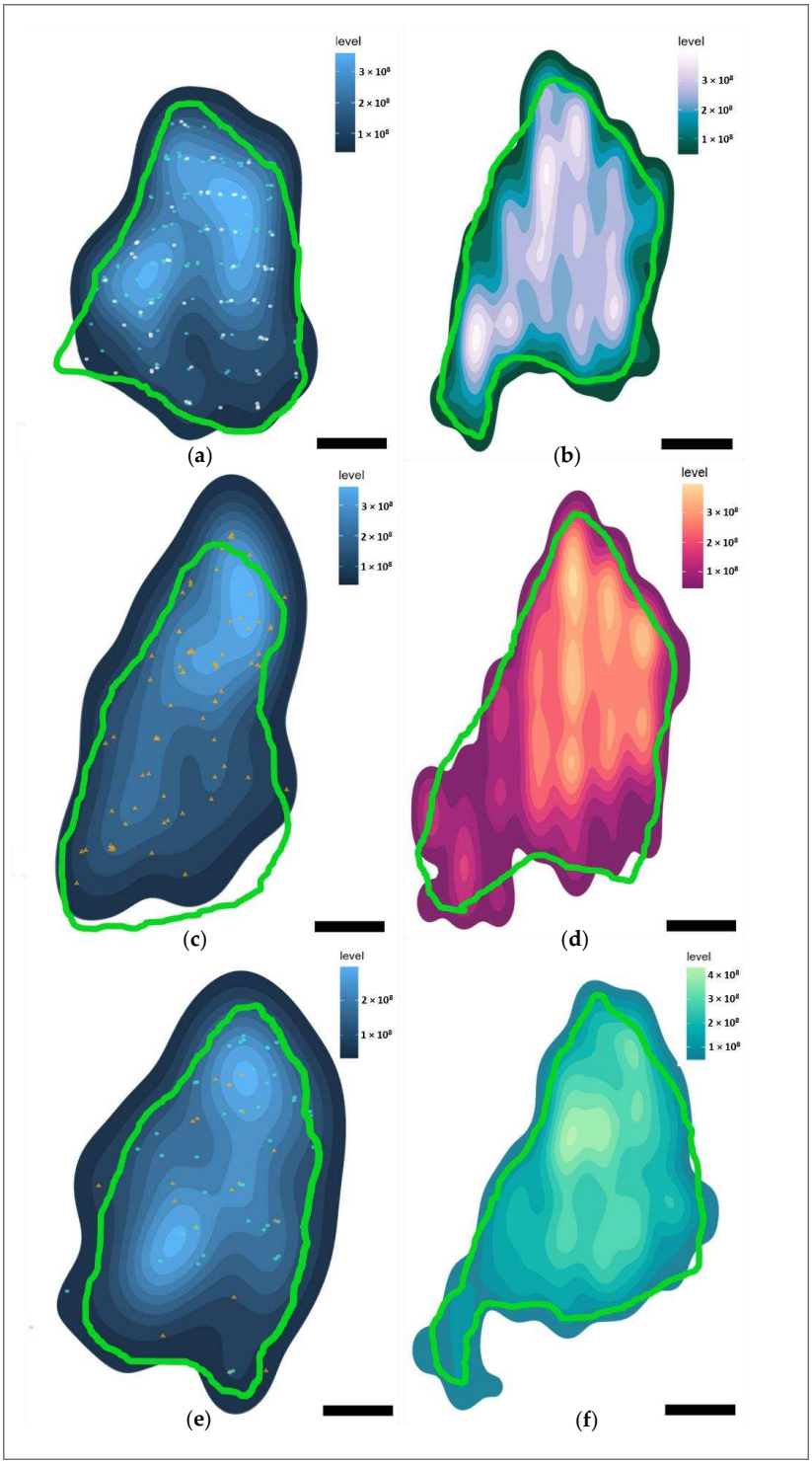

Figure 9. Heatmaps of immunohistochemical marker distributions in the left VCN of Marine 0142 in the coronal plane (caudal perspective). In green—the average contour surrounding the putative VCN area from every 20th serial section. Lighter colors of the heatmaps represent a higher marker density. Scale bar: 2 mm. (**a**) Heatmap display total Aβ-containing neurons, regardless of immunoreactivity type. Turquoise points—neurons with nuclear immunoreactivity. White points—neurons with simultaneous cytoplasmic and nuclear immunoreactivity. (**b**) Heatmap of pNFP-ir axons. (**c**) Heatmap of all fibronectin-ir neurons. Orange points—neurons with cytoplasmic immunoreactivity pattern. (**d**) Heatmap of GFAP-ir astrocytes. (**e**) Heatmap of all TDP-43-ir neurons. Points as in (**a**,**c**). (**f**) Heatmap of Iba-1-ir microglia.

3.5. Intra- and Interspecies Comparisons

To our knowledge, this is the first stereological estimates of neurons and glia ir against the investigated antibodies in the bottlenose dolphin IC and VCN. While the two hemispheres of Marine 0116's brain yielded high-quality 7T-MRI scans, the tissue quality made it unsuitable for immunohistochemistry. The celloidin-embedded Nissl-sections of the right IC and VCN of Dolphin 2 (a bottlenose dolphin; [36]) and the right VCN of a striped dolphin (*Stenella coeruleoalba*) were analyzed for comparison. Values for cochlear nucleus numbers (subdivisions in a dorsal and VCN are indistinct) have previously been reported for healthy individuals versus people with presbycusis by Hinojosa and colleagues (2011) [37], and the former number and density is presented in Figure 10 in comparison with the cetaceans. At 91.47 thousand neurons, human values are about a third (31%) of Marine 0142's VCN (316.38 thousand). The difference is exorbitantly greater when comparing Marine 0142, which was processed minimally and embedded using DPX, to Dolphin 2 (2.15 million neurons), whose brain volume presumably shrunk by at least 50% due to celloidin embedding, thus reflecting on the neurons observed per counting frame and density estimates. While the striped dolphin's brain was processed similarly to Dolphin 2's, its numbers (personal communication, Ava Akbarian, Hof laboratory) are similar to those of Marine 0142, despite its physiologically, species-characteristic smaller brain volume [38].

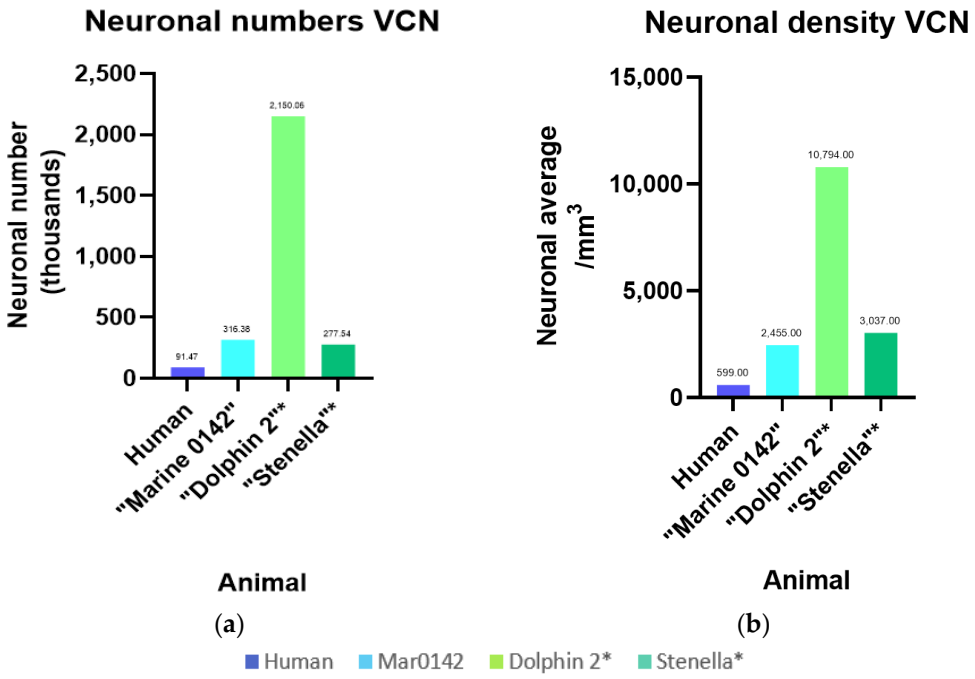

Figure 10. Intra- and interspecies comparison of numbers and densities for the VCN. Human values were taken from existing literature [37]. * Bottlenose Dolphin 2 and the striped dolphin (*Stenella*) VCN neurons were counted using archived, Nissl-stained, celloidin-embedded sections. (**a**) Total number of neurons counted in the VCN; (**b**) Total density neurons referring to the VCN Cavalieri volume.

IC neuronal numbers were only available for Marine 0142 and Dolphin 2 (8.30 million—IC central nucleus, 1.76 million—external cortex, 2.15 million—VCN), and revealed 2-7 times higher values in the celloidin-embedded bottlenose dolphin tissue.

4. Discussion

This study reports a multimodal and quantitative approach to assessing cetacean auditory nuclei, expanding the knowledge of neurochemical signatures and brain connectivity. Stereological probes for systematic random sampling yielded reliable cell counts with coefficients of error (CEs) < 10% for most of the tested markers with regards to total immunoreactivity.

Following our previous work, markers of interest were chosen according to their relevance in the neurodegenerative and neuroprotective processes, as well as in plasticity. Aβ was consistently observed in the nuclei of IC and VCN neurons in 21 bottlenose dolphins (including the specimens from Orekhova and colleagues, 2022 [5]), and the present work shows that intranuclear Aβ is present in 71% of IC central nuclear cells, pointing to a widespread, potentially physiological pattern in a healthy dolphin and matching findings in other cetacean species [14].

As previously described by these authors, a potential neuroprotective role of nuclear Aβ oligomer may facilitate nuclear degradation of misfolded proteins [39,40], particularly assuming repetitive exposure to mild hypoxia that may be experienced by animals with dive intervals of up to ~8 min [41,42]. This hypothesis is worthy of further investigation, as extracellular Aβ aggregation is correlated with AD and used for staging of the disease [43], yet no clear causality has been described [44].

In this context, the localization of fibronectin is of particular interest. Contrary to the expected capillary reactivity, as it was seen in the healthy human control tissue, the bottlenose dolphins examined for this study displayed neuronal cytoplasmic (with and without nuclear signal) and limited glial immunoreactivity in the IC, VCN, and auditory cortex. This corresponded to the pattern seen in a human CTE brain.

As a component soluble in the extracellular matrix (ECM) and insoluble when built into vascular basal membranes, fibronectin is secreted by endothelial, pericytic, and astroglial cells [16]. It may also be expressed on the neuronal cell surface along with other adhesive glycoproteins as part of the ECM, enabling integrin-associated signal transduction and thus reflecting the activity of neuronal, glial, and vascular cells that are responsible for its proteolytic degradation [45]. Following neuronal insults such as stroke and traumatic brain injury (TBI), the hybrid ECM proteins are shown to be acutely down- and chronically upregulated within the scar tissue, shifting from the perivascular to the perineuronal compartment and putatively enabling plastic adaptations to take place. As such, perineuronal immunoreactivity is expected in a CTE brain.

Wang and colleagues (2013) attribute a key neuroprotective role to the "fibronectin-integrin-growth factor receptor-signal transduction-gene and protein expression cascade", highlighting its capacity to compensate TBI-induced synaptic deficits by modulating neuron-glial extrasynaptic transmission [20]. Furthermore, ECM homeostasis is thought to be disturbed as a consequence of hypoxia in fibrotic breast, mesenchymal stem cells, and other tissues [46,47] as well as ischemic conditions, although in the latter case, immunoreactivity is largely restricted to perivascular and diffuse parenchymal and not cell-associated immunoreactivity pattern [48,49]. Moreover, hypoxia may also be a driver of neuroinflammation by promoting Aβ build-up and disrupting calcium homeostasis when the tissue is exposed chronically, although intermittent and acute exposure tends to induce neuroprotective mechanisms [50].

Considering this together with higher myelination [9] and antioxidant protein levels [10] in deeper- and thus longer-diving cetacean species, and generally higher neuroglobin levels in cetaceans versus terrestrial mammals and seals [51], perineural fibronectin appearance in a healthy dolphin brain concurrently with intranuclear Aβ is remarkable and suggests that a neurochemical signature reminiscent of hypoxia may be physiological in dolphins. However, a reliable vascular marker would still be important despite the lack of immunoreactivity in the antibodies tried in this study (Appendix A, Table A1), as TBI may cause chronic vessel-associated neuroinflammation [52].

TDP-43 appeared on average in 87% of counted auditory nuclei neurons, mostly in nuclear (58%), followed by nuclear and cytoplasmic (7%), and only cytoplasmic (21%) patterns. In a recent study on the brains of seven free-ranging common dolphins variably exposed to β-*N*-methylamino-L-alanine (BMAA) and methylmercury, all the specimens were observed to have neuronal cytoplasmic inclusions morphologically reminiscent of AD disease in humans, widespread in different cortical areas and layers independent of BMAA exposure levels, but potentially associated with a synergistic pathology in combination

with high methylmercury levels [4]. Furthermore, *TARDBP*, the gene encoding for TDP-43, was found to be upregulated in these dolphins [4]. However, no quantitative assessment was available for the protein-expression data.

In humans with Guamanian Parkinsonism-dementia complex, hippocampal CA1 neuronal loss was correlated with significantly lower numbers of neurons expressing nuclear TDP-43 and higher numbers of cytoplasmic TDP-43. Healthy controls displayed 43.7% of positive nuclei compared to 22% in this diseased cohort [53]. While human values for the IC and cochlear nuclei are unavailable, the intranuclear 58% in Marine 0142 auditory nuclei may reflect the lack of neuropathological changes in this dolphin, as confirmed by microscopic examination.

Qualitative descriptions of TDP-43 neuronal mislocalization from the nucleus to the cytoplasm in various neurodegenerative disorders abound [54,55], and thus it may be a protein with a similar apoptosis-heralding dynamic, but potentially more chronic expression in the dolphin than the previously described diacylglycerol-ζ [5].

While antibodies against cytoskeleteal neurofilament have successfully been used in cetaceans (SMI-32—[13,56]; NF200—[5,57]), they mostly visualize somatic and dendritic elements. Here we used pNFP to analyze axonal length and density, targeting heavily phosphorylated axonal epitopes [58], which may thus serve as a reference for comparison with other individuals and species in an evolutionary and pathophysiological context.

Validating pNFP for cetaceans may help assess oxidative axonopathy by assessing the ratio of phosphorylated neurofilaments to total neurofilament proteins (using NF200). This has been shown in an acute loss of phosphorylation, quantifying the loss of axonal function in acute oxidative injury [59] and correlating with the duration of some neurodegenerative diseases such as multiple sclerosis [60].

GFAP-expressing astrocyte and Iba-1-expressing microglial numbers and densities may also serve as a baseline, as both cell types are involved in the response to pathogen- [61,62], toxin- [63], age-related, and immune-mediated neuroinflammation [64], and have even been involved in acoustic trauma [65–67]. Future studies may focus on quantifying proteins such as Aβ and fibronectin in glial cell populations using confocal/multiplexing methods, as their involvement has been verified in neurodegeneration and neuroprotection [20,68–70].

Cetaceans display remarkable cognitive abilities, including complex social relationships, mirror self-recognition, the ability to pass along cultural behaviors such as specialized hunting techniques, and even the use of different dialects, traditions, and tools [71–74]. In this regard, comparison of the reported protein expression to individuals with known cognitive decline or deafness, especially in dolphins from aquaria where behavioral assessments are available, would be very valuable venue for upcoming research. Ethically sound functional studies in live, trained dolphins, such as using fMRI, are very difficult due to a variety of logistical and training challenges. Nevertheless, they are likely to become feasible with time, providing unique insight and validation for post-mortem assessments.

While stereological estimates of the above markers are a useful baseline for future comparisons with other individuals and species, cell numbers, and especially densities, depend heavily on the way the tissue was fixed, processed, and probed. While MRI scans do not allow a precise border delineation using cell morphology, they can be helpful to assess in situ volumes as a reference for stereological assessment. In the case of Marine 0142, relatively little processing was performed as opposed to paraffin-embedded tissue. Nevertheless, Cavalieri volume estimates were 77% (IC) and 30% (VCN) of their in situ correlates from the 7T-MRI scans. The difference in the VCN is likely owing to macroscopic damage of the caudal part of the nucleus, which prevented us from obtaining serial sections from its caudal third. For Marine 0116, whose IC and VCN were complete in both scans and sections, Cavalieri volume estimates amounted to 84% and 75% of the MRI-based volume estimates, implying that the volumes inferred from processed brain sections are systematically underestimated.

The comparison to Dolphin 2, a celloidin-embedded, archived bottlenose dolphin specimen, showed that that a processing tissue shrinkage of about 50% can create an artificial

concentration of neuronal numbers of 288%, which increases the average neuronal density by 498%. Therefore, species comparisons must also be undertaken with care. Historic studies have reported quantitative cochlear nucleus volumes and neuronal numbers [75–77] in harbor porpoise (*Phocoena phocoena*), fin whale (*Balaenoptera physalus*), beluga whale (*Delphinapterus leucas*), and common dolphin, revealing that volumes ranged from 6–30 times that of human, and the neurons numbered 6–17 times the average healthy human value. However, many details including age, gender, and history and tissue preparation behind the whale and human specimens are variable or unknown.

In our case, VCN Cavalieri volumes were observed to be 8.4–18.5 times that of the most recent human study [37], 12.9–28.5 times comparing to the volumes of human cochlear nuclei in Hall's (1967) [75] study, and 23–52 times those from Gandolfi and colleague's VCN averages (1980) [78]. Neuronal numbers were between 4.5–70.6 times those of the adult human VCN (3.3–23.5 times that of both cochlear nuclei) compared to the above studies.

Preliminary values for the striped dolphin (celloidin-embedded) are best compared to bottlenose Dolphin 2 due to similarities in processing, and comprise 46% of its volume, 13% of neuronal numbers, and 28% of the total packing density, which may reflect the fact that its brain mass (880.01 g on average) is around 57% that of the bottlenose dolphin (1549.9 g; [79]). This variability highlights that, while quantitative estimates of morphological and neurochemical properties are desirable, many more specimens need to be examined in future using the most tissue-sparing techniques possible, and that a multimodal approach such as used here may be of great use to offset potential artifacts.

Not as much literature is available for the comparison between IC volumes and numbers. The intraspecies trend of a concentration in both neuronal numbers and densities is repeated between Marine 0142 and Dolphin 2 as a likely consequence of celloidin-embedding, and human volumes appear to be between 3.5 to 28 times lower than in the bottlenose dolphins [80]. We could not differentiate a dorsal from an external IC cortex in our specimens; thus, comparisons to these structures were not possible [81].

Furthermore, 7T-MRI-based volumes confirmed that tissue processing caused a shrinkage of 15–25% in these specimens and, as such, the DTI results reported in this study must be seen as preliminary. Connectivity from the VCN and IC of the two bottlenose dolphin hemispheres largely recreated the known delphinid auditory pathway between the brainstem and midbrain nuclei [32,34,38,77,82]. Regarding the high quality of the scans and notwithstanding the limitations of evaluating single hemispheres separately, these specimens merit further detailed connectivity studies that are beyond the scope of the present paper.

As is often the case in marine mammal science, very low sample sizes limit the significance of the acquired data, and scant information on the animals' history, age, sex, and circumstances of death limit health assessments and the interpretation of histopathological data. Cetacean sample acquisition is opportunistic due to ethical and logistic constraints, and is inherently affected by high variability in fixation times and methods, sample integrity, and processing (see Ijsseldijk and colleagues, 2019 [83] for the current protocols of general post-mortem procedures and Orekhova and colleagues, 2022 [5] for VCN, IC, and vestibulocochlear-nerve sampling protocols). Further studies should aim to process tissues in the most sparing way available to enable future comparisons to the quantitative assessments provided in this and other recent studies [4,13].

5. Conclusions

The quantitative, multimodal assessment of the IC and VCN of this study expand the available knowledge on cetacean auditory nuclei neurochemical signature and connectivity, facilitating the recognition of artifacts. The stereological estimates obtained herein heighten the translational potential of dolphins to model the pathophysiology of the human brain, although different responses to neurodegenerative disease may be possible in species evidently adapted to a high-pressure, low-temperature underwater environment. They may also serve as a baseline for stranded cetaceans where pathological findings are inconclusive

and acoustic trauma is suspected [84], as a support to the examination of the fragile inner ear [5,85]. Cumulative and acute toxicity from environmental and anthropogenic sources may also be better quantified [4].

Further studies using similar validatory and multimodal approaches are necessary to solidify the results, allow for functional intra- and interspecies comparisons between other marine and terrestrial animals and create a deeper understanding of cetacean neuroanatomy, physiology, and pathology.

Supplementary Materials: The following supporting information can be downloaded at: https://www.mdpi.com/article/10.3390/vetsci9120692/s1. Table S1: Excel sheet of all calculations of percentages and densities of immunohistochemical markers supplementary to this study.

Author Contributions: Conceptualization, K.O. and P.R.H.; methodology, K.O., B.W., P.R.H., T.G. and J.-M.G.; software, P.R.H., B.W., P.B., A.S. and A.A.; validation, E.S., R.D.G., B.M., M.A.G.S., B.W., A.S. and A.A.; writing—original draft preparation, K.O.; writing—K.O., S.M., P.R.H. and G.D.G.; visualization, K.O., T.G. and J.-M.G.; supervision, P.R.H., S.M., C.C. and P.B. All authors have read and agreed to the published version of the manuscript.

Funding: This research received no external funding.

Institutional Review Board Statement: Not applicable.

Informed Consent Statement: Not applicable.

Data Availability Statement: Data presented in this article are available either in the article or the Supplementary Materials.

Acknowledgments: We would like to thank Merina Varghese and Nicole Ackermans for their technical support for the immunohistochemistry and use of StereoInvestigator. We would also like to acknowledge and thank Ava Akbarian for her work on preliminary estimates for the ventral cochlear nuclei in the striped dolphin specimen discussed in this study.

Conflicts of Interest: The authors declare no conflict of interest.

Appendix A

Table A1. Antibodies tried in bottlenose dolphin brains using immunohistochemistry (IHC) in the pilot study.

Antibody [1]	Host	Reactivity	Clonality	RRID	Catalogue Number	Lowest Dilution IHC
AT-8	Mouse	Human, Mouse, Rat (etc.)	Monoclonal	AB_223647	MN1020	1:1000
CD-31	Rabbit	Human	Polyclonal	AB_726362	ab28364	1:100
Collagen IV	Rabbit	Mouse, Rat, Hamster, Cow, Dog, Human, Pig, Zebrafish, African green monkey, Chinese hamster, Syrian hamster	Polyclonal	AB_445160	ab6586	1:300
Collagen IV	Rabbit	Mouse	Polyclonal	AB_445160	ab19808	1:300
Collagen IV	Rabbit	Human	Monoclonal	AB_2801511	ab214417	1:500
CP-13	Mouse	Human	Monoclonal	AB_2314223	Davies Lab	1:1000
dMBP	Rabbit	Human, Rat	Polyclonal	AB_2140351	ab5864	1:500
GFAP	Rabbit	Mouse, Rat, Human	Monoclonal	AB_880202	ab68426	1:1000
Isolectin B4 [2]	*Bandeiraea simplicifolia*	Non-immune origin	Unspecific binding of glycoproteins	NA	L2140	1:40

Table A1. *Cont.*

Antibody [1]	Host	Reactivity	Clonality	RRID	Catalogue Number	Lowest Dilution IHC
MAP-2	Rabbit	Human	Polyclonal	AB_1853945	HPA008273	1:200
MMP-9	Mouse	Human, Mouse, Rat	Monoclonal	Not available	NBP2-80855	1:300
MOAB-2	Mouse	Human	Monoclonal	AB_2895168	MABN254	1:200
NeuN	Mouse	Avian, Chicken, Ferret, Human, Mouse, Pig, Rat, Salamander	Monoclonal	AB_2298772	MAB377	1:200
PHF1	Mouse	Human	Monoclonal	AB_2315150	Davies Lab	1:500
SMI-32	Mouse	Human, Mouse, Rat	Monoclonal	AB_2715852	801701	1:1000
Vimentin	Mouse	Human, Rat	Monoclonal	AB_306239	ab8069	1:200

[1] Antibodies yielding inconsistent or no evident immunoreactivity were tested in morphologically healthy dolphin brain tissues. Potential immunoreactivity in pathological specimens were not excluded, but these antibodies require validation in cetaceans. [2] Isolectin B4 is not an antibody, but only a protein that can agglutinate cells/glycoproteins/some complex carbohydrates. It agglutinated to vascular glycoproteins in the human and dolphin sections, but the signal was too weak for further use.

Table A2. Full table of all the coefficients or error for the stereological markers counted in this study.

Data File	Marker	Total Markers Counted	Number of Sampling Sites	Estimated Population Using Mean Section Thickness with Counts	CE (Gundersen), m = 0	CE (Gundersen), m = 1	1st Estimated CE (Schmitz-Hof)	2nd Estimated CE (Schmitz-Hof)
				Amyloid-β				
LIC CN	Non-ir	162	239	960,000.06	0.11	0.08	0.099	0.079
LIC CN	Nuclear	484	239	2,868,148.5	0.06	0.05	0.057	0.045
LIC CN	Cytoplasmic	7	239	41481.48	0.38	0.38	0.470	0.378
LIC CN	Nuclear + cytoplasmic	33	239	195,555.56	0.20	0.18	0.202	0.174
LIC CN	All markers	686	239	4,065,185.25	0.05	0.04	0.046	0.038
LIC EC	Non-ir	14	153	82,962.96	0.28	0.27	0.370	0.267
LIC EC	Nuclear	82	153	485,925.94	0.16	0.11	0.172	0.110
LIC EC	Cytoplasmic	1	153	5925.93	1.00	1.00	1.000	1.000
LIC EC	Nuclear + cytoplasmic	95	153	562,963	0.12	0.10	0.157	0.103
LIC EC	All markers	192	153	1,137,777.88	0.1	0.07	0.109	0.072
LVCN	Non-ir	45	137	44,444.45	0.21	0.15	0.312	0.149
LVCN	Nuclear	128	137	126,419.76	0.13	0.09	0.105	0.088
LVCN	Cytoplasmic	11	137	10,864.20	0.34	0.30	0.343	0.302
LVCN	Nuclear + cytoplasmic	65	137	64,197.54	0.14	0.12	0.129	0.124
LVCN	All markers	249	137	245,925.94	0.1	0.07	0.083	0.063
				Fibronectin				
LIC CN	Non-ir	594	235	3,520,000.25	0.05	0.04	0.049	0.041
LIC CN	Cytoplasmic	217	235	1,285,926.13	0.09	0.07	0.085	0.068
LIC CN	Nuclear + cytoplasmic	129	235	764,444.5	0.12	0.09	0.100	0.088
LIC CN	All markers	940	235	5,570,370.5	0.04	0.03	0.045	0.033
LIC EC	Non-ir	147	100	871,111.19	0.10	0.08	0.123	0.082

Table A2. *Cont.*

Data File	Marker	Total Markers Counted	Number of Sampling Sites	Estimated Population Using Mean Section Thickness with Counts	CE (Gundersen), m = 0	CE (Gundersen), m = 1	1st Estimated CE (Schmitz-Hof)	2nd Estimated CE (Schmitz-Hof)
LIC EC	Cytoplasmic	35	100	207,407.41	0.19	0.17	0.192	0.169
LIC EC	Nuclear + cytoplasmic	28	100	165,925.92	0.22	0.19	0.222	0.189
LIC EC	All markers	210	100	1,244,444.5	0.09	0.07	0.103	0.069
LVCN	Non-ir	300	145	296,296.31	0.12	0.06	0.099	0.058
LVCN	Cytoplasmic	77	145	76,049.38	0.12	0.11	0.133	0.114
LVCN	Nuclear + cytoplasmic	62	145	61,234.57	0.14	0.13	0.137	0.127
LVCN	All markers	439	145	433,580.28	0.1	0.05	0.072	0.048
				TDP-43				
LIC CN	Non-ir	555	248	3,288,889	0.07	0.04	0.051	0.042
LIC CN	Nuclear	74	248	438,518.59	0.12	0.12	0.118	0.116
LIC CN	Cytoplasmic	60	248	355,555.56	0.16	0.13	0.170	0.129
LIC CN	Nuclear + cytoplasmic	140	248	829,629.63	0.12	0.09	0.108	0.085
LIC CN	All markers	829	248	49,12593	0.05	0.04	0.044	0.035
LIC EC	Non-ir	130	106	770,370.5	0.14	0.09	0.150	0.088
LIC EC	Nuclear	35	106	207,407.41	0.19	0.17	0.218	0.169
LIC EC	Cytoplasmic	17	106	100,740.75	0.24	0.24	0.253	0.243
LIC EC	Nuclear + cytoplasmic	63	106	373,333.34	0.16	0.13	0.161	0.126
LIC EC	All markers	245	106	1,451,852	0.12	0.07	0.11	0.064
LVCN	Non-ir	151	140	149,135.81	0.14	0.09	0.112	0.081
LVCN	Nuclear	47	140	46,419.76	0.19	0.15	0.150	0.146
LVCN	Cytoplasmic	22	140	21,728.40	0.22	0.21	0.217	0.213
LVCN	Nuclear + cytoplasmic	53	140	52,345.68	0.29	0.15	0.148	0.137
				pNFP				
LIC CN	Axonal	3970	213	2,299,468,544	0.06	0.02	-	-
LIC EC	Axonal	1795	76	1,058,085,632	0.09	0.03	-	-
LVCN	Axonal	1988	115	195,308,656	0.13	0.04	-	-
				Iba-1				
LIC CN	Microglial	2738	227	405,629,632	0.06	0.02	0.035	0.019
LIC EC	Microglial	2135	122	316,296,320	0.08	0.03	0.047	0.022
LVCN	Microglial	1594	139	39,358,024	0.09	0.03	0.055	0.025
				GFAP				
LIC CN	Astrocytic	4840	229	717,036,992	0.05	0.02	0.03	0.014
LIC EC	Astrocytic	2662	96	394,370,400	0.08	0.03	0.058	0.019
LVCN	Astrocytic	3128	137	77,234,568	0.08	0.02	0.043	0.018

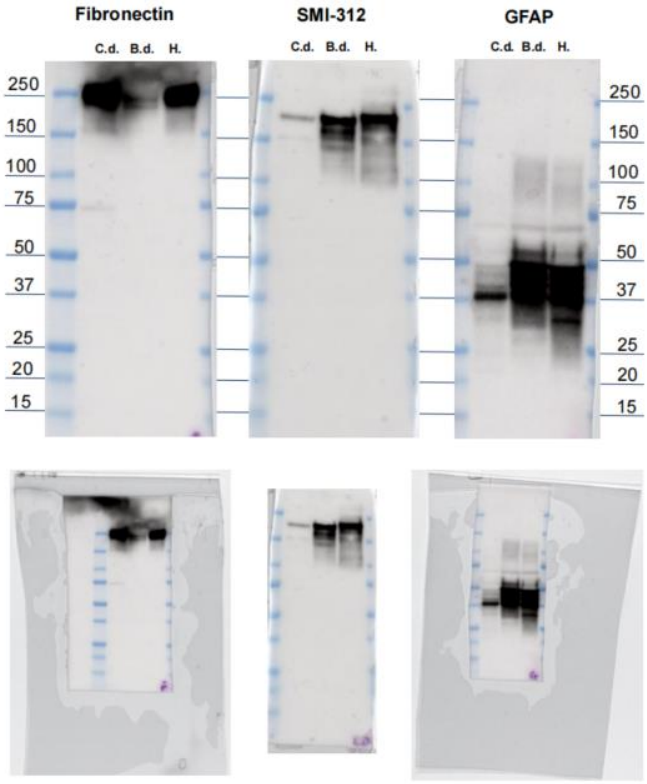

Figure A1. Western blot membranes from fibronectin, SMI-312, and GFAP. Top: Annotated membranes from Western blots of fibronectin, pNFP, and GFAP for C.d. = common dolphin; B.d. = bottlenose dolphin; H. = human control. Values in kDa. Bottom: original uncropped and unlabeled source images.

References

1. Hof, P.E.; Chanis, R.; Marino, L. Cortical complexity in cetacean brains. *Anat. Rec.—Part A Discov. Mol. Cell. Evol. Biol.* **2005**, *287*, 1142–1152. [CrossRef]
2. Gunn-Moore, D.; Kaidanovich-Beilin, O.; Gallego Iradi, M.C.; Gunn-Moore, F.; Lovestone, S. Alzheimer's disease in humans and other animals: A consequence of postreproductive life span and longevity rather than aging. *Alzheimer's Dement.* **2018**, *14*, 195–204. [CrossRef] [PubMed]
3. Di Guardo, G. Cetaceans, models for human disease? *Res. Vet. Sci.* **2018**, *119*, 43–44. [CrossRef] [PubMed]
4. Davis, D.A.; Garamszegi, S.P.; Banack, S.A.; Dooley, P.D.; Coyne, T.M.; McLean, D.W.; Rotstein, D.S.; Mash, D.C.; Cox, P.A. Bmaa, methylmercury, and mechanisms of neurodegeneration in dolphins: A natural model of toxin exposure. *Toxins* **2021**, *13*, 697. [CrossRef] [PubMed]
5. Orekhova, K.; Centelleghe, C.; Di Guardo, G.; Graïc, J.M.; Cozzi, B.; Trez, D.; Verin, R.; Mazzariol, S. Systematic validation and assessment of immunohistochemical markers for central nervous system pathology in cetaceans, with emphasis on auditory pathways. *PLoS ONE* **2022**, *17*, e026909. [CrossRef] [PubMed]
6. Fernández, A.; Edwards, J.F.; Rodríguez, F.; Espinosa De Los Monteros, A.; Herráez, P.; Castro, P.; Jaber, J.R.; Martín, V.; Arbelo, M. "Gas and fat embolic syndrome" involving a mass stranding of beaked whales (*Family ziphiidae*) exposed to anthropogenic sonar signals. *Vet. Pathol.* **2005**, *42*, 446–457. [CrossRef] [PubMed]
7. Gupta, R.; Sen, N. Traumatic brain injury: A risk factor for neurodegenerative diseases. *Rev. Neurosci.* **2016**, *27*, 93–100. [CrossRef] [PubMed]
8. Lillie, M.A.; Vogl, A.W.; Gerard, S.G.; Raverty, S.; Shadwick, R.E. Retia mirabilia: Protecting the cetacean brain from locomotion-generated blood pressure pulses. *Science* **2022**, *377*, 1452–1456. [CrossRef] [PubMed]
9. Ridgway, S.H.; Brownson, R.H.; Van Alstyne, K.R.; Hauser, R.A. Higher neuron densities in the cerebral cortex and larger cerebellums may limit dive times of delphinids compared to deep-diving toothed whales. *PLoS ONE* **2019**, *14*, e0226206. [CrossRef]
10. Cantú-Medellín, N.; Byrd, B.; Hohn, A.; Vázquez-Medina, J.P.; Zenteno-Savín, T. Differential antioxidant protection in tissues from marine mammals with distinct diving capacities. Shallow/short vs. deep/long divers. *Comp. Biochem. Physiol.—Part A Mol. Integr. Physiol.* **2011**, *158*, 438–443. [CrossRef]

11. Manger, P.R.; Patzke, N.; Spocter, M.A.; Bhagwandin, A.; Karlsson, K.; Bertelsen, M.F.; Alagaili, A.N.; Bennett, N.C.; Mohammed, O.B.; Herculano-Houzel, S.; et al. Amplification of potential thermogenetic mechanisms in cetacean brains compared to artiodactyl brains. *Sci. Rep.* **2021**, *11*, 5486. [CrossRef]
12. Marino, L.; Butti, C.; Connor, R.C.; Fordyce, R.E.; Herman, L.M.; Hof, P.R.; Lefebvre, L.; Lusseau, D.; McCowan, B.; Nimchinsky, E.A.; et al. A claim in search of evidence: Reply to Manger's thermogenesis hypothesis of cetacean brain structure. *Biol. Rev.* **2008**, *83*, 417–440. [CrossRef] [PubMed]
13. Nieder, C.; Rosene, D.L.; Mortazavi, F.; Oblak, A.L.; Ketten, D.R. Morphology and unbiased stereology of the lateral superior olive in the short-beaked common dolphin, *Delphinus delphis* (Cetacea, Delphinidae). *J. Morphol.* **2022**, *283*, 446–461. [CrossRef]
14. Simona, S.; Antonio, E.D.L.M.; Yania, P. Amyloid-beta peptide and phosphorylated tau in the frontopolar cerebral cortex and in the cerebellum of toothed whales: Aging vs. hypoxia Summary Statement. *Biol. Open* **2020**, *9*, bio054734.
15. Jo, M.; Lee, S.; Jeon, Y.M.; Kim, S.; Kwon, Y.; Kim, H.J. The role of TDP-43 propagation in neurodegenerative diseases: Integrating insights from clinical and experimental studies. *Exp. Mol. Med.* **2020**, *52*, 1652–1662. [CrossRef]
16. Reed, M.J.; Damodarasamy, M.; Banks, W.A. The extracellular matrix of the blood-brain barrier: Structural and functional roles in health, aging, and Alzheimer's disease. *Tissue Barriers* **2019**, *7*, 1651157. [CrossRef]
17. Wang, J.; Milner, R. Fibronectin promotes brain capillary endothelial cell survival and proliferation through alpha5beta1 and alphavbeta3 integrins via MAP kinase signalling. *J. Neurochem.* **2006**, *96*, 148–159. [CrossRef]
18. Boero, J.A.; Ascher, J.; Arregui, A.; Rovainen, C.; Woolsey, T.A. Increased brain capillaries in chronic hypoxia. *J. Appl. Physiol.* **1999**, *86*, 1211–1219. [CrossRef]
19. LaManna, J.C.; Chavez, J.C.; Pichiule, P. Structural and functional adaptation to hypoxia in the rat brain. *J. Exp. Biol.* **2004**, *207*, 3163–3169. [CrossRef]
20. Wang, J.T.; Yin, L.; Chen, Z. Neuroprotective role of fibronectin in neuron-glial extrasynaptic transmission. *Neural Regen. Res.* **2013**, *8*, 376–382. [CrossRef]
21. Hof, P.R.; Van Der Gucht, E. Structure of the cerebral cortex of the humpback whale, *Megaptera novaeangliae* (Cetacea, Mysticeti, Balaenopteridae). *Anat. Rec. Part A Discov. Mol. Cell. Evol. Biol.* **2006**, *31*, 175. [CrossRef]
22. Ackermans, N.L.; Varghese, M.; Williams, T.M.; Grimaldi, N.; Selmanovic, E.; Alipour, A.; Balchandani, P.; Reidenberg, J.S.; Hof, P.R. Evidence of traumatic brain injury in headbutting bovids. *Acta Neuropathol.* **2022**, *144*, 5–26. [CrossRef]
23. Boonstra, J.T.; Michielse, S.; Roebroeck, A.; Temel, Y.; Jahanshahi, A. Dedicated container for postmortem human brain ultra-high field magnetic resonance imaging. *Neuroimage* **2021**, *235*, 118010. [CrossRef]
24. Griswold, M.A.; Jakob, P.M.; Heidemann, R.M.; Nittka, M.; Jellus, V.; Wang, J.; Kiefer, B.; Haase, A. Generalized autocalibrating partially parallel acquisitions (GRAPPA). *Magn. Reson. Med.* **2002**, *47*, 1202–1210. [CrossRef]
25. Jenkinson, M.; Smith, S. A global optimisation method for robust affine registration of brain images. *Med. Image Anal.* **2001**, *5*, 143–156. [CrossRef]
26. Jenkinson, M.; Bannister, P.; Brady, M.; Smith, S. Improved optimization for the robust and accurate linear registration and motion correction of brain images. *Neuroimage* **2002**, *17*, 825–841. [CrossRef]
27. McNab, J.A.; Jbabdi, S.; Deoni, S.C.L.; Douaud, G.; Behrens, T.E.J.; Miller, K.L. High resolution diffusion-weighted imaging in fixed human brain using diffusion-weighted steady state free precession. *Neuroimage* **2009**, *46*, 775–785. [CrossRef]
28. Andersson, J.L.R.; Sotiropoulos, S.N. An integrated approach to correction for off-resonance effects and subject movement in diffusion MR imaging. *Neuroimage* **2016**, *125*, 1063–1078. [CrossRef] [PubMed]
29. Yeh, F.C.; Verstynen, T.D.; Wang, Y.; Fernández-Miranda, J.C.; Tseng, W.Y.I. Deterministic Diffusion Fiber Tracking Improved by Quantitative Anisotropy. *PLoS ONE* **2013**, *8*, e80713. [CrossRef]
30. Yushkevich, P.A.; Piven, J.; Hazlett, H.C.; Smith, R.G.; Ho, S.; Gee, J.C.; Gerig, G. User-guided 3D active contour segmentation of anatomical structures: Significantly improved efficiency and reliability. *Neuroimage* **2006**, *31*, 1116–1128. [CrossRef]
31. Gundersen, H.J.G.; Jensen, E.B.V.; Kiêu, K.; Nielsen, J. The efficiency of systematic sampling in stereology—Reconsidered. *J. Microsc.* **1999**, *193*, 199–211. [CrossRef] [PubMed]
32. Ogawa, T.; Arifuku, S. On the Acoustic System in the Cetacean Brains. *Sci. Rep. Whales Res. Inst.* **1948**, *2*, 1–20.
33. Graaf, A.S.d. *Anatomical Aspects of the Cetacean Brain Stem*; Van Gorcum: Assen, The Netherlands, 1967.
34. Zook, J.M.; DiCaprio, R.A. A Potential System of Delay-Lines in the Dolphin Auditory Brainstem. In *Sensory Abilities of Cetaceans*; Springer: Boston, MA, USA, 1990; pp. 181–193. [CrossRef]
35. Malmierca, M.S. Anatomy and Physiology of the Mammalian Auditory System. In *Encyclopedia of Computational Neuroscience*; Springer: Berlin/Heidelberg, Germany, 2013; pp. 1–36. [CrossRef]
36. Morgane, P.J.; Jacobs, M.S.; McFarland, W.L. The anatomy of the brain of the bottlenose dolphin (*Tursiops truncatus*). Surface configurations of the telencephalon of the bottlenose dolphin with comparative anatomical observations in four other cetacean species. *Brain Res. Bull.* **1980**, *5*, 1–107. [CrossRef]
37. Hinojosa, R.; Nelson, E.G. Cochlear nucleus neuron analysis in individuals with presbycusis. *Laryngoscope* **2011**, *121*, 2641–2648. [CrossRef]
38. Cozzi, B.; Huggenberger, S.; Oelschläger, H. *Anatomy of Dolphins: Insights into Body Structure and Function*; Academic Press: Waretown, NJ, USA, 2016; ISBN 9780124072299.
39. von Mikecz, A. Pathology and function of nuclear amyloid: Protein homeostasis matters. *Nucleus* **2014**, *5*, 311–317. [CrossRef]
40. Hefter, D.; Draguhn, A. APP as a protective factor in acute neuronal insults. *Front. Mol. Neurosci.* **2017**, *10*, 22. [CrossRef]

41. Ridgway, S.H. Diving by cetaceans. In *Diving in Animals and Man*; Brubakk, A.O., Kanwisher, J.W., Sundnes, G., Eds.; Royal Norwegian Society of Science and Letters: Trondheim, Norway, 1986; pp. 33–62.
42. Klatsky, L.J.; Wells, R.S.; Sweeney, J.C. Offshore Bottlenose Dolphins (*Tursiops truncatus*): Movement and Dive Behavior Near the Bermuda Pedestal. *J. Mammal.* **2007**, *88*, 59–66. [CrossRef]
43. Thal, D.R.; Rüb, U.; Orantes, M.; Braak, H. Phases of A beta-deposition in the human brain and its relevance for the development of AD. *Neurology* **2002**, *58*, 1791–1800. [CrossRef]
44. Morris, G.P.; Clark, I.A.; Vissel, B. Questions concerning the role of amyloid-β in the definition, aetiology and diagnosis of Alzheimer's disease. *Acta Neuropathol.* **2018**, *136*, 663–689. [CrossRef]
45. Ulbrich, P.; Khoshneviszadeh, M.; Jandke, S.; Schreiber, S.; Dityatev, A. Interplay between perivascular and perineuronal extracellular matrix remodelling in neurological and psychiatric diseases. *Eur. J. Neurosci.* **2021**, *53*, 3811–3830. [CrossRef]
46. Labrousse-Arias, D.; Martínez-Ruiz, A.; Calzada, M.J. Hypoxia and Redox Signaling on Extracellular Matrix Remodeling: From Mechanisms to Pathological Implications. *Antioxid. Redox Signal.* **2017**, *27*, 802–822. [CrossRef] [PubMed]
47. Lee, S.H.; Lee, Y.J.; Han, H.J. Role of hypoxia-induced fibronectin-integrin β1 expression in embryonic stem cell proliferation and migration: Involvement of PI3K/Akt and FAK. *J. Cell. Physiol.* **2011**, *226*, 484–493. [CrossRef] [PubMed]
48. Michalski, D.; Spielvogel, E.; Puchta, J.; Reimann, W.; Barthel, H.; Nitzsche, B.; Mages, B.; Jäger, C.; Martens, H.; Horn, A.K.E.; et al. Increased Immunosignals of Collagen IV and Fibronectin Indicate Ischemic Consequences for the Neurovascular Matrix Adhesion Zone in Various Animal Models and Human Stroke Tissue. *Front. Physiol.* **2020**, *11*, 575598. [CrossRef] [PubMed]
49. Edwards, D.N.; Bix, G.J. Roles of blood-brain barrier integrins and extracellular matrix in stroke. *Am. J. Physiol. Cell Physiol.* **2019**, *316*, C252–C263. [CrossRef]
50. Lall, R.; Mohammed, R.; Ojha, U. What are the links between hypoxia and Alzheimer’s disease? *Neuropsychiatr. Dis. Treat.* **2019**, *15*, 1343–1354. [CrossRef]
51. Schneuer, M.; Flachsbarth, S.; Czech-Damal, N.U.; Folkow, L.P.; Siebert, U.; Burmester, T. Neuroglobin of seals and whales: Evidence for a divergent role in the diving brain. *Neuroscience* **2012**, *223*, 35–44. [CrossRef]
52. Gama Sosa, M.A.; De Gasperi, R.; Pryor, D.; Perez Garcia, G.S.; Perez, G.M.; Abutarboush, R.; Kawoos, U.; Hogg, S.; Ache, B.; Janssen, W.G.; et al. Low-level blast exposure induces chronic vascular remodeling, perivascular astrocytic degeneration and vascular-associated neuroinflammation. *Acta Neuropathol. Commun.* **2021**, *9*, 167. [CrossRef]
53. Oyanagi, K.; Yamazaki, M.; Hashimoto, T.; Asakawa, M.; Wakabayashi, K.; Takahashi, H. Hippocampal sclerosis in the parkinsonism-dementia complex of Guam: Quantitative examination of neurons, neurofibrillary tangles, and TDP-43 immunoreactivity in CA1. *Neuropathology* **2015**, *35*, 224–235. [CrossRef]
54. Neumann, M.; Sampathu, D.M.; Kwong, L.K.; Truax, A.C.; Micsenyi, M.C.; Chou, T.T.; Bruce, J.; Schuck, T.; Grossman, M.; Clark, C.M.; et al. Ubiquitinated TDP-43 in frontotemporal lobar degeneration and amyotrophic lateral sclerosis. *Science* **2006**, *314*, 130–133. [CrossRef]
55. Atkinson, R.; Leung, J.; Bender, J.; Kirkcaldie, M.; Vickers, J.; King, A. TDP-43 mislocalization drives neurofilament changes in a novel model of TDP-43 proteinopathy. *Dis. Model. Mech.* **2021**, *14*, dmm047548. [CrossRef]
56. Hof, P.R.; Glezer, I.I.; Archin, N.; Janssen, W.G.; Morgane, P.J.; Morrison, J.H. The primary auditory cortex in cetacean and human brain: A comparative analysis of neurofilament protein-containing pyramidal neurons. *Neurosci. Lett.* **1992**, *146*, 91–95. [CrossRef] [PubMed]
57. Morell, M.; Raverty, S.A.; Mulsow, J.; Haulena, M.; Barrett-Lennard, L.; Nordstrom, C.A.; Venail, F.; Shadwick, R.E. Combining Cochlear Analysis and Auditory Evoked Potentials in a Beluga Whale With High-Frequency Hearing Loss. *Front. Vet. Sci.* **2020**, *7*, 534917. [CrossRef] [PubMed]
58. Ulfig, N.; Nickel, J.; Bohl, J. Monoclonal antibodies SMI 311 and SMI 312 as tools to investigate the maturation of nerve cells and axonal patterns in human fetal brain. *Cell Tissue Res.* **1998**, *291*, 433–443. [CrossRef]
59. Redondo, J.; Hares, K.; Wilkins, A.; Scolding, N.; Kemp, K. Reductions in kinesin expression are associated with nitric oxide-induced axonal damage. *J. Neurosci. Res.* **2015**, *93*, 882–892. [CrossRef]
60. Schirmer, L.; Antel, J.P.; Brück, W.; Stadelmann, C. Axonal Loss and Neurofilament Phosphorylation Changes Accompany Lesion Development and Clinical Progression in Multiple Sclerosis. *Brain Pathol.* **2011**, *21*, 428. [CrossRef]
61. Nasuhidehnavi, A.; Yap, G.S. Microglia and astrocyte responses to neuropathogenic protozoan parasites. *Fac. Rev.* **2021**, *10*, 69. [CrossRef]
62. Pintore, M.D.; Mignone, W.; Di Guardo, G.; Mazzariol, S.; Ballardini, M.; Florio, C.L.; Goria, M.; Romano, A.; Caracappa, S.; Giorda, F.; et al. Neuropathologic findings in cetaceans stranded in Italy (2002–14). *J. Wildl. Dis.* **2018**, *54*, 295–303. [CrossRef]
63. Yin, H.Z.; Yu, S.; Hsu, C.I.; Liu, J.; Acab, A.; Wu, R.; Tao, A.; Chiang, B.J.; Weiss, J.H. Intrathecal infusion of BMAA induces selective motor neuron damage and astrogliosis in the ventral horn of the spinal cord. *Exp. Neurol.* **2014**, *261*, 1–9. [CrossRef]
64. Finger, C.E.; Moreno-Gonzalez, I.; Gutierrez, A.; Moruno-Manchon, J.F.; McCullough, L.D. Age-related immune alterations and cerebrovascular inflammation. *Mol. Psychiatry* **2021**, *27*, 803–818. [CrossRef]
65. Wang, W.; Zhang, L.S.; Zinsmaier, A.K.; Patterson, G.; Leptich, E.J.; Shoemaker, S.L.; Yatskievych, T.A.; Gibboni, R.; Pace, E.; Luo, H.; et al. Neuroinflammation mediates noise-induced synaptic imbalance and tinnitus in rodent models. *PLoS Biol.* **2019**, *17*, e3000307. [CrossRef]
66. Chang, K.-H.; Jin, S.-Y.; Park, J.-W.; Park, G.-E.; Lee, K.-A.; Jun, B.-C.; Yeo, S.-W. Expression of Glial Fibrillay Acidic Protein in the Central Auditory Pathway of Rats after Loud Noise Exposure. *Korean J. Audiol.* **2010**, *14*, 12–15.

67. Säljö, A.; Bao, F.; Hamberger, A.; Haglid, K.G.; Hansson, H.A. Exposure to short-lasting impulse noise causes microglial and astroglial cell activation in the adult rat brain. *Pathophysiology* **2001**, *8*, 105–111. [CrossRef]
68. Ries, M.; Sastre, M. Mechanisms of Aβ Clearance and Degradation by Glial Cells. *Front. Aging Neurosci.* **2016**, *8*, 160. [CrossRef]
69. Gerrits, E.; Brouwer, N.; Kooistra, S.M.; Woodbury, M.E.; Vermeiren, Y.; Lambourne, M.; Mulder, J.; Kummer, M.; Möller, T.; Biber, K.; et al. Distinct amyloid-β and tau-associated microglia profiles in Alzheimer's disease. *Acta Neuropathol.* **2021**, *141*, 681–696. [CrossRef]
70. Tom, V.J.; Doller, C.M.; Malouf, A.T.; Silver, J. Astrocyte-Associated Fibronectin Is Critical for Axonal Regeneration in Adult White Matter. *J. Neurosci.* **2004**, *24*, 9282. [CrossRef]
71. Marino, L.; Connor, R.C.; Fordyce, R.E.; Herman, L.M.; Hof, P.R.; Lefebvre, L.; Lusseau, D.; McCowan, B.; Nimchinsky, E.A.; Pack, A.A.; et al. Cetaceans have complex brains for complex cognition. *PLoS Biol.* **2007**, *5*, 0966–0972. [CrossRef]
72. Reiss, D.; Marino, L. Mirror self-recognition in the bottlenose dolphin: A case of cognitive convergence. *Proc. Natl. Acad. Sci. USA* **2001**, *98*, 5937–5942. [CrossRef]
73. Smith, T.G.; Siniff, D.B.; Reichle, R.; Stone, S. Coordinated behavior of killer whales, Orcinus orca, hunting a crabeater seal, Lobodon carcinophagus. *Can. J. Zool.* **1981**, *59*, 1185–1189. [CrossRef]
74. Morlock, G.E.; Ziltener, A.; Geyer, S.; Tersteegen, J.; Mehl, A.; Schreiner, T.; Kamel, T.; Brümmer, F. Evidence that Indo-Pacific bottlenose dolphins self-medicate with invertebrates in coral reefs. *iScience* **2022**, *25*, 104271. [CrossRef]
75. Hall, J.G. Hearing and Primary Auditory Centres of the Whales. *Acta Oto-Laryngologica* **2009**, *63*, 244–250. [CrossRef]
76. Bullock, T.H.; Gurevich, V.S. Soviet literature on the nervous system and psychobiology of Cetacea. *Int. Rev. Neurobiol.* **1979**, *21*, 47–127. [CrossRef] [PubMed]
77. Jansen, J.; Jansen, J.K.S. The nervous system of Cetacea. In *Biology of Marine Mammals*; Andersen, H.T., Ed.; Academic Press: New York, NY, USA, 1969; pp. 175–252.
78. Gandolfi, A.; Horoupian, D.S.; De Teresa, R.M. Quantitative and cytometric analysis of the ventral cochlear nucleus in man. *J. Neurol. Sci.* **1981**, *50*, 443–455. [CrossRef] [PubMed]
79. Huggenberger, S.; Oelschläger, H.A.; Cozzi, B.; Centelleghe, C.; Banzato, T.; Demma, M.; Oelschläger, J.; Gorter, U. *Atlas of the Anatomy of Dolphins and Whales/Stefan Huggenberger, Helmut Oelschläger, Bruno Cozzi; in Collaboration with Cinzia Centelleghe [and 3 Others]; with the Assistance of Tommaso Banzato [and 8 Others]*; Massimo, D., Jutta, O., Eds.; Academic Press: Waretown, NJ, USA, 2019.
80. Sitek, K.R.; Gulban, O.F.; Calabrese, E.; Johnson, G.A.; Lage-Castellanos, A.; Moerel, M.; Ghosh, S.S.; De Martino, F. Mapping the human subcortical auditory system using histology, postmortem MRI and in vivo MRI at 7T. *Elife* **2019**, *8*, e48932. [CrossRef] [PubMed]
81. Sitek, K.R.; Calabrese, E.; Johnson, G.A.; Ghosh, S.S.; Chandrasekaran, B. Structural Connectivity of Human Inferior Colliculus Subdivisions Using in vivo and post mortem Diffusion MRI Tractography. *Front. Neurosci.* **2022**, *16*, 751595. [CrossRef]
82. Malkemper, E.P.; Oelschläger, H.H.A.; Huggenberger, S. The dolphin cochlear nucleus: Topography, histology and functional implications. *J. Morphol.* **2012**, *273*, 173–185. [CrossRef]
83. Ijsseldijk, L.L.; Brownlow, A.C.; Mazzariol, S. Best Practice on Cetacean Post Mortem Investigation and Tissue Sampling; Joint ACCOBAMS and ASCOBANS document. 2019. Available online: osf.io/zh4ra/ (accessed on 15 April 2022).
84. Obusan, M.C.M.; Caras, J.A.A.; Lumang, L.S.L.; Calderon, E.J.S.; Villanueva, R.M.D.; Salibay, C.C.; Siringan, M.A.T.; Rivera, W.L.; Masangkay, J.S.; Aragones, L.V. Bacteriological and histopathological findings in cetaceans that stranded in the Philippines from 2017 to 2018. *bioRxiv* **2020**. [CrossRef]
85. Morell, M.; Brownlow, A.; McGovern, B.; Raverty, S.A.; Shadwick, R.E.; André, M. Implementation of a method to visualize noise-induced hearing loss in mass stranded cetaceans. *Sci. Rep.* **2017**, *7*, srep41848. [CrossRef]

Addendum II: Semi-quantitative Comparisons of Bottlenose Dolphin Auditory Pathway Fiber Tracts

In publication III, the seed-to-end, seed-to-terminative and end-to-end fiber tracts between the auditory nerve (AN), VCN, lateral lemniscus (LL), IC central nucleus (CN), external cortex (EC) and brachium, and medial geniculate nucleus (MGN) are enumerated in Figure 2. However, it was beyond the scope of that paper to compare the DTI results of the left hemisphere of that animal (Marine 0142) and a second bottlenose dolphin, Marine 0116, for which both, separate hemispheres (Figure 9) were scanned using a 7T-MRI using the same parameters as described in Publication III.

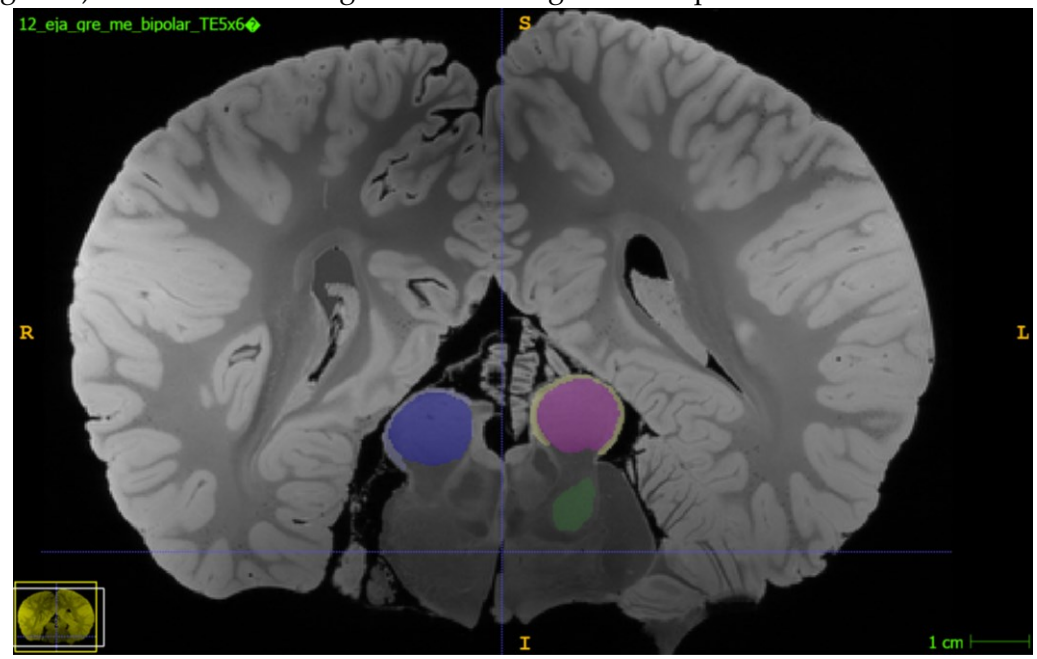

Figure 9. Coronal cross-section image from the MRI scan of Marine 0116 at the level of the IC. The IC central nuclei (right—blue; left—pink) and external cortices (right—light blue; left—yellow), as well as the left lateral lemniscus (green) are masked for subsequent segmentation. Rostral perspective.

Here the semi-quantitative results of Marine 0116 two hemispheres are presented in comparison to each other, and to the left hemisphere of Marine 0142. Table 6 shows the number of tracts leaving or reaching each nucleus when it is considered as a seed, ending point (End) and region of interest (ROI). Tables 7, 8 and 9 display the seed-to-end, seed-to-terminative, and end-to-end connections calculated using Yeh and colleagues' (2013) deterministic fiber tracking algorithm.

Table 6. Number of tracts calculated for the displayed auditory nuclei.

	Seed			End			ROI		
Nucleus	R_Mar 0116	L_Mar 0116	L_Mar 0142	R_Mar 0116	L_Mar 0116	L_Mar 0142	R_Mar 0116	L_Mar 0116	L_Mar 0142
AN	874356	756301	526077	22	497	44	2387	2125	1675
VCN	744339	561069	471679	641	1194	875	3184	4381	8297
LL	285499	297663	578325	562	488	1652	1853	1493	7456
IC CN	304960	296055	453041	3014	1581	5630	7252	4082	9967
IC EC	283986	426052	369924	2058	3789	1602	8367	6793	7498
Brachium	907062	840455	719650	60	251	4371	9195	6582	17159
MGN	891313	662599	972942	1140	4569	294	12906	11143	20251

Table 7. Number of seed (2nd row)-to-end (1st column) tracts calculated between the auditory nuclei of the right and left hemispheres of Marine 0116 (unmarked in 1st column), and the left hemisphere of Marine 0142 (marked in 1st column). Bar icons represent numerical comparisons between the three hemispheres for each nucleus (separated by thick borders).

SEED to END							
Nucleus	**AN**	**VCN**	**LL**	**IC CN**	**IC EC**	**Brachium**	**MGN**
R_AN		155068	1	2	1	0	0
L_AN		185447	47	31	2	2	0
L_AN 0142		10275	1458	2023	636	224	6
R_VCN	3940		2	12	1	0	0
L_VCN	54464		301	1041	8	34	0
L_VCN 0142	3990		2255	9382	545	257	2
R_LL	0	675		38262	130	1308	1
L_LL	70	11185		41803	8465	2165	0
L_LL 0142	41	21553		209522	13062	5839	438
R_IC CN	0	10075	22856		26803	1406	9075
L_IC CN	327	35364	2267		61999	507	11220
L_IC CN 0142	1	3801	102948		73043	53266	3310
R_IC EC	0	901	479	69327		1297	11935
L_IC EC	35	3105	977	66442		779	64515
L_IC EC 0142	1	3379	36366	256602		46687	3015
R_Brachium	907062	814	3208	208598	249895		72329
L_Brachium	0	0	0	109858	529071		220802
LBrachium 0142	0	44	2570	157946	98229		10013
R_MGN	1	197	154	203242	139173	3225	
L_MGN	0	0	0	43814	247389	19304	
L_MGN 0142	0	0	0	107473	23863	170078	

Table 8. Number of seed (2nd row)-to-terminative (1st column) tracts calculated between the auditory nuclei of the right and left hemispheres of Marine 0116 (unmarked in 1st column), and the left hemisphere of Marine 0142 (marked in 1st column). Bar icons represent numerical comparisons between the three hemispheres for each nucleus (separated by thick borders).

SEED to TERMINATIVE							
Nucleus	**AN**	**VCN**	**LL**	**IC CN**	**IC EC**	**Brachium**	**MGN**
R_AN		270554	874356	874356	874356	874356	874356
L_AN		238313	497	756301	756301	756301	756301
L_AN 0142		5790	43	526077	526077	526077	526077
R_VCN	353638		744335	744339	744339	744339	744339
L_VCN	276819		558557	561069	561069	561069	561069
L_VCN 0142	423519		458304	471679	471679	471679	471679
R_LL	285499	285435		260016	279080	273122	285499
L_LL	297654	297052		291212	288003	294461	297663
L_LL 0142	578322	556501		485482	531809	576179	578325
R_IC CN	304960	304960	270065		157721	240842	296446
L_IC CN	296055	296055	280948		133364	259471	290102
L_IC 0142	453041	453041	374458		253621	352316	440863
R_IC EC	283986	283986	283607	205114		133561	232997
L_IC EC	426052	426052	423097	332300		162224	306688
L_IC EC 0142	369924	369924	364115	174086		276873	354561
R_Brachium	907062	907062	904901	862921	839467		707084
L_Brachium	840455	840455	840421	738023	554315		435838
Lbrachium 0142	719650	719650	718951	619578	661183		516932
R_MGN	891313	891313	891313	891190	888651	807592	
L_MGN	662599	662599	662599	657386	631432	555674	
L_MGN 0142	972942	972942	972942	971207	972420	920253	

Table 9. Number of end-to-end tracts calculated between the auditory nuclei of the right and left hemispheres of Marine 0116 (unmarked in 1st column), and the left hemisphere of Marine 0142 (marked in 1st column). Bar icons represent numerical comparisons between the three hemispheres for each nucleus (separated by thick borders).

END to END							
Nucleus	**AN**	**VCN**	**LL**	**IC CN**	**IC EC**	**Brachium**	**MGN**
R_AN		1	0	0	0	0	0
L_AN		0	0	1	0	0	0
L_AN 0142		0	0	0	0	0	0
R_VCN	1		2	48	0	0	0
L_VCN	0		2	175	1	0	0
L_VCN 0142	0		12	63	11	1	0
R_LL	0	2		149	0	6	0
L_LL	0	2		33	0	2	0
L_LL 0142	0	12		988	46	32	0
R_IC CN	0	48	149		10	0	72
L_IC CN	1	175	33		28	0	97
L_IC 0142	0	63	988		362	380	37
R_IC EC	0	0	0	10		2	65
L_IC EC	0	1	0	28		0	337
L_IC EC 0142	0	11	46	362		56	17
R_Brachium	0	0	6	0	2		0
L_Brachium	0	0	2	0	0		4
Lbrachium 0142	0	1	32	380	56		3
R_MGN	0	0	0	72	65	0	
L_MGN	0	0	0	97	337	4	
L_MGN 0142	0	0	0	37	17	3	

In a semi-quantitative comparison, there are more seed-to-end tracts in the nuclei of the left hemisphere of Marine 0116. The nuclei of the brainstem (from AN to LL) sprout more connections in Marine 0142, although looking further towards the brachium and thalamus, the right-side IC brachium and MGN of Marine 0116 exhibit higher numbers of tracts.

Seed-to-terminative connections (i.e., any tracts ending or passing through the second nucleus named in the first column of Tables 8, 9, and 10 are counted) appear balanced out between the left and right hemispheres of Marine 0116. Tracts seeded from the AN in this dolphin result as more numerous, because more nerve tissue was available bilaterally as opposed to in Marine 0142. Another potential confounder lies in the right VCN of Marine 0116, which was not easily distinguishable from the surrounding tissue including the AN due to a reduced difference in signal intensity and positioning of the brain within its scanning container. It is possible that its volume is overestimated, and thus more connections are expected from a larger masking area.

End-to-end connections are low in number but consistent between the VCN and IC CN, the LL and IC CN, CN IC, and CN EC to MGB in both examined dolphins, and in Marine 0142 additionally IC brachium to the IC CN and EC. This highlights the important role that the IC plays as an integration center for auditory and non-auditory information within the brain. No left-to-right asymmetry was noted from these tract numbers on the brainstem and midbrain level, and more animals of both sexes and different age groups would be required to assess asymmetry systematically in the future (Wright et al., 2018).

The DTI data of the two bottlenose dolphins yielded additional qualitative findings regarding cortical connectivity. The areas of the lateral gyrus corresponding to the primary visual cortex, as

well as the suprasylvian and ectosylvian gyri delineated as A1 and A2 in the literature were segmented in the middle rostrocaudal third of the brain scans (Figure 10a). While we could not assess contralateral connections due to the physical separation of the left and right hemispheres in Marine 0116, we could visualize the unilateral tracts of the two sides simultaneously. When the right and left IC were set as ending regions, the tracts of the left side appeared more pronounced than on the right (Figure 10b). This could be incidental, but importantly, the fiber tracts reached the lateral gyrus, which is traditionally classified as a primary visual cortex, omitting entirely the putatively auditory suprasylvian and ectosylvian gyri. Another unexpected finding was that the VCN, when set as an ending region, projected fibers into the area of the somatosensory cortex (Figure 10c). This was consistent between the two scanned dolphin brains. The connection from the midbrain and thalamic auditory nuclei to the temporal cortex described in older (Revishchin and Garey, 1990) and more recent literature (Berns et al., 2015a) was re-created, although Marine 0142 also displayed a strong connection to the paralimbic lobe (Figure 10d).

Due to the unusual lack of a connection between any of the segmented brainstem and midbrain nuclei to A1/A2, both a more restricted (Figure 10e, f) and expanded area of the visual and A1/A2 (Figure 10a) cortices were examined. However, consistently, the V1 appeared to connect to the auditory pathway (Figure 10f), while A1/A2 connected only with itself (Figure 10e), resembling a pattern of corticocortical connections of association areas in terrestrial mammals (Zalesky and Fornito, 2009; Wang et al., 2012).

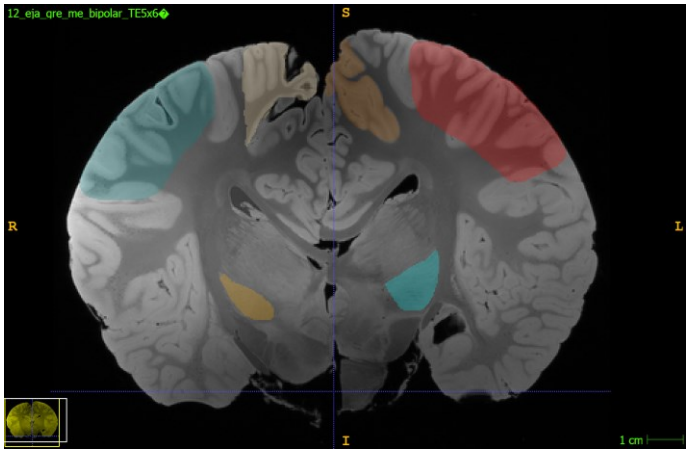

(**a**)

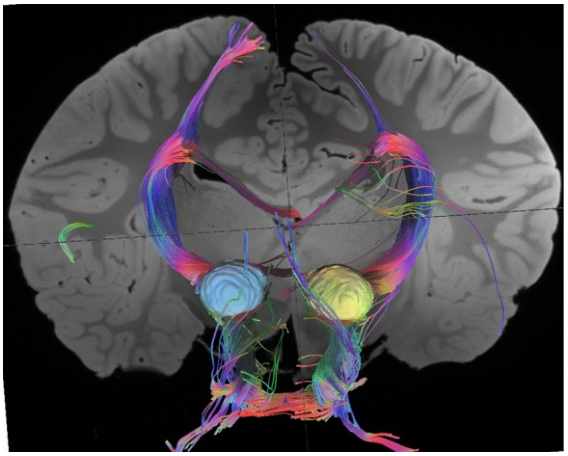

(**b**)

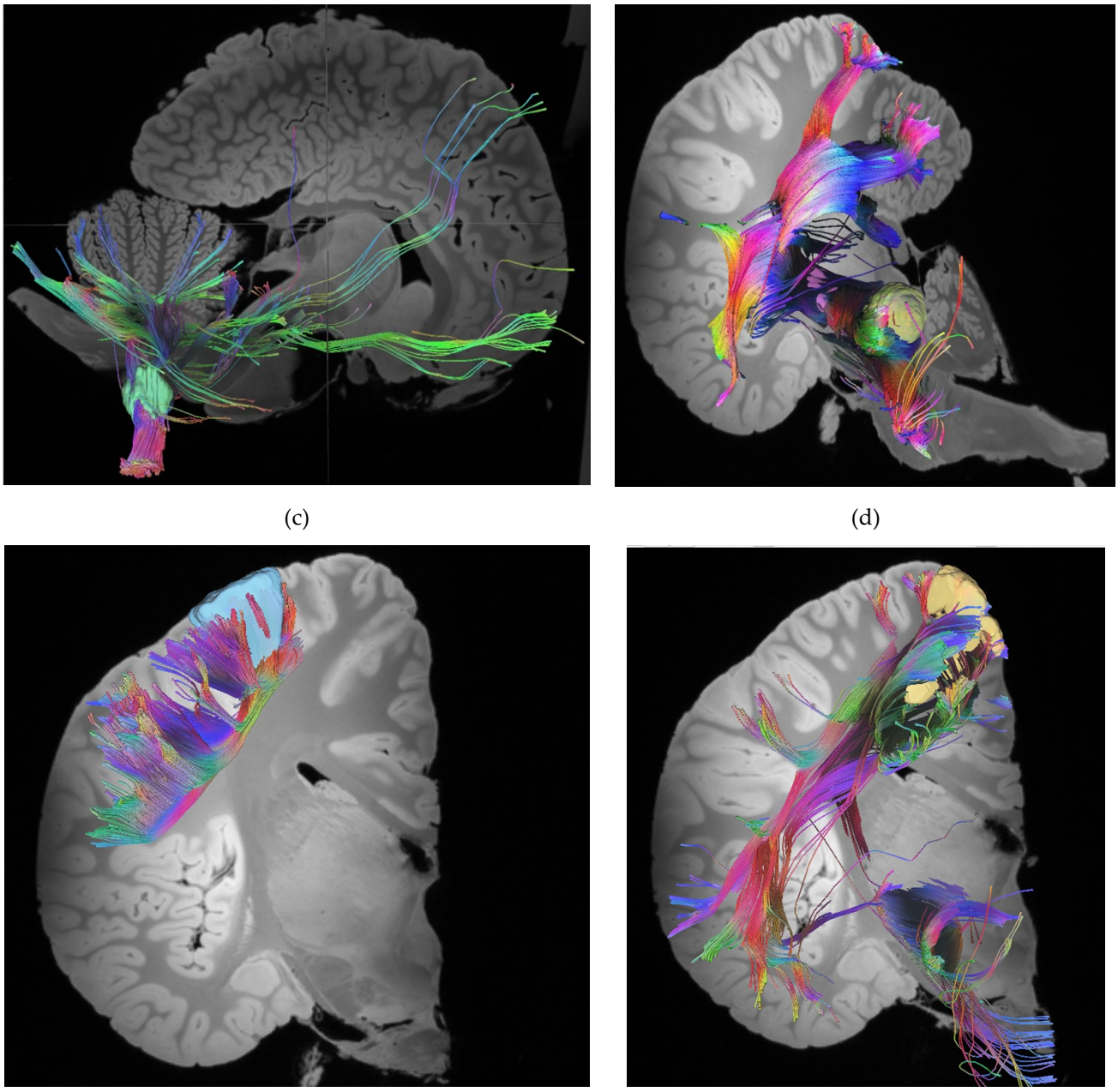

(c) (d)

(e) (f)

Figure 10. DTI images of Marine 0116 (a, b, c) and Marine 0142 (d, e, f). (a) Areas of the lateral gyrus corresponding to the primary visual cortex (masked in tan and brown on the right and left sides, respectively), as well as the suprasylvian and ectosylvian gyri delineated as A1 and A2 in the literature (turquoise on the right; red on the left) were segmented in the middle rostrocaudal third of the brain. Rostral perspective. The MGN is masked orange on the right and light blue on the left. (b) Fiber tracts calculated from the right and left IC as ending regions. Caudal perspective. (c) Fiber tracts calculated from the right VCN, set as an ending region, projected fibers (light green) into the area of the somatosensory cortex. Right lateral perspective. (d) Fibers calculated from the left MGN as a ROI display connections to the temporal, visual and paralimbic lobes. Left caudolateral perspective. (e) Fiber tracts calculated from the A1 (as a ROI) are of the suprasylvian gyrus (blue) show corticocortical connections within the A1/A2 cortical domain. Caudal perspective. (f) Fiber tracts calculated from the primary visual cortex (as an End) of the lateral gyrus (restrictively masked in yellow) connect to the temporal lobe, MGN, and IC. Caudal perspective.

While deterministic fiber tracking provides semi-quantitative to qualitative information and does not reflect the number of axons composing a given anatomical tract, it may nevertheless

be useful in assessing multiple animals' volumes of different nuclei of interest *in situ*, provided they are delineated and assessed in a standardized way. The present findings are intended as an example for the type of analyses that can be performed in *post-mortem* dolphin brains and are further considered in the Discussion.

Addendum III: Stereological Assessment of Morphological Neuronal Types in the Bottlenose Dolphin VCN

In addition to designing the probes for stereological analysis of the immunoreactivity of various antibodies in publication III, the archived coronal sections of the right VCN of Bottlenose dolphin 2 (Dolphin 2) were analyzed for the different morphological subpopulations of the VCN as reported for two other species of cetacean—short-beaked common and La Plata (*Pontoporia blainvillei*) dolphins—by Malkemper and colleagues (2012). Using a grid size of 400 × 400 µm, with the systematic random sampling layout at 100 % of this region of interest, optical dissector height at 20 µm with 5 µm top and bottom guard zones and manual focus, every 40th section (originally cut at 35 µm thickness) was evaluated for the morphologies summarized in Table 10. The other methodological steps coincide with those reported in Publication III. The aim was to evaluate the feasibility of quantifying different morphological subpopulations within the VCN in order to infer the functional organization of this nucleus.

Table 10. Morphological subtypes assessed in this project, their putative functions and their references. Images are from Malkemper et al. (2012), and the scalebar is set to 100 µm.

Morphological cell type	Functional significance (terrestrial mammals)	Reference
Small spherical cells 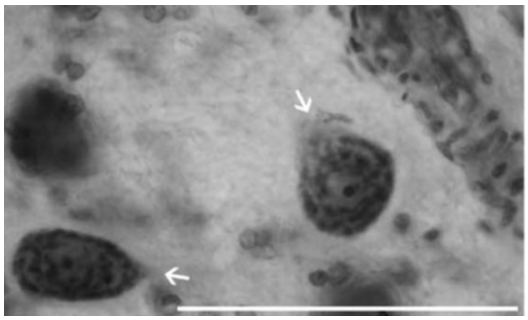	Likely involvement in directional hearing. They connect to the ipsilateral lateral superior olive with excitatory terminals. Diameter: 25-30 µm	Cant and Benson, (2003); Grothe, (2003)
Small globular cells 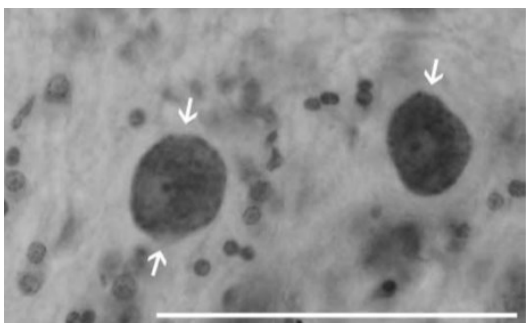	Predominantly project towards the contralateral medial nucleus of the trapezoid body, ending in the very large calices of Held. From there, the next connection reaches the lateral nucleus of the lateral superior olive with inhibitory input. Potential involvement in ultrasonic echolocation.	Malkemper et al., (2012)

	Diameter: ~30 μm	
Giant cells 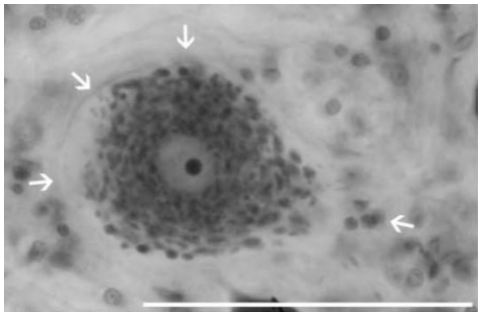	Send inhibitory connections to the IC and contralateral (Cant and Benson, 2003).They are normally found in the DCN, which is only rudimentary in cetaceans. Projections putatively constitute dorsal acoustic stria in cetaceans (De Graaf, 1967). Diameter: 50-60 μm	Cant and Benson (2004) De Graaf (1967)
Multipolar cells 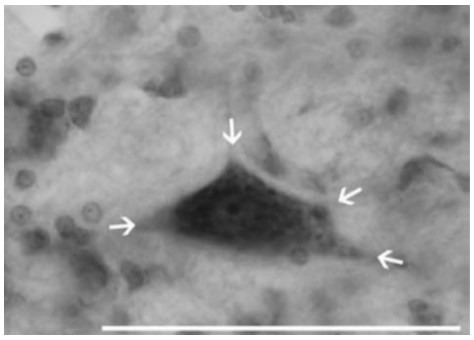	Umbrella term for a group of further subtypes e.g., type I send excitatory input to contralateral IC and ipsilateral DCN (involved in speech recognition); type II emit inhibitory input to contralateral VCN and bilaterally to the DCN. Diameter: 30-40 μm	Cant and Benson, (2003)
Octopus cells 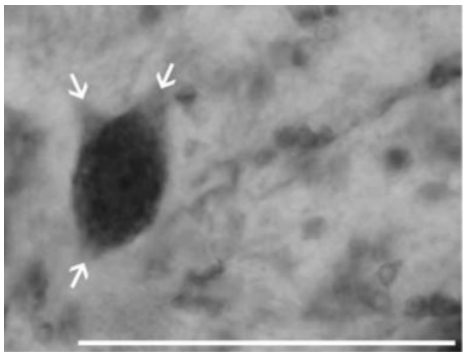	Projections predominantly to the contralateral ventral nucleus of the lateral lemniscus, which in turn sends inhibitory input to the IC. Involved in speech recognition and processing of other complex sounds. Diameter: 25-40 μm	Cant and Benson, (2003)
Small multipolar cells 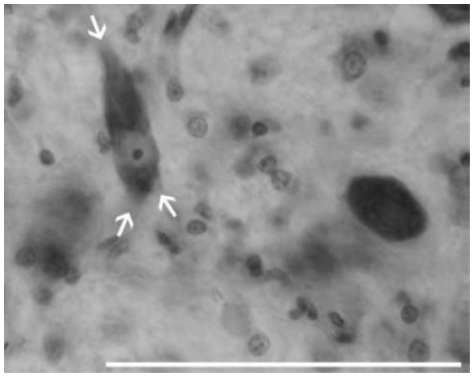	Function unknown. They may sometimes appear as a dorsomedial (and in odontocetes potentially also dorsolateral) "cap" around the VCN. Diameter: 20-30 μm	Osen, (1969); Moore and Osen (1979).

The Cavalieri volume of the right VCN was calculated and used to estimate the density of the counted neurons. Number estimates, percentages, densities and coefficients of error (CEs) of the VCN of Dolphin 2 are presented in Table 11.

Table 11. Results of the stereological assessment of the right VCN neuronal subpopulations using the optical disector probe (StereoInvestigator). CE—coefficient of error as calculated according to Gundersen (1999) and Schmitz and Hof (2005).

Neuronal by morphological type	Total markers counted	Percentage from total (%)	Estimated population using mean section thickness with counts	Density referring to VCN Cavalieri volume corrected for overprojection (neurons/mm^3)	CE (Gundersen), m=0	CE (Gundersen), m=1	1st estimated CE (Schmitz-Hof)	2nd estimated CE (Schmitz-Hof)
Small spherical	29	6.1	172243	867	0.19	0.19	0.22	0.19
Small globular	27	5.7	160364	807	0.19	0.19	0.18	0.19
Giant	9	1.9	53455	269	0.33	0.33	0.33	0.33
Multipolar	82	17.3	487031	2451	0.12	0.11	0.10	0.11
Small multipolar	314	66.2	1864973	9385	0.08	0.06	0.08	0.06
Octopus	13	2.7	77212	389	0.30	0.28	0.27	0.28
All neurons	474	100	2815278	14168	0.06	0.05	0.06	0.05

The results obtained allowed an estimate of the total number and density of neurons present in the dolphin VCN that could be compared to those of Marine 0142 in publication III. The CE is only sufficiently low considering the sum of all the neurons counted but rise to > 0.1 when looking at each different morphology. The oversample-resample probe in StereoInvestigator allowed us to confirm that this sampling design was on the lower limit for a precise estimate of the neuronal numbers, as shown in the visualization of the predicted variation of the estimates assuming a reduction of the sampling density by several factors (Figure 11). A two-fold reduction of the number of sampling sites would already imply a variation in the neuronal number estimate of around 400,000. For this reason, a higher sampling density was used to estimate different immunoreactivity patterns in the VCN of Marine 0142 in Publication III.

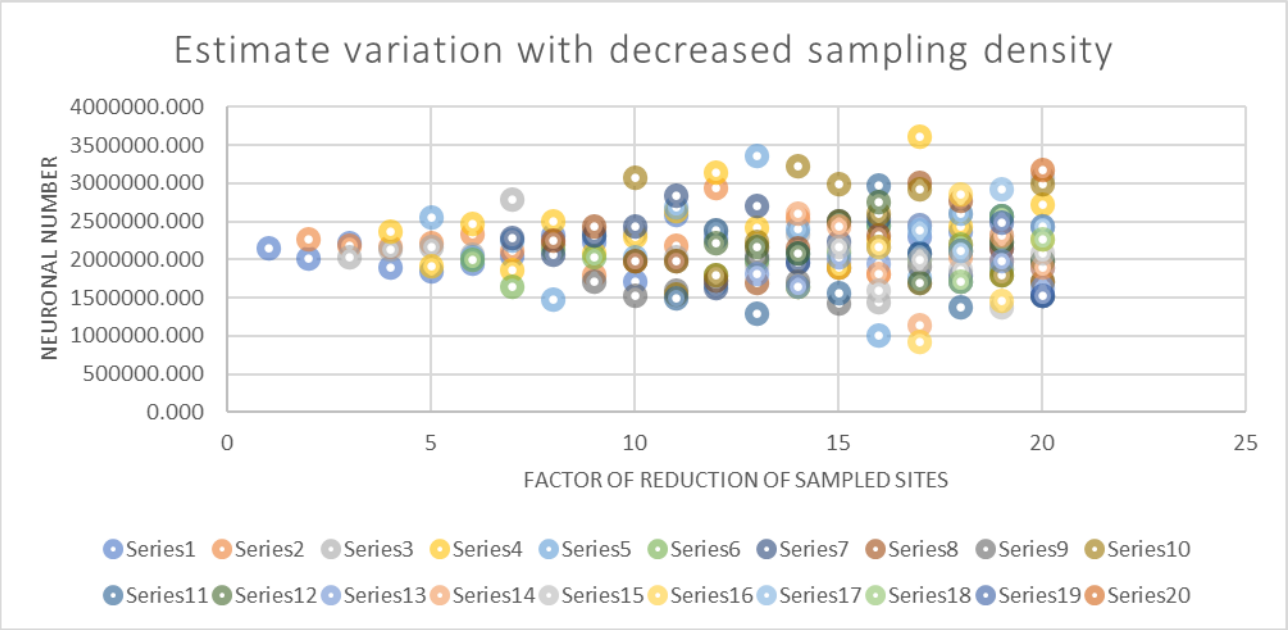

Figure 11. Oversample-resample probe results from StereoInvestigator. Series 1-20 represent the predicted alternative estimates obtained using a theoretical reduction of the number of sampling sites represented by the factor on the X-axis. It is visible that this variability increases strongly starting from a two-fold reduction of the oversampled number (i.e., a quarter of the sampling sites actually used), ending with a potential variation of approximately 2 million neurons at the factor 20.

The most often found morphological cell type were the small multipolar and multipolar neurons, followed by the small spherical and globular cells. No clear indication of large spherical cells was present, similar to the finding in common dolphin and unlike that of the La Plata dolphin made by Malkemper and colleagues (2012). However, as in those studies, the similarity of this neuronal type to other spherical cells and *post-mortem* degradation of the Nissl substance may confound the findings. A similar limitation is inherent in the search for octopus cells, in which the characteristic parallel alignment of the dendrites appears at a certain distance from the cell soma, and depending on the orientation of the cut and section thickness, this might encumber their detection (Malkemper et al., 2012).

In this context, it was not possible to delineate the four subdivisions previously described in the cetacean VCN: partes anterior, posterior, dorsomedialis, and dorsolateralis. In general, only every 10th section of the series was available in the archived materials of Dolphin 2, and not each one was intact enough to assess the complete VCN—hence the sampling interval of every 40th section. The cytoarchitectural borders between the different segments could not be determined with certainty, and the sampling density would have had to be much higher to account for the smaller volume of each subnucleus. It is possible that certain types of tissue processing and embedding may affect the ratios of subnuclei to one another due to irregular shrinking of axonal fiber-rich versus cell-rich areas.

Therefore, no information on the distribution of the different cell types is assessed here, but future studies could focus on assessing this using similar heatmaps as seen in Figure 9 of publication III. To the best of our knowledge, so far only cetaceans from the high to very-high frequency hearing groups have been assessed for VCN morphology (common dolphin, La Plata dolphin, harbor porpoise, bottlenose dolphin), and the morphological cell types mostly correspond to this high frequency specialized-hearing. Conversely, large spherical cells, associated with low

frequency signal processing, were seen in the La Plata dolphin, a specialist in high frequency clicks (Malkemper et al., 2012; Von Fersen, 2000). Assessing further cetacean species belonging to the mid- and low-frequency groups (Southall et al., 2019) could advance understanding of the correlation between morphological and functional features of the dolphin auditory pathway. The number estimates provided in this addendum could serve as a baseline for quantitative comparisons of this manner for upcoming research.

Discussion

Evidence of individually variable effects of noise is accumulating for cetaceans, ranging from reproductive disturbance to inability to communicate and forage in environmental niches that they evolved to fit over millions of years. These observations, deduced from behavioral studies, are argued to be vague and without undisputable evidence of causal correlation to acoustic overexposure. Due to the scarcity of objective, evidence-based approaches to mitigate anthropogenic underwater noise, the global community is currently balancing between erring on the safe side—with millions of euros flowing into mitigation measures whose efficacy remains unproven—or committing mistakes with potentially long-lasting effects on the biodiversity and eco-sustainability on our planet.

Pathophysiological and morphological data from routine *post-mortem* examinations of stranded cetaceans helps reduce uncertainty inherent in such approaches, especially if they can be correlated reliably to in-vivo audiograms. The publications and addenda presented within this dissertation contribute to the beginning of a systematic investigation of cetacean auditory CNS morphology and function. They should contribute to customizing regional management strategies to diverse and highly specialized marine species.

The direct effects of AOE on the anatomy and physiology of the auditory apparatus range from subcellular component alterations such as intra- and extracellular molecule redistributions (Shinkawa et al., 2019; Kurabi et al., 2017), structural inner ear hair cell and stereocilia damage (Raphael and Altschuler; 1991), over more systemic disruptions including vasospasm, ischemia/reperfusion damage, inflammatory and apoptotic processes, synapto- (Kujawa and Liberman, 2009) and neuropathy (Moser and Starr, 2016), to CNS changes. The latter include synaptic plasticity as well as changes in excitatory-inhibitory balance and grey and white matter volume of the brain (Schneider et al., 2009; Mühlau et al., 2006). Alone, none of these processes is pathognomonic to NIHL, but in combination they can be integrated into a signature of biomolecular and morphological events indicative of acoustic trauma.

Biomarkers of Neurodegeneration

The 11 protein biomarkers validated for bottlenose dolphins in our three years of research have increased information yield from microscopic analysis of cetacean central auditory nuclei. This represents a third of all the antibodies we investigated (33). Preliminary statistical analyses yielded

significant differences between lesion-free adults and those with lesions, as well as between younger and older adult dolphins for Apaf-1 and DGK-ζ. Systematic-random sampling yielded reliable cell counts with coefficients of error < 10% for most of the markers assessed using stereology: Aβ, TDP-43, fibronectin, phosphorylated neurofilament protein, Iba1, and GFAP. The benefits of studying each one is discussed in the presented papers.

In summary, the validated markers are deemed instrumental in analyzing auditory and non-auditory pathology, as well as basal physiology. Their expression can help interpret the pathogenesis of various afflictions, covering a range of apoptotic (Apaf-1, DGK- ζ, Bcl-2), neuroinflammatory (Aβ, TDP-43, GFAP, Iba1), structural (NF200, phosphorylated neurofilament), and ECM (fibronectin) changes. This can help us assess neurodegeneration beyond the classical search for AD-like neurodegeneration marked by tau pathology, neurofibrillary tangles, and amyloid plaques (Vacher et al., 2022; Gunn-Moore et al., 2018). In a complex brain belonging to animals that survive into senescence, many other age- and exposure-associated causes of neurodegeneration can be expected.

In pinnipeds, a lot of progress has been made in the assessment of neuropathology related to domoic acid toxicity: loss of hippocampal neurons, multifocal neuronal degeneration, gliosis, and connectivity changes have all been recorded (Buckmaster et al., 2014; Silvagni et al., 2015; Cook et al., 2018). The latter changes are consistent with findings in human medial temporal lobe epilepsy (Ramsdell & Gulland, 2014). Links to autism spectrum disorders (Lahvis, 2017) and other neurodevelopmental hindrances (Ramsdell and Zabka, 2008; Lefebvre et al., 2018) are also probable, since domoic acid is a known neuroteratogen (Doucette and Tasker, 2016). Similar mechanisms are entirely plausible in cetaceans, but little work has been done in assessing hippocampal morphology in disease states. This is partly because this structure is discreet, and positioned deeper within the brain, making it slightly more challenging to sample (Morgane et al., 1980; Patzke et al., 2015), and partly because studies so far have not revealed significant neurochemical findings within this region (Parolisi et al., 2018). However, other centers of the limbic system that are well developed, such as the amygdala and the paralimbic lobe, could represent structures evolved to fulfil the purpose of processing and memorizing sensory and emotional information (Marino, 2015), and should be explored further in terms of significant changes in the face of neurodegenerative insults. The central auditory pathway should be included here because, lacking an olfactory stimulus, the greatest connections to learning and memory are likely to be associated with acoustic information.

Meanwhile, a pilot study using induced neuronal cell cultures reprogrammed from melon-headed whale fibroblasts has assessed *in vitro* neurotoxicity of a persistent organic pollutant (POP) compound—4-hydroxy- 2′,3,5,5′-tetrachlorobiphenyl (4′OH-CB72)—and recorded significant differences in transcriptomes of whales compared to humans related to "oxidative phosphorylation, chromatin degradation, axonal transport, and neurodegenerative diseases" (Ochiai et al., 2021). One of the findings included an aberrant expression of genes regulating ECM organization, which fits well with our observation of divergent fibronectin expression in dolphin versus healthy human brain tissue. However, lacking information on the dolphin's life history, an alternative explanation could be this animal's own exposure to POPs in its marine environment.

Infectious diseases share many characteristics amongst themselves and with age-related, pollutant- and trauma-associated neurodegeneration: neuronal apoptosis and necrosis, gliosis and satellitosis, loss of synaptic connections, deposits of misfolded proteins and pigments, increased permeability of the blood-brain-barrier, edema, spongiosis, vasculopathy and immune cell infiltration. While the validated protein biomarkers can be useful in assessing many of these changes at an earlier disease stage than that characterized by morphological lesions visible in the routine hematoxylin-eosin stain (e.g., by quantifying the formation of rod-shaped microglia using an antibody against Iba1), reliable markers of vascular integrity and plasticity could not be consistently validated. In particular, despite the unsuccessful attempts to use several antibodies targeting collagen IV to visualize capillary networks using (the gold standard) enzymatic antigen retrieval, other attempts could be made using the same antibodies and alternative retrieval methods, as has worked for human brains with traumatic lesions (Enna Selmanovic, personal communication). Similarly, while markers such as the microtubule-associated protein 2 (MAP2) and Sternberger-Meyer Immunochemicals catalog #32 (SMI-32) yielded inconsistent results in our analyses, they have worked in other studies in cetaceans (e.g., Ochiai et al., 2021; Nieder et al., 2022), and should not be excluded from future work.

In the case of plasticity markers, the search can be made much more systematic, encompassing more brain regions, antibodies and epitopes, attempts using higher antibody concentrations and stronger demasking protocols. In adult rats, the unipolar brush cells of the dorsal cochlear nucleus have been shown to express doublecortin and hypothesized to have a crucial role in the changes in auditory to non-auditory sensory integration involved in tinnitus (Manohar et al., 2012; Baizer et al., 2012). Parolisi and colleagues (2018) noted a lack of doublecortin expression in the subventricular zone and hippocampus of the bottlenose dolphin. Considering the function-based need driving plastic processes both in physiological and pathological conditions, their presence in the auditory midbrains of lab animals with tinnitus, and the generally discreet morphology of the odontocete hippocampus; investigation of such markers along the "hypertrophied" (Bullock and Gurevich, 1979) cetacean central auditory pathway may hold promise. Ochiai and colleagues (2021) reported upregulated *synaptophysin* and *stathmin* mRNA expression compared to the human profile. Both genes are associated with neuroplasticity, and *stathmin* affects fear and anxiety processing in humans (Brocke et al., 2010). This underlines the possible advantages in assessing both proteins and transcriptome for assessing negative effects of anthropogenic activities on cetacean mental health, potentially opening the door to examining the "pessimistic biases" mentioned in the introduction (Bateson et al., 2007).

Baseline Neuroprotective Microenvironment in Cetacean Brains

In both the presented and previous studies, evidence is mounting that the cetacean (and pinniped) CNS is protected from habitual, diving-associated cellular stress (Krüger et al., 2019; Geßner et al., 2020; Schneuer et al., 2011; Ridgway et al., 2019; Cantú-Medellín et al., 2011). Some of these mechanisms are already discussed in Publications II and III. One of the most recurrent findings is that of intranuclear neuronal Aβ across brain regions and species consisting of both deeper and shallower divers (publication II, III; Sacchini et al., 2020; Vacher et al., 2022). While the

percentage of neurons displaying this immunoreactivity pattern varied, this nevertheless hints that the findings are not artifactual or caused by using an unspecific antibody isoform. However, further assessment conclusively differentiating the Aβ-42 oligomer from the vessel-affine Aβ-40, and from APP would improve understanding of their expression in cetaceans (Vacher et al., 2022).

Intermittent hypoxia and hypothermia are two conditions commonly present in marine mammal brains during their dives, as well as during unihemispheric sleep (Ridgway et al., 2006), and in hibernating species during their torpor. These scenarios are of great interest in *in vitro* and laboratory settings to study neurodegenerative disease pathogenesis. While the seals' strategy of neuroprotection during deep dives appears to be one of hypometabolism, cetaceans maintain high brain activity and have rather evolved a compendium of enzymatic and metabolic buffers against hypoxic insults, similarly to the naked mole rat—*Heterocephalus glaber* (Krüger, 2019). Some molecules linked with reducing ROS concentrations, including the antioxidant enzymes displayed in Figure 12, as well as genes associated with anti-apoptotic (e.g., COMM domain containing 6) and ECM genes have been shown to be overexpressed in comparison with cattle and human transcriptomes (Krüger, 2019; Ochiai, 2021). These findings fit in with what we have observed in our immunohistochemistry results of perineuronal and periglial fibronectin, an important ECM component that can support extrasynaptic transmission (Wang et al., 2013). Furthermore, Krüger and colleagues (2019) have discussed that, in addition to the ability to compensate for any metabolic deficits underwater very efficiently with an enhanced aerobic capacity when on the surface, cetaceans are outfitted with protein isomers that allow a quick switch between aerobic and anaerobic metabolism.

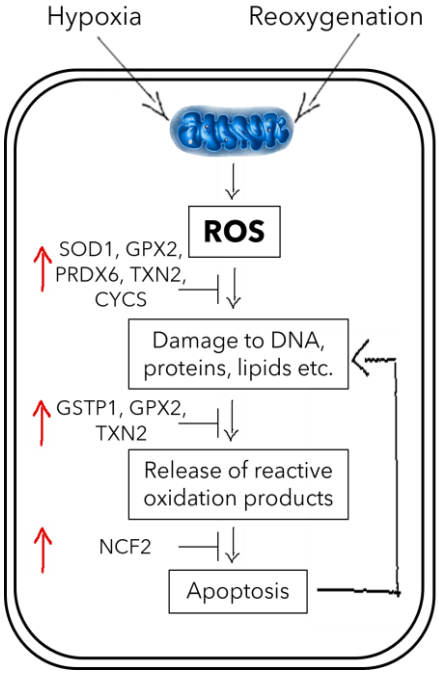

Figure 12. Genes associated with antioxidant proteins enriched in cetacean compared to cattle brains. Modified from Krüger (2019), as modified from Hayes et al. (1999).

Tau proteins are microtubule associated proteins that are important in cellular stability and axonal transport between the neuronal soma and the synapse. In disease states, they become hyperphosphorylated and can form neurofibrillary tangles (NFTs), of which paired helical fragments (PHFs) are a hallmark component (Bullman et al., 2008). A recent study showed high

incidence of both neuronal and plaque-associated Aβ and phosphorylated tau in a cohort of elderly specimens from several cetacean species. However, the authors mentioned that only one pilot whale was positive for NFTs, and phosphorylated tau-8 antibody, an antibody targeting PHFs, was non-reactive in any of the animals. Thus, this forensic evidence does not allow us to draw the conclusion of cognitive decline in any of the cetaceans, as humans are not guaranteed to display clinical signs of AD even with up to 40 % probability of displaying AD-like pathology (Nelson et al., 2009).

Moreover, hyperphosphorylation of tau is not irreversible. Hibernating species, regardless of whether they evolved to continuous dormancy or torpor-arousal cycles and were obligate or facultative hibernators, have been shown to have higher phosphorylated tau levels during the inactive period, returning to normal soon after it (Gattoni et al., 2019). Vacher and colleagues (2022) found increased phosphorylated tau in the neurons of older cetaceans, and of a bottlenose dolphin calf with a non-suppurative encephalitis associated with *Yersinia pseudotuberculosis* infection. As such, it is plausible that, as in hibernators during torpor, hypoxic and hypothermic conditions over a lifetime of frequent diving may cumulate in a semi-permanent expression of phosphorylated tau (without its more advanced pathological form of PHFs), and acute insults associated with infections may trigger increased expression even in younger animals. In hibernators, this has been proposed as a neuroprotective process associated with increased neuronal plasticity and downregulated apoptosis, differential phosphorylation of heavy neurofilaments and regulation of calcium buffering proteins (Gattoni et al., 2019).

This neuroprotective effect may be restricted by the duration and level of hypothermia, however. Species that maintain a high body temperature during hibernation, such as black bears, display permanent phosphorylated tau aggregation in old age. Marine mammals may reduce their body temperatures slightly during diving, but they remain relatively warm in comparison to a hibernator with a core temperature close to 0 C° (Logan and Storey, 2017). Thus, they are not spared the appearance of Aβ-plaques and NFTs approaching senescence, a phenomenon that may be somewhat prolonged by the epimeletic behavior of pod members.

Nevertheless, these signs in conjunction with other anatomical (Retia mirabilia, Lille et al., 2022; strong myelination, Ridgway et al., 2019), physiological (bradycardia, high hematocrit values, myoglobin, neuroglobin) adaptations render cetaceans unique models for both neurodegenerative disease and for translational studies of neuroprotective benefits of intermittent hypoxia training (Rybnikova et al., 2022; Burtscher et al., 2021). Just as studying hibernators has inspired first neuroprotective molecules against AD-like neurodegeneration (de Veij Mestdagh et al., 2022), growing evidence points towards enough similarities and intriguing differences in neurochemical programming between humans and cetaceans to merit its own branch of research.

White Matter Connectivity

Another aspect touched upon in our publications is white matter connectivity in *post-mortem* cetacean brains, assessed in 7T-MRI scans with DTI and deterministic fiber tracking (Yeh et al., 2013). While the unihemispheric connections of the brainstem and midbrain auditory nuclei of the

two bottlenose dolphin brains were consistent with previous literature (De Graaf, 1967; Ogawa and Arifuku, 1948; Zook and DiCaprio, 1990), cortical connectivity not only shows a strong connection to the temporal, visual and paralimbic cortical areas, but does not reliably visualize any connection to the putative A1/A2 regions of the suprasylvian and ectosylvian gyri as established in the electrophysiological work of the 1960s (Sokolov et al. 1972, Ladygina et al., 1978). Instead, these regions appear to send and receive reciprocal fibers amongst themselves, consistent with associative cortico-cortical connections. The projections to the temporal cortices can, however, be correlated to past work, as both retrograde tracer (Revishchin and Garey, 1990) and 3T-MRI studies (Berns et al., 2015a) have established similar connections in harbor porpoises and bottlenose dolphins.

Other unexpected fiber tracts included those from the VCN to the area of the somatosensory cortex. At first, we believed this could be an artifact due to the putative crossing over of fibers with those of the pulvinar or elliptic nucleus connections, as overlap between the visual and auditory thalamus is expected (Berns et al., 2015a). However, our segmentation and tracing revealed no evident overlap between the fibers to and from the mentioned nuclei. Given that retrograde tracing from the suprasylvian, ectosylvian, and lateral gyri of harbor porpoises using tracer dyes labelled neurons in the pulvinar, ventrobasal, and the posterior nuclear complex (Revishchin and Garey, 1990), according to the nomenclature of Kruger (1959), and that fibers tracked from DTI do not correspond to neuronal fascicles, this must nevertheless remain a potential explanation. In particular, the most anteriorly injected areas of the suprasylvian gyrus, which corresponded to the areas labelled as somatosensory using electrophysiological methods (Lende and Welker, 1972; Sokolov et al., 1972; Ladygina et al., 1978), have been traced caudally towards the ventrobasal and ventropostero-inferior nuclei (Revishchin and Garey, 1990). Another explanation could be a too-large margin for filtering the length of the tracts.

There is a strong decussation of auditory and visual fibers at the level of the thalamic radiation, as visualized based on tracer studies and macroscopically in the MRI images obtained in our studies (Figure 13). This could also have influenced the fiber vectors in the deterministic tracking algorithm.

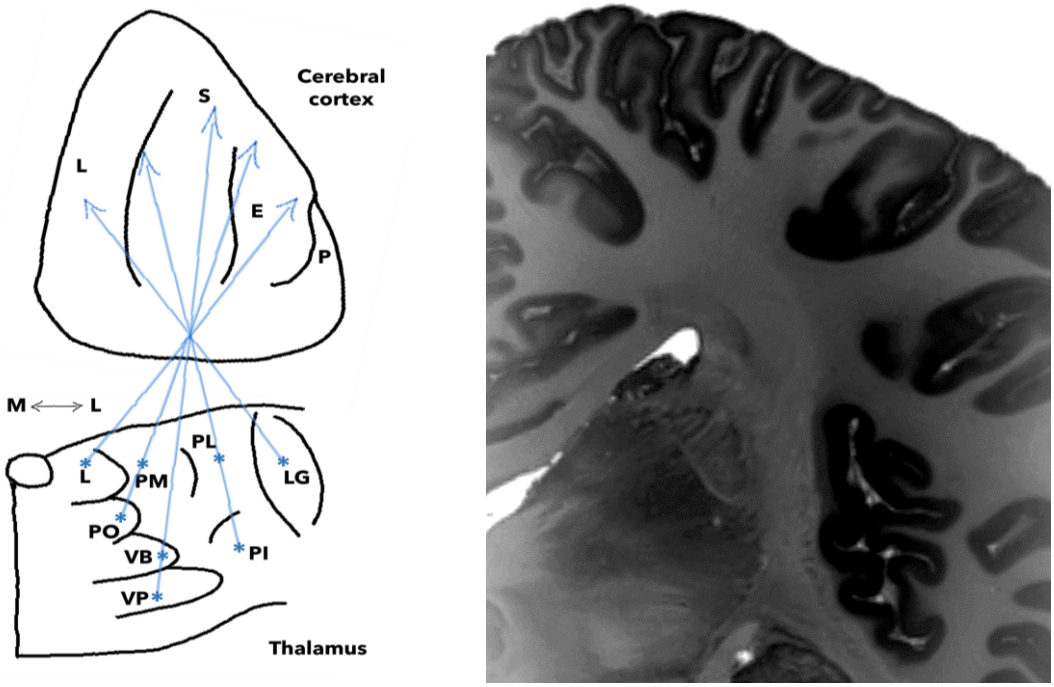

(**a**) (**b**)

Figure 13. Complex crossing over of fiber bundles in the thalamocortical projection may confound DTI findings. (a) Retrograde tracer studies demonstrated that central parts of the medial geniculate nucleus connect to the auditory area of the suprasylvian gyrus, and dorsal medial geniculate nucleus connects to A2 of the ectosylvian gyrus, and to the temporal lobe (image modified from Revishchin and Garey, 1990). (b) 7T-MRI scan of a bottlenose dolphin (Marine 0142) displays a mosaic of crossing fibers and varying signal intensity at the same level of the brain (image contrast enhanced to underline these differences).

The lack of an attached second hemisphere could present a major confounder, as contralateral connections cannot be assessed *in situ*. However, through meticulous integration into existing literature, these ultra-high-resolution scans can serve as a basis for an atlas of unilateral connectomes, and unexpected findings such as those mentioned above can be verified with further MRI scanning of whole cetacean brains as well as potentially future fMRI correlates from highly trained dolphins such as those of the US Navy (U.S. Navy, 2022), and *post-mortem* imaging of effectively blind cetaceans, such as some river dolphins. Ideally, thalamic topographical (and potentially tonotopic) mapping may be undertaken to verify the descriptive work of Kruger (1959), Krasnoshchekova and Figurina (1980) regarding the thalamocortical connections of an extended number of cetacean species.

Normalizing virtopsies prior to necropsies is a useful step for assessing in situ pathology and connecting the situation across the entire body (Tsui et al., 2020). In doing so, pathologists reduce the probability of being blinded by a first fulminant finding (such as severe pneumonia), opting rather for an integrative approach considering all the relevant macro-, microscopic and functional evidence.

Limitations

The field of cetacean pathology has the inherent limitation of a small sample size. A study is considered "systematic" once the number of specimens per species surpasses three, which naturally leads to difficulties in inference of correlation of causes of pathology and death to outside factors. This is a result of numerous logistical and ethical hurdles, including unpredictability of stranding events, variable accessibility, personnel training, equipment, and collaboration of the local authorities in a race against the rapid autolysis of cetaceans due to their insulating blubber, size, and exposure to the elements. Bureaucratic contexts may further slow down or preclude international shipment of fresh samples.

This makes it especially challenging to organize samples to adequately represent different subpopulations, age groups, and sex differences concerning physiological and pathological parameters, thereby increasing the difficulty of finding an adequate positive control for acoustic trauma. In many cases, a certain cause of death cannot be established due to missing information, since free-ranging animals are rarely monitored to the extent that spontaneous events, such as sound exposure, can be perceived using tags at the moment of insult. Fortunately, scientific advances may soon allow a more complete picture of marine mammals' age using DNA methylation (Peters et al., 2023), and passive acoustic monitoring will help contextualize MSEs without clear alternative causes of stranding and death. With efficient and transparent

collaboration among stranding networks on the national and international levels and the establishment of brain banks, sample sizes can be boosted and samples serving as positive controls for more rare, confirmed scenarios, such as blast or AOE, can be exchanged. We could begin to assess the prevalence of more discreet changes, such as presence and distribution of neuropigments such as lipofuscin and neuromelanin (Sacchini et al., 2022), changes associated with methylmercury accumulation, reference ranges of changes such as "gliosis", and neurochemical dynamics of co-infections.

Regarding more technical aspects of our studies, several limitations should be mentioned. Not all the Uhlen pillars touched upon in the Methodology section could be implemented (MacNeil et al., 2020). Genetic validation is still outstanding for most of the tested antibodies. Ideally, customized antibodies and mRNA probes would be developed to target the specific marine mammal species in question. These, as well as multiplexed in-situ hybridization, are becoming increasingly available to study the remarkable capabilities of cetacean brains (Brigid Maloney, personal communication), paving the way to address these limitations.

Another technical caveat is the difficulty to automate the evaluation of immunohistochemical reactivity, due to a relatively high background signal. Both stereological and Histoscore approaches represented a first attempt at gauging the respective antibodies' usefulness, and automatization was put aside in favor of flexibility to assess different patterns of immunoreactivity (e.g., cytoplasmic versus nuclear). This was very time-consuming, and once a key panel of antibodies becomes more established, machine learning techniques such as those suggested in counting the auditory nerve fibers in this work or using open-source software such as QuPath® and ImageJ® is suggested. Since the publication of paper II, where a scoring system of 1-3 is used, Vacher and colleagues (2022) have used a 5-level scoring for their immunohistochemical results. These inconsistencies make it difficult to cross-reference and categorize relevant findings across studies. In general, however, studies on the dolphin brain are becoming more systematic and multidisciplinary (Davis et al., 2019; Nieder et al., 2022; Vacher et al., 2022; Kot et al., 2020, Krüger et al., 2020), as well as starting to focus beyond "just" AD-like pathology (Ochiai et al., 2021; Davis et al., 2021; Sacchini et al., 2022), which bodes well for the future of cetacean conservation medicine.

With the advent of a more integrated approach to cetacean neuropathology, further challenges will need to be tackled. If we are to differentiate between NIHL and ARHL, we need to unravel physiological baselines species by species and different age/gender/environmental type. However, Rabinowitz (2012) points out that such classification automatically leads to over-/underestimation of the pathology owing to noise, which is why NIOSH (the US occupational noise regulating agency) renounces age-corrected audiograms. Zhan (2010) argues that ARHL may not, alone, be responsible for hearing loss, but rather accumulate progressively depending on the individual's noise exposure history. In general, many aspects of cetacean aging remains to be investigated, since recent findings imply a high incidence of both hearing loss and neurodegenerative changes (Mann et al., 2010; Vacher et al., 2022; Davis et al., 2021). Considering the homologies of the mammalian auditory apparatus, lower noise exposures in marine mammal ecosystems may contribute significantly to welfare and life expectancy of vulnerable species, prolonging the time frame in which they could reproduce.

Central repercussions of peripheral hearing damage e.g., in the form of tinnitus, are likely (Eggermont and Roberts, 2004), but may potentially be confounded in their expression due to the

numerous decussations at different levels of the auditory pathway. For example, plasticity can often be detected to varying degrees in central auditory components ipsi- versus contralateral to the exposed ear (measuring for GAP-43 protein expression *post-mortem*, Michler et al., 2002; or using fMRI *in-vivo*, Heggdal et al., 2016) depending on the side of unilateral sensorineural hearing loss. In general: the further "up" or afferent along the auditory pathway one looks, the longer a significant response may need to become morphologically visible. Thus, a general acute response to a noxious stimulus including AOE may be an intracellular accumulation of radicals (e.g., Ohinata et al., 2000; Henderson et al., 2006).

If one decides to explore radical levels within cetacean tissues, however, where higher baseline antioxidant enzyme levels (Cantú-Medellín et al., 2019; Wilhelm Filho et al., 2002) and more pronounced myelination within the CNS compared to terrestrial mammals (Ridgway et al., 2019) are the rule, one must consider potential differences in the ability to compensate for hypoxic conditions and resist lipid peroxidation processes across taxa. Generalizations within the cetacean order should be avoided and the selection of an umbrella species might rather be done considering the species' specific ecology.

In any case, apart from the allostatic load that AOE and masking likely impose on marine fauna (NRC, 2005), if inference from individuals to populations became possible, a potential vicious circle of effects may be expected at different levels. For example, chronic noise/particle motion vibrations could evoke reproductive disruptions and a higher likelihood of preterm births, as has been found in humans (Penkov et al., 1996; Seidel, 1993; Seidel and Heide, 1986), and then preterm neonates might be much more likely to have sensorineural hearing loss (Schulmann-Galambos, 1979), resulting in a higher susceptibility to NIHL and exacerbation of congenital auditory pathology through anthropogenic sound (Moser and Starr, 2016). It is possible that noise affects marine mammals at an even earlier life stage (as it does in fish larvae exposed to explosions; e.g., Govoni et al., 2003; 2008), since fetal response to impulsive sounds is mostly unknown.

Pierson et al. (1994) measured auditory brain stem responses in sheep fetuses before, immediately, and several hours after exposure to impulsive noise with peak pressures of approximately 166 dB re 20 μPa, and noted a slight threshold shift of 10-15 dB for 1 and 2 kHz tone-burst stimuli. Despite this shift being much more subtle than that of the pregnant ewe (50 dB threshold shift), the long-term effects of AOE on the development and susceptibility of the fetus to NIHL later in life remain untested. Extrapolations from this type of study from terrestrial to aquatic mammals are problematic, as it is unclear whether the proposed attenuation of sound from the external (aerial) to the intrauterine environment is valid in a larger number of animals, and the differences to sound conduction from a marine environment are entirely unknown. Compounded with the known effects of hearing loss associated with heavy metal, chemical and POP exposure (Rosati et al., 2020), however, the problem becomes one of a potential scale that should not be ignored.

Conclusions and Perspectives

The cetacean brain has kept the fascination of many a generation of scientists, and its further investigation should continue to unravel functional adaptations and their interplay with physiological and pathological stimuli. Insights gained, such as the examination of its connectome, proteome and transcriptome, could help discover fundamental evolutionary mechanisms behind the development of such a complex brain, as well as benefit the understanding of the pathogenesis of both cetacean and human neurodegenerative conditions.

Veterinary evidence-based medicine shows strong potential for expanding the diagnostic spectrum of NIHL by complementing standard necropsy protocols (Ijsseldijk et al., 2019). Both the peripheral and central nervous auditory systems of stranded cetaceans should be considered by implementing the knowledge acquired in human medical research and laboratory animal models. This may help provide clarity regarding the onset of LOBE to policymakers currently attempting to standardize thresholds for safe underwater practices (Commission Decision (EU) 2017/848) and avoid costly over-precautionary measures in the spirit of optimizing the ALARP principle ("As Low as Reasonably Practical" in terms of residual impact on marine fauna after risk-oriented mitigation; Bröker, 2019; IOGP, 2010). It will also play a role in assessing the true impact of conflicts such as the Russia-Ukraine war affecting the Black Sea, with the use of sea mines, explosives, and sonar on marine mammal populations (Karina Vishnyakova, personal communication), helping to provide an evidence-based scaffold to ecocide allegations. To make such a diagnostic tool viable, unknowns regarding the functional anatomy, physiology, and molecular homeostasis in the tissues of interest are being systematically addressed, with tissue banks being a vital cornerstone to reach worldwide.

No mechanism reported so far is pathognomonic for AOE—it is a balance of degenerative and reparative processes that must always be integrated with the general health status of the animal and observed in the context of a spatiotemporal association to an AOE. Tissue integrity depends on the individual balance between pro- and anti-inflammatory and -apoptotic mechanisms, and recovery is a question of available molecular resources, although still unpredictable from the scale of the hearing threshold shift. The role of recovery between single pulses or during breaks in the underwater noise activity is also unclear (Kastelein et al., 2019b).

Despite the significant knowledge gradient in favor of extensively studied laboratory animals to marine mammals and, even more so, to non-mammalian vertebrates (fishes and sea turtles), there is great potential in applying established techniques in less-studied species, including non-model domestic and companion animals. This could enable maximum yield of information from rare specimens on pathophysiological processes including NIHL and bioaccumulation and provide novel insights for refining diagnostics in humans. Due to the difficulties of visualizing the ultrastructure of large brains, there are similar unknowns in both cetaceans and humans, e.g., regarding the topography of the acoustic radiation (Maffei et al., 2019) or the relationship between NIHL, ARHL, excitotoxic synaptic CNS damage and cognitive decline (Moser and Starr, 2016), awaiting research. Given a multidisciplinary approach and the adoption of techniques that have been successful in various other terrestrial and marine fauna (from confocal, scanning electron and light-sheet microscopy to genetic analysis), the development of

sophisticated, comprehensive NIHL diagnostics along the auditory pathways in marine mammals may be achieved (Panganiban et al., 2018; Coyat et al., 2019; Pende et al., 2020). Simultaneous approaches to numerous more available species such as sea turtles, fish, and even invertebrates (Popper et al., 2020) would provide a wider field for comparison and help assess direct and indirect impacts of AOE on lower constituents of the marine food chain.

The objective remains to attain measurable, repeatable standardized protocols to fingerprint subtle and cumulative detrimental health effects owing to anthropogenic noise (Bröker, 2019; Popper et al., 2020). For this, baseline values of select biomarkers for at least a few representative species within a given ecosystem will be required. Considering that this issue in humans is highly prevalent (Rabinowitz, 2012; WHO, 2021), developing a practical method to assess the true status of potentially overexposed animals, both in marine and terrestrial environments, is of utmost importance. In this regard, veterinarians have a role to play, combining their expertise in evaluating pathology pertaining to sound exposure with techniques already available for lab animals that have yet to be applied to our species of interest.

The applications mentioned in this study—combinations of virtopsy, novel modeling, genetic, and *in vitro* techniques in addition to conventional immunohistochemistry and histopathology—are increasingly available and could become part of routine *post-mortem* investigation. This will widen the diagnostic spectrum and fortify risk assessment and regulatory frameworks concerning sylvatic species under the One Health principle. From there, inference from individuals to populations and from several umbrella species to the marine mammal stock in international waters may acquire an evidence-based backbone, facilitating cohesive and risk-oriented wildlife management and legislation born out of multidisciplinary collaboration.

Acknowledgements

This is it! Time to say thank you to all the strong and wonderful people who have helped me out throughout these three years of a-PhD italiano. Especially that people that have raised be up to be strong enough to finish this challenging last year of it: my mum and dad, brother, grandparents, Marco (and our funny, funny dog!), his family, and the extended BCA family—Sandro, Cinzia, Tommaso, Jean-Marie, Steffen, Bruno, Guido, Laura, Valentina, Davide, Rossella, Enrico, Ranieri, Giuseppe, Alessandro, Massimo, Emek, Lucrezia and Claudia. Thank you to Dr. Enrico Orvieto for having helped me from afar in matters of both veterinary and human pathology, and Dr. Frances Gulland for having been so encouraging and helpful, and the big surprise I found on my desk one day. It would not have been anywhere near as fun without the great team across the Atlantic in the center of the world, New York—you gave me much more than mentorship and new knowledge! I see you as lifelong friends and colleagues, my brain buds and lab queens, and am flattered to have made your acquaintance. I am grateful to Dr. Lori Marino for having helped me connect with you. I would never have started this journey without a Greek holiday and Joan Gonzalvo's Ionian Dolphin Project, so eternal kudos to him.

All my buddies from Germany, Malta and Gran Canaria that have been steadfast in never quite letting me go—I miss and love you all and would like to tell you that you absolutely contributed to my sanity in these times. Finally, to my last, squeezed out years of being a student: goodbye and thanks for all the fish!

References

1. Abbott, S. D., Hughes, L. F., Bauer, C. A., Salvi, R. & Caspary, D. M. (1999). Detection of glutamate decarboxylase isoforms in rat inferior colliculus following acoustic exposure. *Neuroscience*, 93(4), 1375-1381.
2. ACCOBAMS (2019b). Methodological Guidance on Underwater Noise Mitigation Measures. Available online: https://accobams.org/wp-content/uploads/2019/04/MOP7.Doc31Rev1_Methodological-Guide-Noise.pdf (Accessed: December 17, 2022)
3. ACCOBAMS (2021). Activities Report Regarding QUIETMED2 Project. ACCOBAMS-SC14/2021/Inf12 Available online: https://accobams.org/wp-content/uploads/2021/09/SC14.Inf12_Report-QM2.pdf (Accessed: December 17, 2022)
4. ACCOBAMS Resolution 2.16 (2004). Assessment and Impact Assessment of Man-made Noise. Available online: https://www.accobams.org/wp-content/uploads/2016/06/ACCOBAMS_MOP2_Res.2.16.pdf (Accessed: June 15, 2020)
5. ACCOBAMS Resolution 3.10 (2007). Guidelines to Address the Impact of Anthropogenic Noise on Marine Mammals in the ACCOBAMS Area. Available online: https://www.accobams.org/wp-content/uploads/2016/06/ACCOBAMS_MOP3_Res.3.10.pdf (Accessed: June 15, 2020)
6. ACCOBAMS Resolution 4.17 (2010). Guidelines to Address the Impact of Anthropogenic Noise on Cetaceans in the ACCOBAMS Area. Available online: https://www.accobams.org/wp-content/uploads/2016/06/ACCOBAMS_MOP4_Res.4.17.pdf (Accessed: June 15, 2020)
7. ACCOBAMS Resolution 5.15 (2013). Addressing the Impact of Anthropogenic Noise. Available online: https://www.accobams.org/wp-content/uploads/2016/06/ACCOBAMS_MOP5_Res.5.15.pdf (Accessed: June 15, 2020)
8. ACCOBAMS Resolution 6.17 (2016a). Anthropogenic Noise. Available online: https://www.accobams.org/wp-content/uploads/2016/06/ACCOBAMS_MOP6_Res6.17.pdf (Accessed: December 17, 2022)
9. ACCOBAMS Resolution 6.18 (2016b). Implementation of an ACCOBAMS Certification for highly qualified Marine Mammal Observers. Available online: https://accobams.org/wp-content/uploads/2019/12/Res.7.13_Anthropogenic-Noise.pdf (Accessed: June 15, 2020)
10. ACCOBAMS Resolution 7.13 (2019a). Addressing the Impact of Anthropogenic Noise. Available online: https://accobams.org/wp-content/uploads/2019/12/Res.7.13_Anthropogenic-Noise.pdf (Accessed: June 15, 2020)
11. Accomando, A.W.; Mulsow, J.; Branstetter, B.K.; Schlundt, C.E.; Finneran, J.J. (2020). Directional hearing sensitivity for 2–30 kHz sounds in the bottlenose dolphin (*Tursiops truncatus*). *The Journal of the Acoustical Society of America*, 147, 388–398.
12. Ackermans, N. L., Varghese, M., Wicinski, B., Torres, J., De Gasperi, R., Pryor, D., ... & Hof, P. R. (2021). Unconventional animal models for traumatic brain injury and chronic traumatic encephalopathy. *Journal of neuroscience research*, 99(10), 2463-2477.
13. Alderson, A. M., Diamantopoulos, E., And Downman, C. B. (1960). Auditory cortex of the seal (*Phoca vitulina*). J. Anat. 94, 506–11. Available online: http://www.ncbi.nlm.nih.gov/pubmed/13682212 (Accessed: May 19, 2020)
14. Allen Brain Atlas (2020). Available online: https://mouse.brain-map.org/ (Accessed: May 2, 2020)

15. Altschuler, R. A., Lim, H. H., Ditto, J., Dolan, D., & Raphael, Y. (1996). Protective mechanisms in the cochlea: heat shock proteins. *Auditory system plasticity and regeneration*, 202-212.
16. Anderson, C., Rothwell, I.H., Bell, K., Denny, H., Kallenberg, R.C., & Wakefield, J.H. (1954). Annual Report for 1954. Juneau: Alaska Department of Fisheries. 92 pp.
17. André, M., Delory, E., Degollada, E., Alonso, J., del Rio, J., van der Schaar, M., ... & Morell, M. (2007). Identifying cetacean hearing impairment at stranding sites. *Aquatic Mammals*, 33(1), 100.
18. André, M., Morell, M., Alex, M., Solé Carbonell, M., der Schaar, V., Malcolm, M. C. R., et al. (2009). Best practices in management, assessment and control of underwater noise pollution. Available online: https://upcommons.upc.edu/handle/2117/22457 (Accessed: May 19, 2020)
19. Arbelo M, Espinosa de los Monteros A, Herráez P, Suárez-Bonnet A, Andrada M, Rivero M, et al. Primary central nervous system T-cell lymphoma in a common dolphin (*Delphinus delphis*) (2014). *Journal of Comparative Pathology*, 150 (2–3), 336–340.
20. ASCOBANS MOP4 (2003). Effects of Noise and of Vessels. Available online: https://www.cms.int/sites/default/files/document/ScC16_Inf_12_3_ASCOBANS_Ocean_Noise_Response_Eonly_0.pdf (Accessed: June 15, 2020)
21. ASCOBANS MOP5 (2006). Adverse Effects of Sound, Vessels and Other Forms of Disturbance on Small Cetaceans. Available online: https://www.cms.int/sites/default/files/document/ScC16_Inf_12_3_ASCOBANS_Ocean_Noise_Response_Eonly_0.pdf (Accessed: June 15, 2020)
22. ASCOBANS MOP6 (2009). Adverse Effects of Underwater Noise on Marine Mammals during Offshore Construction Activities for Renewable Energy Production. Available online: https://www.cms.int/sites/default/files/document/ScC16_Inf_12_3_ASCOBANS_Ocean_Noise_Response_Eonly_0.pdf (Accessed: June 15, 2020)
23. Au W.W.L., Pawloski D. (1992). Cylinder wall thickness difference discrimination by an echolocating Atlantic bottlenose dolphin. *Journal of Comparative Physiology* A 170(1), 41-7.
24. Au W.W.L., Turl C.W.W. (1983). Target detection in reverberation by an echolocating Atlantic bottlenose dolphin (*Tursiops truncatus*). *The Journal of the Acoustical Society of America* 73, 1676.
25. Au, W.W.L., Popper, A. N., & Fay, R. R. (2000). Hearing by whales and dolphins. Springer Science & Business Media.
26. Austin, M. E., Hannay D. E., & Bröker, K. C. (2018). Acoustic characterization of exploration drilling in the Chukchi and Beaufort Seas. *The Journal of the Acoustical Society of America*, 144(1).
27. Australian Government Department of the Environment, Water, Heritage and the Arts (DEWHA) (2008). Environment Protection and Biodiversity Conservation Act. Policy Statement 2.1 – Interaction between off-shore seismic exploration and whales. Available online: https://www.environment.gov.au/system/files/resources/8d928995-0694-414e-a082-0ea1fff62fc8/files/seismic-whales.pdf (Accessed: June 15, 2020)
28. Axer, M., Strohmer, S., Grassel, D., Bucker, O., Dohmen, M., Reckfort, J., et al. (2016). Estimating fiber orientation distribution functions in 3D-polarized light imaging. *Frontiers in Neuroanatomy* 10, 40.

29. Baily J.L., Morrison L.R., Patterson I.A., Underwood C., Dagleish M.P. (2013) Primitive Neuroectodermal tumour in a striped dolphin (*Stenella coeruleoalba*) with features of ependymoma and neural tube differentiation (medulloepithelioma). *Journal of Comparative Pathology*, 149(4), 514–519.
30. Bain, D.E. & Williams, R. (2006) Long-range effects of air gun noise on marine mammals: Responses as a function of received sound level and distance. – IWC- SC/58E35. Available online: https://tethys.pnnl.gov/publications/long-range-effects-air gun-noise-marine-mammals-responses-function-received-sound-level (Accessed: May 30, 2020)
31. Baizer, J. S., Manohar, S., Paolone, N. A., Weinstock, N., & Salvi, R. J. (2012). Understanding tinnitus: the dorsal cochlear nucleus, organization and plasticity. *Brain research*, 1485, 40-53.
32. Balcomb III, K. C., & Claridge, D. E. (2001). A mass stranding of cetaceans caused by naval sonar in the Bahamas. *Bahamas Journal of Science*, 8(2), 2-12.
33. Barton, B. A. (2002). Stress in fishes: A diversity of responses with particular reference to changes in circulating corticosteroids. *Integrative and Comparative Biology*, 42(3), 517–525.
34. Bateson, M. (2007). Environmental noise and decision making possible implications of increases in anthropogenic noise for information processing in marine mammals. *International Journal of Comparative Psychology*, 20, 169–178.
35. Bernaldo de Quirós, Y., Fernandez, A., Baird, R. W., Brownell Jr, R. L., Aguilar de Soto, N., Allen, D., ... & Schorr, G. (2019). Advances in research on the impacts of anti-submarine sonar on beaked whales. *Proceedings of the Royal Society B*, 286(1895), 20182533.
36. Berns, G. S., Cook, P. F., Foxley, S., Jbabdi, S., Miller, K. L., & Marino, L. (2015a). Diffusion tensor imaging of dolphin brains reveals direct auditory pathway to temporal lobe. *Proceedings of the Royal Society B: Biological Sciences*, 282(1811).
37. Berns, G.S. (2015b). "Functional MRI of dolphins?". Available online: https://practicalfmri.blogspot.com/2015/10/functional-mri-of-dolphins.html (Accessed 21/12/2022)
38. Blackwell, S. B., Lawson, J. W., & Williams, M. T. (2004). Tolerance by ringed seals (*Phoca hispida*) to impact pipe-driving and construction sounds at an oil production island. *The Journal of the Acoustical Society of America*, 115(5).
39. Bohne, B. A., Bozzay, D. G., & Thomas, J. A. (1986). Evaluation of inner ear pathology in Weddell seals. *Antarctic journal of the United States*, 21(5), 208.
40. Bohne, B. A., Thomas, J. A., Yohe, E. R., & Stone, S. H. (1985). Examination of potential hearing damage in Weddell Seals (*Leptonychotes weddelli*) in McMurdo Sound, Antarctica. *Antarctic Journal of the United States*, 20, 174-176.
41. Bolle, L. J., de Jong, C. A., Bierman, S. M., van Beek, P. J., Wessels, P. W., Blom, E., van Damme, C. J., Winter, H. V., & Dekeling, R. P. (2016). "Effect of pile-driving sounds on the survival of larval fish," in The Effects of Noise on Aquatic Life II eds. A. N. Popper & A. Hawkins (New York: Springer), 91-100.
42. Bradley, D. L., & Stern, R. (2008). Underwater sound and the marine mammal acoustic environment. Report prepared for the US Marine Mammal Commission. Available online: https://www.mmc.gov/wp-content/uploads/sound_bklet.pdf (Accessed: December 13, 2020)

43. Brocke B, Lesch KP, Armbruster D, Moser DA, Müller A, Strobel A, Kirschbaum C. (2010). Stathmin, a gene regulating neural plasticity, affects fear and anxiety processing in humans. *American Journal of Medical Genetics, Part B: Neuropsychiatric Genetics*, 153B(1), 243-51.
44. Bröker, K. C. (2019). An Overview of Potential Impacts of Hydrocarbon Exploration and Production on Marine Mammals and Associated Monitoring and Mitigation Measures. *Aquatic Mammals*, 45(6).
45. Bröker, K. C., Gailey, G., Muir, J., & Racca, R. (2015). Monitoring and impact mitigation during a 4D seismic survey near a population of gray whales off Sakhalin Island, Russia. *Endangered Species Research*, 28.
46. Brozoski, T. J., Bauer, C. A., & Caspary, D. M. (2002). Elevated fusiform cell activity in the dorsal cochlear nucleus of chinchillas with psychophysical evidence of tinnitus. *Journal of Neuroscience*, 22(6).
47. Buckmaster PS, Wen X, Toyoda I, Gulland FM, Van Bonn W. (2014). Hippocampal neuropathology of domoic acid-induced epilepsy in California sea lions (*Zalophus californianus*). *Journal of Comparative Neurology*, 522(7), 1691-706.
48. Buckstaff, K.C. (2004). Effects of watercraft noise on the acoustic behavior of bottlenose dolphins, *Tursiops truncatus*, in Sarasota Bay, Florida. *Marine Mammal Science*, 20, 709–725.
49. Bullmann, T., Stieler, J., Holzer, M., Härtig, W., & Arendt, T. (2008). Hibernation, Starvation and Hypothermia–Models for Alzheimer's Disease. Available online: http://ishiilab.jp/member/bullmann-t/Bullmann2008_English.pdf (Accessed: December 12, 2022)
50. Bullock, T. H., Grinnell, A. D., Ikezono, E., Kameda, K., Katsuki, Y., Nomoto, M., ... & Yanagisawa, K. (1968). Electrophysiological studies of central auditory mechanisms in cetaceans. *Zeitschrift für vergleichende Physiologie*, 59(2), 117-156.
51. Bullock, T.H.; Gurevich, V.S. (1979). Soviet literature on the nervous system and psychobiology of Cetacea. *International Review of Neurobiology*, 21, 47–127.
52. Burtscher, J., Mallet, R. T., Burtscher, M., & Millet, G. P. (2021). Hypoxia and brain aging: neurodegeneration or neuroprotection? *Ageing Research Reviews*, 68, 101343.
53. Canlon, B., Borg, E., & Flock, Å. (1988). Protection against noise trauma by pre-exposure to a low level acoustic stimulus. *Hearing research*, 34(2), 197-200.
54. Cant N.B., Benson C.G. (2003). Parallel auditory pathways: Projection patterns of the different neuronal populations in the dorsal and ventral cochlear nuclei. *Brain Research Bulletin*, 60, 457–474.
55. Cantú-Medellín N., Byrd B., Hohn A., Vázquez-Medina J.P., Zenteno-Savín T. (2011). Differential antioxidant protection in tissues from marine mammals with distinct diving capacities. Shallow/short vs. deep/long divers. *Comparative biochemistry and physiology. Part A, Molecular & integrative physiology*, 158, 438–443.
56. Caspary, D. M., Ling, L., Turner, J. G., and Hughes, L. F. (2008). Inhibitory neurotransmission, plasticity and aging in the mammalian central auditory system. *Journal of Experimental Biology*, 211, 1781–1791.
57. Castellote, M.; Clark, C.W.; Lammers, M.O. (2012). Acoustic and behavioural changes by fin whales (*Balaenoptera physalus*) in response to shipping and air gun noise. *Biological Conservation*, 147, 115–122.
58. Cernak, I., Wang, Z., Jiang, J., Bian, X., & Savic, J. (2001a). Cognitive deficits following blast injury-induced neurotrauma: possible involvement of nitric oxide. *Brain Injury*, 15(7).
59. Cernak, I., Wang, Z., Jiang, J., Bian, X., and Savic, J. (2001b). Ultrastructural and functional characteristics of blast injury- induced neurotrauma. *Journal of Trauma and Acute Care Surgery*, 50.

60. Chen, I. H., Chou, L. S., Chou, S. J., Wang, J. H., Stott, J., Blanchard, M., ... & Yang, W. C. (2018). Sound exposure-induced cytokine gene transcript profile changes in captive bottlenose dolphin (*Tursiops truncatus*) blood identified by a probe-based qRT-PCR. *Journal of Veterinary Medical Science*, 17-0548.
61. Cherry, E. C. (1953). Some experiments on the recognition of speech, with one and with two ears. *The Journal of the Acoustical Society of America*, 25, 975–979.
62. Cook, P. F., Berns, G. S., Colegrove, K., Johnson, S., & Gulland, F. (2018). Postmortem DTI reveals altered hippocampal connectivity in wild sea lions diagnosed with chronic toxicosis from algal exposure. *Journal of Comparative Neurology*, 526(2), 216-228.
63. Cook, P. F., Hoard, V. A., Dolui, S., Frederick, B. D., Redfern, R., Dennison, S. E., ... & Inglis, B. A. (2021). An MRI protocol for anatomical and functional evaluation of the California sea lion brain. *Journal of Neuroscience Methods*, 353, 109097.
64. Coppola, C. L., Enns, R. M., & Grandin, T. (2006). Noise in the animal shelter environment: building design and the effects of daily noise exposure. *Journal of Applied Animal Welfare Science*, 9(1).
65. Costantini, I., Axer, M., Magnain, C., & Hof, P. R. (2022). The human brain multiscale imaging challenge. *Frontiers in Neuroanatomy*,16, 107.
66. Costantini, I., Morgan, L., Yang, J., Balbastre, Y., Varadarajan, D., Pesce, L., ... & Hof, P. R. (2021). A multimodal imaging and analysis pipeline for creating a cellular census of the human cerebral cortex. *bioRxiv*.
67. Coyat, C., Cazevieille, C., Baudoux, V., Larroze-Chicot, P., Caumes, B., & Gonzalez-Gonzalez, S. (2019). Morphological consequences of acoustic trauma on cochlear hair cells and the auditory nerve. *International Journal of Neuroscience*, 129(6).
68. Cozzi, B., Huggenberger, S., & Oelschläger, H. A. (2016). Anatomy of dolphins: insights into body structure and function. London: Academic Press. 192.
69. Cranford, T. W., Krysl, P., and Amundin, M. (2010). A New Acoustic Portal into the Odontocete Ear and Vibrational Analysis of the Tympanoperiotic Complex. *PLoS ONE* 5, e11927.
70. Cranford, T. W., Krysl, P., and Hildebrand, J. A. (2008). Acoustic pathways revealed: simulated sound transmission and reception in Cuvier's beaked whale (*Ziphius cavirostris*). *Bioinspiration & Biomimetics*, 3, 016001.
71. Croft, D. P., Johnstone, R. A., Ellis, S., Nattrass, S., Franks, D. W., Brent, L. J., Mazzi, S., Balcomb, K. C., Ford, J. K., Cant, M. A. (2017). Reproductive Conflict and the Evolution of Menopause in Killer Whales. *Current Biology*, 27, 298–304.
72. Cummings B.J., Head E., Afagh A.J., Milgram N.W., Cotman C.W. (1996). B- Amyloid accumulation correlates with cognitive dysfunction in the aged canine. *Neurobiology of Learning and Memory*, 66, 11–23.
73. Dahlheim, M., Castellote, M. (2016). Changes in the acoustic behavior of gray whales *Eschrichtius robustus* in response to noise. *Endangered Species Research*, 31, 227–242.
74. Dähne, M., Tougaard, J., Carstensen, J., Rose, A., & Nabe-Nielsen, J. (2017). Bubble curtains attenuate noise from offshore wind farm construction and reduce temporary habitat loss for harbour porpoises. *Marine Ecology Progress Series*, 580, 221-237.
75. Danil, K., & St Leger, J. A. (2011). Seabird and dolphin mortality associated with underwater detonation exercises. *Marine Technology Society Journal*, 45(6), 89-95.

76. Danil, K., Beaulieu-McCoy, N., Dennison, S., Rotstein, D., Rowles, T., Wilkin, S. (2021). Uncommon Stranding Event of Bottlenose Dolphins (*Tursiops truncatus*) in San Diego, California (October 2015). NOAA Tech. Memo. NMFS-SWFSC-641, 26 p.
77. Davis D.A., Mondo K., Stern E., Annor A.K., Murch S.J., Coyne T.M., Brand L.E., Niemeyer M.E., Sharp S., Bradley W.G., Cox P.A., Mash D.C. (2019). Cyanobacterial neurotoxin BMAA and brain pathology in stranded dolphins. *PLoS ONE*, 14(3), e0213346.
78. Davis, D. A., Garamszegi, S. P., Banack, S. A., Dooley, P. D., Coyne, T. M., McLean, D. W., ... & Cox, P. A. (2021). BMAA, Methylmercury, and mechanisms of neurodegeneration in dolphins: A natural model of toxin exposure. *Toxins*, 13(10), 697.
79. De Clerck, S.; Samarra, F.I.; Svavarsson, J.; Mouy, X.; Wensveen, P. (2019). Noise influences the acoustic behavior of killer whales, *Orcinus orca*, in Iceland. Proceedings of the Meetings on Acoustics 5ENAL, Den Haag, The Netherlands, 7 July 2019, p. 040003.
80. De Graaf, A.S. (1967). Anatomical Aspects of the Cetacean Brain Stem. Assen: Von Gorcum. 1–169.
81. de Veij Mestdagh, C. F., Koopmans, F., Breiter, J. C., Timmerman, J. A., Vogelaar, P. C., Krenning, G., ... & van Kesteren, R. E. (2022). The hibernation-derived compound SUL-138 shifts the mitochondrial proteome towards fatty acid metabolism and prevents cognitive decline and amyloid plaque formation in an Alzheimer's disease mouse model. *Alzheimer's Research & Therapy*, 14(1), 1-17.
82. De Vreese, S., André, M., Cozzi, B., Centelleghe, C., van der Schaar, M., & Mazzariol, S. (2020). Morphological evidence for the Sensitivity of the ear canal of odontocetes as shown by immunohistochemistry and transmission electron Microscopy. *Scientific reports*, 10(1).
83. Dekeling, R. P. A., Tasker, M. L., Van der Graaf, A. J., Ainslie, M. A., Andersson, M. H., André, M., ... & Dalen, J. (2014). Monitoring Guidance for Underwater Noise in European Seas, Part II: Monitoring Guidance Specifications. A guidance document within the Common Implementation Strategy for the Marine Strategy Framework Directive by MSFD Technical Subgroup on Underwater Noise. Available online: https://op.europa.eu/en/publication-detail/-/publication/15e008aa-30a3-4d84-a7eb-8d1318a6094d/language-en (Accessed: June 1, 2020)
84. Department of Conservation (DOC) Te Papa Atawhai. (2013). 2013 code of conduct for minimising acoustic disturbance to marine mammals from seismic survey operations. Available online: https://www.doc.govt.nz/our-work/seismic-surveys-code-of-conduct (Accessed: June 1, 2020)
85. Di Filippo, M., Sarchielli, P., Picconi, B., & Calabresi, P. (2008). Neuroinflammation and synaptic plasticity: theoretical basis for a novel, immune-centred, therapeutic approach to neurological disorders. *Trends in pharmacological sciences*, 29(8).
86. Di Guardo, G., Proietto, U., Di Francesco, C. E., Marsilio, F., Zaccaroni, A., Scaravelli, D., ... & Casalone, C. (2010). Cerebral toxoplasmosis in striped dolphins (*Stenella coeruleoalba*) stranded along the Ligurian Sea coast of Italy. *Veterinary Pathology*, 47(2), 245-253.
87. Di Guardo, G. (2018). Cetaceans, models for human disease? Research in veterinary science, 119, 43-44.
88. Di Guardo, G., Di Francesco, C. E., Eleni, C., Cocumelli, C., Scholl, F., Casalone, C., ... & Mazzariol, S. (2013). Morbillivirus infection in cetaceans stranded along the Italian coastline: pathological, immunohistochemical and biomolecular findings. *Research in Veterinary Science*, 94(1), 132-137.

89. Díaz-Delgado, J., Sacchini, S., Suárez-Bonnet, A., Sierra, E., Arbelo, M., Espinosa, A., ... & Fernández, A. (2015). High-grade astrocytoma (glioblastoma multiforme) in an Atlantic spotted dolphin (*Stenella frontalis*). *Journal of comparative pathology*, 152(2-3), 278-282.
90. Dierauf, L., & Gulland, F.M.D. (Eds.). (2001). CRC Handbook of Marine Mammal Medicine: Health, Disease, and Rehabilitation, Second Edition (2nd ed.). CRC Press.
91. Dietz, R., Sonne, C., Basu, N., Braune, B., O'Hara, T., Letcher, R. J., ... & Aars, J. (2013). What are the toxicological effects of mercury in Arctic biota?. *Science of the Total Environment*, 443, 775-790.
92. Domingo, M., Vilafranca, M., Visa, J., Prats, N., Trudgett, A., & Visser, I. (1995). Evidence for chronic morbillivirus infection in the Mediterranean striped dolphin (*Stenella coeruleoalba*). *Veterinary microbiology*, 44(2-4), 229-239.
93. Donner, J., Kaukonen, M., Anderson, H., Möller, F., Kyöstilä, K., Sankari, S., ... & Lohi, H. (2016). Genetic panel screening of nearly 100 mutations reveals new insights into the breed distribution of risk variants for canine hereditary disorders. *PloS ONE*, 11(8), e0161005.
94. Doucette, T. A., & Tasker, R. A. (2015). Perinatal domoic acid as a neuroteratogen. In Neurotoxin modeling of brain disorders—Life-long outcomes in behavioral teratology ed. Kostrzewa, R. M., & Archer, T. (New York: Springer), 87-110.
95. Drira, A., Bouzidi, M., Maglio, A., Pavan, G., Salivas, M., (2018). "Modelling underwater sound fields from noise events contained in the ACCOBAMS impulsive noise register to address cumulative impact and acoustic pollution assessment, in": Proceedings of Euronoise 2018. Available online: http://euronoise2018.eu/docs/papers/465_Euronoise2018.pdf, 2819–2824. (Accessed: 5 April, 2020)
96. Du, X., Choi, C. H., Chen, K., Cheng, W., Floyd, R. A., & Kopke, R. D. (2011). Reduced formation of oxidative stress biomarkers and migration of mononuclear phagocytes in the cochleae of chinchilla after antioxidant treatment in acute acoustic trauma. *International Journal of Otolaryngology*.
97. Dunlop, R. A., Noad, M. J., McCauley, R. D., Kniest, E., Slade, R., Paton, D., & Cato, D. H. (2016). Response of humpback whales (*Megaptera novaeangliae*) to ramp-up of a small experimental air gun array. *Marine Pollution Bulletin*, 103(1-2).
98. EC (1992). Council Directive 92/43/EEC of 21 May 1992 on the conservation of natural habitats and of wild fauna and flora. Available online: https://eur-lex.europa.eu/legal-content/EN/TXT/?uri=celex%3A31992L0043 (Accessed: December 12, 2022)
99. EC (2008) Council Directive 2008/120/EC of 18 December, laying down minimum standards for the protection of pigs. European Council. Available online: http://data.europa.eu/eli/dir/2008/120/2019-12-14 (Accessed: June 1, 2020)
100. Edrén SME, Teilmann J, Dietz R, Carstensen J. (2004) Effect from the construction of Nysted offshore wind farm on seals in Rødsand seal sanctuary based on remote video monitoring. Technical report to Energy E2 A/S. NationalEnvironmental Research Institute, Roskilde. Available online: https://tethys.pnnl.gov/sites/default/files/publications/NERI_Seal_Visual_Monitoring_at_Nysted.pdf (Accessed; April 14, 2020)
101. Eggermont, J. J., & Roberts, L. E. (2004). The neuroscience of tinnitus. *Trends in Neurosciences*, 27(11).

102. Elgoyhen, A. B., Langguth, B., De Ridder, D., & Vanneste, S. (2015). Tinnitus: perspectives from human neuroimaging. *Nature Reviews Neuroscience*, 16(10).
103. Ellis, S., Franks, D. W., Nattrass, S., Currie, T. E., Cant, M. A., Giles, D., Balcomb, K. C., Croft, D. P. (2018). Analyses of ovarian activity reveal repeated evolution of post-reproductive lifespans in toothed whales. *Scientific Reports*, 8, 12833, 1–10.
104. Erbe, C., Dunlop, R., & Dolman, S. (2018). Effects of noise on marine mammals. In Effects of anthropogenic noise on animals, eds. Slabbekoorn, H., Dooling, R. J., Popper, A. N., & Fay, R. R. (New York: Springer), 277-309.
105. EU (2008). Marine Strategy Framework Directive (2008/56/EC). European Parliament and the Council. Available online: http://data.europa.eu/eli/dir/2008/56/oj (Accessed: June 1, 2020)
106. EU (2010). Commission Decision (EU) 2010/477EU(2). European Parliament and the Council. Available online: http://data.europa.eu/eli/dec/2010/477(2)/oj (Accessed: July 17, 2020)
107. EU (2011). Directive 2011/92/EU of the European Parliament and of the Council of 13 December 2011 on the assessment of the effects of certain public and private projects on the environment. Available online: https://eur-lex.europa.eu/legal-content/EN/TXT/?uri=CELEX%3A32011L0092 (Accessed on: December 12, 2022)
108. EU (2014). Commission Decision (EU) 2014/89/EU. Maritime Spatial Plannng Directive. Available online: https://op.europa.eu/en/publication-detail/-/publication/14d91dc4-4b1c-4284-b2fe-6446e407e938 (Accessed: December 12, 2022)
109. EU (2017). Commission Decision (EU) 2017/848. European Parliament and the Council. Available online: http://data.europa.eu/eli/dec/2017/848/oj (Accessed: June 1, 2020)
110. Evans, P.G.H., Lewis, E.J. and Fisher, P. (1993). A Study of the Possible Effects of Seismic Testing Upon Cetaceans in the Irish Sea. Sea Watch Foundation, Oxford, via André et al., 2009.
111. Evans, W.W.andPowell, B. A. (1967). Discrimination of Different Metallic Plates by an Echolocating Delphinid in Animal sonar systems eds. Busnel, R.-G., Fish J.F. (Boston: Springer), 363–382.
112. Fast, R.; Schütt, T.; Toft, N.; Møller, A.; Berendt, M. (2013). An observational study with long-term follow-up of canine cognitive dysfunction: Clinical characteristics, survival, and risk factors. *Journal of Veterinary Internal Medicine*, 27, 822–829.
113. Fernández, A., Arbelo, M., Martín, V., (2013). No mass strandings since sonar ban, 317-317 Nature 497, 317.
114. Fernández, A., Edwards, J. F., Rodriguez, F., De Los Monteros, A. E., Herraez, P., Castro, P., ... & Arbelo, M. (2005). "Gas and fat embolic syndrome" involving a mass stranding of beaked whales (family Ziphiidae) exposed to anthropogenic sonar signals. *Veterinary Pathology*, 42(4), 446-457.
115. Fetoni, A. R., De Bartolo, P., Eramo, S. L. M., Rolesi, R., Paciello, F., Bergamini, C., ... & Troiani, D. (2013). Noise-induced hearing loss (NIHL) as a target of oxidative stress-mediated damage: cochlear and cortical responses after an increase in antioxidant defense. *Journal of Neuroscience*, 33(9).
116. Finneran J.J., Schlundt C.E., Dear R. (2002). Temporary shift in masked hearing thresholds in odontocetes after exposure to single underwater impulses from a seismic watergun. *The Journal of the Acoustical Society of America,* 111, 2929–2940.
117. Finneran, J. J. (2003b). Whole-lung resonance in a bottlenose dolphin (*Tursiops truncatus*) and white whales (*Delphinapterus leucas*). *The Journal of the Acoustical Society of America,* 114, 529-535.

118. Finneran, J. J. (2015b). Noise-induced hearing loss in marine mammals: A review of temporary threshold shift studies from 1996 to 2015. *The Journal of the Acoustical Society of America*, 138(3).
119. Finneran, J. J. (2020). Conditioned attenuation of dolphin monaural and binaural auditory evoked potentials after preferential stimulation of one ear. *The Journal of the Acoustical Society of America*, 147(4).
120. Finneran, J. J., Dear, R., Carder, D. A., & Ridgway, S. H. (2003a). Auditory and behavioral responses of California sea lions (*Zalophus californianus*) to single underwater impulses from an arc-gap transducer. *The Journal of the Acoustical Society of America*, 114(3).
121. Finneran, J. J., Schlundt, C. E., Branstetter, B. K., Trickey, J. S., Bowman, V., & Jenkins, K. (2015b). Effects of multiple impulses from a seismic air gun on bottlenose dolphin hearing and behavior. *The Journal of the Acoustical Society of America*, 137(4).
122. Finneran, J. J., Schlundt, C. E., Branstetter, B. K., Trickey, J. S., Bowman, V., & Jenkins, K. (2015a). Effects of multiple impulses from a seismic air gun on bottlenose dolphin hearing and behavior. *The Journal of the Acoustical Society of America*, 137(4).
123. Finneran, J. J., Schlundt, C. E., Branstetter, B., and Dear, R. L. (2007). "Assessing temporary threshold shift in a bottlenose dolphin (*Tursiops truncatus*) using multiple simultaneous auditory evoked potentials," *The Journal of the Acoustical Society of America,* 122.
124. Finneran, J.J. (2016). Auditory Weighting Functions and TTS/PTS Exposure Functions for Marine Mammals Exposed to Underwater Noise; Space and Naval Warfare Systems Center Pacific: San Diego, CA, USA.
125. Fisheries and Oceans Canada (DFO) (2016). Statement of Canadian practice with respect to the mitigation of seismic sound in the marine environment. Ottawa, ON: Fisheries and Oceans Canada. Available online: https://www. dfo-mpo.gc.ca/oceans/publications/seismic-sismique/ index-eng.html#s02 (Accessed: May 30, 2020)
126. Foote, A.D. (2008). Mortality rate acceleration and post-reproductive lifespan in matrilineal whale species. *Biology Letters*, 4, 189–191.
127. Foote, A.D.; Osborne, R.W.; Hoelzel, A.R. (2004). Whale-call response to masking boat noise. Nature, 428, 910.
128. Fuentes-Santamaría, V., Alvarado, J. C., Melgar-Rojas, P., Gabaldón-Ull, M. C., Miller, J. M., & Juiz, J. M. (2017). The role of glia in the peripheral and central auditory system following noise overexposure: contribution of TNF-α and IL-1β to the pathogenesis of hearing loss. *Frontiers in Neuroanatomy*, 11, 9.
129. Furutani R. (2008). Laminar and cytoarchitectonic features of the cerebral cortex in the Risso's dolphin (*Grampus griseus*), striped dolphin (*Stenella coeruleoalba*), and bottlenose dolphin (*Tursiops truncatus*). *Journal of Anatomy*, 213(3), 241-8.
130. Garofolo G, Zilli K, Troiano P, Petrella A, Marotta F, Di Serafino G, Ancora M, Di Giannatale E. (2014). *Brucella ceti* from two striped dolphins stranded on the Apulia coastline, Italy. *Journal of Medical Microbiology*, 63, 325–329.
131. Gattoni, G., & Bernocchi, G. (2019). Calcium-binding proteins in the nervous system during hibernation: neuroprotective strategies in hypometabolic conditions? *International Journal of Molecular Sciences*, 20(9), 2364.
132. Gazzetta Ufficiale (GU) no. 53 03/03/2005 - LEGGE 10 febbraio 2005, n. 27. ö Ratifica ed esecuzione dell'Accordo sulla conservazione dei cetacei del Mar Nero, del Mediterraneo e dell'area atlantica contigua, con annessi ed Atto Finale, fatto a Monaco il 24 novembre 1996.

133. Gedamke, J., Gales, N., & Frydman, S. (2011). Assessing risk of baleen whale hearing loss from seismic surveys: The effect of uncertainty and individual variation. *The Journal of the Acoustical Society of America*, 129(1).

134. Geßner, C., Krüger, A., Folkow, L. P., Fehrle, W., Mikkelsen, B., & Burmester, T. (2022). Transcriptomes Suggest That Pinniped and Cetacean Brains Have a High Capacity for Aerobic Metabolism While Reducing Energy-Intensive Processes Such as Synaptic Transmission. *Frontiers in Molecular Neuroscience*, 15.

135. Gil-Loyzaga, P., Carricondo, F., Bartolomé, M. V., Iglesias, M. C., Rodríguez, F., & Poch-Broto, J. (2010). Cellular and molecular bases of neuroplasticity: brainstem effects after cochlear damage. *Acta Oto-laryngologica*, 130(3).

136. Giorda, F., Crociara, P., Iulini, B., Gazzuola, P., Favole, A., Goria, M., ... & Grattarola, C. (2022). Neuropathological Characterization of Dolphin Morbillivirus Infection in Cetaceans Stranded in Italy. *Animals*, 12(4), 452.

137. Girdlestone, C. D. (2018). A comparative morphometric analysis of the sensory hair cells of the cochleas of echolocating mammals (Masters dissertation). British Columbia (BC, Canada): University of British Columbia.

138. Glezer, I. I., Hof, P. R., and Morgane, P. J. (1998). Comparative analysis of calcium-binding protein-immunoreactive neuronal populations in the auditory and visual systems of the bottlenose dolphin (*Tursiops truncatus*) and the macaque monkey (*Macaca fascicularis*). *Journal of Chemical Neuroanatomy*, 15, 203–237.

139. Goold, J.C. and Fish, P.J. (1998). Broadband spectra of seismic survey air-gun emissions, with reference to dolphin auditory thresholds. *The Journal of the Acoustical Society of America*, 103.

140. Gordon, J., Gillespie, D., Potter, J., Frantzis, A., Simmonds, M., Swift, R. & Thompson, D. (2004). The effects of seismic surveys on marine mammals. *Marine Technology Society Journal*, 37, 16-34.

141. Gordon, J.; Antunes, R.; Jaqet, N. & Würsig, B. (2006). An investigation of sperm whale headings and surface behaviour before, during and after seismic line changes in the Gulf of Mexico. IWC SC/58/E45, 10.

142. Götz, T., & Janik, V. M. (2010). Aversiveness of sounds in phocid seals: psycho-physiological factors, learning processes and motivation. *Journal of Experimental Biology*, 213(9).

143. Govoni, John J., West, M. A., Settle, L. R., Lynch, R. T., & Greene, M. D. (2008). Effects of Underwater Explosions on Larval Fish: Implications for a Coastal Engineering Project. *Journal of Coastal Research*, 2, 228–233.

144. Govoni, John Jeffrey, Settle, L. R., & West, M. A. (2003). Trauma to Juvenile Pinfish and Spot Inflicted by Submarine Detonations. *Journal of Aquatic Animal Health*, 15(2), 111–119.

145. Graham, K. M., Burgess, E. A., Rolland, R. M. (2021). Stress and reproductive events detected in North Atlantic right whale blubber using a simplified hormone extraction protocol. *Conservation Physiology*, 9(1).

146. Granados-Zapata, A.; Robles-Malagamba, M.J.; González-Barrientos, R.; Kot, B.C.-W.; Barquero-Calvo, E.; Cordero-Chavaría, M.; Suárez-Esquivel, M.; Guzmán-Verri, C.; Palacios-Alfaro, J.D.; Tien-Sung, C.; Moreno, E.; Hernández-Mora, G. (2022). Pathological Studies and Postmortem Computed Tomography of Dolphins with Meningoencephalomyelitis and Osteoarthritis Caused by *Brucella ceti*. *Oceans*, 3, 189-203.

147. Grattarola, C., Giorda, F., Iulini, B., Pintore, M. D., Pautasso, A., Zoppi, S., ... & Casalone, C. (2016). Meningoencephalitis and *Listeria monocytogenes*, *Toxoplasma gondii* and *Brucella spp*. coinfection in a dolphin in Italy. *Diseases of Aquatic Organisms*, 118(2), 169-174.

148. Gray, H., and Van Waerebeek, K. (2011). Postural instability and akinesia in a pantropical spotted dolphin, *Stenella attenuata*, in proximity to operating air guns of a geophysical seismic vessel. *Journal for Nature Conservation*, 19(6), 363-367.

149. Gröhn, H., Gillick, B. T., Tkac, I., Bednarik, P., Mascali, D., Deelchand, D. K., ... & Eberly, L. E. (2019). Influence of Repetitive Transcranial Magnetic Stimulation on Human Neurochemistry and Functional Connectivity: A Pilot MRI/MRS Study at 7 T. *Frontiers in Neuroscience*, 13, 1260.
150. Gröschel, M., Basta, D., Ernst, A., Mazurek, B., & Szczepek, A. J. (2018). Acute noise exposure is associated with intrinsic apoptosis in murine central auditory pathway. *Frontiers in Neuroscience*, 12.
151. Grothe B. (2003). New roles for synaptic inhibition in sound localization. *Nature Reviews Neuroscience*, 4, 1–11.
152. Guan, S., & Brookens, T. (2021). The use of psychoacoustics in marine mammal conservation in the United States: From science to management and policy. *Journal of Marine Science and Engineering*, 9(5), 507.
153. Gundersen, H.J.G.; Jensen, E.B.V.; Kiêu, K.; Nielsen, J. (1999). The efficiency of systematic sampling in stereology—Reconsidered. *Journal of Microscopy*, 193, 199–211.
154. Gunn-Moore D, Kaidanovich-Beilin O, Gallego Iradi MC, Gunn-Moore F, Lovestone S. (2018). Alzheimer's disease in humans and other animals: A consequence of postreproductive life span and longevity rather than aging. *Alzheimer's and Dementia*, 14(2), 195-204.
155. Guofu, G., & Kaiya, Z. (1992). Fiber analysis of the optic and cochlear nerves of small cetaceans. In Marine Mammal Sensory Systems eds. Wartzok, D., Ketten, D.R. (Boston: Springer), 39-52.
156. Ha, J., Cho, Y. S., Kim, S. J., Cho, S. H., Kim, J. P., Jung, Y. H., ... & Seo, S. W. (2020). Hearing loss is associated with cortical thinning in cognitively normal older adults. *European Journal of Neurology*, 27(6).
157. Hall, J.G. Hearing and Primary Auditory Centres of the Whales (1967). *Acta Oto-Laryngologica* 2009, 63, 244–250.
158. Hamel, P. E., Giglio, R. F., Cassle, S. E., Farina, L. L., Leone, A. M., & Walsh, M. T. (2020). Postmortem computed tomography and magnetic resonance imaging findings in a case of coinfection of dolphin morbillivirus and aspergillus fumigatus in a juvenile bottlenose dolphin (*Tursiops truncatus*). *Journal of Zoo and Wildlife Medicine*, 51(2), 448-454.
159. Hastings, M. C., Reid, C. A., Grebe, C. C., Hearn, R. L. & Colman, J. G. (2008). The effects of seismic air gun noise on the hearing sensitivity of tropical reef fishes at Scott Reef, Western Australia. Underwater Noise Measurement, Impact and Mitigation, *Proceedings of the Institute of Acoustics*, 30 (5).
160. Hatch, L.T., Wahle, C.M., Gedamke, J., Harrison, J., Laws, B., Moore, S.E., Stadler, J.H., Van Parijs, S.M., (2016). Can you hear me here? Managing acoustic habitat in US waters. *Endangered Species Research*, 30, 171–186.
161. Hayes, J. D., & McLellan, L. I. (1999). Glutathione and glutathione-dependent enzymes represent a co-ordinately regulated defence against oxidative stress. *Free Radical Research*, 31 (4), 273–300.
162. Hayes, K. R., Ylitalo, G. M., Anderson, T. A., Urbán R, J., Jacobsen, J. K., Scordino, J. J., ... & Godard-Codding, C. A. (2022). Influence of Life-History Parameters on Persistent Organic Pollutant Concentrations in Blubber of Eastern North Pacific Gray Whales (*Eschrichtius robustus*). *Environmental Science & Technology*, 56(23), 17119-17130.
163. Heggdal, P. O. L., Brännström, J., Aarstad, H. J., Vassbotn, F. S., & Specht, K. (2016). Functional-structural reorganisation of the neuronal network for auditory perception in subjects with unilateral hearing loss: review of neuroimaging studies. *Hearing Research*, 332, 73-79.
164. Helfert, R. H., Glatz III, F. R., Wilson, T. S., Ramkumar, V., & Hughes, L. F. (2002). Hsp70 in the inferior colliculus of Fischer-344 rats: effects of age and acoustic stress. *Hearing Research*, 170(1-2).

165. Hemilä, S., Nummela, S., & Reuter, T. (1995). What middle ear parameters tell about impedance matching and high frequency hearing. *Hearing Research*, 85(1-2).
166. Hemilä, S., Nummela, S., & Reuter, T. (1999). A model of the odontocete middle ear. Hearing Research, 133(1-2).
167. Henderson, D., Bielefeld, E. C., Harris, K. C., & Hu, B. H. (2006). The role of oxidative stress in noise-induced hearing loss. *Ear and Hearing*, 27(1).
168. Hildebrand, J. (2004) Overview of Human-Made Sound Sources in the Marine Environment. Presentation to the joint MMC and JNCC Workshop, London 28 September 2004. Scripps Institution of Oceanography, University of California San Diego, LA Jolla, CA. Available online: http://mmc.gov/sound/internationalwrkshp/pdf/hildebrand.pdf (Accessed April 25, 2020)
169. Hildebrand, J. A. (2005). Impacts of anthropogenic sound. In Marine mammal research: conservation beyond crisis eds. Reynolds, J.E. et al. (Baltimore:The Johns Hopkins University Press), 101- 124.
170. Hof, P. R., Chanis, R., & Marino, L. (2005). Cortical complexity in cetacean brains. *The Anatomical Record Part A: Discoveries in Molecular, Cellular, and Evolutionary Biology*: An Official Publication of the American Association of Anatomists, 287(1), 1142-1152.
171. Hof, P. R., Glezer, I. I., Archin, N., Janssen, W. G., Morgane, P. J., and Morrison, J. H. (1992). The primary auditory cortex in cetacean and human brain: A comparative analysis of neurofilament protein-containing pyramidal neurons. *Neuroscience Letters*, 146, 91–95.
172. Holt, M.M.; Noren, D.P.; Veirs, V.; Emmons, C.K.; Veirs, S. (2009). Speaking up: Killer whales (Orcinus orca) increase their call amplitude in response to vessel noise. *The Journal of the Acoustical Society of America*, 125, EL27–EL32.
173. Houser, D.S., Finneran, J.J., (2006). A comparison of underwater hearing sensitivity in bottlenose dolphins (Tursiops truncatus) determined by electrophysiological and behavioral methods. *The Journal of the Acoustical Society of America*, 120, 1713–1722.
174. Hurley, P. A., Crook, J. M., & Shepherd, R. K. (2007). Schwann cells revert to non-myelinating phenotypes in the deafened rat cochlea. *European Journal of Neuroscience*, 26(7), 1813-1821.
175. IJsseldijk, L. L., Brownlow, A. C., & Mazzariol, S. (2019). Data from: Best practice on cetacean post mortem investigation and tissue sampling. Joint ACCOBAMS and ASCOBANS Document. Istanbul. Available online: https://accobams.org/wp-content/uploads/2019/04/MOP7.Doc33_Best-practices-on-cetacean-post-mortem-investigation.pdf (Accessed: February 10, 2020)
176. Illustration by Amy Dozier for the JONAS project in Thomsen, F., Mendes, S., Bertucci, F., Breitzke, M., Ciappi, E., Cresci, A. Debusschere, E., Ducatel, C., Folegot, F., Juretzek, C., Lam, F-P., O'Brien, J., dos Santos, M. E. (2021) Addressing underwater noise in Europe: Current state of knowledge and future priorities. Kellett, P., van den Brand, R., Alexander, B., Muniz Piniella, A., Rodriguez Perez, A., van Elslander, J., Heymans, J. J. eds. *Future Science Brief 7* of the European Marine Board, Ostend, Belgium.
177. International Association of Oil and Gas Producers (IOGP) (2010). HSE management – Guidelines for working together in a contract environment (IOGP Report 423). Available online: https://wiki.seg.org/images/3/3e/ IOGP_423.pdf (Accessed: February 10, 2020)

178. Isojunno, S., Wensveen, P. J., Lam, F. P. A., Kvadsheim, P. H., von Benda-Beckmann, A. M., López, L. M. M., ... & Miller, P. J. (2020). When the noise goes on: received sound energy predicts sperm whale responses to both intermittent and continuous navy sonar. *Journal of Experimental Biology*, 223(7).

179. IWC (International Whaling Commission). (2007). Report of the scientific committee. Annex K. Report of the Standing Working Group on environmental concerns. *Journal of Cetacean Research and Management*, 9 (Suppl.), 227–296.

180. Jacobs, Bob, Rally, Heather, Doyle, Catherine, O'Brien, Lester, Tennison, Mackenzie and Marino, Lori. (2022). Putative neural consequences of captivity for elephants and cetaceans. *Reviews in the Neurosciences*, 33 (4), 439-465.

181. Jacobs, S. R., y Terhune, J. M. (2002). The effectiveness of acoustic harassment devices in the Bay of Fundy, Canada: Seal reactions and a noise exposure model. *Aquatic Mammals*, 28, 147-158.

182. Jain, R. K., Pingle, S. K., Tumane, R. G., Thakkar, L. R., Jawade, A. A., Barapatre, A., & Trivedi, M. (2018). Cochlear proteins associated with noise-induced hearing loss: An update. *Indian Journal of Occupational and Environmental Medicine*, 22(2).

183. Jakob-Hoff, R., Kingan, M., Fenemore, C., Schmid, G., Cockrem, J. F., Crackle, A., ... & Descovich, K. (2019). Potential impact of construction noise on selected zoo animals. *Animals*, 9(8).

184. Jefferson, T. A., Webber, M. A., & Pitman, R. (2011). Marine mammals of the world: a comprehensive guide to their identification. Elsevier.

185. Jepson, P. D., Arbelo, M., Deaville, R., Patterson, I. A. P., Castro, P., Baker, J. R., ... & Rodriguez, F. (2003). Gas-bubble lesions in stranded cetaceans. *Nature*, 425(6958), 575-576.

186. Jepson, P. D., Bennett, P. M., Allchin, C. R., Law, R. J., Kuiken, T., Baker, J. R., ... & Kirkwood, J. K. (1999). Investigating potential associations between chronic exposure to polychlorinated biphenyls and infectious disease mortality in harbour porpoises from England and Wales. *Science of the Total Environment*, 243, 339-348.

187. Johnson, M. P., & Tyack, P. L. (2003). A digital acoustic recording tag for measuring the response of wild marine mammals to sound. *IEEE Journal of Oceanic Engineering*, 28(1), 3-12.

188. Joint Nature Conservaion Comittee (2010). JNCC guidelines for minimising the risk of injury and disturbance to marine mammals from seismic surveys Available online: http://www.utm.csic.es/sites/default/files/2018-01/JNCC_Guidelines_Seismic%20Guidelines_Aug%202010.pdf (Accessed: December 12, 2022)

189. Kaltenbach, J.A., Afman, C.E., (2000). Hyperactivity in the dorsal cochlear nucleus after intense sound exposure and its resemblance to tone-evoked activity: a physiological model for tinnitus. *Hearing Research*, 140.

190. Kaltenbach, J.A., Godfrey, D.A., Neumann, J.B., McCaslin, D.L., Afman, C.E., Zhang, J., (1998). Changes in spontaneous neural activity in the dorsal cochlear nucleus following exposure to intense sound: relation to threshold shift. *Hearing Research*. 124.

191. Karlidağ, T., Yalçin, Ş., Öztürk, A., Üstündağ, B., Gök, Ü., Kaygusuz, I., & Susaman, N. (2002). The role of free oxygen radicals in noise induced hearing loss: effects of melatonin and methylprednisolone. *Auris Nasus Larynx*, 29(2), 147-152.

192. Kastak D. and Schusterman, R. (1998). Low-frequency amphibious hearing in pinnipeds: Methods, measurements, noise, and ecology. *The Journal of the Acoustical Society of America*, 103.

193. Kastak, D., Mulsow, J., Ghoul, A., & Reichmuth, C. (2008). Noise-induced permanent threshold shift in a harbor seal. *The Journal of the Acoustical Society of America*, 123(5).

194. Kastelein, R. A., Helder-Hoek, L., and Gransier, R. (2019a). Frequency of greatest temporary hearing threshold shift in harbor seals (*Phoca vitulina*) depends on fatiguing sound level. *The Journal of the Acoustical Society of America*, 145.

195. Kastelein, R. A., Helder-Hoek, L., Kester, R., Van Huisman, R., and Gransier, R. (2019b). Temporary hearing threshold shift in harbor porpoises (*Phocoena phocoena*) due to one-sixth octave noise and at 16 kHz. *Aquatic Mammals*, 45.

196. Kastelein, R. A., Helder-Hoek, L., Van de Voorde, S., von Benda-Beckmann, A. M., Lam, F. P. A., Jansen, E., ... & Ainslie, M. A. (2017). Temporary hearing threshold shift in a harbor porpoise (*Phocoena phocoena*) after exposure to multiple air gun sounds. *The Journal of the Acoustical Society of America*, 142(4).

197. Kastelein, R. A., von Benda-Beckmann, A. M., Lam, F. P. A., Jansen, E., & de Jong, C. A. (2019c). Effect of a Bubble Screen on the Behavioral Responses of Captive Harbor Porpoises (*Phocoena phocoena*) Exposed to Air gun Sounds. *Aquatic Mammals*, 45(6).

198. Kenned,y S., Lindstedt I.J., Mcaliskey, M.M., Mcconnell, S.A., Mccullough, S.J. (1992). Herpesviral encephalitis in a harbor porpoise (*Phocoena phocoena*). *Journal of Zoo and Wildlife Medicine*, 23, 374–9.

199. Kern, A., Siebert, U., Cozzi, B., Hof, P.R., Oelschläger, H.H.A. (2011). Stereology of the neocortex in odontocetes: qualitative, quantitative, and functional implications. *Brain, Behavior and Evolution*, 77, 79–90.

200. Kesarev, V.E. (1970). Some data on neuronal organization of the dolphin neocortex. *Arkhiv Anatomii, Gistologii i Embriologii*, 59 (8), 71–77.

201. Ketten, D. R. (1994). Functional analyses of whale ears: adaptations for underwater hearing. *In I.E.E.E. Proceedings Underwater Acoustics*, 1, 264-270.

202. Ketten, D. R. (1995). Estimates of blast injury and acoustic trauma zones for marine mammals from underwater explosions in Sensory Systems of Aquatic Mammals, 391-407.

203. Ketten, D. R. (1997). Structure and function in whale ears. *Bioacoustics*, 8(1-2), 103-135.

204. Ketten, D. R. (2000). Cetacean Ears inHearing by Whales and Dolphins. W. Au, R. Fay, and A. Popper eds., Springer Handbook of Auditory Research, (New York: Springer), 43-108.

205. Ketten, D. R., & Montie, E. W. (2008). Imaging procedures for stranded marine mammals. Woods Hole Oceanographic Institution, MA, USA. Available online: https://csi.whoi.edu/content/imaging-procedures-stranded-marine-mammals/index.html (Accessed: September 30, 2020)

206. Ketten, D. R., Cramer, S., Arruda, J., Prahl, S., Williams, S. R., & Dunnigan, B. (2008). CT and MRI techniques for analysis of trauma and disease in marine mammals. In Florida Marine Mammal Health Conference, 2008, Gainesville, FL.

207. Ketten, D. R., Lien, J. & Todd, S. (1993). Blast injury in humpback whale ears: Evidence and implications. J. Acoust. Soc. Am. 94, 1849–1850. Abstract available online: https://csi.whoi.edu/biblio/blast-injury-humpback-whale-ears-evidence-and-implications/ (Accessed: September 30, 2020)

208. Kim, S. Y., Heo, H., Kim, D. H., Kim, H. J., & Oh, S. H. (2018). Neural Plastic changes in the subcortical auditory neural pathway after single-sided deafness in adult mice: a MEMRI study. *BioMed Research International*.

209. Koschinski, S. (2011). Underwater noise pollution from munitions clearance and disposal, possible effects on marine vertebrates, and its mitigation. *Marine Technology Society Journal*, 45(6), 80-88.

210. Knudsen S.K., Øen E.O. (2003). Blast-induced neurotrauma in whales. *Neuroscience Research*, 46(3), 377-86.

211. Kot, B. C., Tsui, H. C., Chung, T. Y., & Lau, A. P. (2020). Postmortem neuroimaging of cetacean brains using computed tomography and magnetic resonance imaging. *Frontiers in Marine Science*, 7, 544037.

212. Kragh, I.M.; McHugh, K.; Wells, R.S.; Sayigh, L.S.; Janik, V.M.; Tyack, P.L.; Jensen, F.H. (2019). Signal-specific amplitude adjustment to noise in common bottlenose dolphins (*Tursiops truncatus*). *Journal of Experimental Biology*, 222, 1–11.

213. Krasnoshchekova, E. I., & Figurina, I. I. (1980). Cortical projections of the dolphin cerebral geniculate body. *Arkhiv Anatomii, Gistologii i Embriologii*, 78, 19-24.

214. Kraus, K. S., Ding, D., Jiang, H., Kermany, M. H., Mitra, S., & Salvi, R. J. (2013). Up-regulation of GAP-43 in the chinchilla ventral cochlear nucleus after carboplatin-induced hearing loss: Correlations with inner hair cell loss and outer hair cell loss. *Hearing Research*, 302.

215. Kraus, K. S., Ding, D., Jiang, H., Lobarinas, E., Sun, W., & Salvi, R. J. (2011). Relationship between noise-induced hearing-loss, persistent tinnitus and growth-associated protein-43 expression in the rat cochlear nucleus: does synaptic plasticity in ventral cochlear nucleus suppress tinnitus? *Neuroscience*, 194.

216. Krey, A., Ostertag, S.K., Chan, H.M. (2015). Assessment of neurotoxic effects of mercury in beluga whales (*Delphinapterus leucas*), ringed seals (*Pusa hispida*), and polar bears (*Ursus maritimus*) from the Canadian Arctic. *Science of The Total Environment*, 509-510, 237-247.

217. Krüger, A. (2019). Molecular basis of hypoxia tolerance in the whale brain (Doctoral dissertation). Hamburg (Deutschland): Staats-und Universitätsbibliothek Hamburg Carl von Ossietzky.

218. Krüger, A., Fabrizius, A., Mikkelsen, B., Siebert, U., Folkow, L. P., and Burmester, T. (2020). Transcriptome analysis reveals a high aerobic capacity in the whale brain. *Comparative biochemistry and physiology. Part A, Molecular & integrative physiology*, 240, 110593.

219. Kruger, L. (1959). The thalamus of the dolphin (*Tursiops truncatus*) and comparison with other mammals. *Journal of Comparative Neurology*, 111, 133-194.

220. Kujawa, S. G., and Liberman, M. C. (2009). Adding insult to injury: cochlear nerve degeneration after "temporary" noise-induced hearing loss. *Journal of Neuroscience*, 29, 14077–14085.

221. Kurabi, A., Keithley, E. M., Housley, G. D., Ryan, A. F., and Wong, A. C.-Y. (2017). Cellular mechanisms of noise-induced hearing loss. *Hearing Research*, 349.

222. Ladygina, T. F., & Supin, A. I. (1977). [Localization of the sensory projection areas in the cerebral cortex of the dolphin, Tursiops truncatus]. *Zhurnal Evoliutsionnoi Biokhimii i Fiziologii*, 13(6), 712–718. Available online: http://www.ncbi.nlm.nih.gov/pubmed/602532 (Accessed: May 16, 2020)

223. Ladygina, T. F., Mass, A. M. & Supin, A. Y. (1978). Multiple sensory projections in the dolphin cerebral cortex. *Zhurnal Vysshef Nervnoi Deyatel'nosti Imeni L P. Pavlova*, 28, 1047-1053.

224. Lahvis, G.P. (2017). What California sea lions exposed to domoic acid might teach us about autism: lessons for predictive and preventive medicine. *EPMA Journal*, 8, 229–235.

225. Lefebvre, K. A., Hendrix, A., Halaska, B., Duignan, P., Shum, S., Isoherranen, N., ... & Gulland, F. M. (2018). Domoic acid in California sea lion fetal fluids indicates continuous exposure to a neuroteratogen poses risks to mammals. *Harmful Algae*, 79, 53-57.

226. Lemes, M., Wang, F., Stern, G. A., Ostertag, S. K., Chan, H. M. (2011). Methylmercury and selenium speciation in different tissues of beluga whales (Delphinapterus leucas) from the western Canadian Arctic. *Environmental Toxicology and Chemistry*, 30, 2732-2738.

227. Lende, R. A. & Welker, W. I. (1972). An unusual sensory area in the cerebral neocortex of the bottlenose dolphin, *Tursiops truncatus*. *Brain Research*,45, 555-560.

228. Liberman, M. C. (2016). Noise-induced hearing loss: permanent versus temporary threshold shifts and the effects of hair cell versus neuronal degeneration. In The Effects of Noise on Aquatic Life II, 1-7, eds. Popper, A. N., & Hawkins (New York: Springer), 1-7.

229. Lillie, M. A., Vogl, A. W., Gerard, S. G., Raverty, S., & Shadwick, R. E. (2022). Retia mirabilia: Protecting the cetacean brain from locomotion-generated blood pressure pulses. *Science*, 377(6613), 1452-1456.

230. Lim, D. J., & Melnick, W. (1971). Acoustic damage of the cochlea: A scanning and transmission electron microscopic observation. *Archives of Otolaryngology*, 94(4), 294-305.

231. Liu, Y. M., Li, X. D., Guo, X., Liu, B., Lin, A. H., & Rao, S. Q. (2010). Association between polymorphisms in SOD1 and noise-induced hearing loss in Chinese workers. *Acta oto-laryngologica*, 130(4).

232. Lobarinas, E., Sun, W., Stolzberg, D., Lu, J., & Salvi, R. (2008). Human brain imaging of tinnitus and animal models. *Seminars in Hearing*, 29(4).

233. Logan, S. M., & Storey, K. B. (2017). Avoiding apoptosis during mammalian hibernation. *Temperature*, 4(1), 15-17.

234. Lowe, C.L., Hunt, K.E., Robbins, J., Seton, R.E., Rogers, M., Gabriele, C.M., Neilson, J.L., Landry, S., Teerlink, S.S., Buck, C.L. (2021). Patterns of cortisol and corticosterone concentrations in humpback whale (*Megaptera novaeangliae*) baleen are associated with different causes of death. *Conservation Physiology*, 23, 9(1), coab096.

235. Lucá, R.; Giacominelli-Stuffler, R.; Mazzariol, S.; Roperto, S.; Cocumelli, C.; Di Guardo, G. (2017). Neuronal and astrocytic involvement in striped dolphins (*Stenella coeruleoalba*) with morbilliviral encephalitis. *Acta Virologica*, 61, 495–497.

236. Lucke, K.; Siebert, U.; Lepper, P.A.; Blanchet, M.-A. (2009). Temporary shift in masked hearing thresholds in a harbor porpoise (*Phocoena phocoena*) after exposure to seismic air gun stimuli. *The Journal of the Acoustical Society of America*, 125, 4060–4070.

237. Luís, A.R.; Couchinho, M.N.; dos Santos, M.E. (2014). Changes in the acoustic behavior of resident bottlenose dolphins near operating vessels. *Marine Mammal Science*, 30, 1417–1426.

238. MacNeil, T., Vathiotis, I. A., Martinez-Morilla, S., Yaghoobi, V., Zugazagoitia, J., Liu, Y., & Rimm, D. L. (2020). Antibody validation for protein expression on tissue slides: a protocol for immunohistochemistry. *Biotechniques*, 69(6), 460-468.

239. Madsen, P. T., Møhl, B., Nielsen, B. K., y Wahlberg, M. (2002). Male sperm whale behavior during exposures to distant seismic survey pulses. *Aquatic Mammals*, 28, 231- 240.

240. Madsen, P.T., Wahlberg, M., Tougaard, J., Lucke, K., Tyack, P. (2006). Wind turbine underwater noise and marine mammals: implications of current knowledge and data needs. *Marine Ecology - Progress Series*, 309.

241. Maffei, C., Sarubbo, S., & Jovicich, J. (2019). A missing connection: A review of the macrostructural anatomy and tractography of the acoustic radiation. *Frontiers in Neuroanatomy*, 13.

242. Maglio, A., Salivas, M., Lemesnager, P., Arenas, D., Ruiz, P., Sánchez, M., (2018). QUIETMED Deliverable D4.1: International Impulsive Noise Register for the Mediterranean Basin. Joint Programme on Noise (D11) for the Implementation of the Second Cycle of the MSF in the Mediterranean Sea. Available online: http://www.quietmed-project.eu/wp-content/uploads/2019/01/QUIETMED_D4.1_Joint-register-for-impulsivenoise-in-the-MED_final.pdf. (Accessed July 4, 2020)

243. Malkemper, E. P., Oelschläger, H. H. A., & Huggenberger, S. (2012). The dolphin cochlear nucleus: Topography, histology and functional implications. *Journal of Morphology*, 273(2), 173-185.

244. Malme, C. I., Würsig, B., Bird, J. E., & Tyack, P. (1986). Behavioral responses of gray whales to industrial noise: feeding observations and predictive modeling (No. PB-88-249057/XAB). BBN Labs. Inc., Cambridge, MA, USA.

245. Mann, D., Hill-Cook, M., Manire, C., Greenhow, D., Montie, E., Powell, J., ... & Hoetjes, P. (2010). Hearing loss in stranded odontocete dolphins and whales. *PloS ONE*, 5(11), e13824.

246. Manohar, S., Paolone, N.A., Bleichfeld, M., Hayes, S.H., Salvi, R.J., Baizer, J.S., (2012). Expression of doublecortin, a neuronal migration protein, in unipolar brush cells of the vestibulocerebellum and dorsal cochlear nucleus of the adult rat. *Neuroscience*, 202, 169–183.

247. Marino, L. (2015). The brain: Evolution, structure, and function. In Dolphin communication and cognition: Past, present, and future, eds. Herzing, D.L. & Johnson C.M. (Cambridge: MIT Press) 3-18.

248. Marino, L., Sherwood, C. C., Delman, B. N., Tang, C. Y., Naidich, T. P., & Hof, P. R. (2004a). Neuroanatomy of the killer whale (*Orcinus orca*) from magnetic resonance images. *The Anatomical Record Part A: Discoveries in Molecular, Cellular, and Evolutionary Biology*: An Official Publication of the American Association of Anatomists, 281(2), 1256-1263.

249. Marino, L., Sudheimer, K. D., Pabst, D. A., Mclellan, W. A., Filsoof, D., & Johnson, J. I. (2002). Neuroanatomy of the common dolphin (*Delphinus delphis*) as revealed by magnetic resonance imaging (MRI). *The Anatomical Record*: An Official Publication of the American Association of Anatomists, 268(4), 411-429.

250. Marino, L., Sudheimer, K., Mclellan, W. A., & Johnson, J. I. (2004b). Neuroanatomical structure of the spinner dolphin (*Stenella longirostris orientalis*) brain from magnetic resonance images. *The Anatomical Record Part A: Discoveries in Molecular, Cellular, and Evolutionary Biology*: An Official Publication of the American Association of Anatomists, 279(1), 601-610.

251. Marino, L., Sudheimer, K., Pabst, D. A., Mclellan, W. A., & Johnson, J. I. (2003). Magnetic resonance images of the brain of a dwarf sperm whale (*Kogia simus*). *Journal of Anatomy*, 203(1), 57-76.

252. Marsh, H., Kasuya, T. (1968). Evidence for reproductive senescence in female cetaceans. Report of the International Whaling Commission 8, 57–74.

253. Martin, W.E., Haun, C.K., Barrows, H.S., Cravioto, H. (1970). Nematode damage to brain of striped dolphin, Lagenorhynchus obliquidens. *Transactions of the American Microscopical Society*, 89, 200–5.

254. Martin, M.J.; Gridley, T.; Elwen, S.H.; Jensen, F.H. (2018). Heaviside's dolphins (*Cephalorhynchus heavisidii*) relax acoustic crypsis to increase communication range. *Proceedings of the Royal Society B: Biological Sciences*, 285, 20181178.

255. Martin, S. B., Matthews, M. N. R., MacDonnell, J. T., & Bröker, K. (2017). Characteristics of seismic survey pulses and the ambient soundscape in Baffin Bay and Melville Bay, West Greenland. *The Journal of the Acoustical Society of America*, 142(6).

256. Martin, S. B., Morris, C., Bröker, K., & O'Neill, C. (2019). Sound exposure level as a metric for analyzing and managing underwater soundscapes. *The Journal of the Acoustical Society of America*, 146(1).

257. Maulucci, G., Troiani, D., Eramo, S. L. M., Paciello, F., Podda, M. V., Paludetti, G., ... & Fetoni, A. R. (2014). Time evolution of noise induced oxidation in outer hair cells: role of NAD (P) H and plasma membrane fluidity. *Biochimica et Biophysica Acta (BBA)-General Subjects*, 1840(7), 2192-2202.

258. May, J., Ramachandran, V., & Cacace, A. T. (2011). Tinnitus and vestibular schwannoma: overview and clinical correlations. In Textbook of Tinnitus eds. Møller, A. R., Langguth, B., DeRidder, D., & Kleinjung, T. (New York: Springer), 317-325.

259. McAuliffe, K., & Whitehead, H. (2005). Eusociality, menopause and information in matrilineal whales. *Trends in Ecology & Evolution*, 20(12), 650.

260. McCauley, R.D., Fewtrell, J., Duncan, A. J., Jenner, C., Jenner, M. N., Penrose, J. D., ... & McCabe, K. (1999). Marine Mammal Seismic Surveys: Analysis and Propagation of Air-Gun Signals; and Effects of Air-Gun Exposure on Humpback Whales, Sea Turtles, Fishes and Squid. Curtin University, Centre for Marine Science and Technology. Available online: http://citeseerx.ist.psu.edu/viewdoc/download?doi=10.1.1.646.3324&rep=rep1&type=pdf (Accessed: July 7, 2020)

261. McDonald, M.A., Hildebrand, J.A. and Webb, S.C. (1995). Blue and fin whales observed on a seafloor array in the Northeast Pacific. *The Journal of the Acoustical Society of America*, 98 (2, Pt 1).

262. McKnight, J. C., Bennett, K. A., Bronkhorst, M., Russell, D. J., Balfour, S., Milne, R., ... & Thompson, D. (2019). Shining new light on mammalian diving physiology using wearable near-infrared spectroscopy. *PLoS Biology*, 17(6), e3000306.

263. Menzel, M., Reuter, J. A., Grassel, D., Huwer, M., Schlomer, P., Amunts, K., et al. (2021). Scattered light imaging: resolving the substructure of nerve fiber crossings in whole brain sections with micrometer resolution. *Neuroimage*, 233, 117952.

264. Merchant, N. D., Andersson, M. H., Box, T., Le Courtois, F., Cronin, D., Holdsworth, N., ... & Norro, A. M. (2020). Impulsive noise pollution in the Northeast Atlantic: Reported activity during 2015–2017. *Marine Pollution Bulletin*, 152.

265. Merchant, N.D., Faulkner, R.C., Martinez, R. (2018). Marine noise budgets in practice. Conserv. Lett. 11, e12420.

266. Michler, S. A., and Illing, R. B. (2002). Acoustic trauma induces reemergence of the growth- and plasticity-associated protein GAP-43 in the rat auditory brainstem. *Journal of Comparative Neurology*, 451, 250–266.

267. Miclard J, Mokhtari K, Jouvion G, Wyrzykowski B, Van Canneyt O, Wyers M, et al. Microcystic meningioma in a dolphin (*Delphinus delphis*): immunohistochemical and ultrastructural study. *Journal of Comparative Pathology*, 135 (4), 254–258.

268. Miller, PJO; Johnson, MP; Madsen, PT; Biassoni, N; Quero, M; Tyack, PL. (2009). Using at-sea experiments to study the effects of air guns on the foraging behavior of sperm whales in the Gulf of Mexico. *Deep Sea Research Part I*. 56 (7).

269. Miranda, J. A., Shepard, K. N., McClintock, S. K., & Liu, R. C. (2014). Adult plasticity in the subcortical auditory pathway of the maternal mouse. *PloS ONE*, 9(7), e101630.

270. Moller, A.R., (2000). Similarities between severe tinnitus and chronic pain. *Journal of the American Academy of Audiology*, 11, 115–124.

271. Montie, E. W., Schneider, G. E., Ketten, D. R., Marino, L., Touhey, K. E., and Hahn, M. E. (2007). Neuroanatomy of the subadult and fetal brain of the Atlantic white-sided dolphin (*Lagenorhynchus acutus*) from in situ magnetic resonance images. *Anatomical Record*, 290, 1459–1479.

272. Montie, E. W., Schneider, G., Ketten, D. R., Marino, L., Touhey, K. E., & Hahn, M. E. (2008). Volumetric neuroimaging of the atlantic white-sided dolphin (*Lagenorhynchus acutus*) brain from in situ magnetic resonance images. *The Anatomical Record: Advances in Integrative Anatomy and Evolutionary Biology*, 291(3), 263-282.

273. Montie, E. W., Wheeler, E., Pussini, N., Battey, T. W., Barakos, J., Dennison, S., ... & Gulland, F. (2010). Magnetic resonance imaging quality and volumes of brain structures from live and postmortem imaging of California sea lions with clinical signs of domoic acid toxicosis. *Diseases of Aquatic Organisms*, 91(3), 243-256.

274. Moore, J.K., Osen, K.K. (1979). The cochlear nuclei in man. Am J Anat, 154, 393–418.

275. Morell, M. (2012). Ultrastructural analysis of odontocete cochlea (Doctoral dissertation). Barcelona (Catalunya): Universitat Politècnica de Catalunya.

276. Morell, M., Brownlow, A., McGovern, B., Raverty, S. A., Shadwick, R. E., & André, M. (2017). Implementation of a method to visualize noise-induced hearing loss in mass stranded cetaceans. *Scientific Reports*, 7(1), 1-8.

277. Morell, M., IJsseldijk, L. L., Piscitelli-Doshkov, M., Ostertag, S., Estrade, V., Haulena, M., ... & Shadwick, R. E. (2022). Cochlear apical morphology in toothed whales: Using the pairing hair cell—Deiters' cell as a marker to detect lesions. *The Anatomical Record*, 305(3), 622-642.

278. Morell, M., Raverty, S. A., Mulsow, J., Haulena, M., Barrett-Lennard, L., Nordstrom, C. A., ... & Shadwick, R. E. (2020a). Combining cochlear analysis and auditory evoked potentials in a beluga whale with high-frequency hearing loss. *Frontiers in Veterinary Science*, 7, 534917.

279. Morell, M., Vogl, A. W., IJsseldijk, L. L., Piscitelli-Doshkov, M., Tong, L., Ostertag, S., ... & Shadwick, R. E. (2020b). Echolocating whales and bats express the motor protein prestin in the inner ear: A potential marker for hearing loss. *Frontiers in Veterinary Science*, 429.

280. Morgane, P. J., Jacobs, M. S., & McFarland, W. L. (1980). The anatomy of the brain of the bottlenose dolphin (*Tursiops truncatus*). Surface configurations of the telencephalon of the bottlenose dolphin with comparative anatomical observations in four other cetacean species. *Brain Research Bulletin*, 5(3), 1-107.

281. Morimitsu, T., Kawano, H., Torihara, K., Kato, E., Koono, M. (1992). Histopathology of eighth cranial nerve of mass stranded dolphins at Goto Islands, Japan. *Journal of Wildlife Diseases*, 28(4), 656-8.

282. Morimitsu, T., Nagai, T., Ide, M., Kawano, H., Naichuu, A., Koono, M., Ishii, A. (1987). Mass stranding of Odontoceti caused by parasitogenic eighth cranial neuropathy. *Journal of Wildlife Diseases*, 23(4), 586-90.

283. Mortensen, H. S., Pakkenberg, B., Dam, M., Dietz, R., Sonne, C., Mikkelsen, B., & Eriksen, N. (2014). Quantitative relationships in delphinid neocortex. *Frontiers in Neuroanatomy*, 8, 132.

284. Moser, T., & Starr, A. (2016). Auditory neuropathy—neural and synaptic mechanisms. *Nature Reviews Neurology*, 12(3).

285. MSFD Common Implementation Strategy. Technical Group on Underwater Noise (TG NOISE) (2022). Available online: https://environment.ec.europa.eu/news/zero-pollution-and-biodiversity-first-ever-eu-wide-limits-underwater-noise-2022-11-29_fr (Accessed: June 15, 2020)
286. Mühlau, M., Rauschecker, J. P., Oestreicher, E., Gaser, C., Röttinger, M., Wohlschläger, A. M., ... & Sander, D. (2006). Structural brain changes in tinnitus. *Cerebral Cortex*, 16(9).
287. Murchison, A.E. (1980) Detection range and range resolution of echolocating bottlenose porpoise (*Tursiops truncatus*). In Animal sonar systems eds. Busnel, R.-G., Fish J.F. (Boston: Springer), 43–70.
288. Nachtigall, P. E., & Supin, A. Y. (2013). A false killer whale reduces its hearing sensitivity when a loud sound is preceded by a warning. *Journal of Experimental Biology*, 216(16).
289. Nachtigall, P. E., & Supin, A. Y. (2014). Conditioned hearing sensitivity reduction in a bottlenose dolphin (Tursiops truncatus). *Journal of Experimental Biology*, 217(15).
290. Nachtigall, P. E., & Supin, A. Y. (2015). Conditioned frequency-dependent hearing sensitivity reduction in the bottlenose dolphin (Tursiops truncatus). *Journal of Experimental Biology*, 218(7).
291. Nachtigall, P. E., Supin, A. Y., Estaban, J. A., & Pacini, A. F. (2016a). Learning and extinction of conditioned hearing sensation change in the beluga whale (*Delphinapterus leucas*). *Journal of Comparative Physiology A*, 202(2).
292. Nachtigall, P. E., Supin, A. Y., Pacini, A. F., & Kastelein, R. A. (2016b). Conditioned hearing sensitivity change in the harbor porpoise (*Phocoena phocoena*). *The Journal of the Acoustical Society of America*, 140(2).
293. Nachtigall, P. E., Supin, A. Ya., Pacini, A. F., & Kastelein, R. A. (2018). Four odontocete species change hear- ing levels when warned of impending loud sound. *Integrative Zoology*, 13(2).
294. Nachtigall, P.E.; Supin, A.Y.; Pawloski, J.; Au, W.W. (2004). Temporary threshold shifts after noise exposure in the bottlenose dolphin (*Tursiops truncatus*) measured using evoked auditory potentials. *Marine Mammal Science*, 20, 673–687.
295. Näslund, J., Haroutunian, V., Mohs, R., Davis, K. L., Davies, P., Greengard, P., & Buxbaum, J. D. (2000). Correlation between elevated levels of amyloid β-peptide in the brain and cognitive decline. *Jama*, 283(12), 1571-1577.
296. National Oceanic and Atmospheric Administration (NOAA) (2002). Report of the Workshop on Acoustic Resonance as a Source of Tissue Trauma in Cetaceans, Silver Spring, Maryland, 24-25 April, 2002. U.S. Department of Commerce, National Oceanic and Atmospheric Administration, National Marine Fisheries Service, Silver Spring, Maryland. Available online: http://www.nmfs.noaa.gov/prot_res/readingrm/MMSURTASS/Res_Wkshp_Rpt_Fin.PDF. 19pp. (Accessed: May 30, 2020)
297. Nelson, P. T., Braak, H., Markesbery, W. R. (2009). Neuropathology and Cognitive Impairment in Alzheimer Disease: A Complex but Coherent Relationship. *Journal of Neuropathology and Experimental Neurology*, 68, 1–14.
298. Newman, S.J., Smith, S.A. (2006). Marine mammal neoplasia: a review. *Veterinary Pathology*, 43, 865–880.
299. Nieder, C., Rosene, D. L., Mortazavi, F., Oblak, A. L., & Ketten, D. R. (2022). Morphology and unbiased stereology of the lateral superior olive in the short-beaked common dolphin, *Delphinus delphis* (*Cetacea, Delphinidae*). *Journal of Morphology*, 283(4), 446-461.

300. Nieukirk, S.L., Mellinger, D.K., Moore, S.E., Klinck, K., Dziak, R.P., and Goslin, J. (2012). Sounds from air guns and fin whales recorded in the mid-Atlantic Ocean, 1999–2009. *The Journal of the Acoustical Society of America*, 131(2), 1102–1112.
301. NMFS. (2016). Technical guidance for assessing the effects of anthropogenic sound on marine mammal hearing: Underwater acoustic thresholds for onset of perma- nent and temporary threshold shifts (NOAA Technical Memorandum NMFS-OPR-55). Washington, DC: National Oceanic and Atmospheric Administration, U.S. Department of Commerce. 178pp.
302. NMFS. (2018). 2018 revision top technical guidance for assessing the effects of anthropogenic sound on marine mammal hearing: Underwater acoustic thresholds for onset of permanent and temporary threshold shifts (83 FR 28824). Washington, DC: National Oceanic and Atmospheric Administration, U.S. Department of Commerce.
303. Nolte, L., Tinne, N., Schulze, J., Heinemann, D., Antonopoulos, G. C., Meyer, H., ... & Ripken, T. (2017). Scanning laser optical tomography for in toto imaging of the murine cochlea. *PloS ONE*, 12(4), e0175431.
304. Norwegian Defense Research Establishment (2021). The Minke Whale Hearing Project. Available online: https://www.ffi.no/en/research/the-minke-whale-hearing-project (Accessed: December 12, 2022)
305. NRC (2005) Board, O. S., & National Research Council. Marine mammal populations and ocean noise: determining when noise causes biologically significant effects. Washington: National Academies Press.
306. Ochiai, M., Nguyen, H. T., Kurihara, N., Hirano, M., Tajima, Y., Yamada, T. K., & Iwata, H. (2021). Directly Reprogrammed Neurons as a Tool to Assess Neurotoxicity of the Contaminant 4-Hydroxy-2′, 3, 5, 5′-tetrachlorobiphenyl (4′ OH-CB72) in Melon-Headed Whales. *Environmental Science & Technology*, 55(12), 8159-8168.
307. Oelschläger, H. H. A., Ridgway, S. H., & Knauth, M. (2010). Cetacean brain evolution: dwarf sperm whale (*Kogia sima*) and common dolphin (*Delphinus delphis*)–an investigation with high-resolution 3D MRI. *Brain, Behavior and Evolution*, 75(1), 33-62.
308. Øen, E.O. (1995a). Killing Methods for Minke and Bowhead Whales (Doctoral Dissertation). The Norwegian School of Veterinary Science, NO- 0033 Oslo, Norway.
309. Øen, E.O. (1995b). A Norwegian penthrite grenade for minke whales: hunting trials with prototypes of penthrite grenades in 1984, 1985 and 1986 and results from the hunt in 1984, 1985 and 1986. *Acta Veterinaria Scandinavica*, 36, 111.
310. Øen, E.O. (1995c). High velocity projectiles for killing whales. Hunting trials using 20 mm high velocity projectiles for minke whales in 1982. *Acta Veterinaria Scandinavica*, 36, 152.
311. Øen, E.O., Mørk, S. (1999). Observations of agonal movements, injuries and pathological changes in minke whales after intra-body detonation of penthrite. Report of the International Whaling Commission. IWC/51/WK 10.
312. Ogawa, T.; Arifuku, S. (1948). On the Acoustic System in the Cetacean Brains. *The Scientific Reports of the Whales Research Institute*, 2, 1–20.
313. Ohinata Y., Miller J.M., Altschuler R.A., Schacht J. (2000). Intense noise induces formation of vasoactive lipid peroxidation products in the cochlea, *Brain Research*, 29.

314. Olesiuk, O. F., Bigg, M. A., Ellis, G. M. (1990). Life History and Population Dynamics of Resident Killer Whale (*Orcinus orca*) in the Coastal Waters of British Columbia and Washington State. *Report of the International Whaling Commission*, Special Issue 12, 209- 243.

315. Osen, K.K. (1969). Cytoarchitecture of the cochlear nuclei in the cat. *Journal of Comparative Neurology*, 136, 453–484.

316. O'Shea, T.J., Homer, B.L., Greiner, E.C., Layton, A.W. (1991). Nasitrema sp.-associated encephalitis in a striped dolphin (*Stenella coeruleoalba*) stranded in the Gulf of Mexico. *Journal of Wildlife Diseases*, 27(4), 706-9.

317. Ostertag, S.K., Shaw, A.C., Basu, N., Chan, H.M. (2014). Molecular and Neurochemical Biomarkers in Arctic Beluga Whales (Delphinapterus leucas) Were Correlated to Brain Mercury and Selenium Concentrations. *Environmental Science & Technology*, 48, 11551-11559.

318. Panganiban, C. H., Barth, J. L., Darbelli, L., Xing, Y., Zhang, J., Li, H., ... & Richard, S. (2018). Noise-induced dysregulation of Quaking RNA binding proteins contributes to auditory nerve demyelination and hearing loss. *Journal of Neuroscience*, 38(10).

319. Park, E., Gottlieb, J. J., Cheung, B., Shek, P. N. & Baker, A. J. (2011). A model of low-level primary blast brain trauma results in cytoskeletal proteolysis and chronic functional impairment in the absence of lung barotrauma. *Journal of Neurotrauma*, 28, 343–347.

320. Parks, S.E.; Clark, C.W.; Tyack, P.L. (2007). Short-and long-term changes in right whale calling behavior: The potential effects of noise on acoustic communication. *The Journal of the Acoustical Society of America*, 122, 3725–3731.

321. Parolisi, R., Cozzi, B., & Bonfanti, L. (2018). Humans and dolphins: decline and fall of adult neurogenesis. *Frontiers in Neuroscience*, 497.

322. Patzke, N., Spocter, M. A., Karlsson, K., Bertelsen, M. F., Haagensen, M., Chawana, R., ... & Manger, P. R. (2015). In contrast to many other mammals, cetaceans have relatively small hippocampi that appear to lack adult neurogenesis. *Brain Structure and Function*, 220(1), 361-383.

323. Pende, M., Vadiwala, K., Schmidbaur, H., Stockinger, A. W., Murawala, P., Saghafi, S., ... & Zurl, M. (2020). A versatile depigmentation, clearing, and labeling method for exploring nervous system diversity. *Science Advances*, 6(22), eaba0365.

324. Penkov, A.; R. Stanislavov and D. Tzvetkov. (1996). Male reproductive function in workers exposed to vibration. *Central European Journal of Public Health*, 4(3), 185-188.

325. Perrin, W.F., Powers, J.E. (1980). Role of a nematode in natural mortality of spotted dolphins. *Journal of Wildlife Management*, 44, 960–3.

326. Peters, K. J., Gerber, L., Scheu, L., Cicciarella, R., Zoller, J. A., Fei, Z., ... & Krützen, M. (2023). An epigenetic DNA methylation clock for age estimates in Indo-Pacific bottlenose dolphins (*Tursiops aduncus*). *Evolutionary Applications*, 16(1), 126-133.

327. Petersen, J., & Valeur, J. (2013). Use of the ALARP prin- ciple for evaluating environmental risks and impacts of produced water discharged to sea (Paper OTC 23902). Presented at the Offshore Technology Conference, Houston, via Bröker (2019).

328. Photopoulou, T., Ferreira, I. M., Best, P. B., Kasuya, T., Marsh, H. (2017). Evidence for a postreproductive phase in female false killer whales *Pseudorca crassidens*. *Frontiers in Zoology*, 14, 1–14.

329. Pierson, L. L., Gerhardt, K. J., Abrams, R. M., Griffiths, S. K., & Peters, A. J. (1994). Effect of impulse noise on the auditory brainstem response of the fetal sheep and the adult ewe: case study. *Military Medicine*, 159(11), 676-680.
330. Pilati, N., Ison, M. J., Barker, M., Mulheran, M., Large, C. H., Forsythe, I. D., ... & Hamann, M. (2012). Mechanisms contributing to central excitability changes during hearing loss. *Proceedings of the National Academy of Sciences*, 109(21).
331. Pilleri G. (1966). Brain lipoma in the Humpback whale, *Megaptera novaeangliae*. *Pathologia Veterinaria*, 3, 341–349.
332. Pilleri G. (1968). Cerebral neurofibroma in the fin whale, *Balaenoptera physalus*. *Pathologia Veterinaria*, 5(1), 35–40.
333. Pintore, M. D., Mignone, W., Di Guardo, G., Mazzariol, S., Ballardini, M., Florio, C. L., ... & Iulini, B. (2018). Neuropathologic findings in cetaceans stranded in Italy (2002–14*). Journal of Wildlife Diseases*, 54(2), 295-303.
334. Popov, V. V., Ladygina, T. F., & Supin, A. Y. (1986). Evoked potentials of the auditory cortex of the porpoise, Phocoena phocoena. *Journal of Comparative Physiology A*, 158(5).
335. Popov, V. V., Supin, A. Y., & Klishin, V. O. (1992). Electrophysiological study of sound conduction in dolphins. In Marine Mammal Sensory Systems, eds. Thomas, J.A., Kastelein, R.A, Supin, A.Y. (Boston: Springer), 269-276.
336. Popov, V., & Supin, A. (1990). Electrophysiological studies of hearing in some cetaceans and a manatee in Sensory Abilities of Cetaceans, ed. Thomas, J. A., Kastelein, R. A. (Boston: Springer), 405-415.
337. Popper, A. N., Hawkins, A. D., & Halvorsen, M. B. (2019). Anthropogenic sound and fishes. Report by ICF for Washington State Department of Transportation, Research Office, 170. Available online: https://www.wsdot.wa.gov/research/reports/fullreports/891-1.pdf (Accessed: May 30, 2020)
338. Popper, A. N., Hawkins, A. D., & Thomsen, F. (2020). Taking the Animals' Perspective Regarding Anthropogenic Underwater Sound. *Trends in Ecology & Evolution*, 35(9), 787-794.
339. Popper, Arthur N., & Hastings, M. C. (2009). The effects of human-generated sound on fish. *Integrative Zoology*, 4(1).
340. Price, G. R. (2007). Validation of the auditory hazard assessment algorithm for the human with impulse noise data. *The Journal of the Acoustical Society of America*, 122(5).
341. Pun, P. B. L., Kan, E. M., Salim, A., Li, Z. H., Ng, K. C., Moochhala, S. M., ... & Lu, J. (2011). Low level primary blast injury in rodent brain. *Frontiers in Neurology*, 2, 19.
342. Rabinowitz, P. M. (2012). The public health significance of noise-induced hearing loss. In Noise-Induced Hearing Loss: Scientific Advances, Springer Handbook of Auditory Research 40, eds. Le Prell, C. G. et al. (New York: Springer), 13-25.
343. Raghanti, M.A., Wicinski, B., Meierovich, R., Warda, T., Dickstein, D.L., Reidenberg, J.S., Tang, C.Y., George, J.C., Thewissen J.G.M., Butti, C., Hof, P.R. (2019). A Comparison of the Cortical Structure of the Bowhead Whale (*Balaena mysticetus*), a Basal Mysticete, with Other Cetaceans. *Anatomical Record*, 302(5), 745-760.
344. Ramsdell, J. S., & Gulland, F. M. (2014). Domoic acid epileptic disease. *Marine Drugs*, 12(3), 1185–1207.
345. Ramsdell, J. S., & Zabka, T. S. (2008). In utero domoic acid toxicity: a fetal basis to adult disease in the California sea lion (*Zalophus californianus*). *Marine Drugs*, 6(2), 262-290.
346. Rankin, S. and Evans, W.E. (1998). Effect of Low Frequency Seismic Exploration Signals on the Cetaceans of the Gulf of Mexico. The World Marine Mammal Science Conference 20-24 January 1998. Abstracts, 110 via André et al. (2009).

347. Raphael, Y., & Altschuler, R. A. (1991). Reorganization of cytoskeletal and junctional proteins during cochlear hair cell degeneration. *Cell Motility and the Cytoskeleton*, 18(3), 215-227.

348. Readnower, R. D., Chavko, M., Adeeb, S., Conroy, M. D., Pauly, J. R., McCarron, R. M., & Sullivan, P. G. (2010). Increase in blood–brain barrier permeability, oxidative stress, and activated microglia in a rat model of blast-induced traumatic brain injury. *Journal of Neuroscience Research*, 88(16).

349. Reichmuth, C., Ghoul, A., Sills, J. M., Rouse, A., & Southall, B. L. (2016). Low-frequency temporary threshold shift not observed in spotted or ringed seals exposed to single air gun impulses. *The Journal of the Acoustical Society of America*, 140(4).

350. Reichmuth, C., Sills, J. M., Mulsow, J., & Ghoul, A. (2019). Long-term evidence of noise-induced permanent threshold shift in a harbor seal (*Phoca vitulina*). The Journal of the Acoustical Society of America, 146(4).

351. Revishchin, A. V., & Garey, L. J. (1990). The thalamic projection to the sensory neocortex of the porpoise, Phocoena phocoena. *Journal of Anatomy*, 169, 85.

352. Richardson, W. J. (Ed.). (1998). Marine mammal and acoustical monitoring of Western Geophysical's open water seismic program in the Alaskan Beaufort Sea, 1998. LGL Limited, Greeneridge Sciences. Available online: ftp://ftp.lgl.com/Public/For%20DRDC/TA2230-3%20Final%20Report.pdf (Accessed: May 15, 2020)

353. Richardson, W. J., Green Jr., C. R., Malme, C. I., and Thomson, D. H. eds. (1995). Marine Mammals and Noise. New York: Academic Press.

354. Ridgway, S.H., Marino, L., Lipscomb, T.P. (2002). Description of a poorly differentiated carcinoma within the brainstem of a white whale (*Delphinapterus leucas*) from magnetic resonance images and histological analysis. *Anatomical Record*, 268 (4), 441–449.

355. Ridgway, S.H. (1972). Cerebral and cerebellar involvement of trematode parasites in dolphins and their possible role in stranding. *Journal of Wildlife Diseases*, 8(1), 33-43.

356. Ridgway, S. H. (1980). Electrophysiological experiments on hearing in odontocetes. In Animal sonar systems eds. Busnel, R.-G., Fish J.F. (Boston: Springer), 483-493.

357. Ridgway, S. H. (1983). Dolphin hearing and sound production in health and illness. In Hearing and other senses: Presentations in honor of E.G. Wever, eds. Fay, R.R. and Gourevitch, G., 247-296.

358. Ridgway, S. H. (2000). The auditory central nervous system of dolphins. In Hearing by Whales and Dolphins, eds. Au, W. W.L., Popper, A. N., Fay, R. R. (New York: Springer), 273-293.

359. Ridgway, S. H., & Hanson, A. C. (2014). Sperm whales and killer whales with the largest brains of all toothed whales show extreme differences in cerebellum. *Brain, Behavior and Evolution*, 83(4), 266-274.

360. Ridgway, S. H., Brownson, R. H., Van Alstyne, K. R., & Hauser, R. A. (2019). Higher neuron densities in the cerebral cortex and larger cerebellums may limit dive times of delphinids compared to deep-diving toothed whales. *PloS ONE*, 14(12).

361. Ridgway, S., Houser, D., Finneran, J., Carder, D., Keogh, M., Van Bonn, W., ... & Hoh, C. (2006). Functional imaging of dolphin brain metabolism and blood flow. *Journal of Experimental Biology*, 209(15), 2902-2910.

362. Roberto, M., Hamernik, R. P., & Turrentine, G. A. (1989). Damage of the auditory system associated with acute blast trauma. *Annals of Otology, Rhinology & Laryngology*, 98(5_suppl).

363. Rolland, R.M.; Parks, S.E.; Hunt, K.E.; Castellote, M.; Corkeron, P.J.; Nowacek, D.P.; Wasser, S.K.; Kraus, S.D. (2012). Evidence that ship noise increases stress in right whales. *Proceedings of the Royal Society B: Biological Sciences*, 279, 2363–2368.

364. Roman, J., & McCarthy, J. J. (2010). The whale pump: marine mammals enhance primary productivity in a coastal basin. *PloS ONE*, 5(10), e13255.

365. Romano, T. A., Keogh, M. J., Kelly, C., Feng, P., Berk, L., Schlundt, C. E., ... & Finneran, J. J. (2004). Anthropogenic sound and marine mammal health: measures of the nervous and immune systems before and after intense sound exposure. *Canadian Journal of Fisheries and Aquatic Sciences*, 61(7).

366. Rosati, R., Jamesdaniel, S. (2020). Environmental Exposures and Hearing Loss. *International Journal of Environmental Research and Public Health*, 17(13), 4879.

367. Rowles et al. (2001). International Whaling Commission. 2001. Report of the Scientific Committee. Annex J. Report of the Standing Working Group on Environmental Concerns. *Journal of Cetacean Research and Management* (Suppl.), 3, 239-62.

368. Ryan, J.P., Joseph, J.E., Margolina, T., Reeves, L.P., Hatch, L., DeVogelaere, A., Southall, B., Stimpert, A., Baumann-Pickering, S. (2020). Quieting of low-frequency vessel noise in Monterey Bay National Marine Sanctuary during the COVID-19 pandemic. *The Journal of the Acoustical Society of America*, 148, 2734.

369. Rybnikova, E. A., Nalivaeva, N. N., Zenko, M. Y., & Baranova, K. A. (2022). Intermittent Hypoxic Training as an Effective Tool for Increasing the Adaptive Potential, Endurance and Working Capacity of the Brain. *Frontiers in Neuroscience*, 16.

370. Sacchini S, Fernández A, Mompeó B, Ramírez R, Arbelo M, Holgersen U, Quesada-Canales O, Castro-Alonso A, Andrada M. (2022). Toothed Whales Have Black Neurons in the Blue Spot. *Veterinary Sciences*, 9(10), 525.

371. Sacchini, S., Díaz-Delgado, J., Espinosa de los Monteros, A., Paz, Y., Bernaldo de Quirós, Y., Sierra, E., ... & Fernández, A. (2020). Amyloid-beta peptide and phosphorylated tau in the frontopolar cerebral cortex and in the cerebellum of toothed whales: aging versus hypoxia. *Biology Open*, 9(11), bio054734.

372. Salvi, R., and Boettcher, F. A. (2008). Animals models of noise-induced hearing loss in Sourcebook of Models for Biomedical Research, ed. P. M. Conn (Totowa: Humana), 289–302.

373. Samson, J., Sheeladevi, R., Ravindran, R., & Senthilvelan, M. (2007). Stress response in rat brain after different durations of noise exposure. *Neuroscience Research*, 57(1).

374. Sarnocińska, J., Teilmann, J., Balle, J. D., van Beest, F. M., Delefosse, M., & Tougaard, J. (2020). Harbor porpoise (*Phocoena phocoena*) reaction to a 3D seismic air gun survey in the North Sea. *Frontiers in Marine Science*, 6.

375. Scardigli, M., Pesce, L., Brady, N., Mazzamuto, G., Gavryusev, V., Silvestri, L., ... & Pavone, F. S. (2021). Comparison of Different Tissue Clearing Methods for Three-Dimensional Reconstruction of Human Brain Cellular Anatomy Using Advanced Imaging Techniques. *Frontiers in Neuroanatomy*, 15.

376. Schmidt-Wilcke, T., Leinisch, E., Gänssbauer, S., Draganski, B., Bogdahn, U., Altmeppen, J., & May, A. (2006). Affective components and intensity of pain correlate with structural differences in gray matter in chronic back pain patients. *Pain*, 125(1-2), 89-97.

377. Schmitz, C., & Hof, P. (2005). Design-based stereology in neuroscience. *Neuroscience*, 130(4), 813-831.

378. Schneider, P., Andermann, M., Wengenroth, M., Goebel, R., Flor, H., Rupp, A., & Diesch, E. (2009). Reduced volume of Heschl's gyrus in tinnitus. *Neuroimage*, 45(3).

379. Schneuer, M., Flachsbarth, S., Czech-Damal, N. U., Folkow, L. P., Siebert, U., & Burmester, T. (2012). Neuroglobin of seals and whales: Evidence for a divergent role in the diving brain. *Neuroscience*, 223, 35–44.

380. Schulman-Galambos, C. & Galambos, R. (1979). Brain stem evoked response audiometry in newborn hearing screening. *Archives of Otolaryngology*, 105(2), 86-90.

381. Seidel, H. (1993). Selected health risks caused by long-term, whole-body vibration. *American Journal of Industrial Medicine*, Apr 23(4).

382. Seidel, H. and R. Heide. (1986). Long-term effects of whole-body vibration: A critical survey of the literature. *International Archives of Occupational and Environmental Health*, 58(1).

383. Shi, X., & Nuttall, A. L. (2003). Upregulated iNOS and oxidative damage to the cochlear stria vascularis due to noise stress. *Brain Research*, 967(1-2).

384. Shin, S., Lyu, A. R., Jeong, S. H., Kim, T. H., Park, M. J., & Park, Y. H. (2019). Acoustic Trauma Modulates Cochlear Blood Flow and Vasoactive Factors in a Rodent Model of Noise-Induced Hearing Loss. *International Journal of Molecular Sciences*, 20(21).

385. Shinkawa, C., Ito, T., Hozumi, Y., Chiba, M., Matsui, H., Goto, K., & Kakehata, S. (2019). Expression and localization of diacylglycerol kinase ζ in guinea pig cochlea and its functional implication under noise-exposure stress conditions. *Histochemistry and Cell Biology*, 151(6).

386. Siebert, U., Stürznickel, J., Schaffeld, T., Oheim, R., Rolvien, T., Prenger-Berninghoff, E., ... & Morell, M. (2022). Blast injury on harbour porpoises (*Phocoena phocoena*) from the Baltic Sea after explosions of deposits of World War II ammunition. *Environment International*, 159, 107014.

387. Sierra, E., Fernández, A., Felipe-Jiménez, I., Zucca, D., Díaz-Delgado, J., Puig-Lozano, R., ... & Arbelo, M. (2020). Histopathological differential diagnosis of meningoencephalitis in cetaceans: *Morbillivirus*, *Herpesvirus*, *Toxoplasma gondii*, *Brucella sp.*, and *Nasitrema sp. Frontiers in Veterinary Science*, 7, 650.

388. Sierra, E.; Sánchez, S.; Saliki, J.T.; Blas-Machado, U.; Arbelo, M.; Zucca, D.; Fernández, A. (2014). Retrospective study of etiologic agents associated with nonsuppurative meningoencephalitis in stranded cetaceans in the Canary Islands. *Journal of Clinical Microbiology*, 52, 2390–2397.

389. Silvagni, P. A., Lowenstine, L. J., Spraker, T., Lipscomb, T. P., & Gulland, F. M. D. (2005). Pathology of domoic acid toxicity in California sea lions (*Zalophus californianus*). *Veterinary Pathology*, 42(2), 184-191.

390. Soares, M., dos Santos, A. B., Weich, T. M., Mânica, G. G., de Bittencourt Junior, P. I. H., Ludwig, M. S., & Heck, T. G. (2019). Heat shock response in noise-induced hearing loss: effects of alanyl-glutamine dipeptide supplementation on heat shock proteins status. *Brazilian Journal of Otorhinolaryngology*.

391. Sokolov, V. E., Ladygina, T. F., & Supin, A. I. (1972). [Localization of sensory zones in the dolphin cerebral cortex]. Doklady Akademii Nauk SSSR, 202(2), 490–493. Available online: http://www.ncbi.nlm.nih.gov/pubmed/4333815 (Accessed: May 16, 2020)

392. Soloway, A.G., 2018. Environmental Noise from Underwater Explosions and the Impact of the Seabed on the Received Levels (Doctoral dissertation). Washington (WA, USA): University of Washington.

393. Soto, S.; Alba, A.; Ganges, L.; Vidal, E.; Raga, J.A.; Alegre, F.; González, B.; Medina, P.; Zorrilla, I.; Martínez, J. (2011). Post-epizootic chronic dolphin morbillivirus infection in Mediterranean striped dolphins Stenella coeruleoalba. *Diseases of Aquatic Organisms*, 96, 187–194.

394. Southall, B. L., Finneran, J. J., Reichmuth, C., Nachtigall, P. E., Ketten, D. R., Bowles, A. E., ... & Tyack, P. L. (2019). Marine mammal noise exposure criteria: Updated scientific recommendations for residual hearing effects. *Aquatic Mammals*, 45(2).

395. Southall, B. L., Rowles, T., Gulland, F., Baird, R. W., & Jepson, P. D. (2013). Final report of the Independent Scientific Review Panel investigating potential contributing factors to a 2008 mass stranding of melon-headed whales (*Peponocephala electra*) in Antsohihy, Madagascar. Independent Scientific Review Panel. Available online: https://www.cascadiaresearch.org/oldsite/Hawaii/Madagascar_ISRP_Final_report.pdf (Accessed: May 16, 2020)

396. Southall, B., Bowles, A., Ellison, W., Finneran, J., Gentry, R., Greene, C. Jr., Kastak, D., Ketten, D., Miller, J., Nachtigall, P., Richardson, W., Thomas, J., Tyack, P. (2007). Marine Mammal Noise Exposure Criteria: Initial Scientific Recommendations. *Aquatic Mammals*, 33(4), 273-275.

397. Southall, B.L., Nowacek, D.P., Bowles, A.E., Senigaglia, V., Bejder, L., Tyack, P.L. (2021). Marine Mammal Noise Exposure Criteria: Assessing the Severity of Marine Mammal Behavioral Responses to Human Noise. *Aquatic Mammals*, 47, 421–464.

398. Southern, S. (2000). Molecular analysis of stress-activated proteins and genes in dolphins and whales: A new technique for monitoring environmental stress. In Annual Conference-American Association of Zoo Veterinarians (240-244). American Association of Zoo Veterinarians; 1998.

399. Stevens, P.E., Hill, H.M., Bruck, J.N. (2021). Cetacean Acoustic Welfare in Wild and Managed-Care Settings: Gaps and Opportunities. *Animals*, 11, 3312.

400. Stone, C.J. (2015b). Implementation of and consideration for revisions to the JNCC guidelines for seismic surveys, JNCC Report No. 463b, JNCC, Peterborough, ISSN 0963-8091. Available online: http://jncc.defra. gov.uk/pdf/JNCC%20Report%20463b_Final.pdf (Accessed: May 30, 2020)

401. Stone, C.J., (2015a). Marine mammal observations during seismic surveys from 1994 - 2010, JNCC Report No. 463a, JNCC, Peterborough, ISSN 0963-8091. Available online: http://jncc.defra.gov.uk/pdf/JNCC%20 Report%20463a_Final.pdf (Accessed: May 15, 2020)

402. Story, B. D., Miller, M. E., Bradbury, A. M., Million, E. D., Duan, D., Taghian, T., ... & Gray-Edwards, H. L. (2020). Canine models of inherited musculoskeletal and neurodegenerative diseases. *Frontiers in Veterinary Science*, 7, 80.

403. Strahan, M.G.; Finneran, J.J.; Mulsow, J.; Houser, D.S. (2020). Effects of dolphin hearing bandwidth on biosonar click emissions. *The Journal of the Acoustical Society of America*, 148, 243–252.

404. Stylianaki I, Komnenou AT, Posantzis D, Nikolaou K, Papaioannou N. (2019). Alzheimer's disease-like pathological lesions in an aged bottlenose dolphin (*Tursiops truncatus*). *Veterinary Record Case Reports*, 7, 1–5.

405. Suneja, S.K., Potashner, S.J. and Benson, C.G. (1998). Plastic changes in glycine and GABA release, and uptake in adult brain stem auditory nuclei after unilateral middle ear ossicle removal and cochlear ablation. *Experimental Neurology*, 151.

406. Tanabe, S., Iwata, H., & Tatsukawa, R. (1994). Global contamination by persistent organochlorines and their ecotoxicological impact on marine mammals. *Science of the Total Environment*, 154(2-3), 163-177.

407. Thomson, D.J.M. Barclay, D.R. (2020). Real-time observations of the impact of COVID-19 on underwater noise *The Journal of the Acoustical Society of America*, 147, 3390–3396.

408. Titov, A.A. (1972). Investigation of sonic activity and phenomenological characteristics of the echolocation analyzer of Black Sea delphinids (Candidatorial dissertation). Karadag (Crimea, Ucraine).
409. Tougaard, J., Henriksen, O. D., Miller, L. E. (2009). Underwater noise from three types of offshore wind turbines: Estimation of impact zones for harbor porpoises and harbor seals. *The Journal of the Acoustical Society of America*, 125(6).
410. Tsui, H. C., Kot, B. C., Chung, T. Y., & Chan, D. K. (2020). Virtopsy as a revolutionary tool for Cetacean Stranding Programs: Implementation and Management. *Frontiers in Marine Science*, 7, 542015.
411. Tuladhar, A. M., & de Leeuw, F. E. (2020). Hearing loss and cortical thickness: an unheard reciprocal association? *European Journal of Neurology*, 27(6).
412. Turl, C.W. (1991). The echolocation ability of the beluga (*Delphinapterus leucas*) to detect targets in clutter. *The Journal of the Acoustical Society of America,* 89, 896.
413. Turnbull, B.S., Cowan, D.F., Sadagopa Ramanujam, V.M., Alcock, N.W. (1998). Do dolphins have protective mechanisms against mercury toxicity? International Association for Aquatic Animal Medicine Conference, 1998.
414. U.S. Navy (2022). Marine Mammal Program. Naval Information Warfare Centre Pacific. Available online: https://www.niwcpacific.navy.mil/marine-mammal-program (Accessed December 14, 2022)
415. Ueda, H. R., Ertürk, A., Chung, K., Gradinaru, V., Chédotal, A., Tomancak, P., & Keller, P. J. (2020). Tissue clearing and its applications in neuroscience. *Nature Reviews Neuroscience*. 21(2), 61-79.
416. UN General Assembly, Convention on the Law of the Sea, 10 December (1982). Available online: https://www.refworld.org/docid/3dd8fd1b4.html (Accessed: July 17, 2020)
417. Unal, E., & Romano, T. A. (2021). Of whales and genes: unraveling the physiological response to stressors in belugas (*Delphinapterus leucas*) at the molecular level. *Journal of Zoological and Botanical Gardens*, 2(4), 559-575.
418. US (1972). Marine Mammal Protection Act (16 U.S.C. Sec. 1361 et seq.) National Oceanic and Atmospheric Administration and U.S. Fish & Wildlife Service. Available online: https://catalog.data.gov/dataset/marine-mammal-protection-act (Accessed: April 29, 2020)
419. Vacher, M. C., Durrant, C. S., Rose, J., Hall, A. J., Spires-Jones, T. L., Gunn-Moore, F., & Dagleish, M. P. (2022). Alzheimer's disease-like neuropathology in three species of oceanic dolphin. European Journal of Neuroscience.
420. Valderrama, J. T., & Torre Vega, Á. D. L. (2022). The hunt for hidden hearing loss in humans: From preclinical studies to effective interventions. *Frontiers in Neuroscience*, 16, 1000304.
421. van Beest, F. M., Nabe-Nielsen, J., Carstensen, J., Teilmann, J., & Tougaard, J. (2015). Disturbance effects on the harbour porpoise population in the North Sea (DEPONS): status report on model development. Available online: https://dce2.au.dk/pub/SR140.pdf (Accessed: April 29, 2020)
422. Van Bressem, M. F., Duignan, P. J., Banyard, A., Barbieri, M., Colegrove, K. M., De Guise, S., ... & Wellehan, J. F. (2014). *Cetacean morbillivirus*: current knowledge and future directions. *Viruses*, 6(12), 5145-5181.
423. Van der Graaf, A. J., Ainslie, M. A., Brensing, K., Dalen, J., Dekeling, René, Robinson, S., et al. (2012). European Marine Strategy Framework Directive Good Environmental Status (MSFD-GES): Report of the Technical Subgroup on Underwater Noise and other forms of energy. Available online: https://ec.europa.eu/environment/marine/pdf/MSFD_reportTSG_Noise.pdf (Accessed: June 15, 2020)

424. van Elk, C., van de Bildt, M., van Run, P., De Jong, A., Getu, S., Verjans, G., ... & Kuiken, T. (2016). Central nervous system disease and genital disease in harbor porpoises (*Phocoena phocoena*) are associated with different herpesviruses. *Veterinary Research*, 47(1), 1-11.

425. von Benda-Beckmann, A.M., Aarts, G., Sertlek, H.¨O., Lucke, K., Verboom, W.C., Kastelein, R.A., Ketten, D.R., van Bemmelen, R., Lam, F.-P.-A., Kirkwood, R.J., Ainslie, M.A., (2015). Assessing the Impact of Underwater Clearance of Unexploded Ordnance on Harbour Porpoises (*Phocoena phocoena*) in the Southern North Sea. *Aquatic Mammals*, 41, 503–523.

426. Von Fersen L, Kamminga C, Seidl A. 2000. Estudios prelimina- ries sobre el comportamiento de un ejemplar de Franciscana (*Pontoporia blainvillei*) en Mundo Marino, Argentina; in UNEP/CMS. Report of the Third Workshop for Coordinated Research and Conservation of the Franciscana Dolphin *Pontoporia blainvillei* in the Southwestern Atlantic. Bonn, Germany, UNEP/CMS Secretariat, United Nations Premises, 30–33.

427. Wakabayashi, K., Fujioka, M., Kanzaki, S., Okano, H. J., Shibata, S., Yamashita, D., ... & Okano, H. (2010). Blockade of interleukin-6 signaling suppressed cochlear inflammatory response and improved hearing impairment in noise-damaged mice cochlea. *Neuroscience Research*, 66(4).

428. Wan, G., & Corfas, G. (2017). Transient auditory nerve demyelination as a new mechanism for hidden hearing loss. *Nature Communications*, 8(1).

429. Wang, H., Brozoski, T.J., Turner, J.G., Ling, L., Parrish, J.L., Hughes, L.F., Caspary, D.M. (2009). Plasticity at glycinergic synapses in dorsal cochlear nucleus of rats with behavioral evidence of tinnitus. *Neuroscience*, 164.

430. Wang, H., Magnain, C., Wang, R., Dubb, J., Varjabedian, A., Tirrell, L. S., et al. (2018). as-PSOCT: Volumetric microscopic imaging of human brain architecture and connectivity. *Neuroimage*, 165, 56–68.

431. Wang, J.T., Yin, L., Chen, Z. (2013). Neuroprotective role of fibronectin in neuron-glial extrasynaptic transmission. *Neural Regeneration Research*, 8, 376–382.

432. Wang, Q., Sporns, O., & Burkhalter, A. (2012). Network analysis of corticocortical connections reveals ventral and dorsal processing streams in mouse visual cortex. *Journal of Neuroscience*, 32(13), 4386-4399.

433. Wang, W., Zhang, L. S., Zinsmaier, A. K., Patterson, G., Leptich, E. J., Shoemaker, S. L., ... & Zhang, J. (2019). Neuroinflammation mediates noise-induced synaptic imbalance and tinnitus in rodent models. *PLoS Biology*, 17, 1–25

434. Wang, Z. T., Supin, A. Y., Akamatsu, T., Duan, P. X., Yang, Y. N., Wang, K. X., & Wang, D. (2021). Auditory evoked potential in stranded melon-headed whales (*Peponocephala electra*): With severe hearing loss and possibly caused by anthropogenic noise pollution. *Ecotoxicology and Environmental Safety*, 228, 113047.

435. Warchol, M. E. (2011). Sensory regeneration in the vertebrate inner ear: differences at the levels of cells and species. *Hearing Research*, 273, 72–79.

436. Watanabe, T., Frahm, J., & Michaelis, T. (2008). Manganese-enhanced MRI of the mouse auditory pathway. *Magnetic Resonance in Medicine*: An Official Journal of the International Society for Magnetic Resonance in Medicine, 60(1).

437. Weeks, C. A., Brown, S. N., Warriss, P. D., Lane, S., Heasman, L., & Benson, T. (2009). Noise levels in lairages for cattle, sheep and pigs in abattoirs in England and Wales. *Veterinary Record*, 165(11).

438. Weilgart, L. (2013). A review of the impacts of seismic air gun surveys on marine life. CBD Expert Workshop on Underwater Noise and its Impacts on Marine and Coastal Biodiversity, 25-27 February 2014, London, UK. Available online: http://www.cbd.int/doc/?meeting=MCBEM-2014-01 (Accessed: December 15, 2022)

439. Weir, C. R., & Dolman 1, S. J. (2007). Comparative review of the regional marine mammal mitigation guidelines implemented during industrial seismic surveys, and guidance towards a worldwide standard. *Journal of International Wildlife Law and Policy*, 10(1).

440. Weir, C.R. (2008). Short-finned pilot whales (Globicephala macrorhynchus) respond to an air gun ramp-up procedure off Gabon. *Aquatic Mammals,* 34(3).

441. Wensveen, P. J., Kvadsheim, P. H., Lam, F. P. A., von Benda-Beckmann, A. M., Sivle, L. D., Visser, F., ... & Miller, P. J. (2017). Lack of behavioural responses of humpback whales (*Megaptera novaeangliae*) indicate limited effectiveness of sonar mitigation. *Journal of Experimental Biology*, 220(22).

442. Wilhelm Filho, D., Sell, F., Ribeiro, L., Ghislandi, M., Carrasquedo, F., Fraga, C. G., Wallauer, J. P., Simoes-Lopes, P. C., & Uhart, M. M. (2002). Comparison between the antioxidant status of terrestrial and diving mammals. *Comparative biochemistry and physiology. Part A, Molecular & integrative physiology*, 133(3), 885–92.

443. Williams C.L., Ponganis P.J. (2013). Muscle Oxygen Saturation Measurements in Diving Mammals and Birds Using NIRS in Application of Near Infrared Spectroscopy in Biomedicine. Handbook of Modern Biophysics, vol 4. Jue T., ed. Masuda K. (Boston: Springer), 109-121.

444. Winsor, M.H. & Mate, B.R. (2006). Seismic survey activity and the proximity of satellite-tagged sperm whales. IWC SC/58/E16, 8. Available online: https://doi.org/10.1080/09524622.2008.9753813 (Accessed: May 13, 2020)

445. Wong, A. C., & Ryan, A. F. (2015). Mechanisms of sensorineural cell damage, death and survival in the cochlea. *Frontiers in Aging Neuroscience*, 7, 58.

446. World Health Organization (WHO) (2021). World Report on Hearing. Geneva: World Health Organization. Available online: https://www.who.int/publications/i/item/9789240020481 (Accessed: March 12, 2022)

447. Wright, A. J., Deak, T., & Parsons, E. C. M. (2011). Size matters: management of stress responses and chronic stress in beaked whales and other marine mammals may require larger exclusion zones. *Marine Pollution Bulletin*, 63(1-4), 5-9.

448. Wright, A. J., Soto, N. A., Baldwin, A. L., Bateson, M., Beale, C. M., Clark, C., ... & Martin, V. (2007). Do marine mammals experience stress related to anthropogenic noise? *International Journal of Comparative Psychology*, 20(2).

449. Wright, A. K., Theilmann, R. J., Ridgway, S. H., & Scadeng, M. (2018). Diffusion tractography reveals pervasive asymmetry of cerebral white matter tracts in the bottlenose dolphin (*Tursiops truncatus*). *Brain Structure and Function*, 223(4).

450. Wright, A., Scadeng, M., Stec, D., Dubowitz, R., Ridgway, S., & Leger, J. S. (2017). Neuroanatomy of the killer whale (*Orcinus orca*): a magnetic resonance imaging investigation of structure with insights on function and evolution. *Brain Structure and Function*, 222(1), 417-436.

451. Wu, P. Z., Liberman, L. D., Bennett, K., De Gruttola, V., O'Malley, J. T., & Liberman, M. C. (2019). Primary neural degeneration in the human cochlea: evidence for hidden hearing loss in the aging ear. *Neuroscience*, 407.

452. Yamashita D, Jiang HY, Schacht J, Miller JM (2004): Delayed production of free radicals following noise exposure. *Brain Research*, 1019.

453. Yamashita, D., Minami, S. B., Kanzaki, S., Ogawa, K., & Miller, J. M. (2008). Bcl-2 genes regulate noise-induced hearing loss. *Journal of Neuroscience Research*, 86(4).

454. Yang, W. C., Chen, C. F., Chuah, Y. C., Zhuang, C. R., Chen, I. H., Mooney, T. A., ... & Chou, L. S. (2021). Anthropogenic sound exposure-induced stress in captive dolphins and implications for cetacean health. *Frontiers in Marine Science*, 8, 606736.

455. Yazvenko, S. B., McDonald, T. L., Blokhin, S. A., Johnson, S. R., Meier, S. K., Melton, H. R., Wainwright, P. W. (2007). Distribution of western gray whales during a seismic survey near Sakhalin Island, Russia. *Environmental Monitoring and Assessment*, 134(1-3).

456. Yeh, F.C., Verstynen, T.D., Wang, Y., Fernández-Miranda, J.C., Tseng, W.Y.I. (2013). Deterministic Diffusion Fiber Tracking Improved by Quantitative Anisotropy. *PLoS ONE*, 8, e80713.

457. Yin, P., Li, S., Li, X. J., & Yang, W. (2022). New pathogenic insights from large animal models of neurodegenerative diseases. *Protein & Cell*, 1-14.

458. Zalesky A, Fornito A. (2009) A DTI-derived measure of cortico-cortical connectivity. *I.E.E.E. Transactions on Medical Imaging*, 28(7), 1023-36.

459. Zeng, C., Nannapaneni, N., Zhou, J., Hughes, L.F., Shore, S. (2009). Cochlear damage changes the distribution of vesicular glutamate transporters associ- ated with auditory and nonauditory inputs to the cochlear nucleus. *Journal of Neuroscience*, 29.

460. Zhan, W., Cruickshanks, K. J., Klein, B. E., Klein, R., Huang, G. H., Pankow, J. S., Gangnon, R. E., & Tweed, T. S. (2010). Generational differences in the prevalence of hearing impairment in older adults. *American Journal of Epidemiology*, 171(2).

461. Zook, J. M., & DiCaprio, R. A. (1990). A potential system of delay-lines in the dolphin auditory brainstem. In Sensory Abilities of Cetaceans eds. Thomas, J.A., Kastelein, R.A. (Boston: Springer), 181-193.

Annex I: Semi-automatic immunostaining protocol

Staining protocol 222cet (base protocol)
Procedure: BMK ultraView DAB Par
BenchMark IHC/ISH Form

```
1 ***** Select EZ Prep *****
2 ***** Start timed stages *****
3 ***** Mixers disabled *****
4 Heat the slides to 75 ° C, and incubate for 4 minutes
5 Adjust the volume of EZ Prep (Discovery)
6 Incubate for 4 minutes
7 Rinse the slide +
8 Adjust the volume of EZ Prep (Discovery)
9 Incubate for 4 minutes
10 Rinse the slide +
11 Adjust the volume of EZ Prep (Discovery)
12 Dispense Coverslip
13 Heat slides to 76 ° C, and incubate for 4 minutes
14 Rinse the slide +
15 Adjust the dewaxing volume
16 Dispense Coverslip
17 Turn off slide heating
18 ***** Activated mixers *****
19 [Short - Cell Conditioning 8 minutes]
20 Rinse the slide +
21 Dispense Cell Conditioner Medium 1
22 Dispense Coverslip for long CC
23 Heat slides to 95 ° C, and incubate for 8 minutes
24 [Reduced - Cell Conditioning 30 minutes]
25 Dispense Cell Conditioner Medium 1
26 Dispense Coverslip
27 Heat the slides to 100 ° C, and incubate for 4 minutes
28 Dispense Coverslip
29 Dispense Cell Conditioner 1
30 Incubate for 4 minutes
31 Dispense Coverslip
32 Dispense EZ Prep and adjust the CC volume
33 Incubate for 4 minutes
34 Dispense Coverslip
35 Dispense Cell Conditioner Medium 1
36 Incubate for 4 minutes
37 Dispense Coverslip
38 Dispense Cell Conditioner 1
39 Incubate for 4 minutes
40 Turn off slide heating
41 Incubate for 8 minutes
42 Rinse the slide +
43 Adjust the volume on the slide
44 Dispense Coverslip
45 ***** Select Reaction Buffer *****
46 Heat slides to 37 ° C, and incubate for 2 minutes
47 Rinse the slide +
48 Adjust the volume on the slide

* One drop corresponds to one aliquot of reagent
```

49 Dispense an aliquot of UV INHIBITOR, add Coverslip and incubate for 4 minutes
50 Rinse the slide +
51 Adjust the volume on the slide
52 Dispense Coverslip
53 ***** Manually apply (Primary Antibody) and incubate for [32 minutes]*****
54 Rinse the slide +
55 Dispense 200 µl + VA of Wash Buffer
56 Dispense an aliquot of UV HRP UNIV MULT, add Coverslip and incubate for 8 minutes
57 Rinse the slide +
58 Adjust the volume on the slide
59 Dispense Coverslip
60 Rinse the slide +
61 Adjust the volume on the slide
62 Dispense Coverslip
63 Rinse the slide +
64 Adjust the volume on the slide
65 Add one aliquot of UV DAB and one aliquot of UV DAB H2O2, add Coverslip and incubate for 8 minutes
66 Rinse the slide +
67 Adjust the volume on the slide
68 Dispense an aliquot of UV COPPER, add Coverslip and incubate for 4 minutes
69 Rinse the slide +
70 Adjust the volume on the slide
71 Dispense Coverslip
72 ***** Start of timed stages *****
73 Rinse the slide +
74 Adjust the volume on the slide
75 Dispense an aliquot of [HEMATOXYLIN] (Counterstain), add Coverslip and incubate for [8 minutes]
76 Rinse the slide +

* One drop corresponds to one aliquot of reagent

Staining protocol 223cet (increased demasking)
Procedure: BMK ultraView DAB Par
BenchMark IHC/ISH Form

1 ***** Select EZ Prep *****
2 ***** Start timed stages *****
3 ***** Mixers disabled *****
4 Heat the slides to 75 ° C, and incubate for 4 minutes
5 Adjust the volume of EZ Prep (Discovery)
6 Incubate for 4 minutes
7 Rinse the slide +
8 Adjust the volume of EZ Prep (Discovery)
9 Incubate for 4 minutes
10 Rinse the slide +
11 Adjust the volume of EZ Prep (Discovery)
12 Dispense Coverslip
13 Heat slides to 76 ° C, and incubate for 4 minutes
14 Rinse the slide +
15 Adjust the dewaxing volume
16 Dispense Coverslip
17 Turn off slide heating
18 ***** Activated mixers *****
19 [Short - Cell Conditioning 8 minutes]
20 Rinse the slide +
21 Dispense Cell Conditioner Medium 1
22 Dispense Coverslip for long CC
23 Heat slides to 95 ° C, and incubate for 8 minutes
24 [Reduced - Cell Conditioning 30 minutes]
25 Dispense Cell Conditioner Medium 1
26 Dispense Coverslip
27 Heat the slides to 100 ° C, and incubate for 4 minutes
28 Dispense Coverslip
29 Dispense Cell Conditioner 1
30 Incubate for 4 minutes
31 Dispense Coverslip
32 Dispense EZ Prep and adjust the CC volume
33 Incubate for 4 minutes
34 Dispense Coverslip
35 Dispense Cell Conditioner Medium 1
36 Incubate for 4 minutes
37 Dispense Coverslip
38 Dispense Cell Conditioner 1
39 Incubate for 4 minutes
40 [Standard - Cell Conditioning 60 minutes]
41 Dispense Coverslip
42 Dispense Cell Conditioner Medium 1
43 Incubate for 4 minutes
44 Dispense Coverslip
45 Dispense Cell Conditioner 1
46 Incubate for 4 minutes
47 Dispense Coverslip
48 Dispense EZ Prep and adjust the CC volume
49 Incubate for 4 minutes
50 Dispense Coverslip
51 Dispense Cell Conditioner Medium 1
52 Incubate for 4 minutes

* One drop corresponds to one aliquot of reagent

53 Dispense Coverslip
54 Dispense Cell Conditioner 1
55 Incubate for 4 minutes
56 Turn off slide heating
57 Incubate for 8 minutes
58 Rinse the slide +
59 Adjust the volume on the slide
60 Dispense Coverslip
61 ***** Select Reaction Buffer *****
62 Heat slides to 37 ° C, and incubate for 2 minutes
63 Rinse the slide +
64 Adjust the volume on the slide
65 Dispense an aliquot of UV INHIBITOR, add Coverslip and incubate for 4 minutes
66 Rinse the slide +
67 Adjust the volume on the slide
68 Dispense Coverslip
69 ***** Manually apply (Primary Antibody) and incubate for [32 minutes]*****
70 Rinse the slide +
71 Dispense 200 µl + VA of Wash Buffer
72 Dispense an aliquot of UV HRP UNIV MULT, add Coverslip and incubate for 8 minutes
73 Rinse the slide +
74 Adjust the volume on the slide
75 Dispense Coverslip
76 Rinse the slide +
77 Adjust the volume on the slide
78 Dispense Coverslip
79 Rinse the slide +
80 Adjust the volume on the slide
81 Add one aliquot of UV DAB and one aliquot of UV DAB H2O2, add Coverslip and incubate for 8 minutes
82 Rinse the slide +
83 Adjust the volume on the slide
84 Dispense an aliquot of UV COPPER, add Coverslip and incubate for 4 minutes
85 Rinse the slide +
86 Adjust the volume on the slide
87 Dispense Coverslip
88 ***** Start of timed stages *****
89 Rinse the slide +
90 Adjust the volume on the slide
91 Dispense an aliquot of [HEMATOXYLIN] (Counterstain), add Coverslip and incubate for [8 minutes]
92 Rinse the slide +

* One drop corresponds to one aliquot of reagent

Annex II: IMAGES FROM ANTIBODY OPTIMIZATION

In this section, the images of the tissues used during the optimization of immunohistochemical protein markers are presented for each tested antibody.

Acronyms correspond to the ones used throughout the main manuscript and Publication II.

Protocol numbers refer to the lab-internal Ventana Benchmark® semi-automatic immunostainer in the veterinary pathology laboratory of the Department of Comparative Biomedicine and Food Science.

Biomarkers of Auditory Pathology

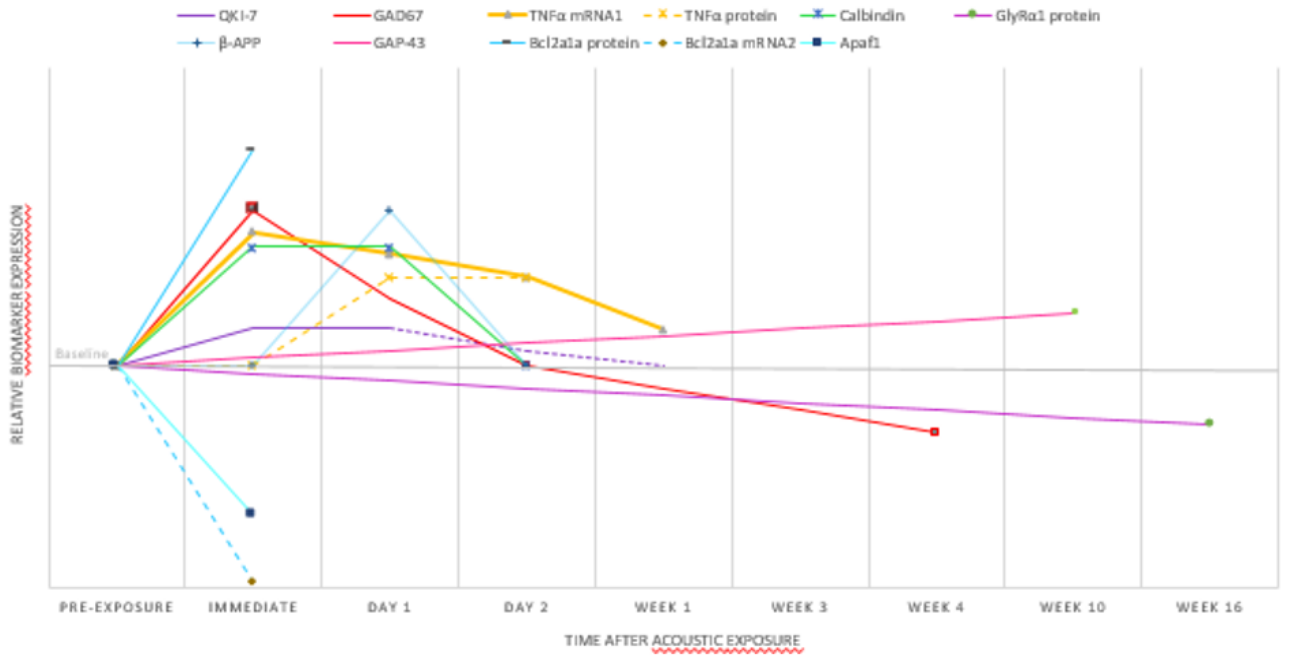

GAP-43

- Established marker for synaptic sprouting and axonal outgrowth; hints toward plasticity
- Expressed physiogically in **Ventral Cochlear Nucleus** (VCN)
- Upregulation within VCN associated with VCN-shrinkage and expression in **Auditory Nerve** (AN) @10 weeks p.e.
- Stronger upregulation within VCN in noise-exposed animals w/o tinnitus

→ **Protective** mechanism

IHC

β-APP

- **β-Amyloid Precursor Protein**, recorded as a marker for **acute axonal** damage in oligodendrocytes and astrocytes of CNS
- Corresponds to DNA-Fragmentation @1 day post-exposure to mild **traumatic blast injury**
- Potential factor in mediating neuroinflammatory response through induction of TNF-α

Microarray, IHC

QKI-7

- Isoform of **Quaking** (RNA-splicing regulator)
- Found upregulated in incomplete recreation of postnatal **myelination** after structural disorganization post-exposure (p.e)
- 77% of glial cells with morphological abnormalities on day one post-exp. (29% in controls); 82% on day 14 p.e.

Microarray, RT-PCR, IHC, TEM

GAD67

- **Glutamate decarboxylase** (67kDa)
- Upregulated in **Inferior Colliculus** (IC) @24h p.e.
- Return to baseline values @48h p.e.
- Drop below baseline values @1 month p.e.
- Represents p.e. changes in inhibitory auditory circuits, may reflect development of central hyperactivity (→ **Tinnitus**)

IHC, Western Blotting

TNFα mRNA1 / TNFα protein

- **Tumor necrosis factor α**, appears to increase in auditory neuroinflammation p.e.
- mRNA upregulation in ipsilateral **Auditory Cortex** (AC) peaks @12h p.e.
- Protein expression reflected @24h p.e. (persists in contralateral AC, while returning to baseline within 10 days in ipsilateral AC

RT-PCR

Calbindin

- Increases in the **medial nucleus of trapezoid body** and their axons in the **lateral superior olive** @24h after functional **deafferentation**
- Baseline levels reached again @5 days p.e.
- Possible decreases in cochlea associated with **conditioning** phenomenon (along with decrease of heat shock proteins)

IHC

GlyRα1 protein

- Decreased in middle- and high-frequency regions of **Dorsal Cochlear Nucleus** (DCN) fusiform cells in rats with **tinnitus** @4 months p.e.
- Represents inhibitory circuit
- Potential marker for plasticity (doublecortin previously found in DCN unipolar brush cells, neighboring fusiform cells)

IHC, *in-situ* hybridization

Bcl2a1a protein / Bcl2a1a mRNA2

- mRNA was upregulated immediately (15min) after trauma in **Cochlear Nucleus (CN), IC and AC**, while Bcl2a1a protein expression was reduced in CN and IC
- Inverse response pattern on genomic and proteomic levels may reflect **cytoprotective, compensatory** mechanism

RT2-qPCR, Western Blot

Apaf1

- Noise exposure decreased expression of **pro-apoptotic protease factor 1** along central auditory pathway (CN, IC, AC) @15 min p.e.
- Trend towards inverse gene-protein pattern
- Along with Bcl2a1a, marker for activation of intinsic apoptosis via mitochondrial dysfunction p.e.

RT2-qPCR, Western Blot

Bottlenose dolphins used in pilot immunohistochemistry runs

Animal	ID 114	ID 319	ID 133
Age/Sex	9 d.o./M	Adult/M	Adult/F
History	DCC: 1 Parco Oltremare s.r.l. 19.06.2007 Meconium aspiration	DCC: 2 Sacca di Goro (FE) 06.05.2014 Septicaemic/endotoxic shock associated with hemolitic *E.coli*	DCC: 1 Parco Oltremare s.r.l. 19.01.2008 Cardiocirculatory schock, necrotizing enteritis, associated with *Enterococcus sp*. and diffuse arterial hypotension
Shape of cortical section as reference to following images			

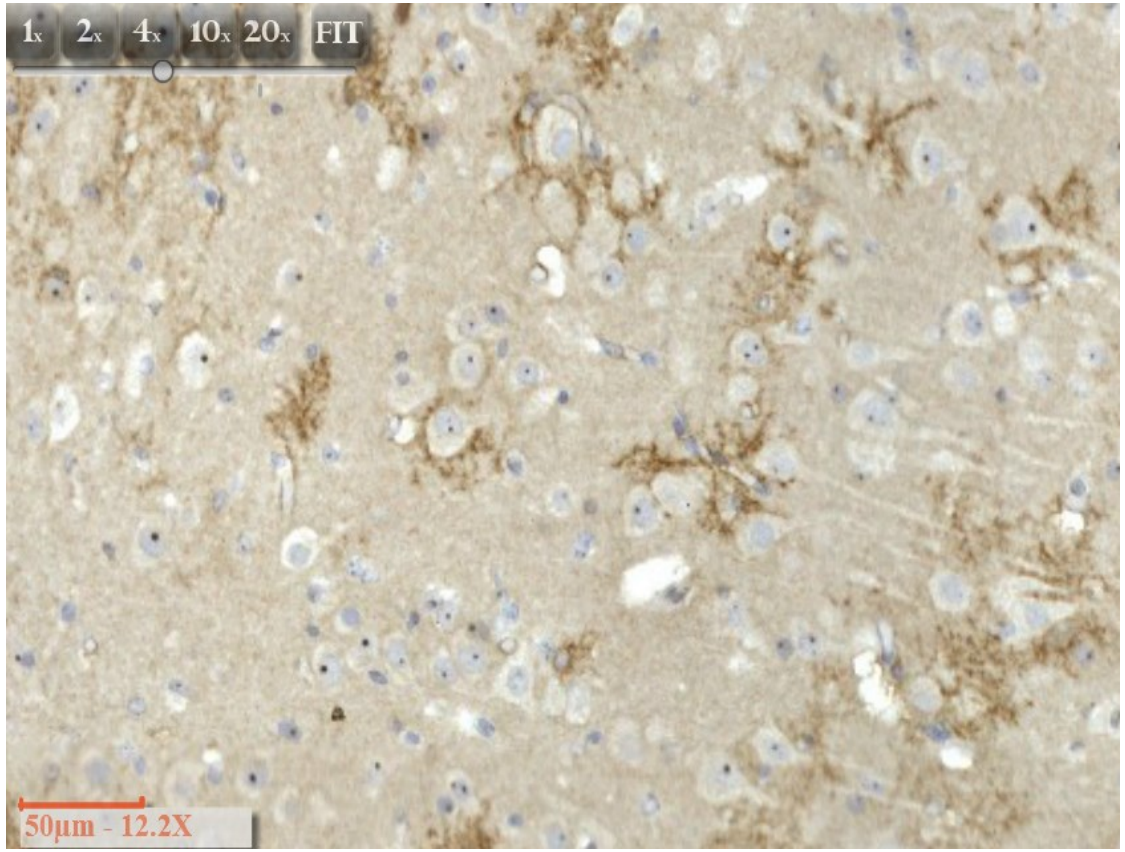

APP: 1:50 dil;
223cet

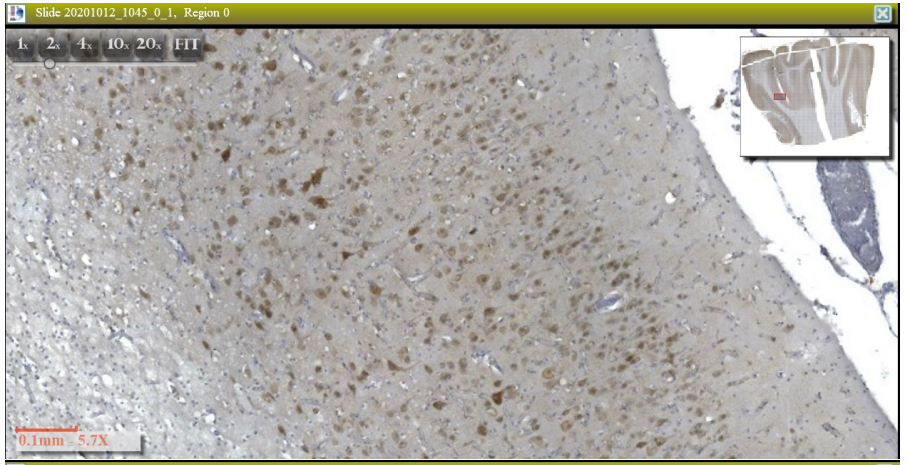

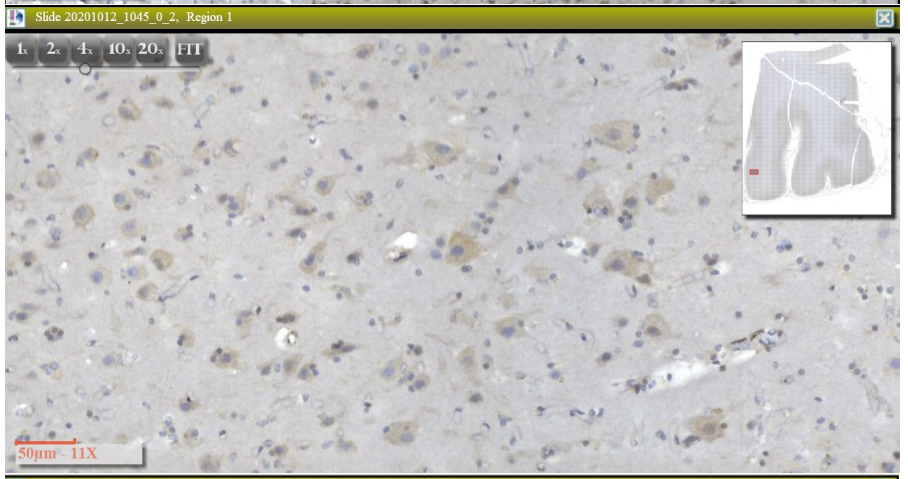

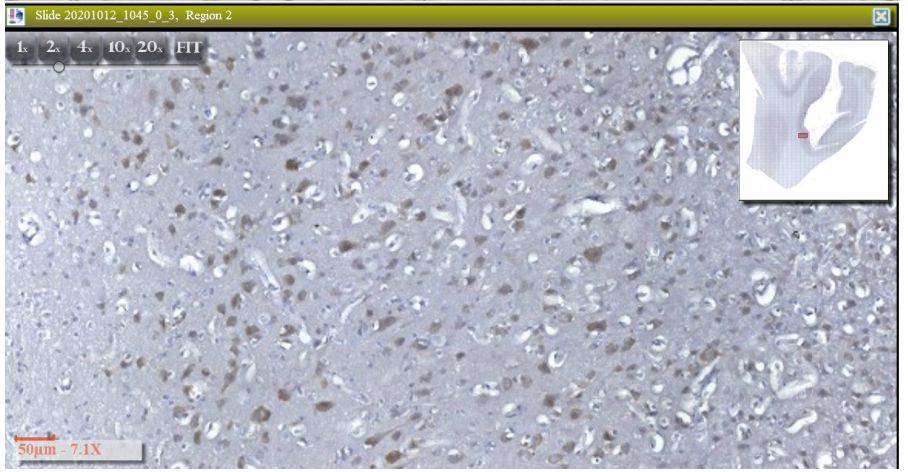

Ischemia and acute oxidative damage

- APP
  - APP
- ROS
  - iNOS
  - Malondialdehyde
  - (ROS)

APP

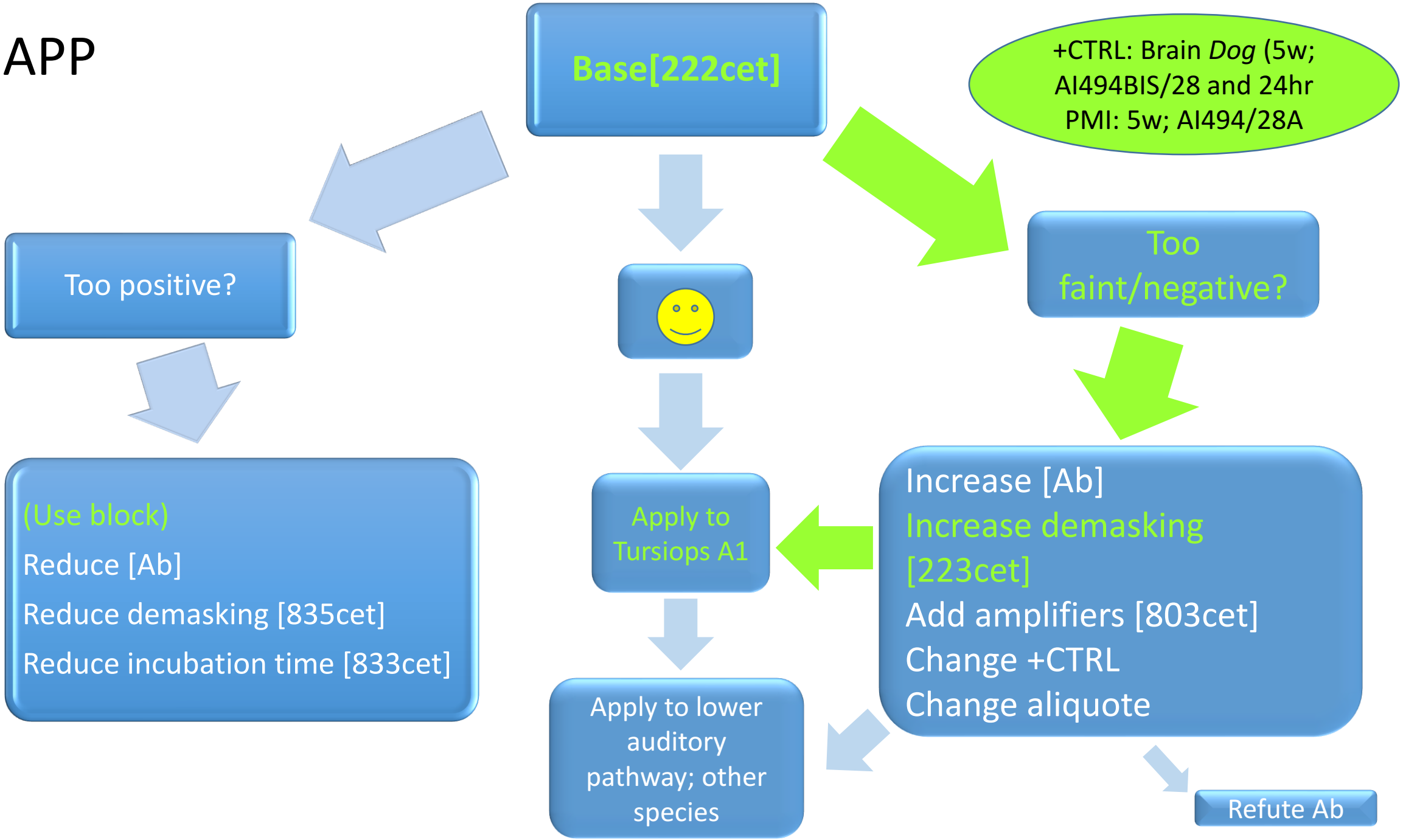
Base[222cet]
+CTRL: Brain *Dog* (5w; AI494BIS/28 and 24hr PMI: 5w; AI494/28A
Too positive?
Too faint/negative?
(Use block)
Reduce [Ab]
Reduce demasking [835cet]
Reduce incubation time [833cet]
Apply to Tursiops A1
Increase [Ab]
Increase demasking [223cet]
Add amplifiers [803cet]
Change +CTRL
Change aliquote
Apply to lower auditory pathway; other species
Refute Ab

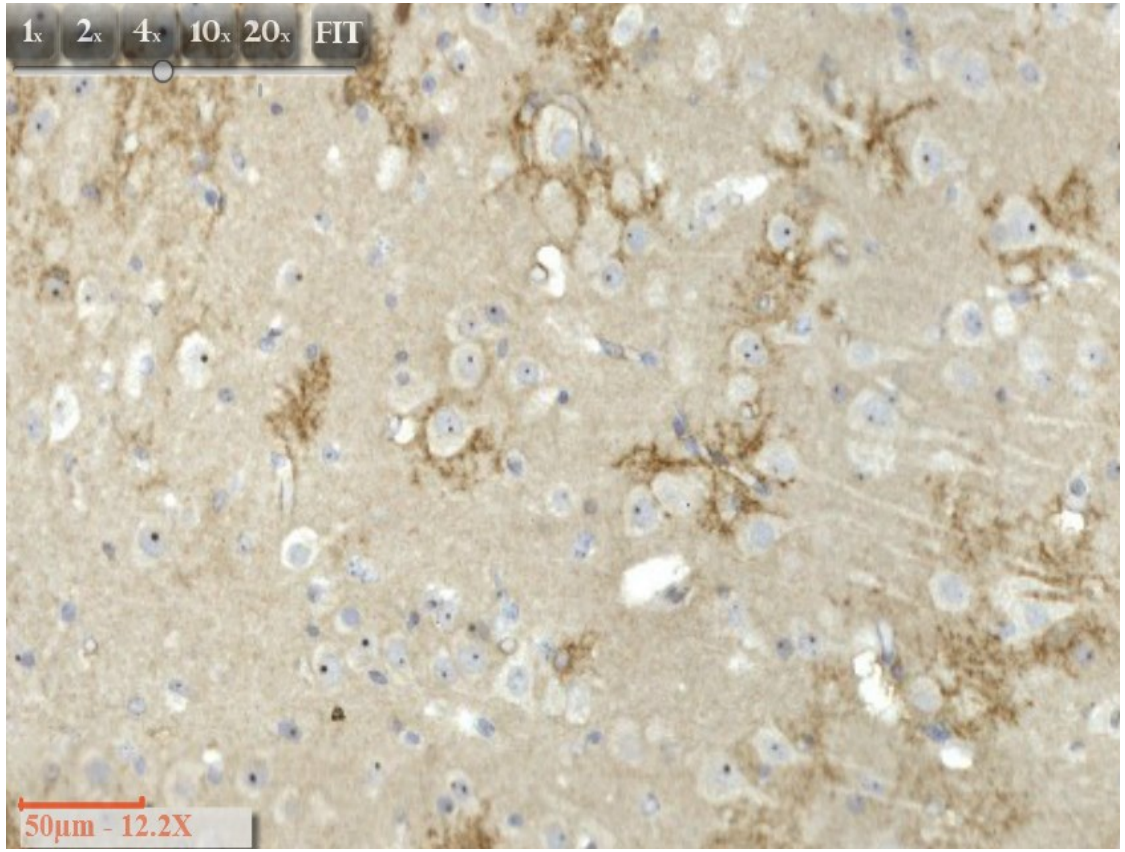

APP: 1:50 dil;
223cet

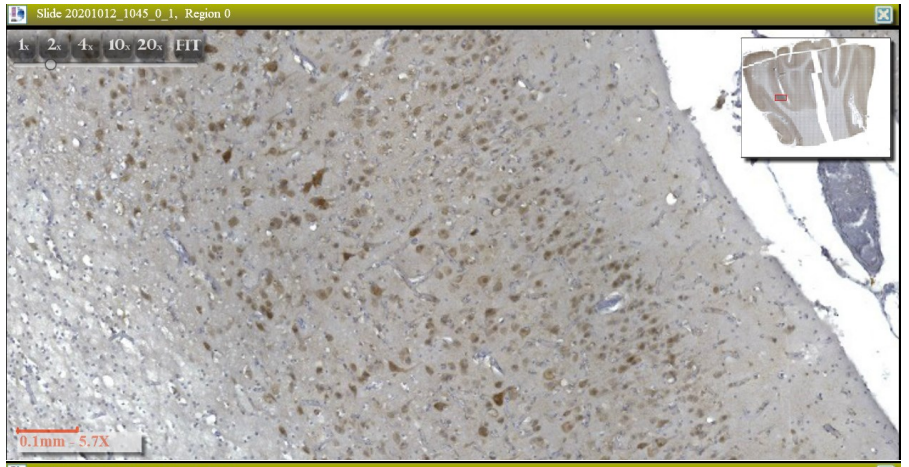

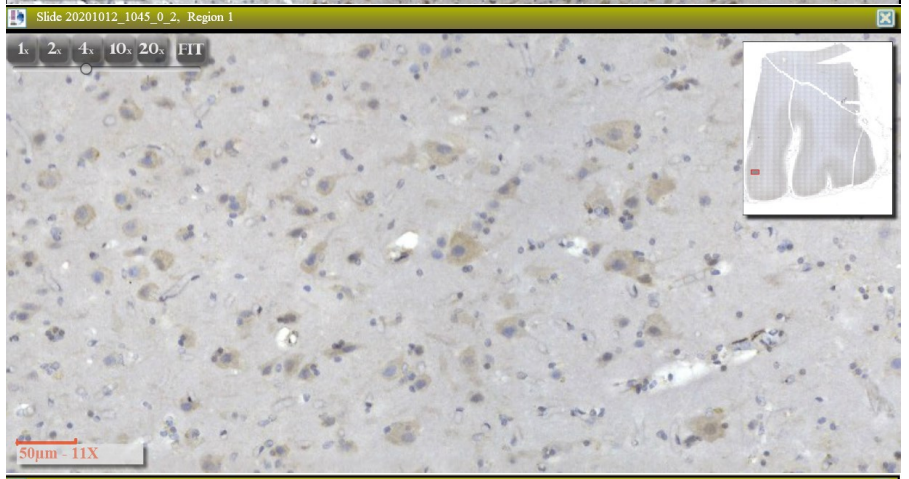

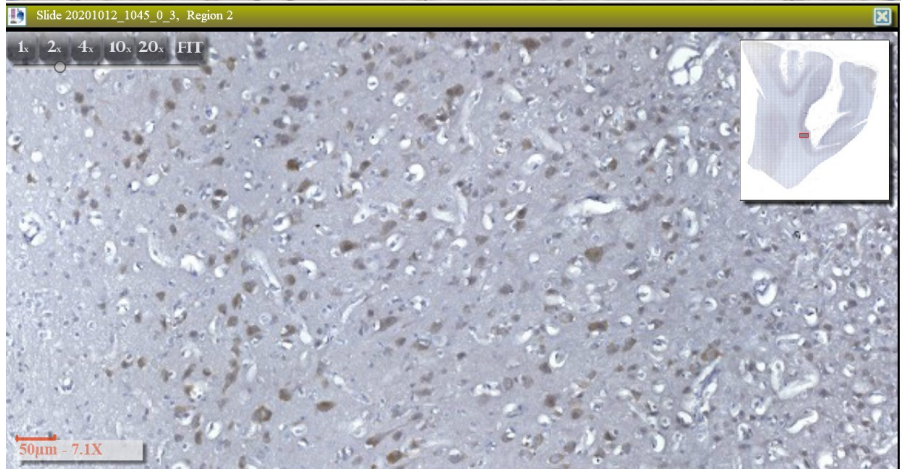

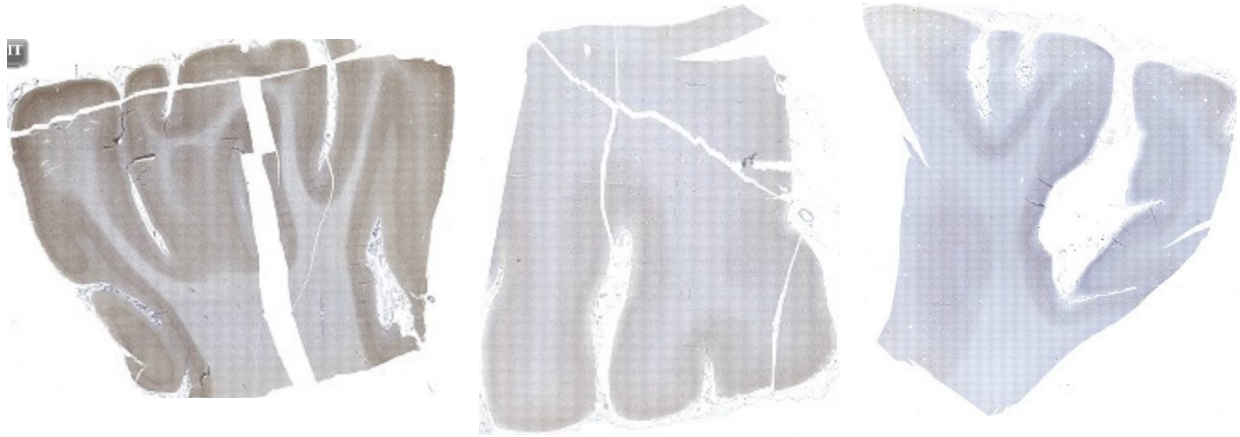

βAPP (clone: H31L21)

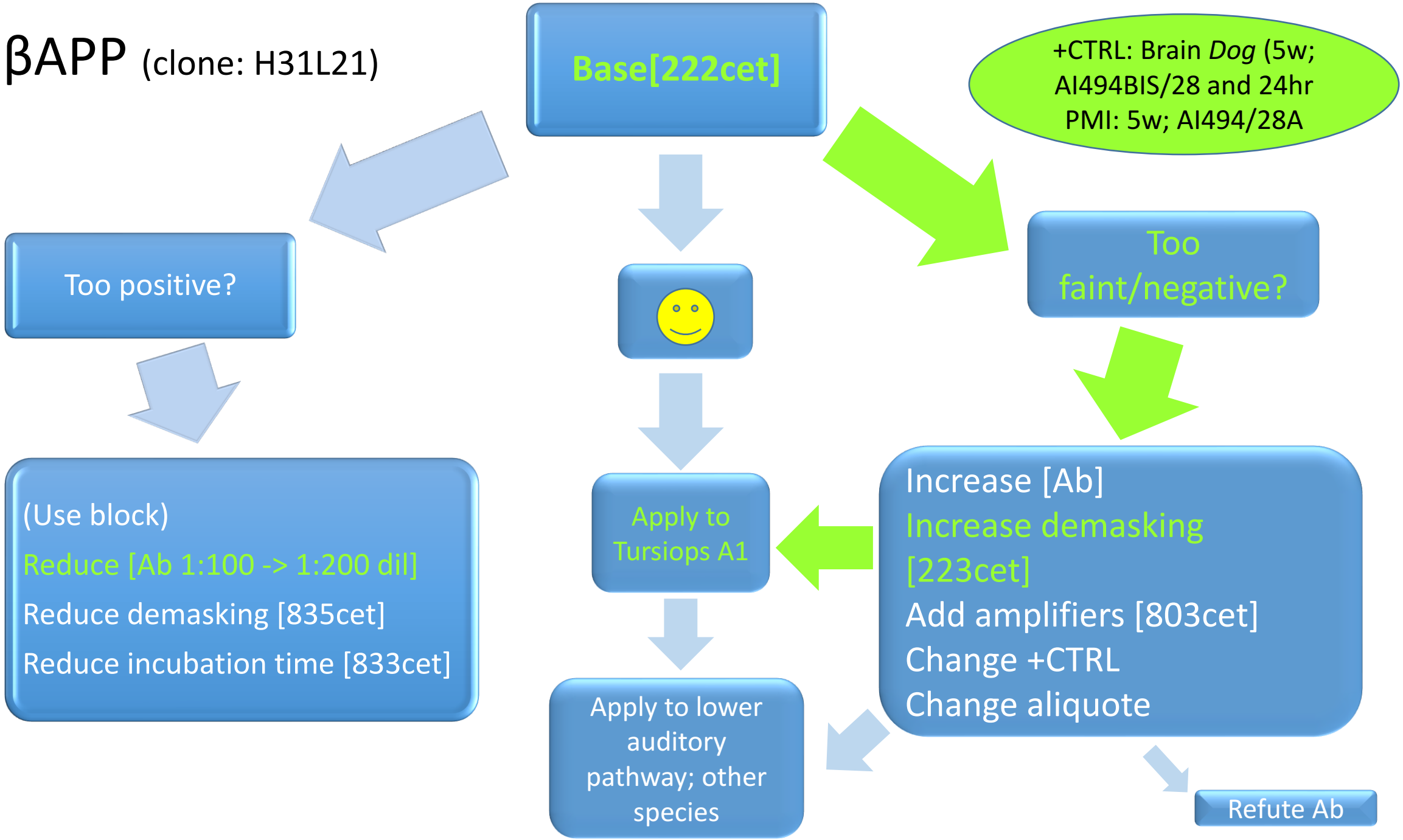

β-APP: 1:200 dil;
223cet

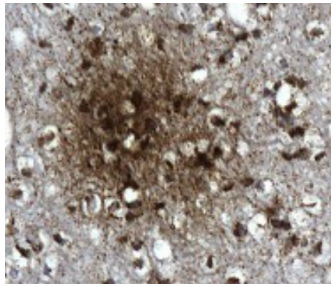

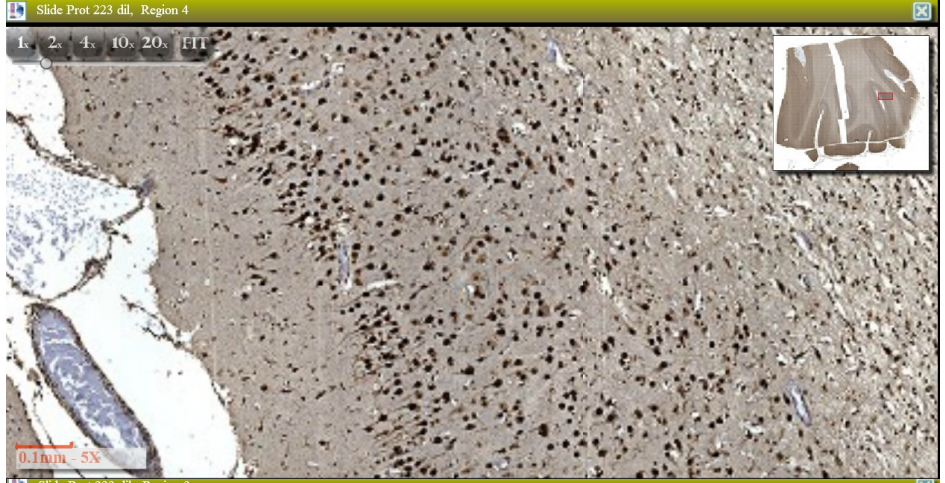

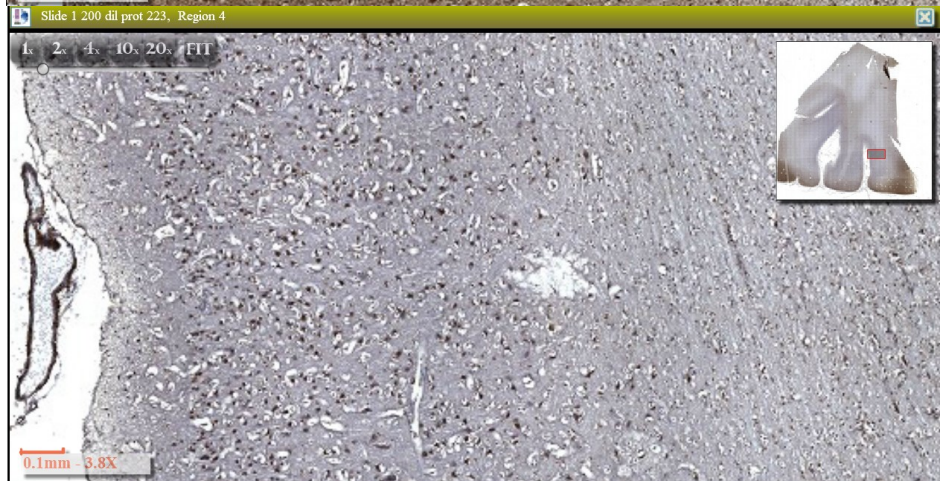

iNOS

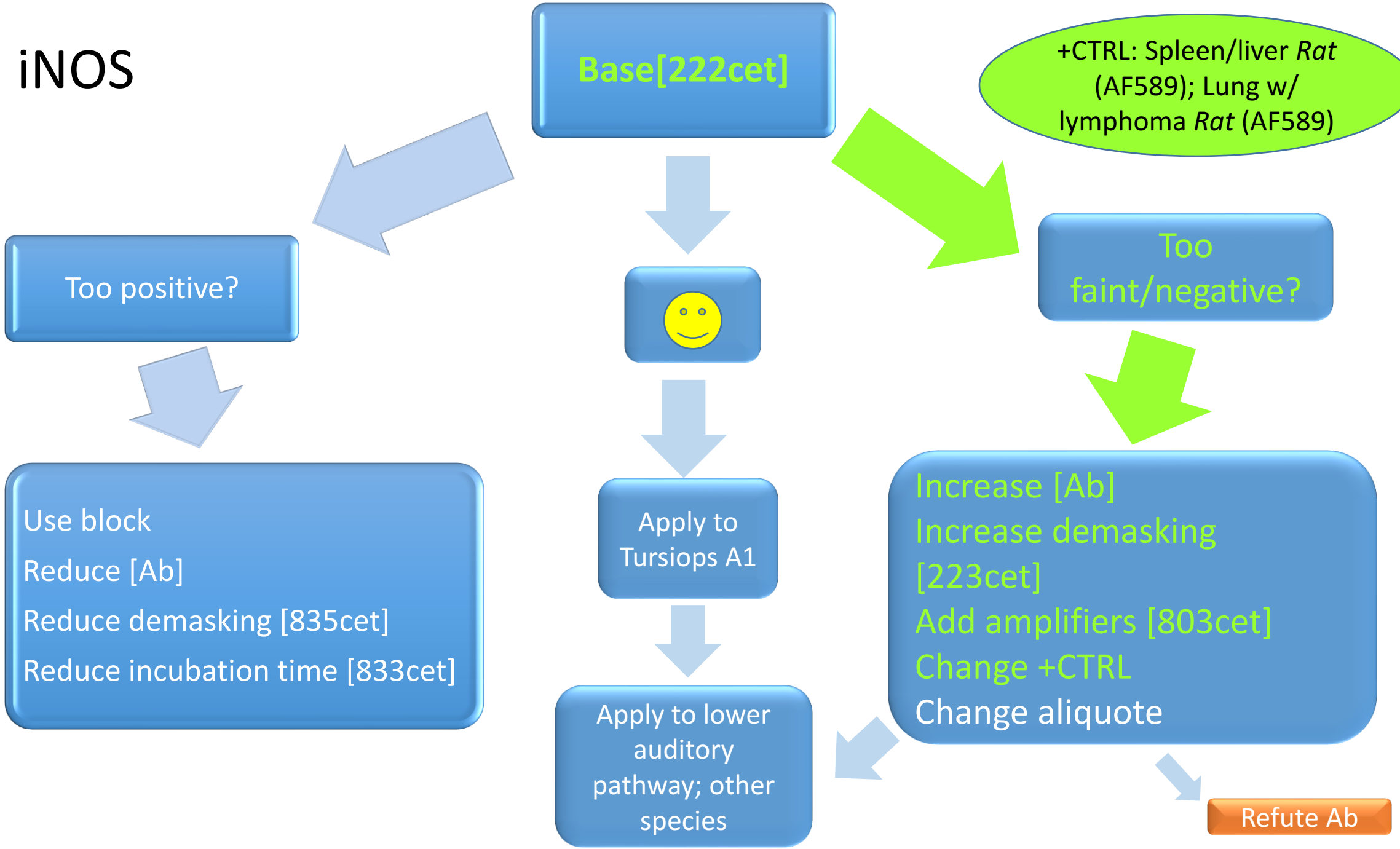
Base[222cet]
+CTRL: Spleen/liver *Rat* (AF589); Lung w/ lymphoma *Rat* (AF589)
Too positive?
Too faint/negative?
Use block
Reduce [Ab]
Reduce demasking [835cet]
Reduce incubation time [833cet]
Apply to Tursiops A1
Increase [Ab]
Increase demasking [223cet]
Add amplifiers [803cet]
Change +CTRL
Change aliquote
Apply to lower auditory pathway; other species
Refute Ab

iNOS Prot 222 cet;
1:100 dil

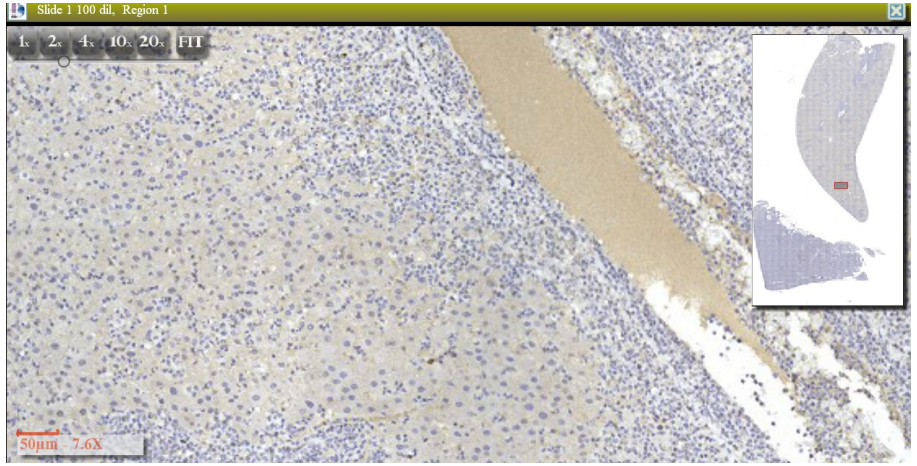

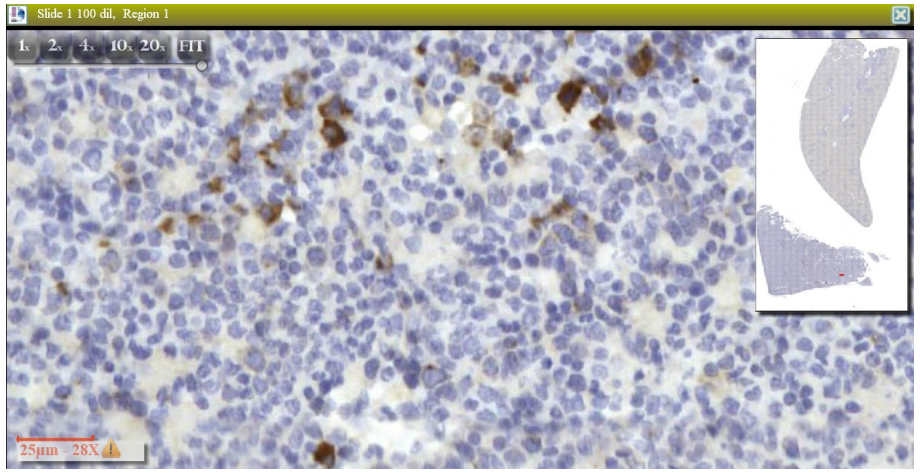

iNOS Prot 223 cet;
1:100 dil

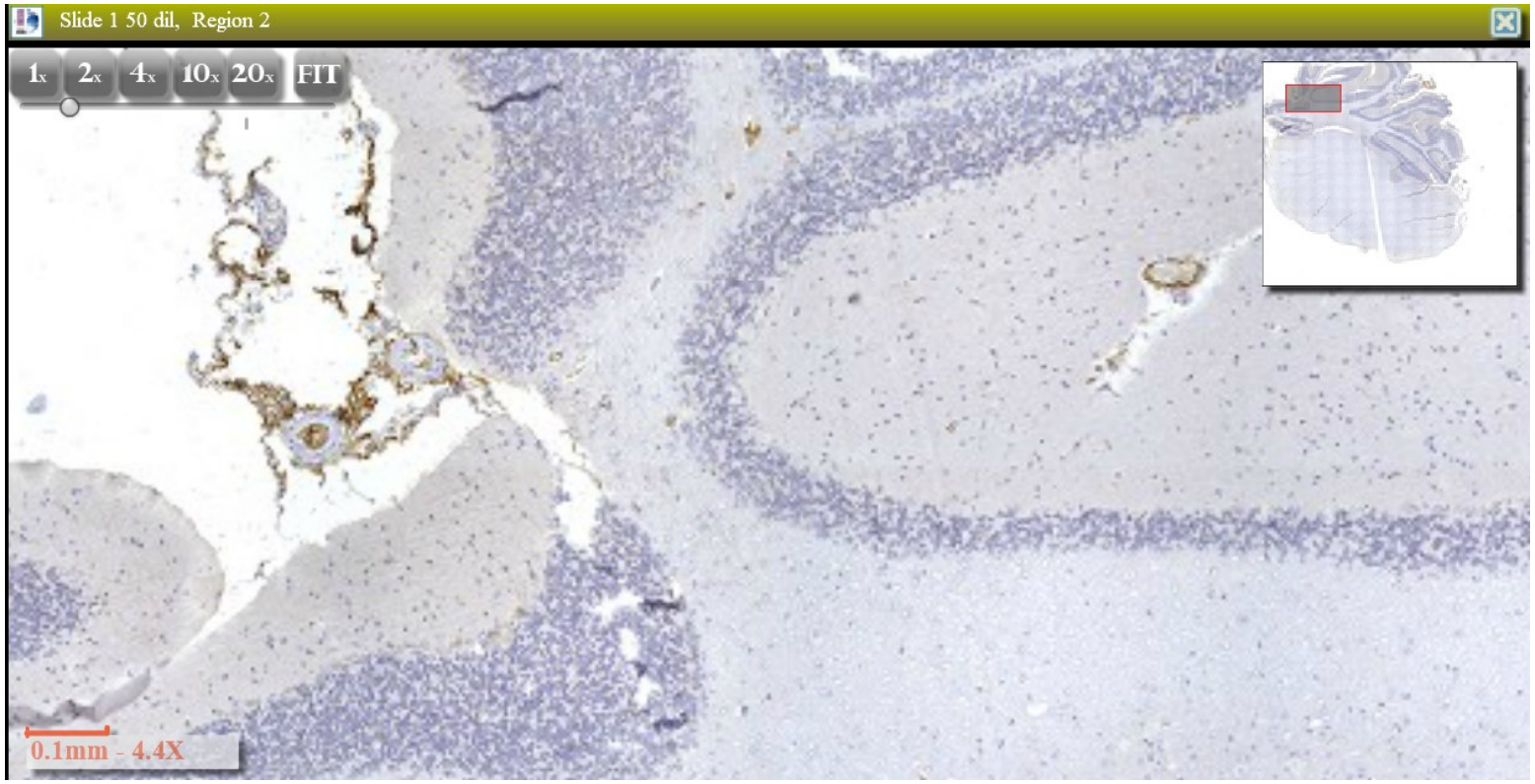

Malondialdehyde

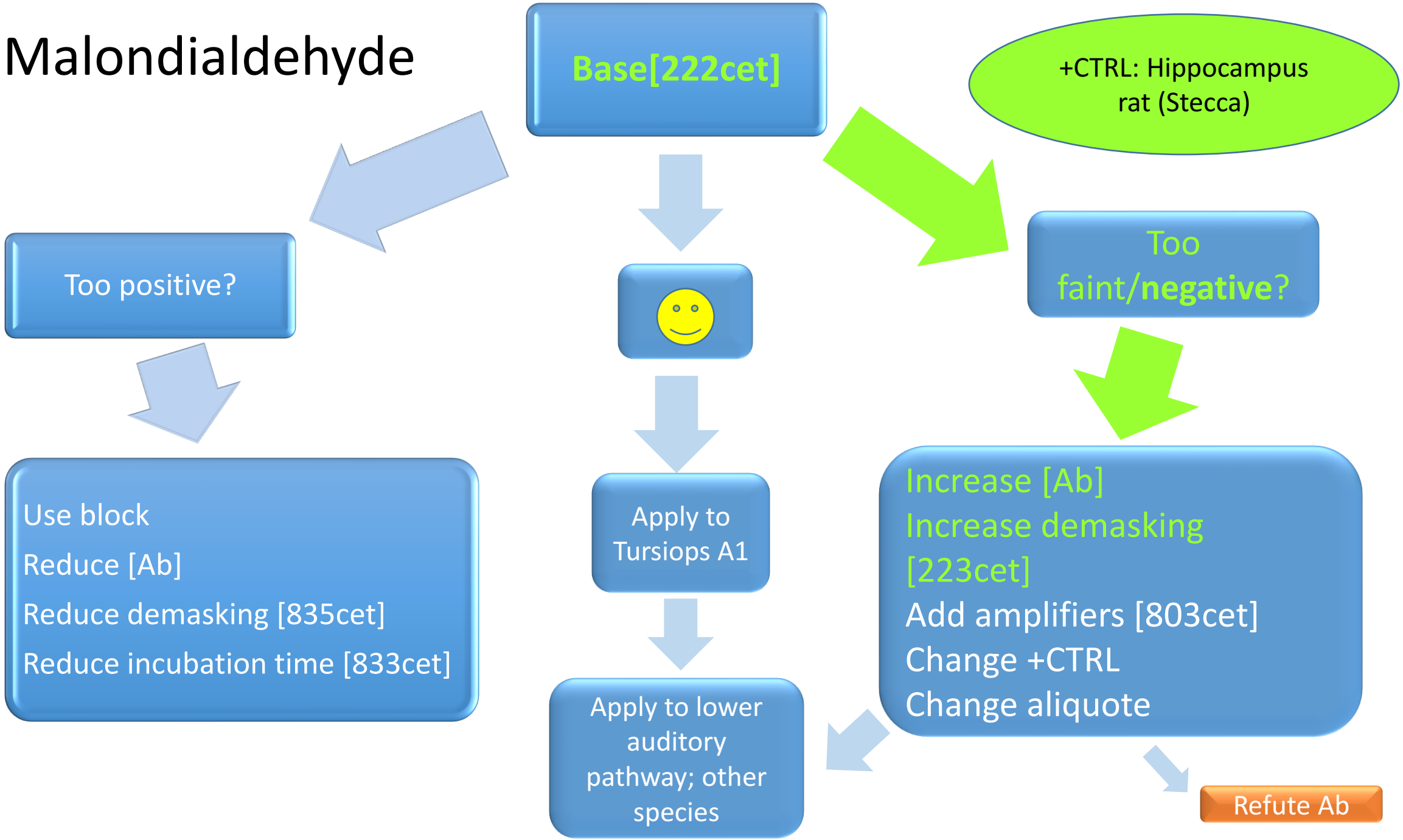

Malondialdehyde
Prot 222 cet; 1:500 dil

Malondialdehyde
Prot **223** cet; 1:500 dil

Malondialdehyde
Prot 222 cet; **1:100** dil

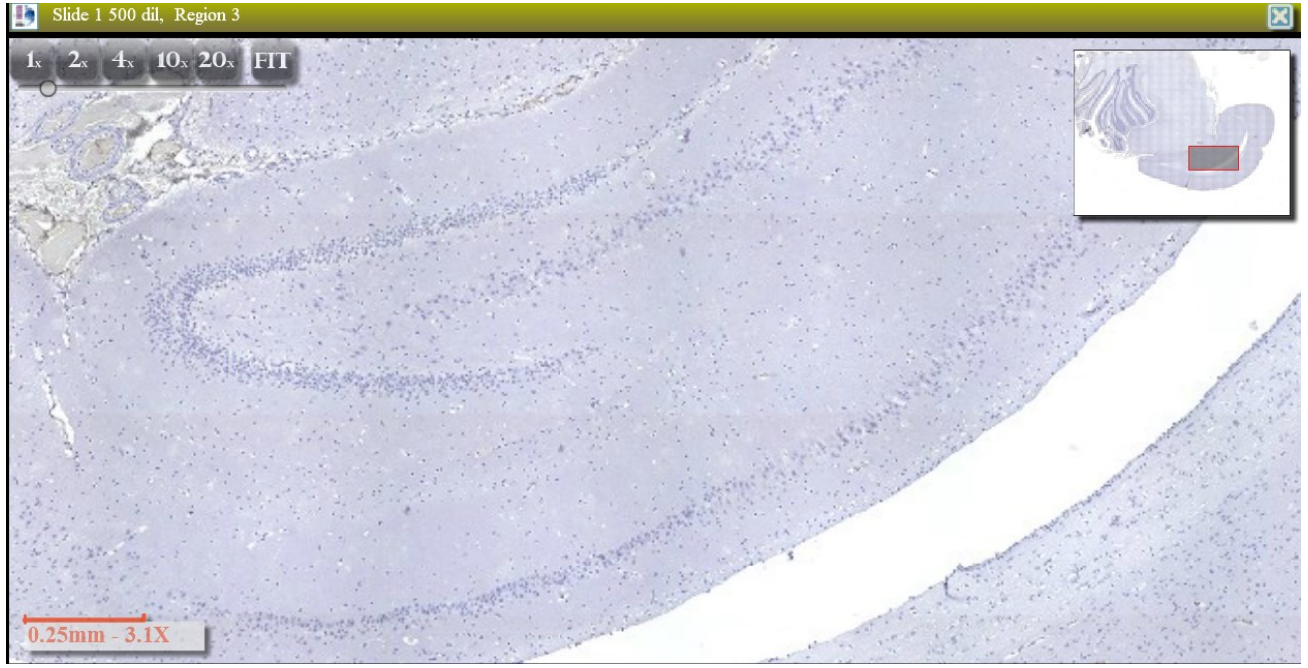

Apoptosis

- p53
- Bcl2
- Apaf1
- DGK-ζ

p53

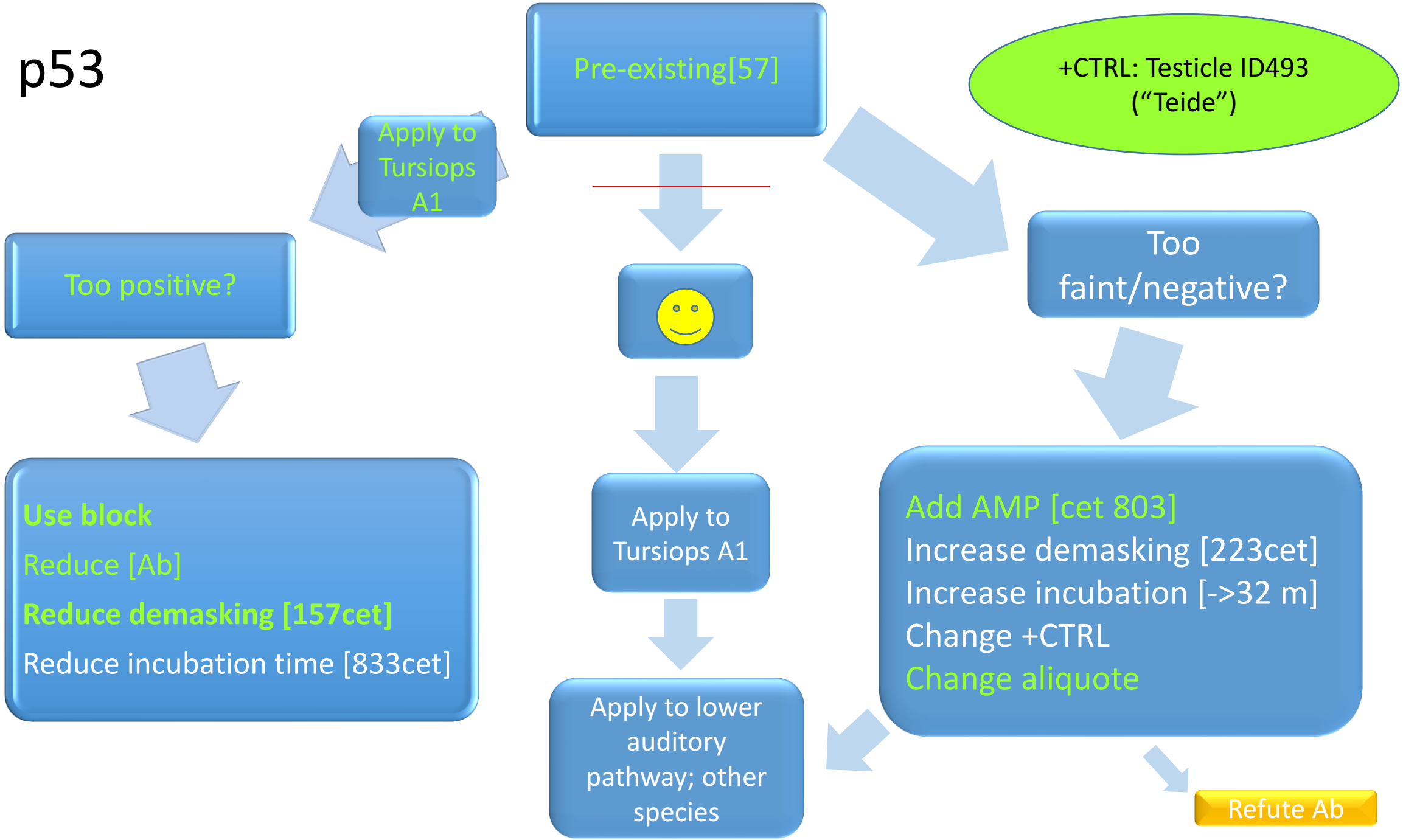
Pre-existing[57]
+CTRL: Testicle ID493 ("Teide")
Apply to Tursiops A1
Too positive?
Too faint/negative?
Use block
Reduce [Ab]
Reduce demasking [157cet]
Reduce incubation time [833cet]
Apply to Tursiops A1
Add AMP [cet 803]
Increase demasking [223cet]
Increase incubation [->32 m]
Change +CTRL
Change aliquote
Apply to lower auditory pathway; other species
Refute Ab

p53, 1:200 dil; 57

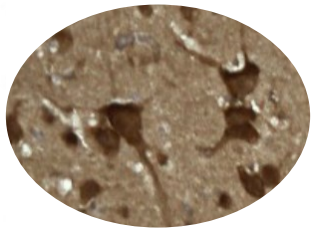

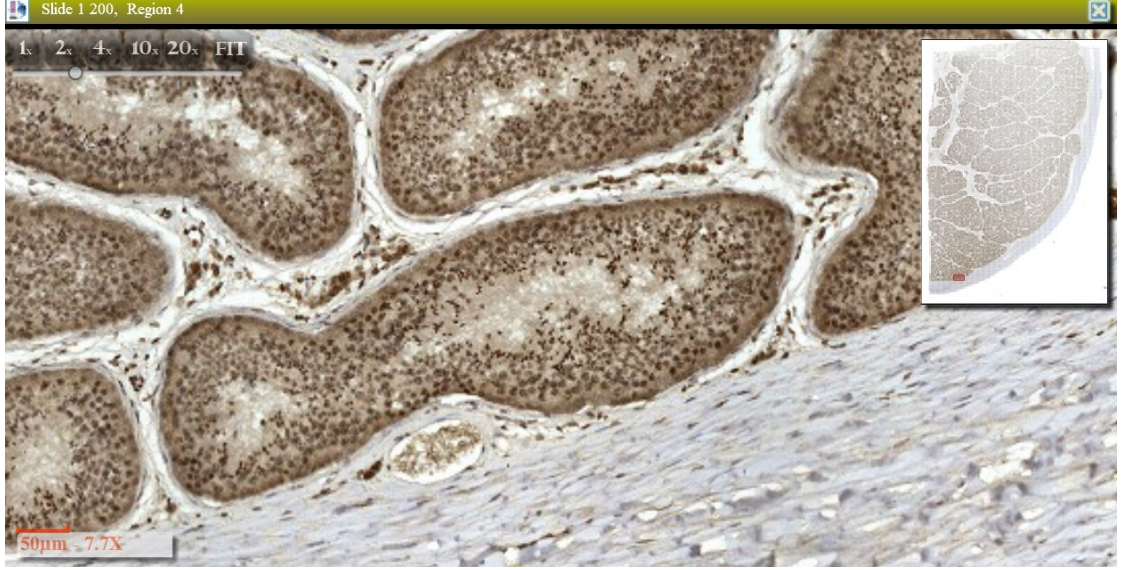

p53, 1:200 block;
57

p53, 1:400 block;
57

p53, 1:200 block; 157 (reduced demasking)

p53, 1:200 block; 3257 (+amplifier) -> **X**

p53, 1:200 block; 357 (reduced demasking +longer incubation->32 min)

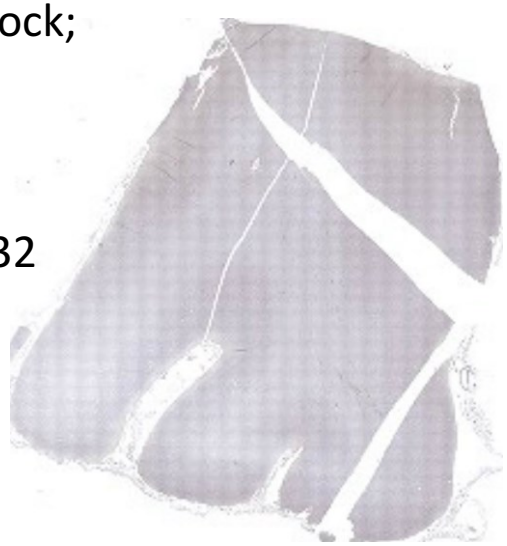

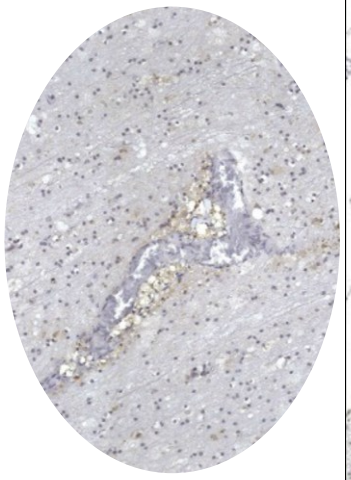

Bcl2

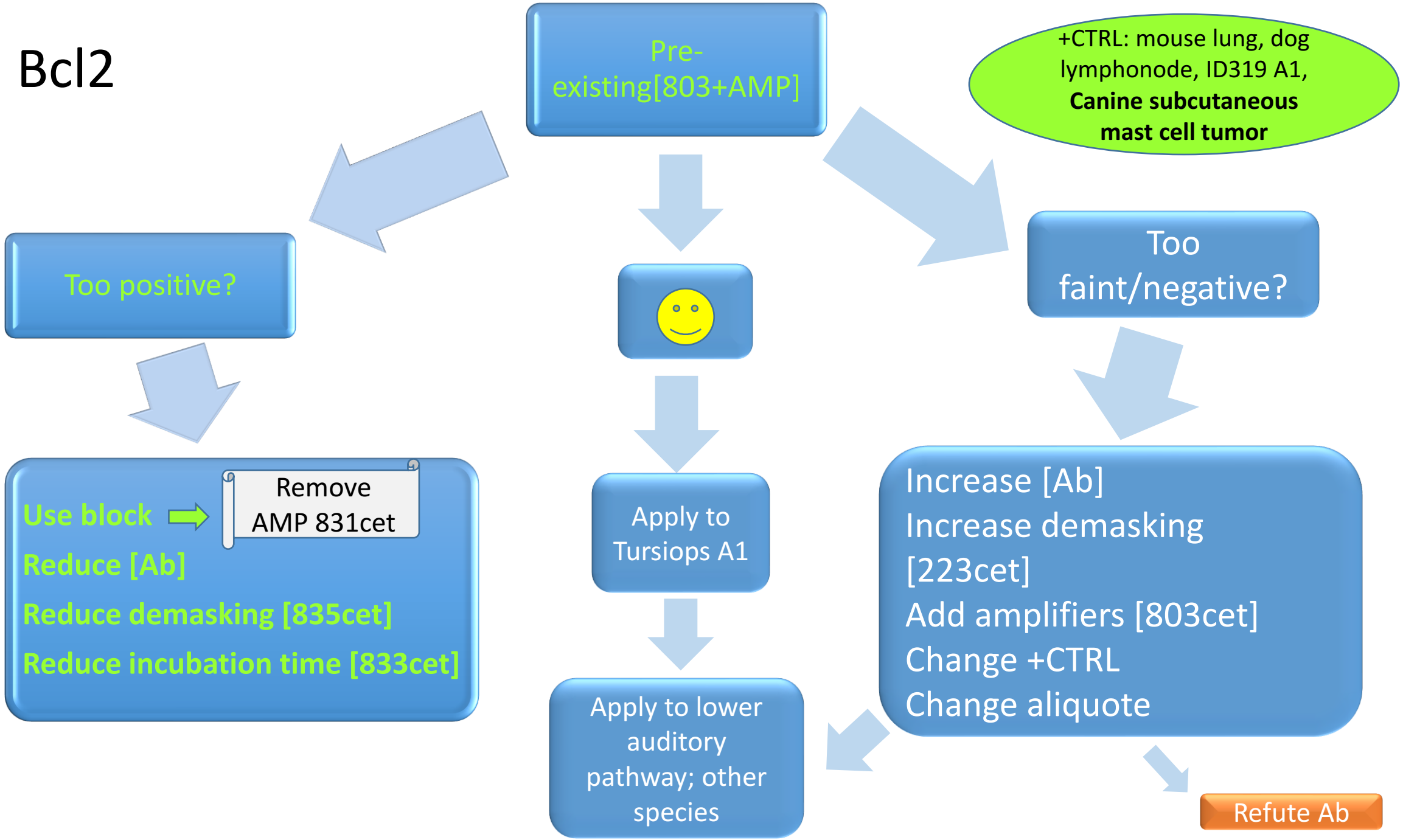
Pre-existing[803+AMP]
+CTRL: mouse lung, dog lymphonode, ID319 A1, **Canine subcutaneous mast cell tumor**
Too positive?
Too faint/negative?
Use block
Remove AMP 831cet
Reduce [Ab]
Reduce demasking [835cet]
Reduce incubation time [833cet]
Apply to Tursiops A1
Increase [Ab]
Increase demasking [223cet]
Add amplifiers [803cet]
Change +CTRL
Change aliquote
Apply to lower auditory pathway; other species
Refute Ab

Bcl2, 1:150 block; 831cet

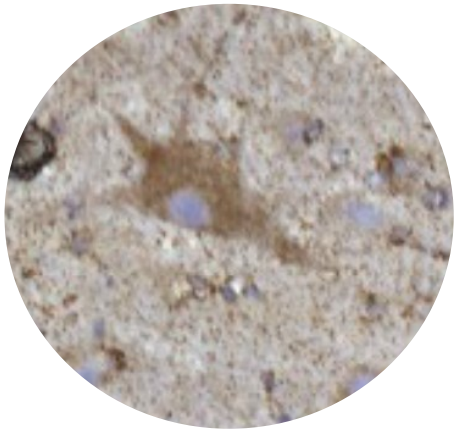

Bcl2, 1:300 block; 831cet

Bcl2, 1:150 block; 833cet

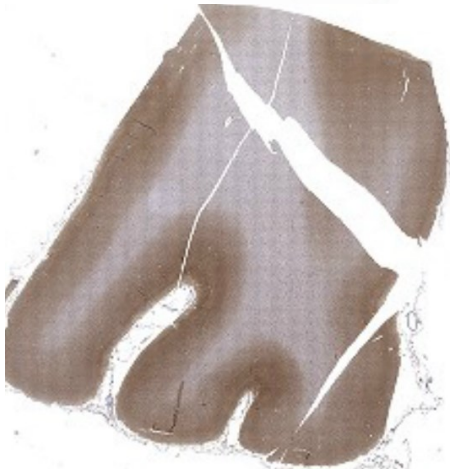

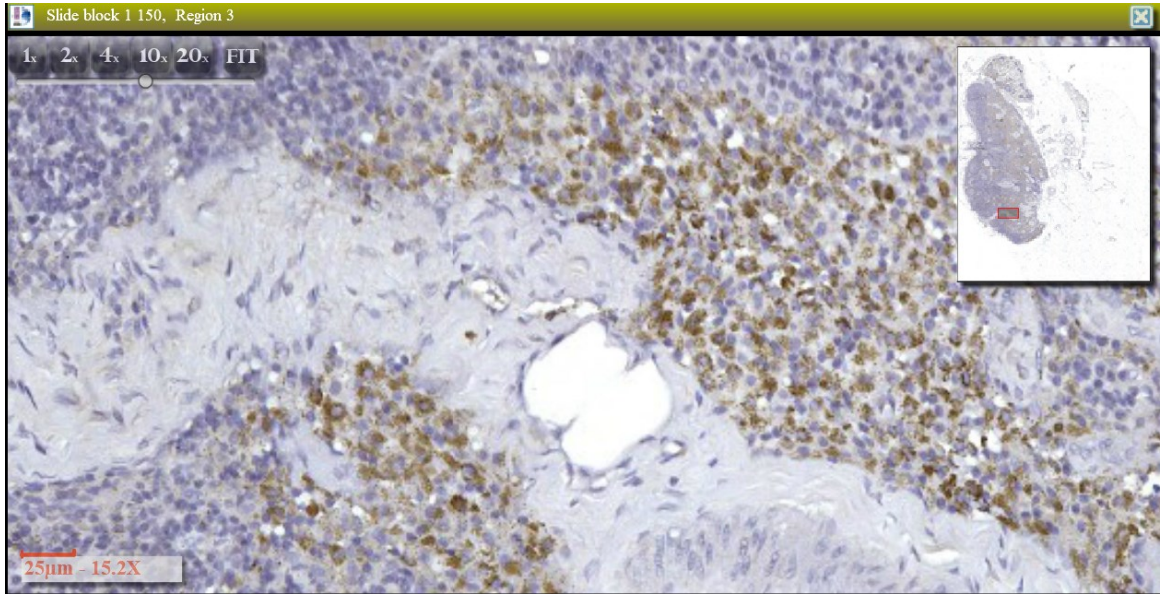

Bcl2, 1:150 block;
835cet. +CTRL
canine
lymphonode

Bcl2, 1:150 block;
835cet

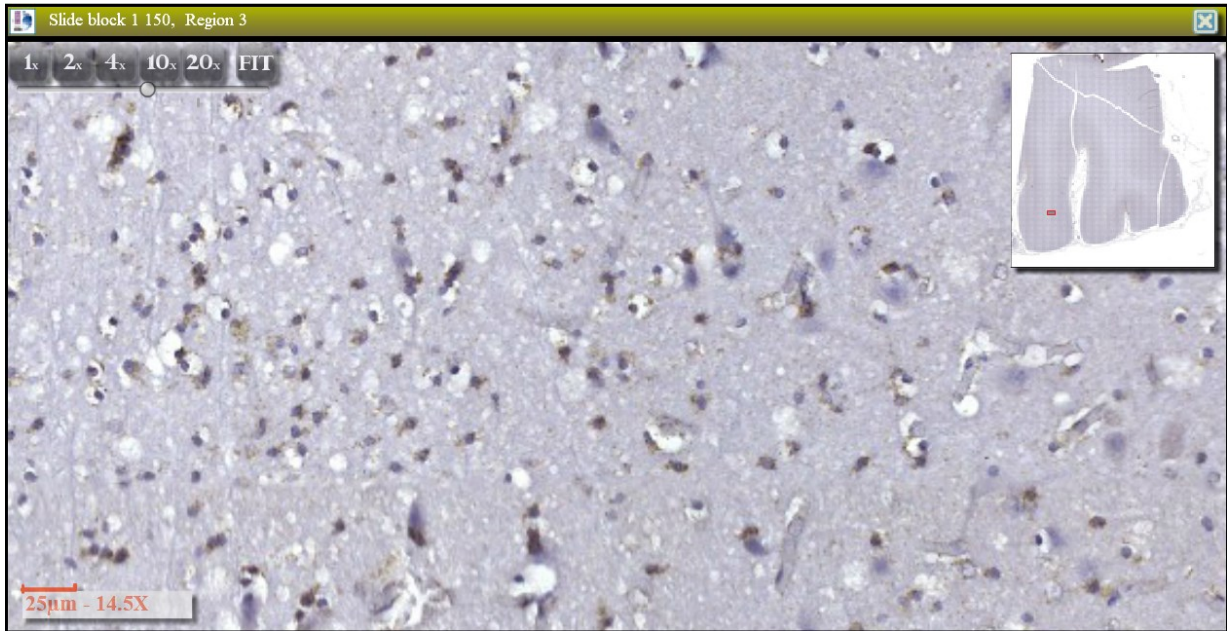

Apaf-1

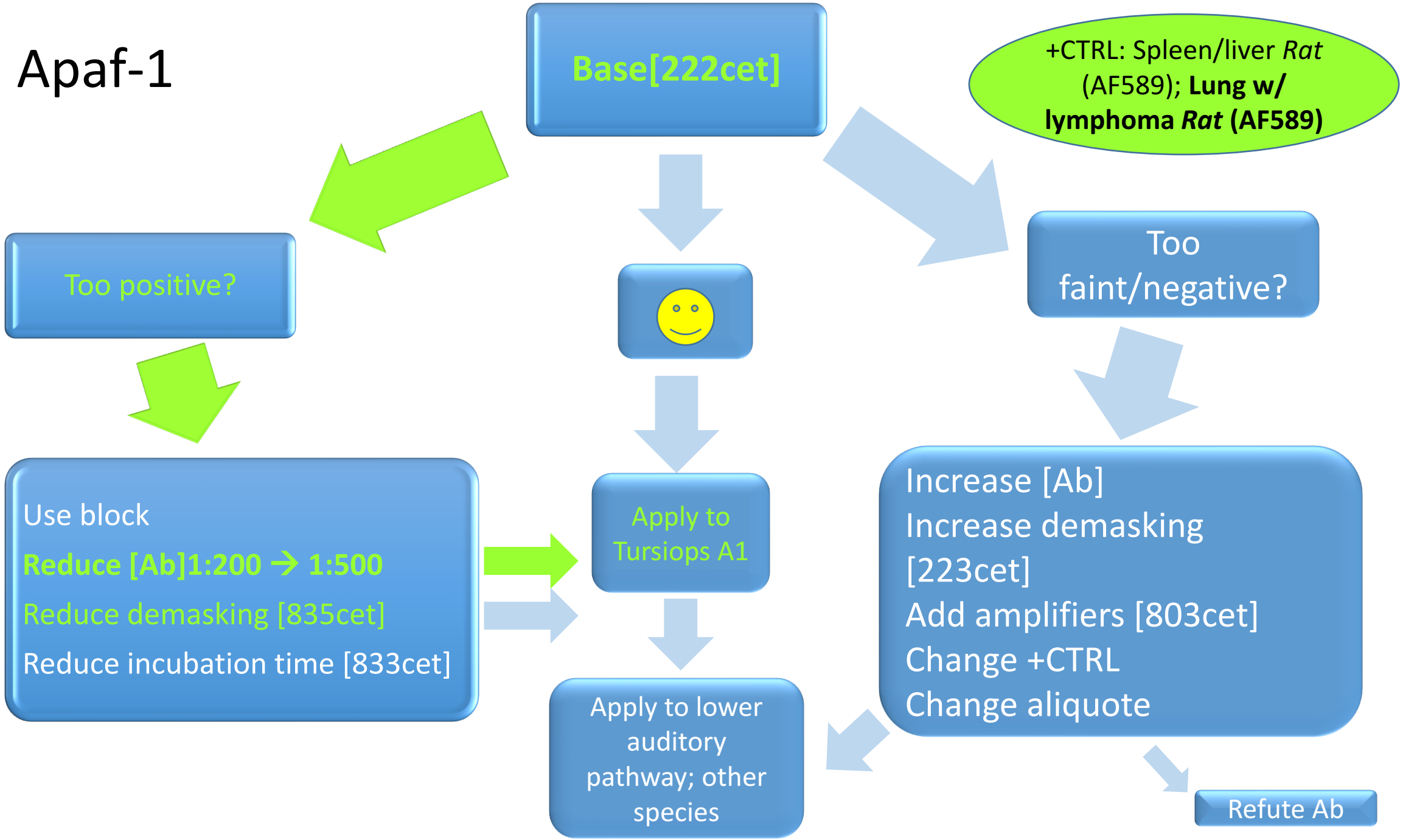
Base[222cet]
+CTRL: Spleen/liver *Rat* (AF589); **Lung w/ lymphoma *Rat* (AF589)**
Too positive?
Too faint/negative?
Use block
Reduce [Ab]1:200 → 1:500
Reduce demasking [835cet]
Reduce incubation time [833cet]
Apply to Tursiops A1
Increase [Ab]
Increase demasking [223cet]
Add amplifiers [803cet]
Change +CTRL
Change aliquote
Apply to lower auditory pathway; other species
Refute Ab

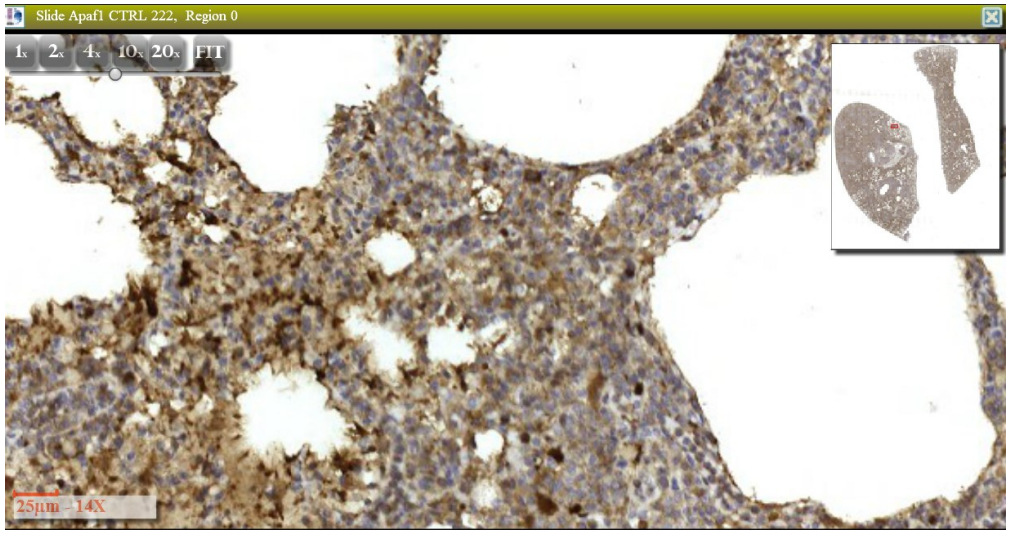

Apaf-1: 1:500 dil; 222cet

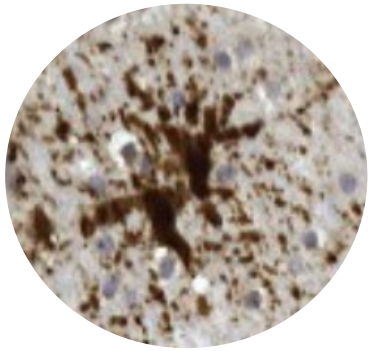

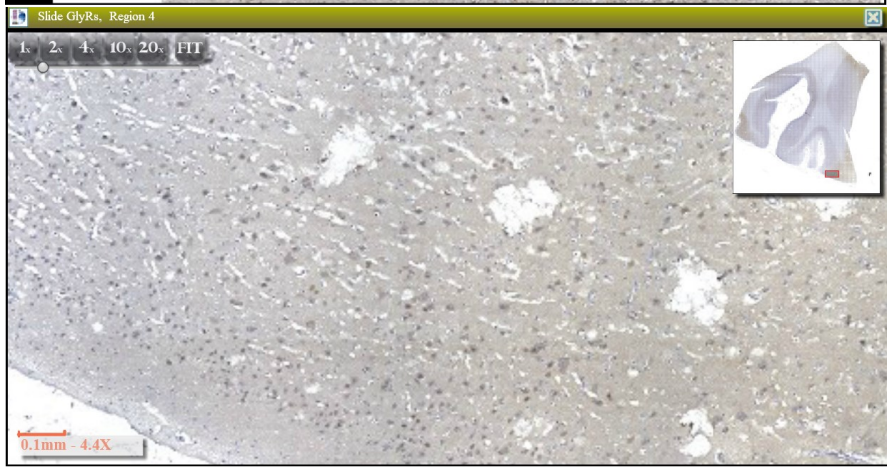

DGK-ζ

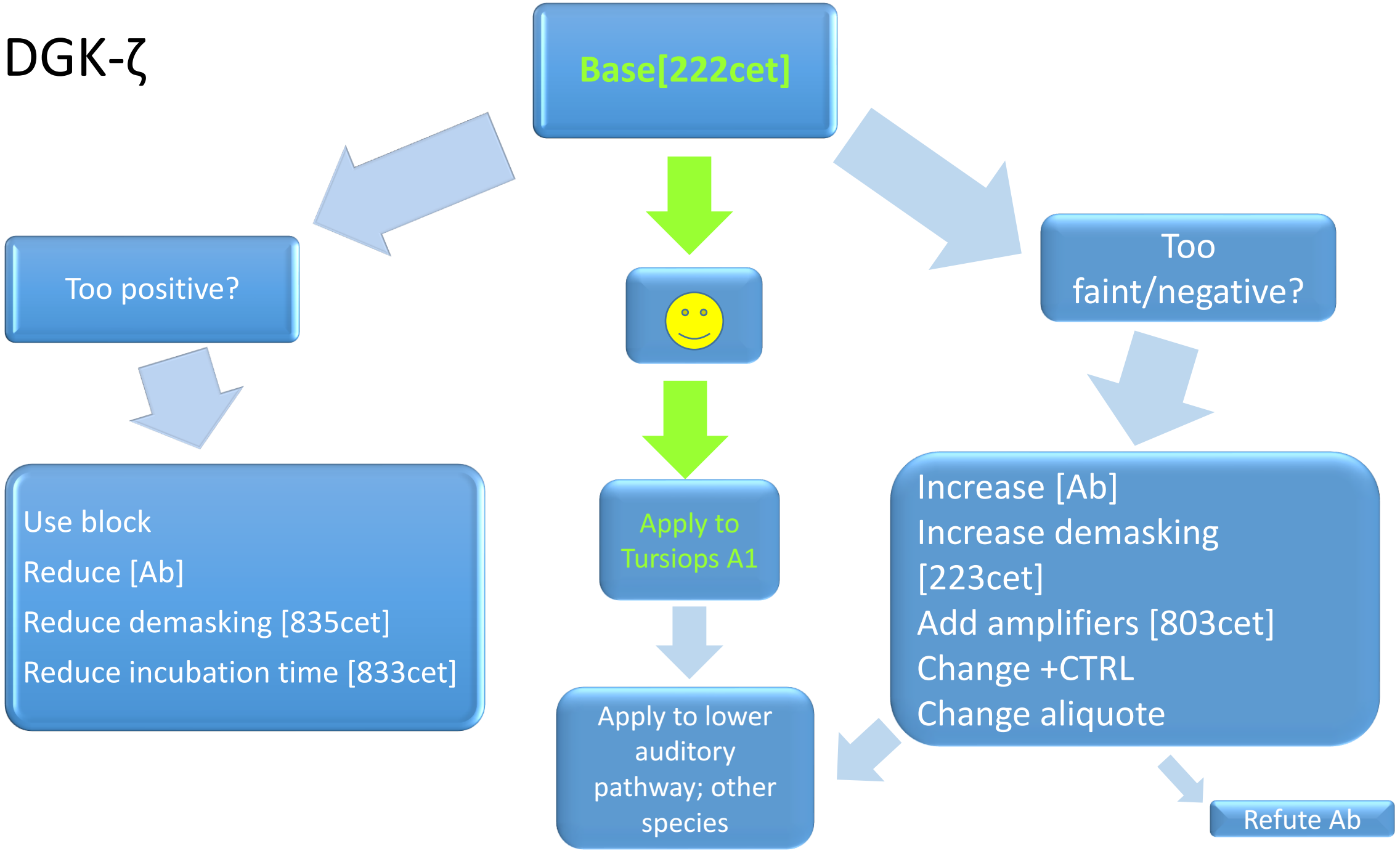
Base[222cet]
Too positive?
Too faint/negative?
Use block
Reduce [Ab]
Reduce demasking [835cet]
Reduce incubation time [833cet]
Apply to Tursiops A1
Apply to lower auditory pathway; other species
Increase [Ab]
Increase demasking [223cet]
Add amplifiers [803cet]
Change +CTRL
Change aliquote
Refute Ab

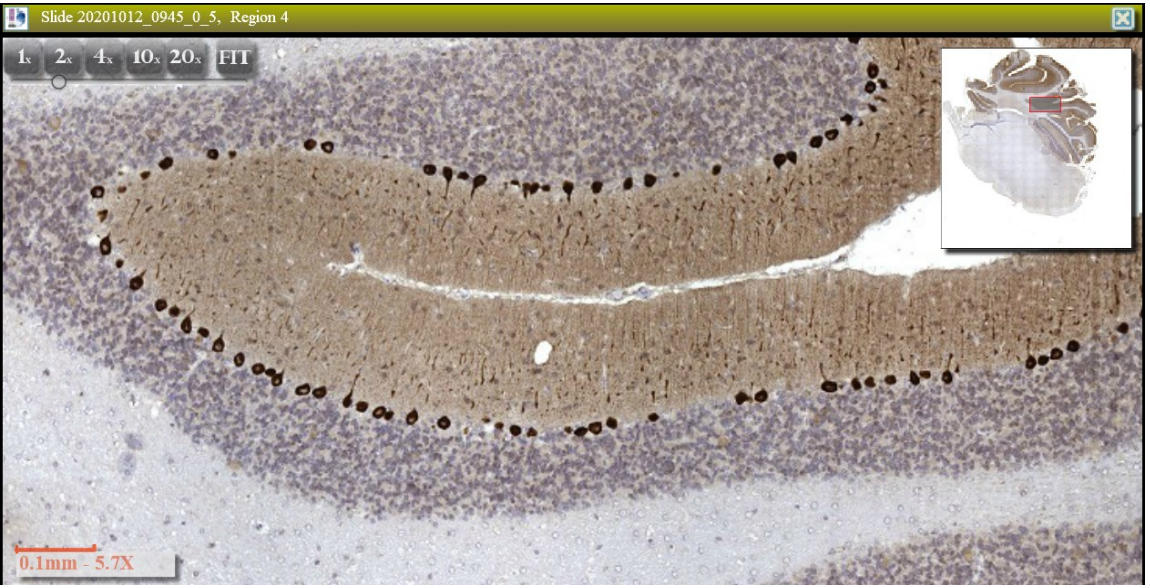

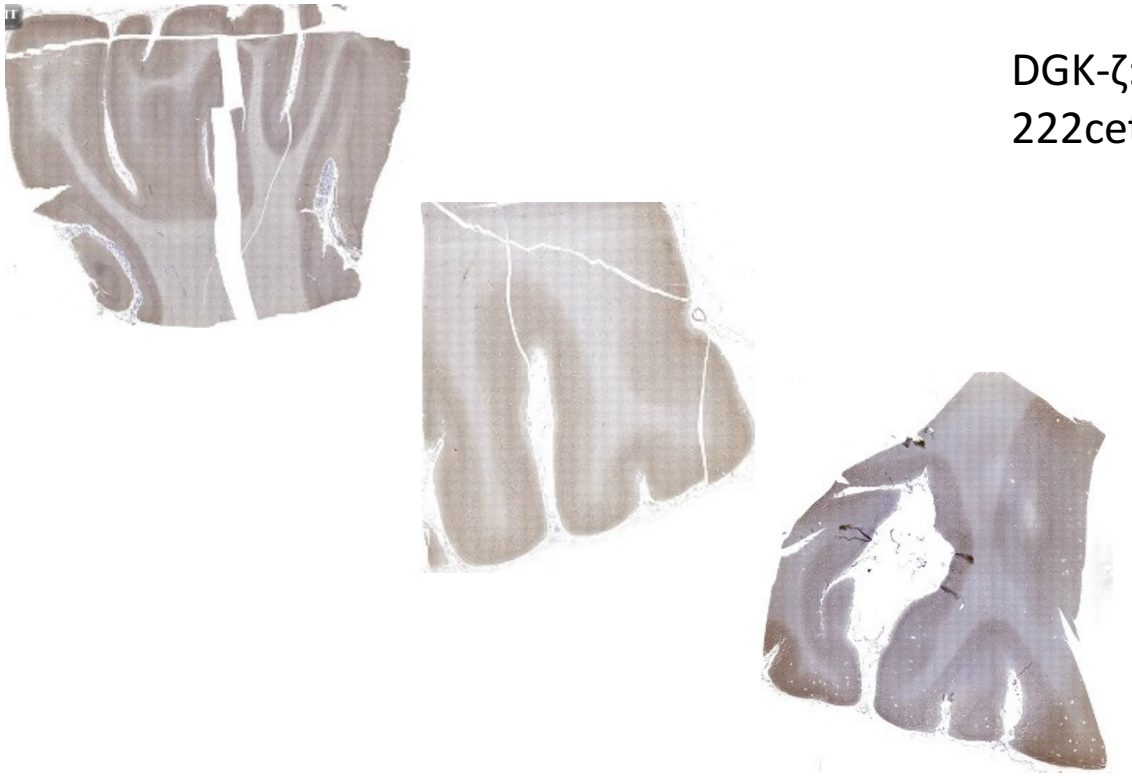

DGK-ζ: 1:50 dil;
222cet

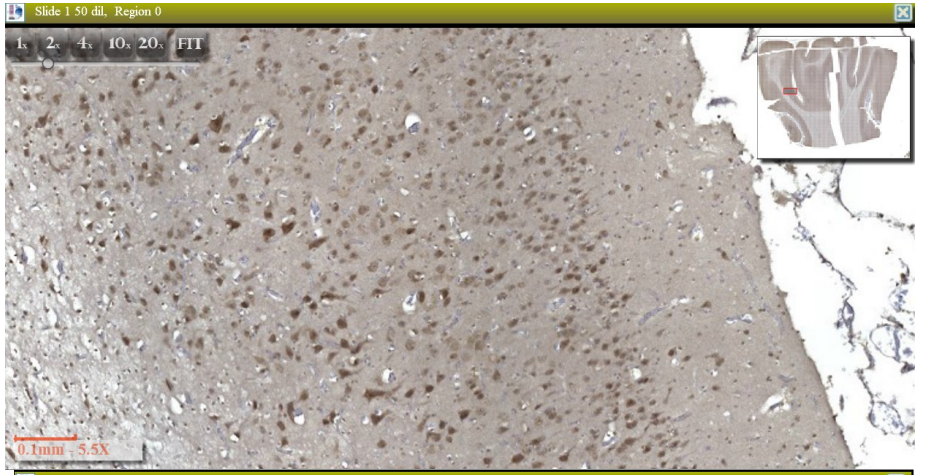

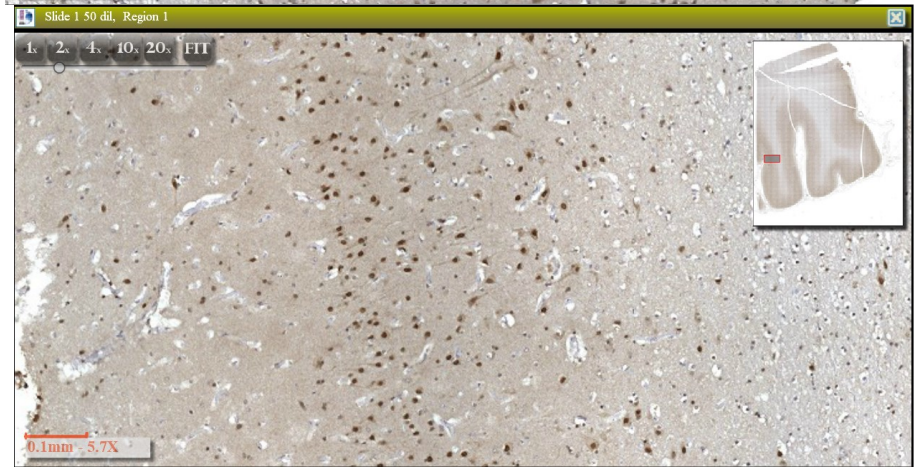

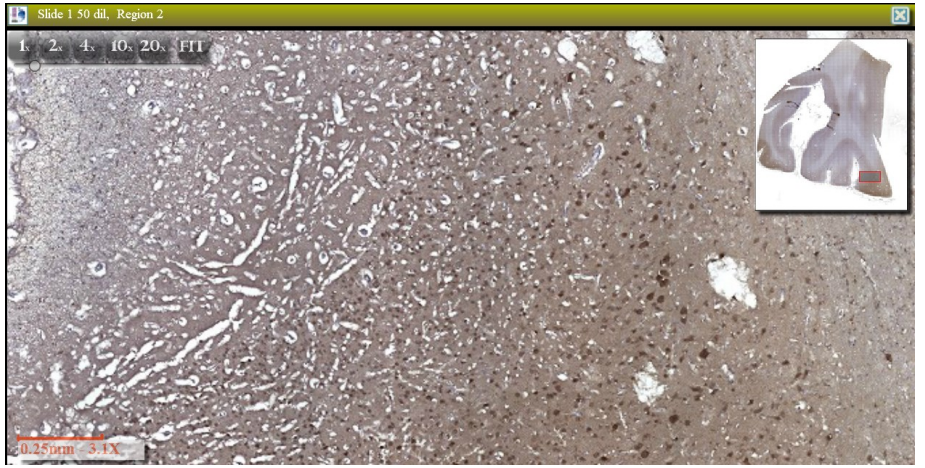

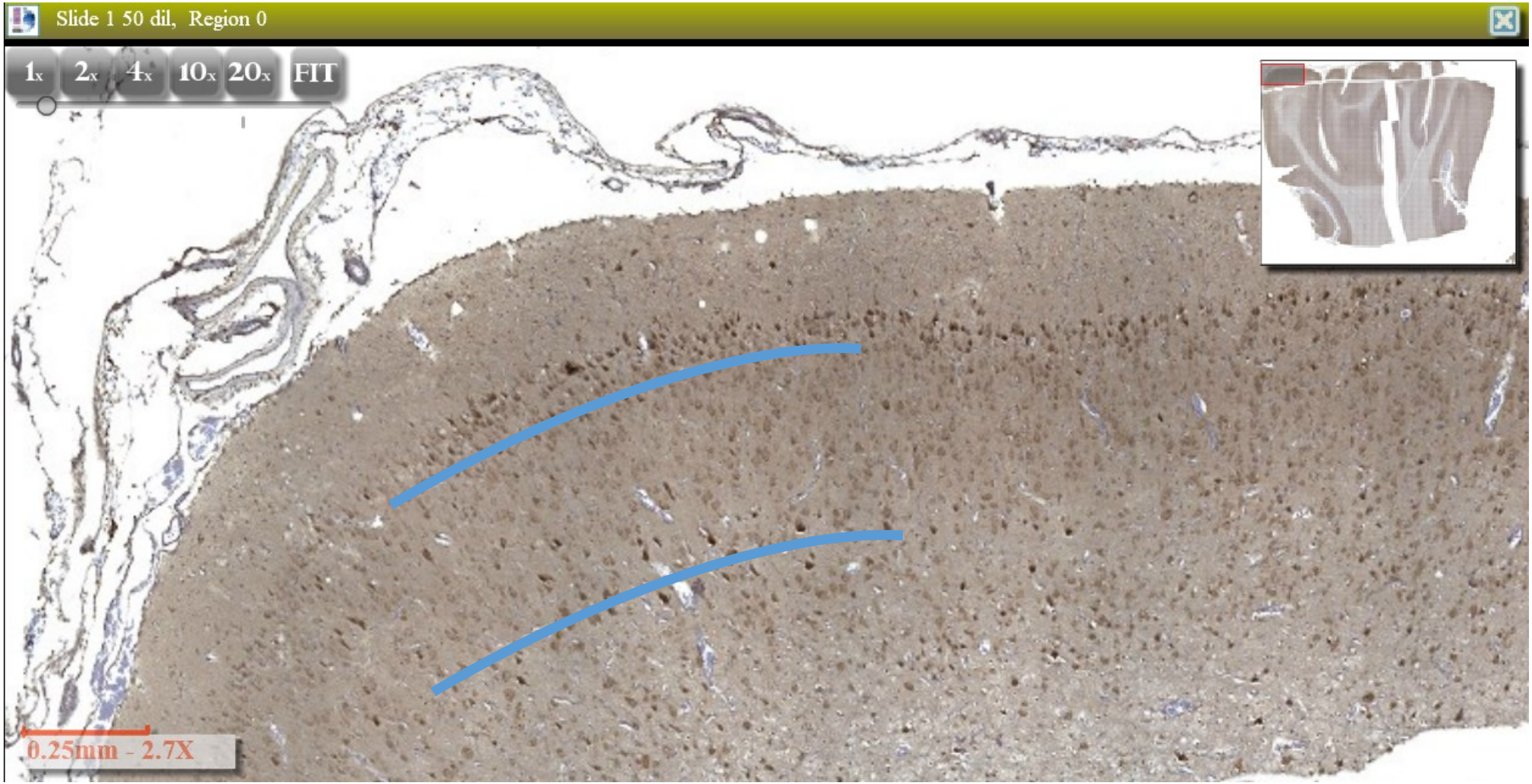

Strongest immunoreactivity in neurons of layers II and V

Inflammation

- TNFα

Metabolic

- Calbindin

TNFα

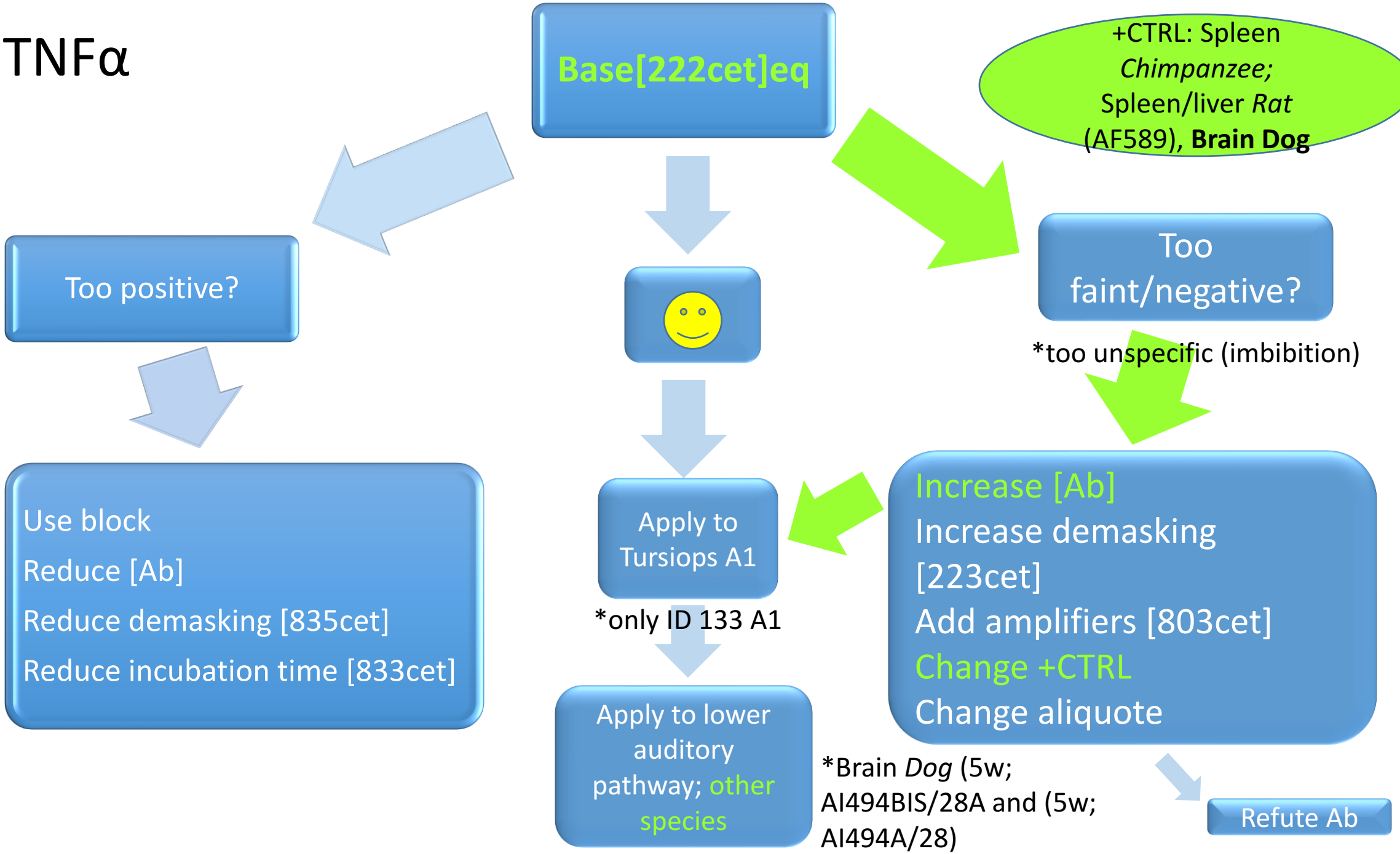
Base[222cet]eq
+CTRL: Spleen *Chimpanzee;* Spleen/liver *Rat* (AF589), **Brain Dog**
Too positive?
Too faint/negative?
*too unspecific (imbibition)
Use block
Reduce [Ab]
Reduce demasking [835cet]
Reduce incubation time [833cet]
Apply to Tursiops A1
*only ID 133 A1
Increase [Ab]
Increase demasking [223cet]
Add amplifiers [803cet]
Change +CTRL
Change aliquote
Apply to lower auditory pathway; other species
*Brain *Dog* (5w; AI494BIS/28A and (5w; AI494A/28)
Refute Ab

TNFα Prot 220/222
cet; 1:50 dil

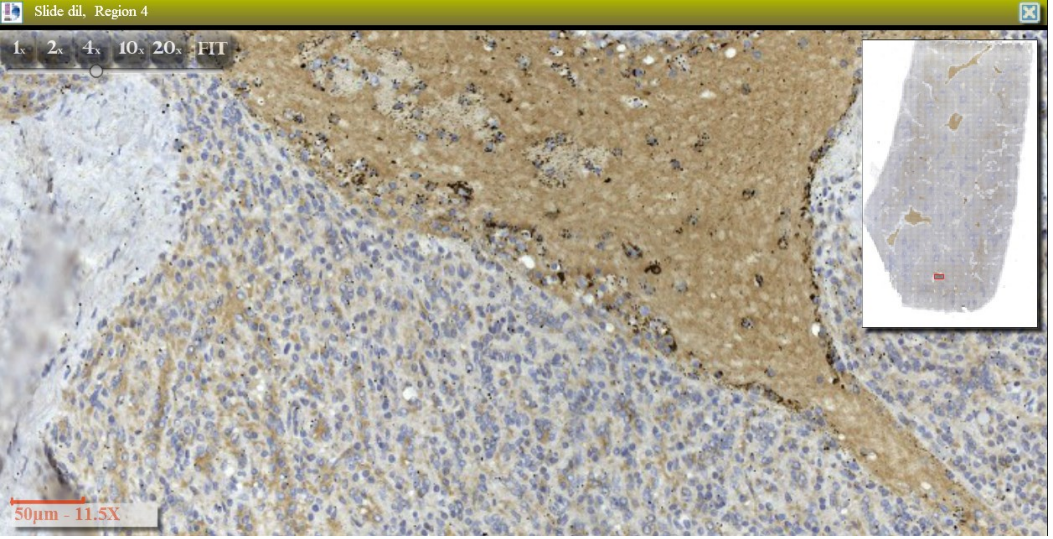

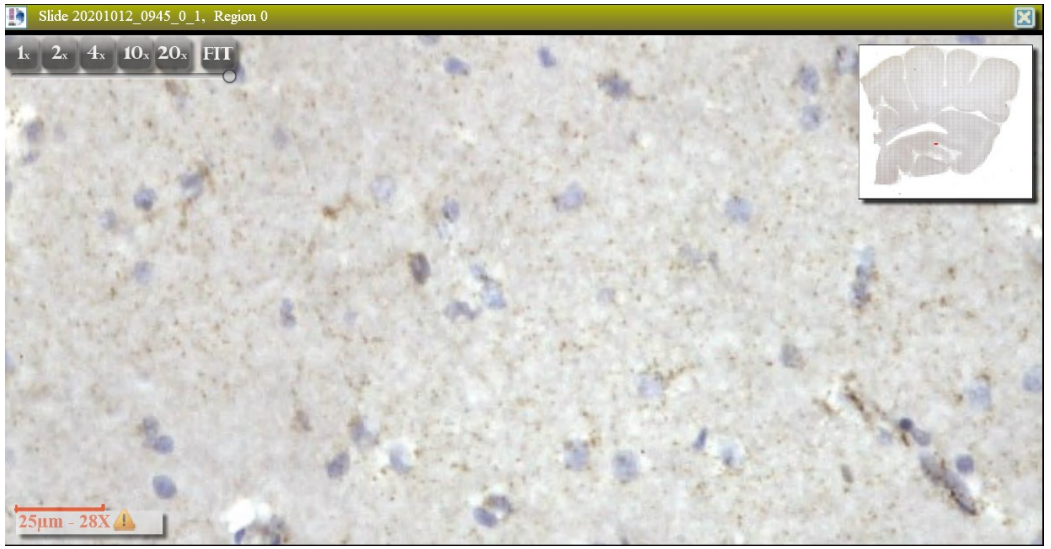

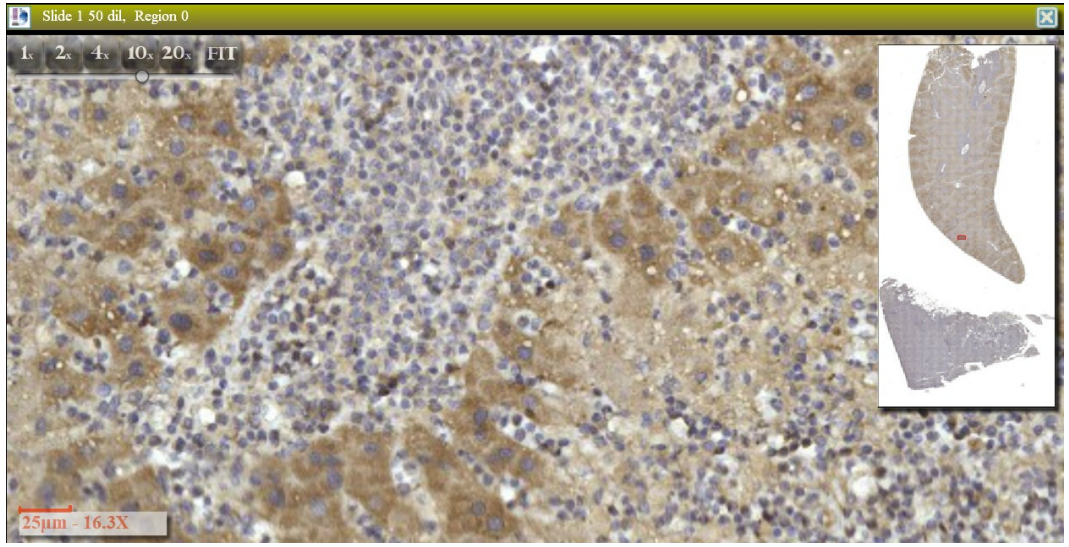

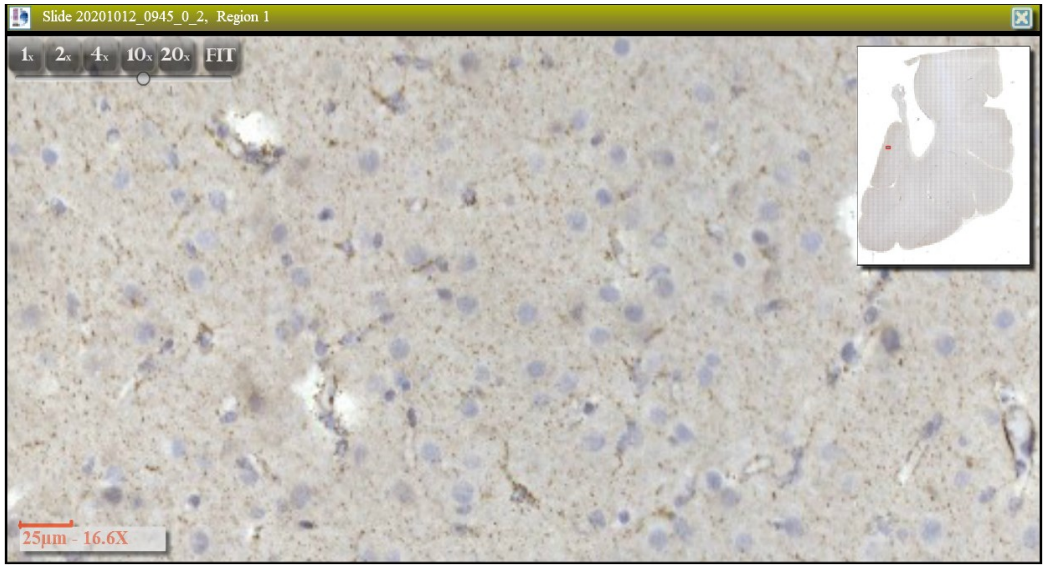

TNFα Prot 220/222
cet; 1:50 dil

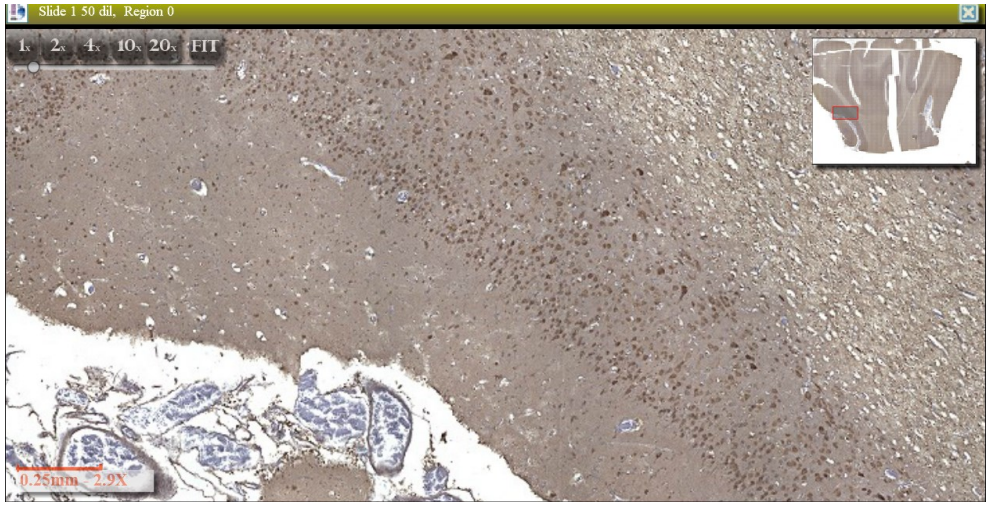

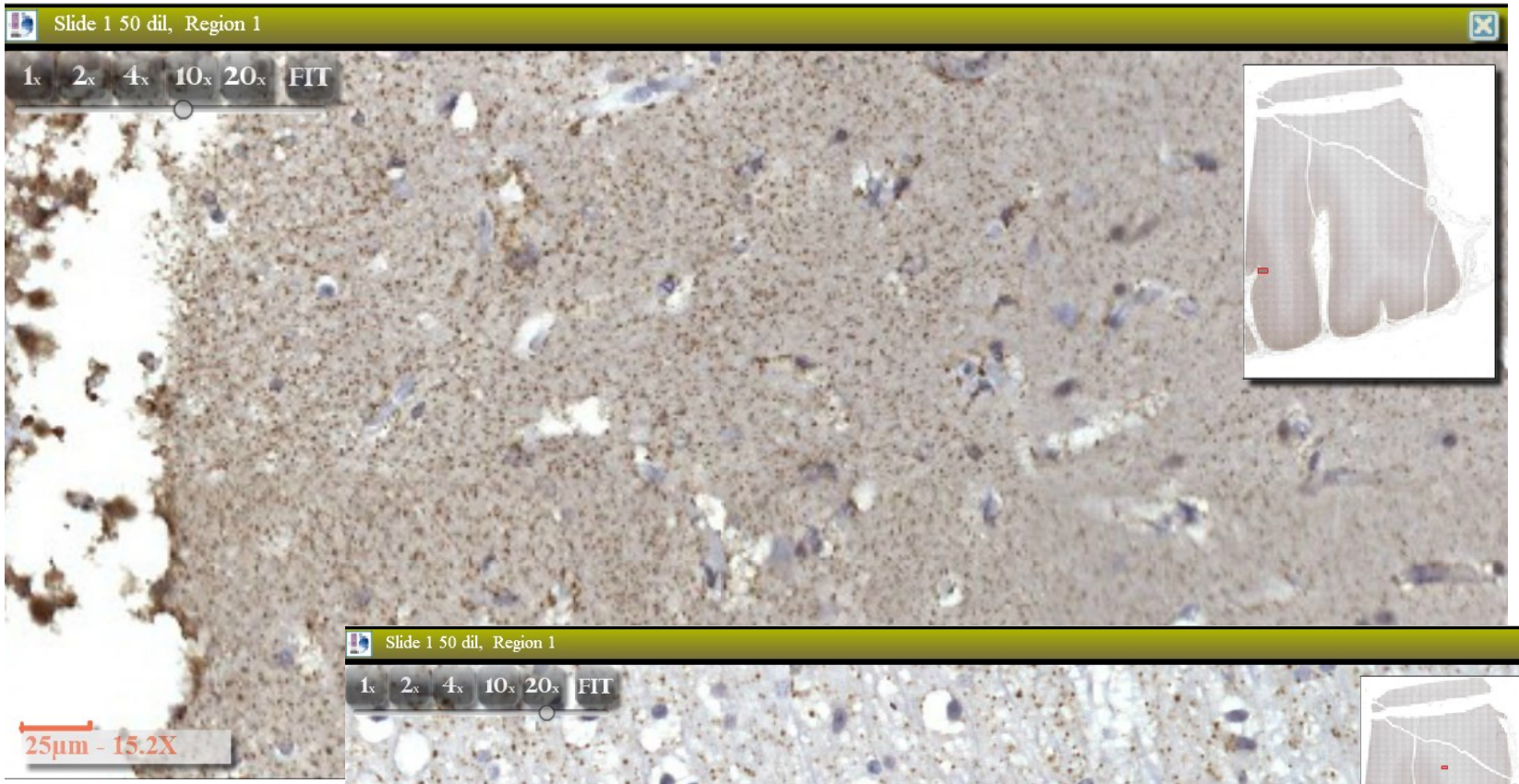
Slide 1 50 dil, Region 1
1x 2x 4x 10x 20x FIT
25µm - 15.2X

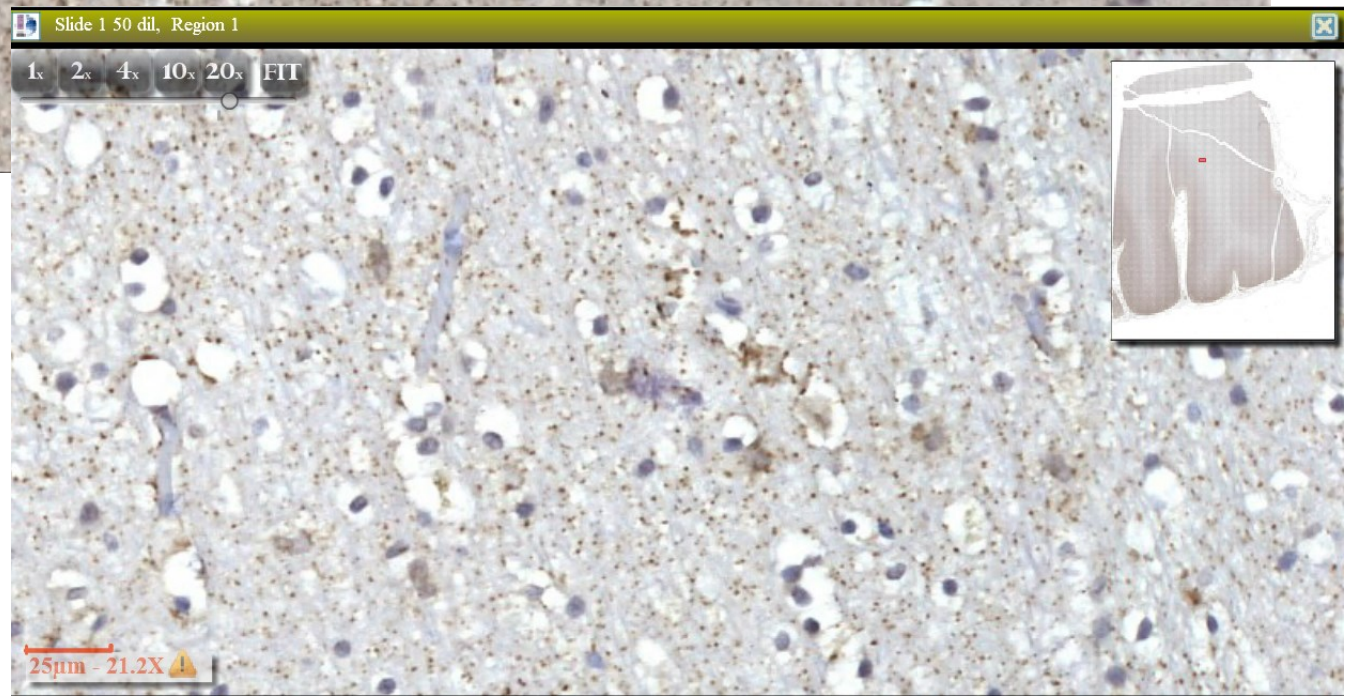
Slide 1 50 dil, Region 1
1x 2x 4x 10x 20x FIT
25µm - 21.2X

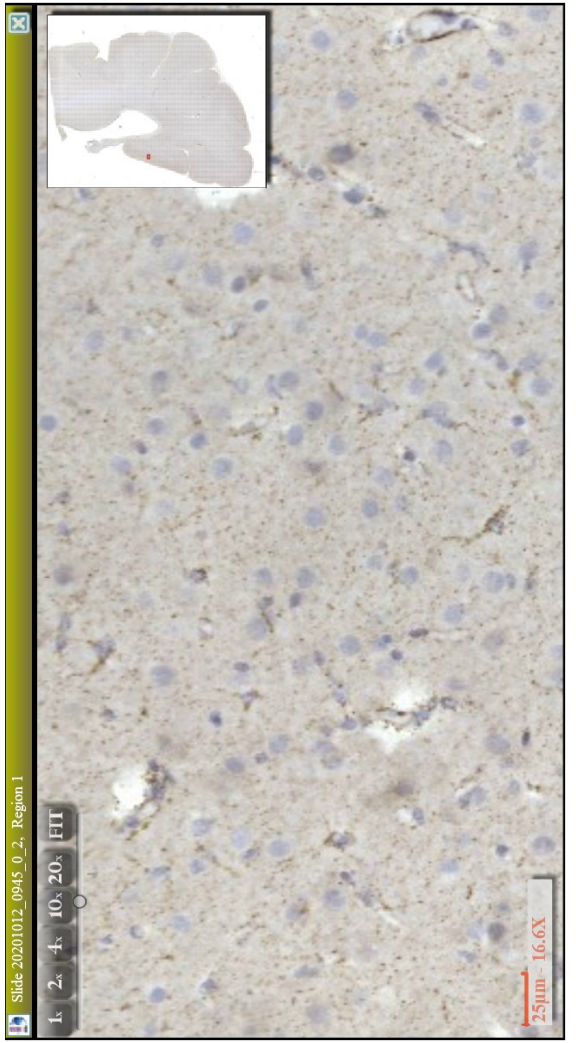
Slide 20201012_0945_0_2, Region 1
1x 2x 4x 10x 20x FIT
25µm - 16.6X

Calbindin

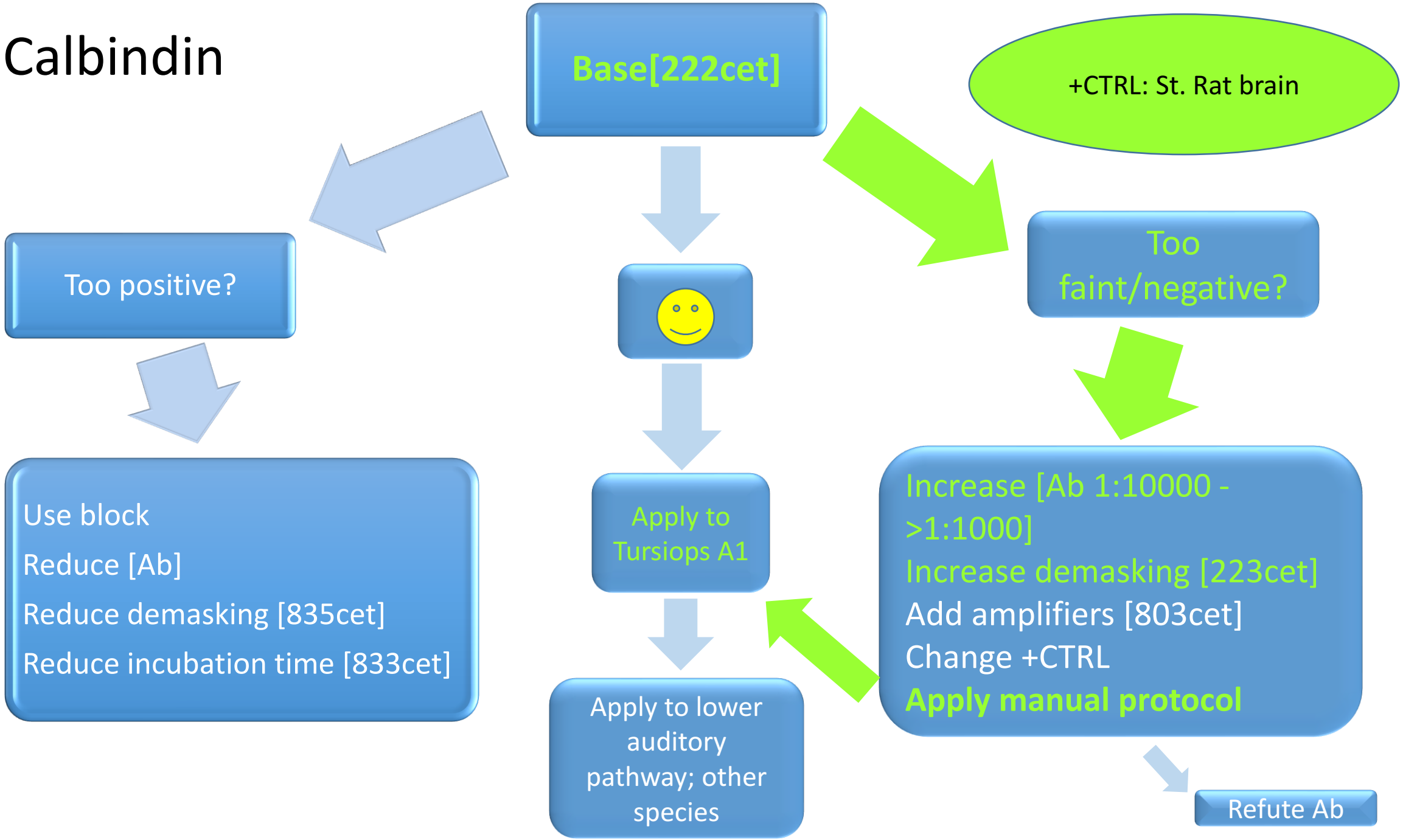
Base[222cet]
+CTRL: St. Rat brain
Too positive?
Too faint/negative?
Use block
Reduce [Ab]
Reduce demasking [835cet]
Reduce incubation time [833cet]
Apply to Tursiops A1
Increase [Ab 1:10000 ->1:1000]
Increase demasking [223cet]
Add amplifiers [803cet]
Change +CTRL
Apply manual protocol
Apply to lower auditory pathway; other species
Refute Ab

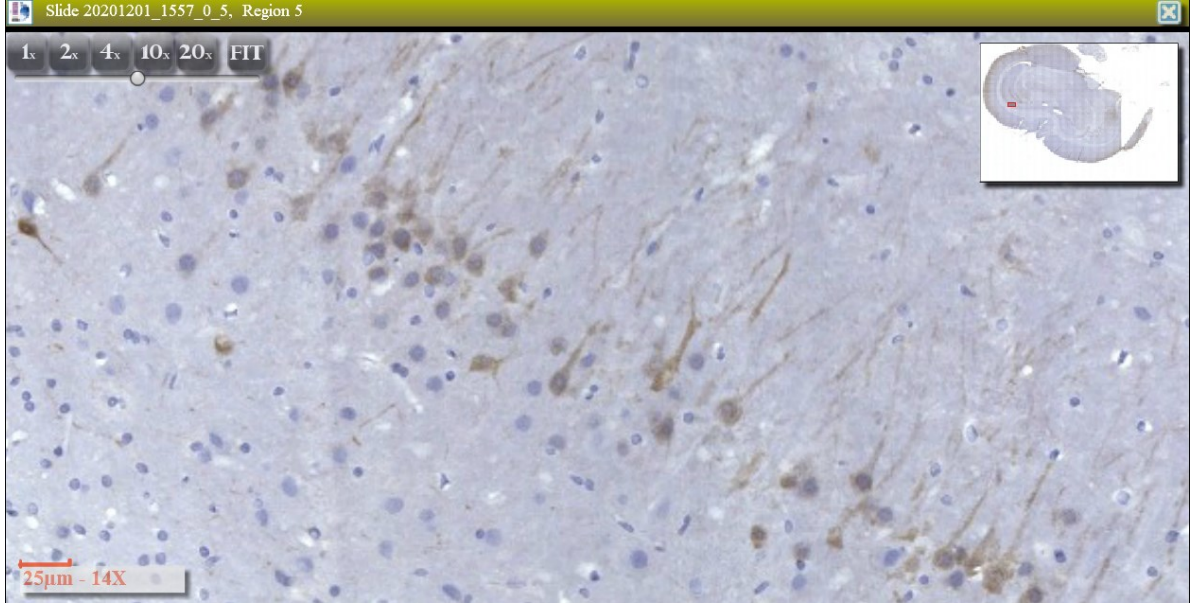

Calbindin Prot 222
cet; 1:2000 dil

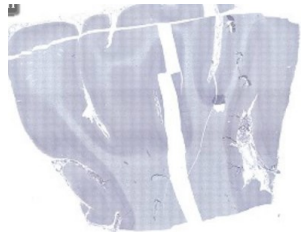

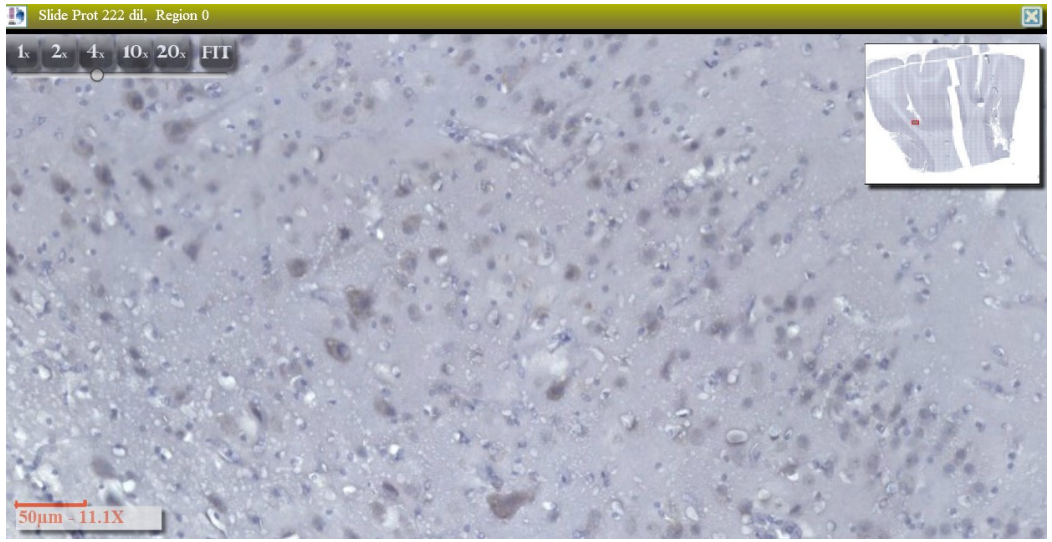

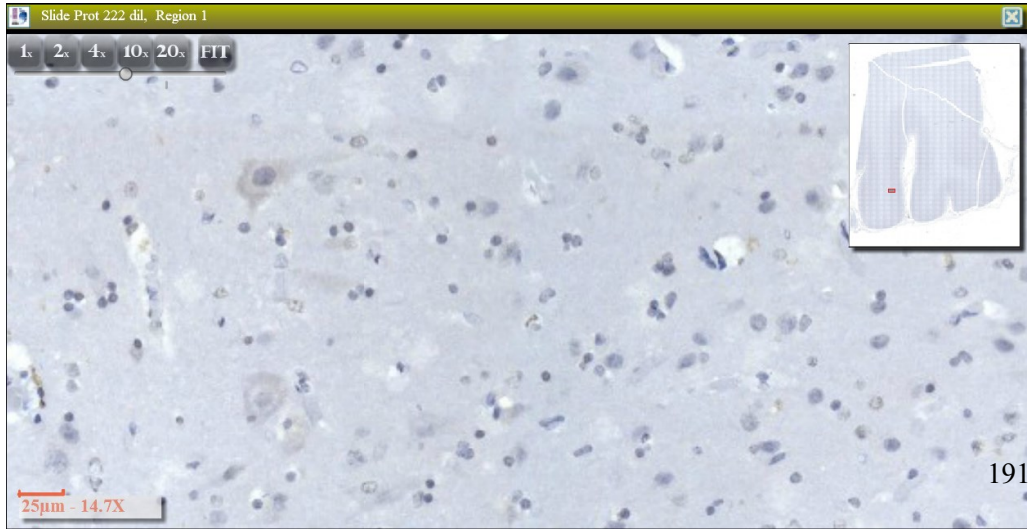

Calbindin Prot 222
cet; 1:2000 dil

Calbindin Prot 222
cet; 1:1000 dil

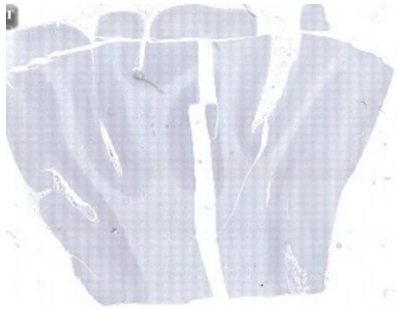

Calbindin Prot 223
cet; 1:2000 dil

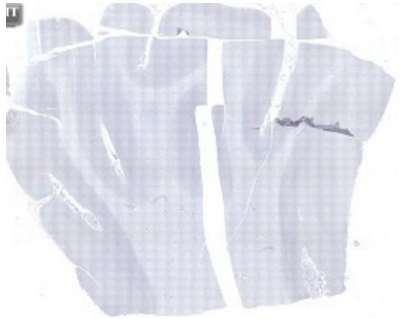

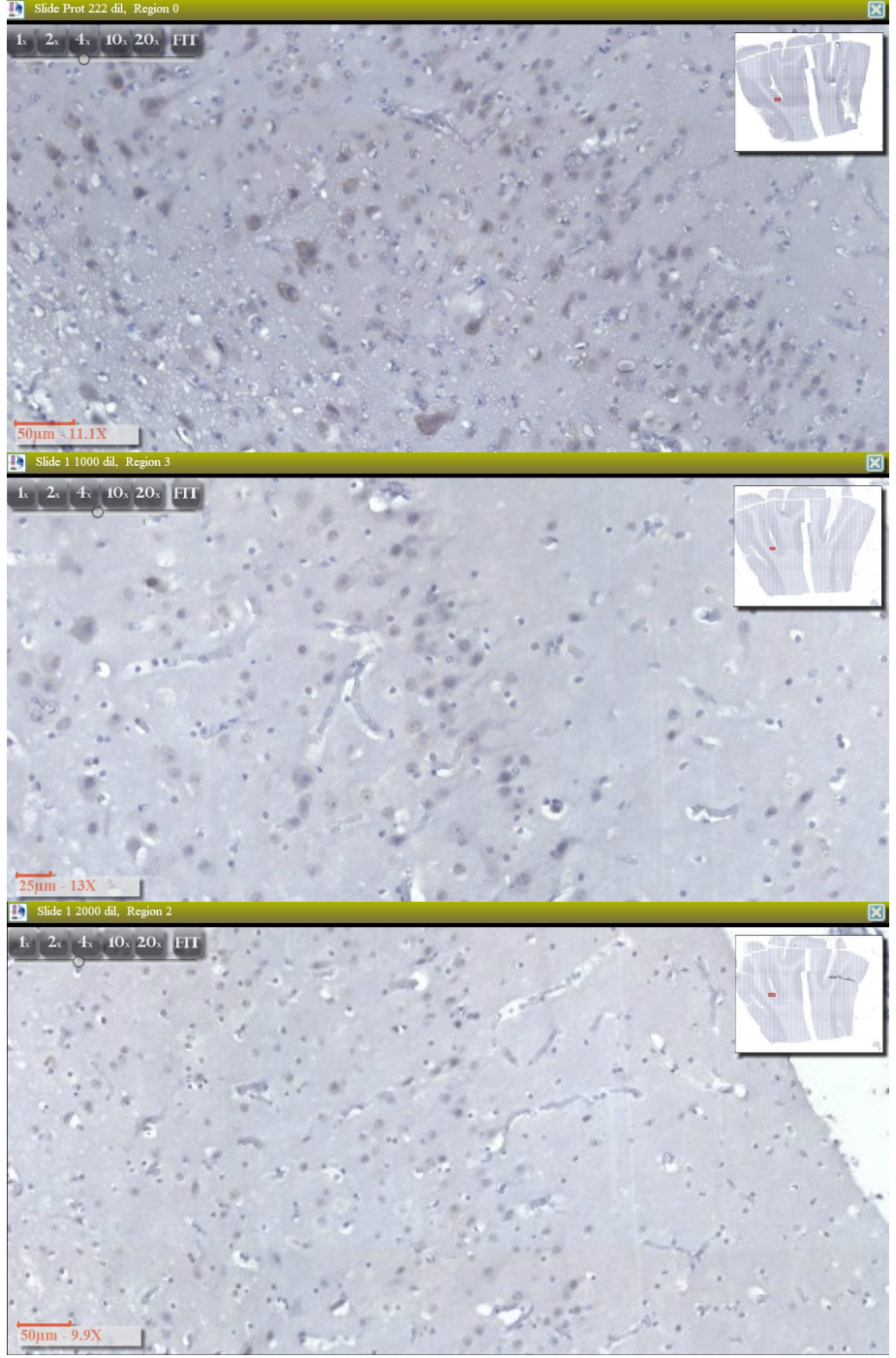

Calbindin Prot 222 (manual) cet;
1:1000 dil;
overnight

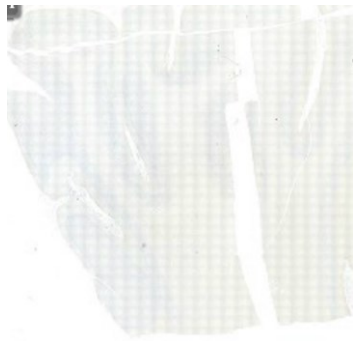

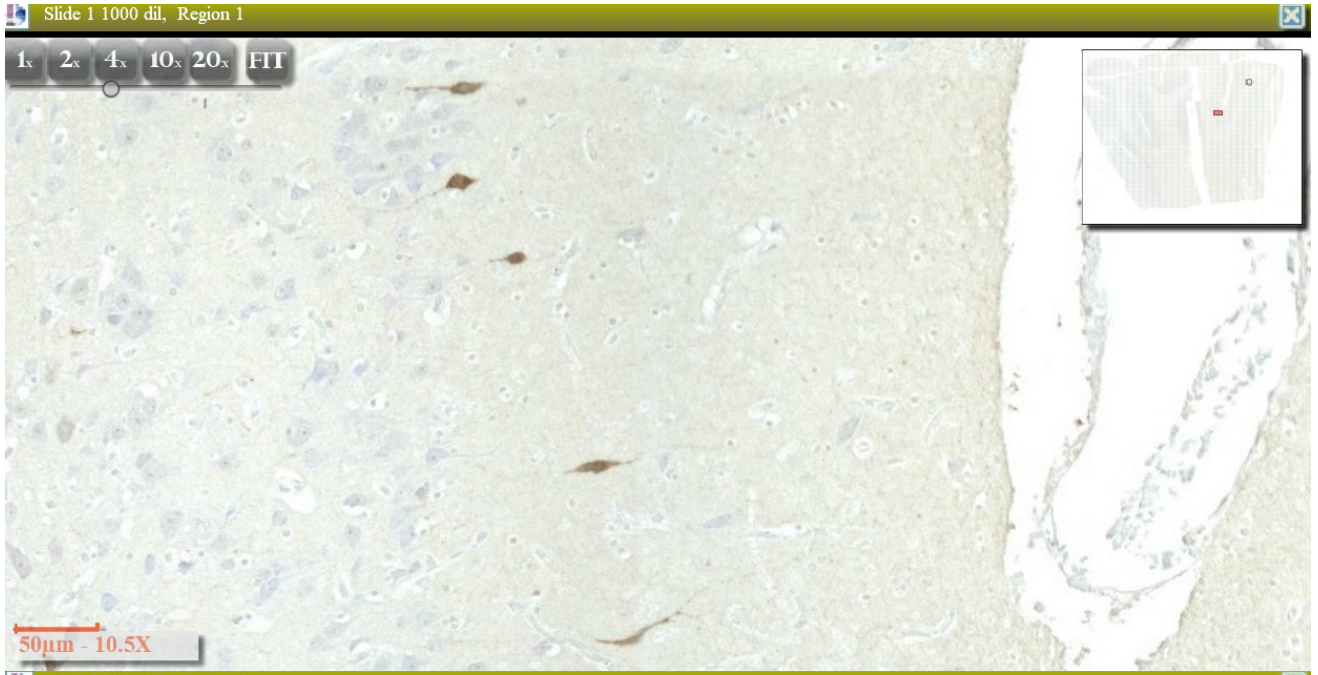

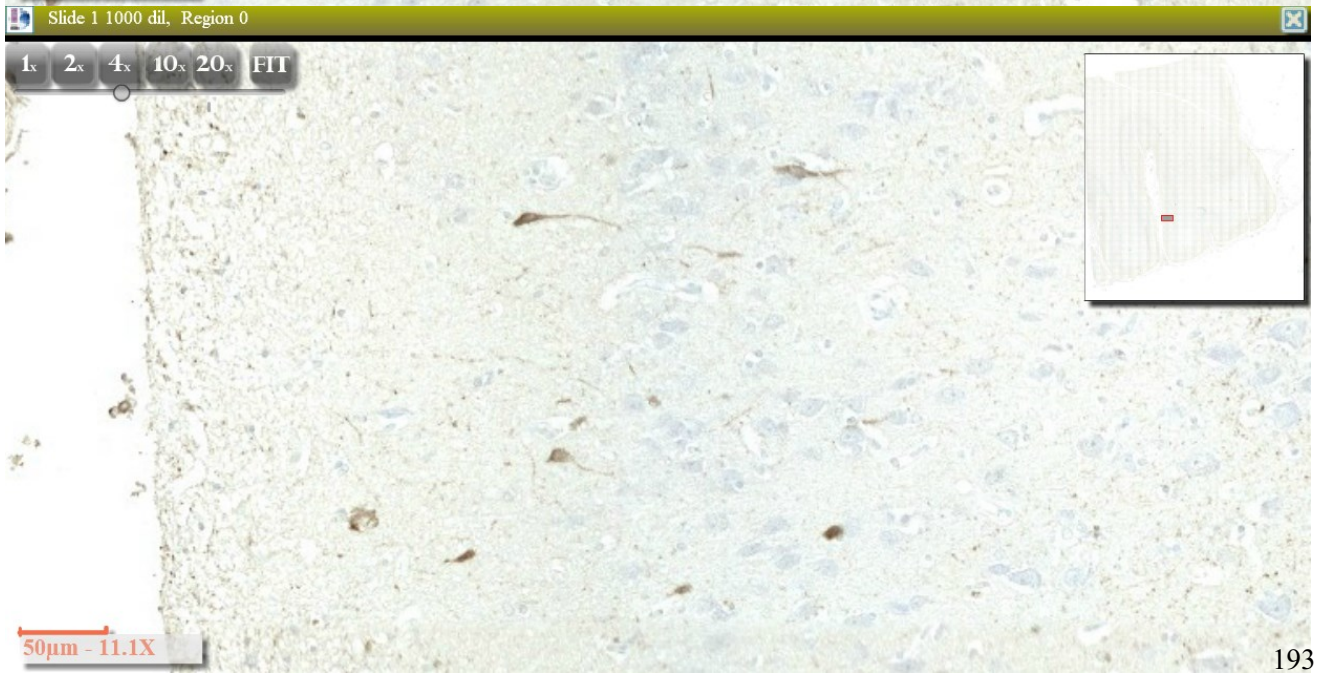

ID 133 light background but no cellular positivity

Plasticity

- GAP43
- Synaptophysin

Structural

- Myelin
  - QKI
- Neuronal cytoskeleton
  - NF200

GAP43

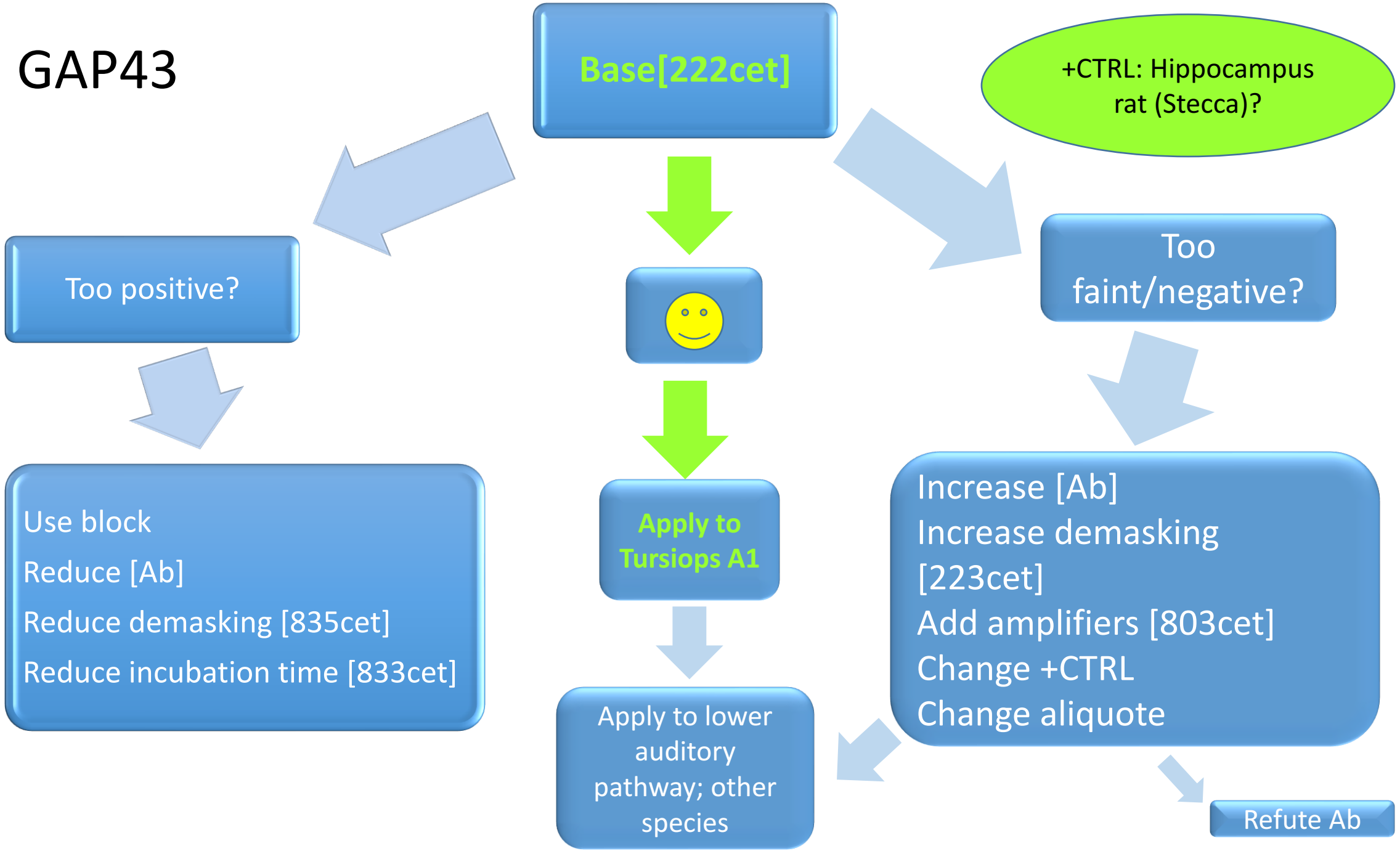
Base[222cet]
+CTRL: Hippocampus rat (Stecca)?
Too positive?
Too faint/negative?
Use block
Reduce [Ab]
Reduce demasking [835cet]
Reduce incubation time [833cet]
Apply to Tursiops A1
Increase [Ab]
Increase demasking [223cet]
Add amplifiers [803cet]
Change +CTRL
Change aliquote
Apply to lower auditory pathway; other species
Refute Ab

GAP43, 1:1000 dil;
222cet

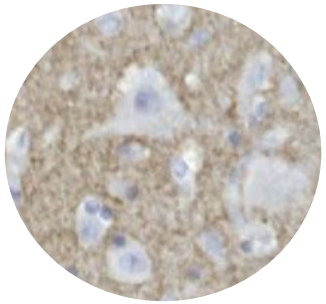

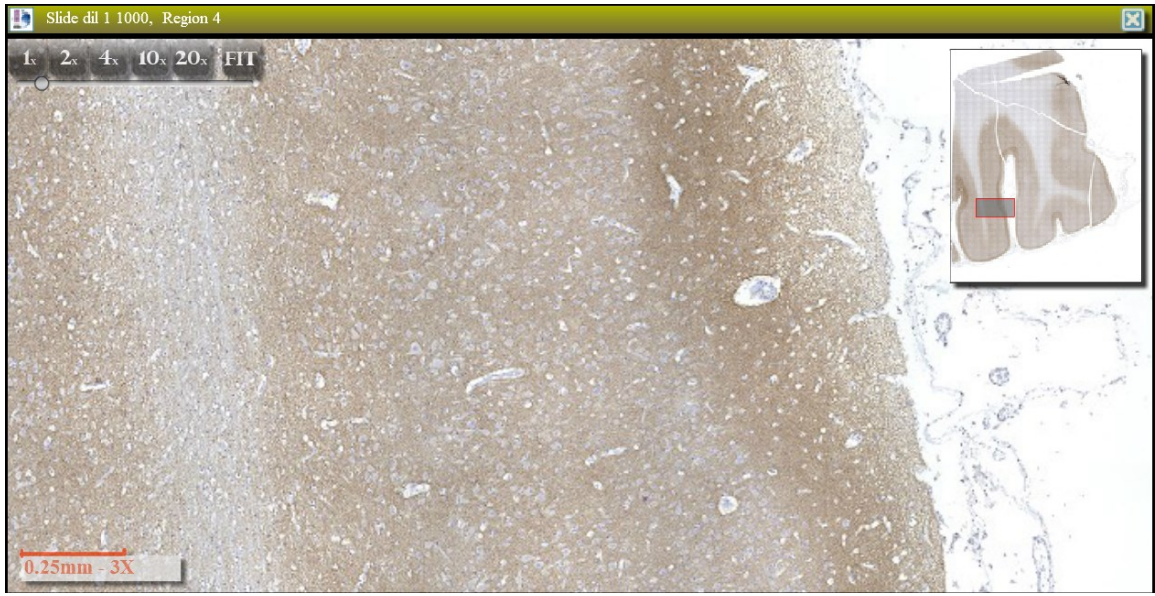

Synaptophysin

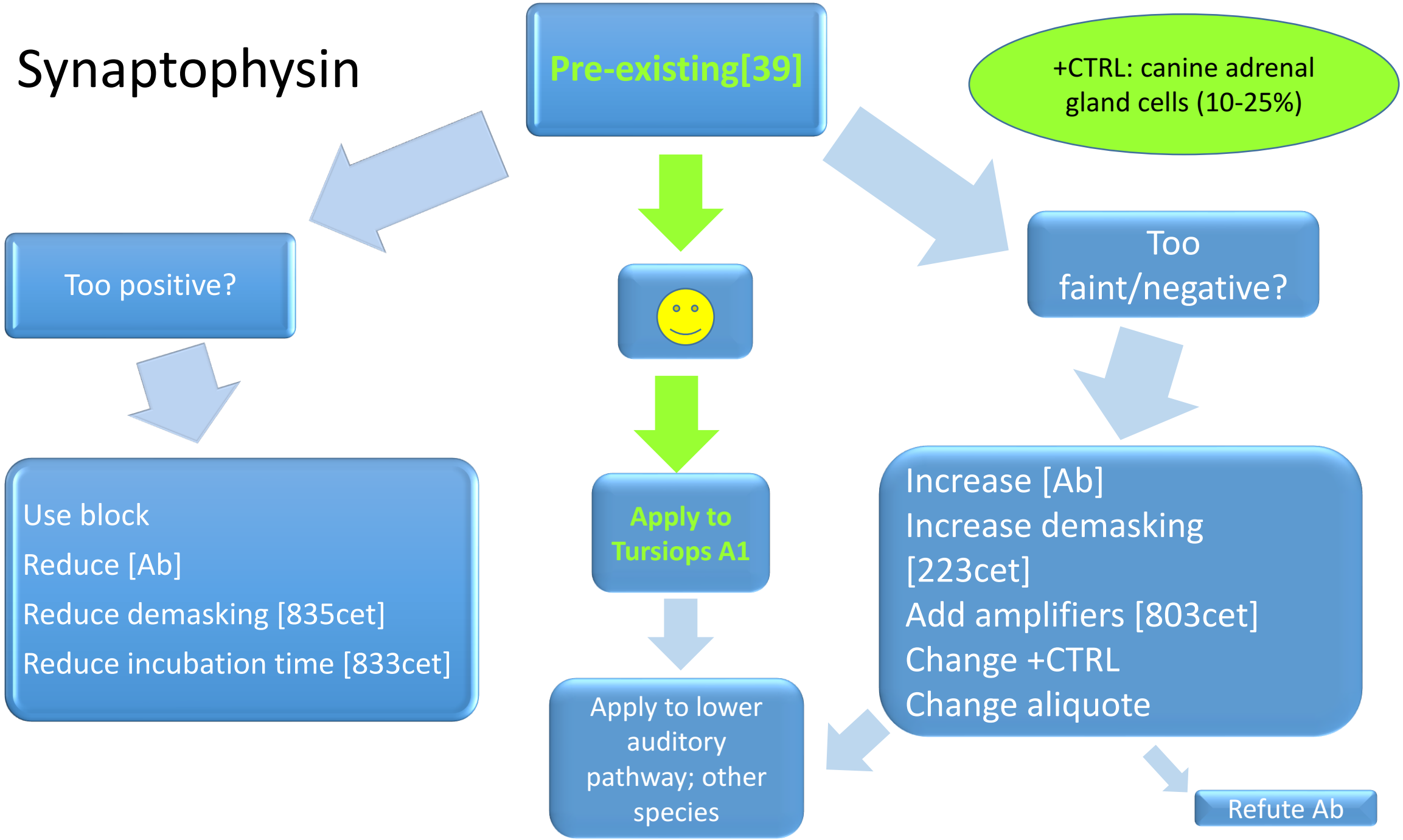

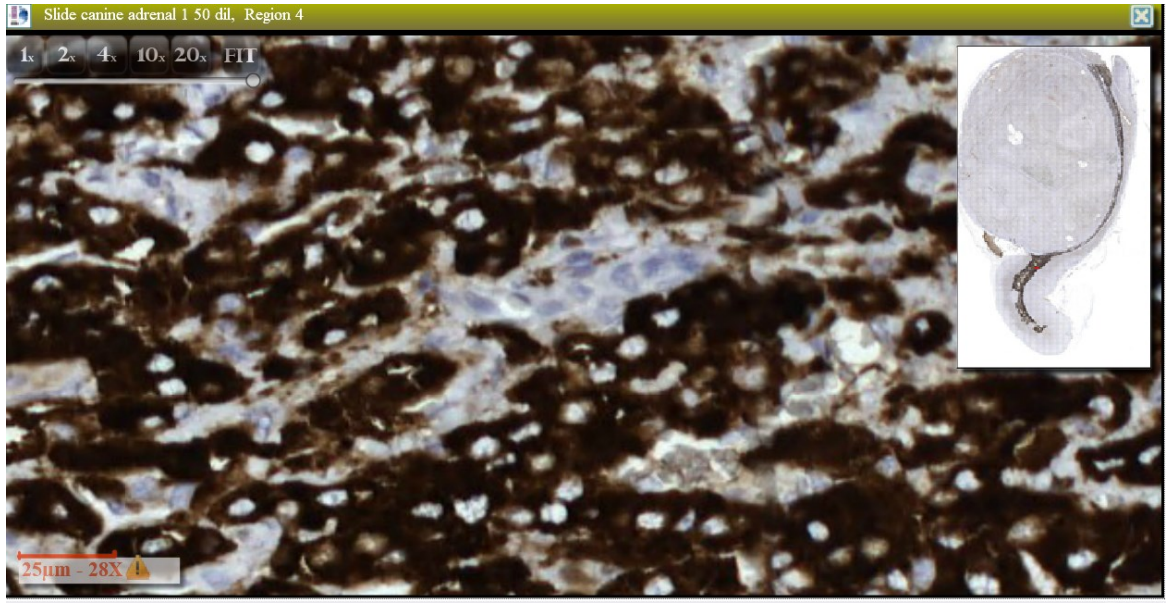

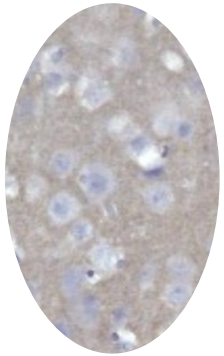

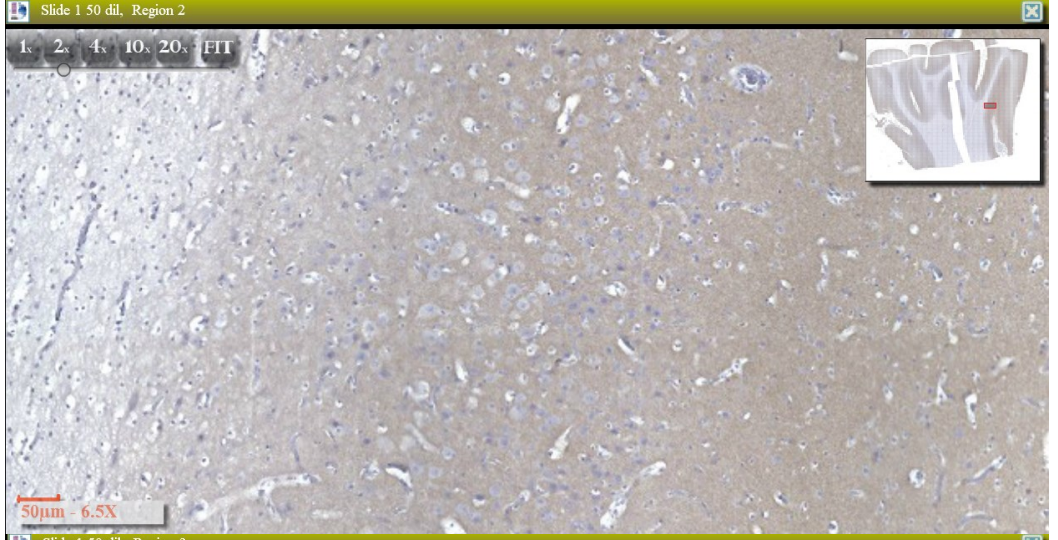

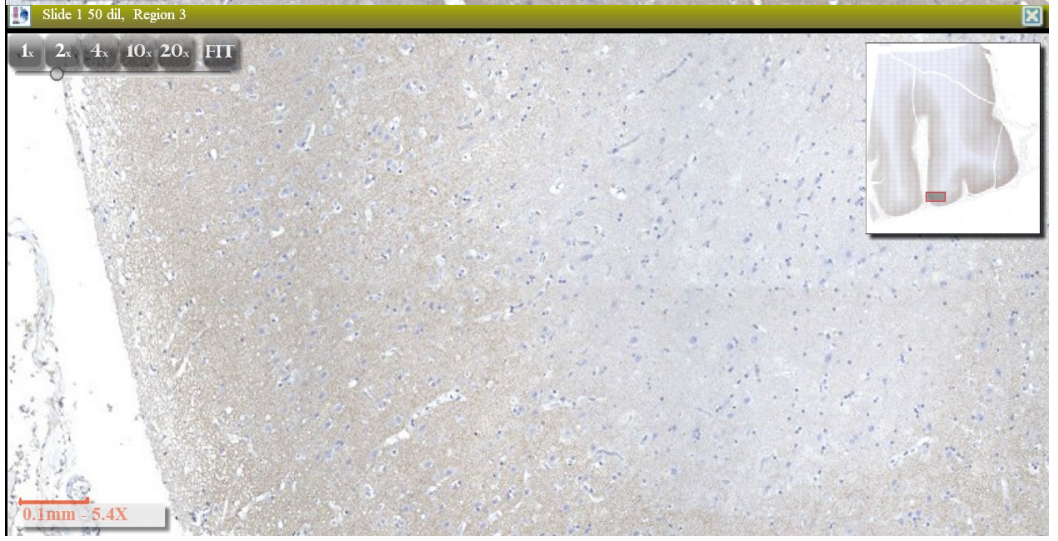

Synaptophysin,
1:50 dil; Prot 39

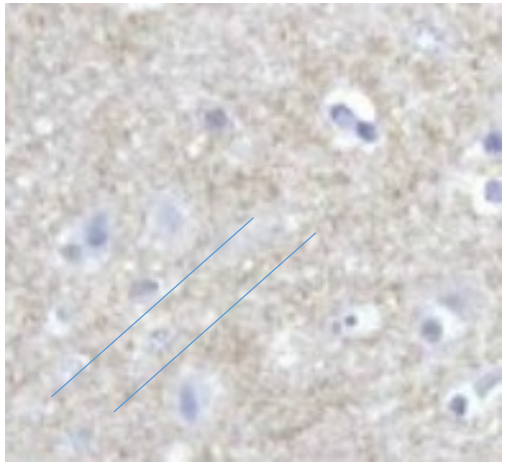

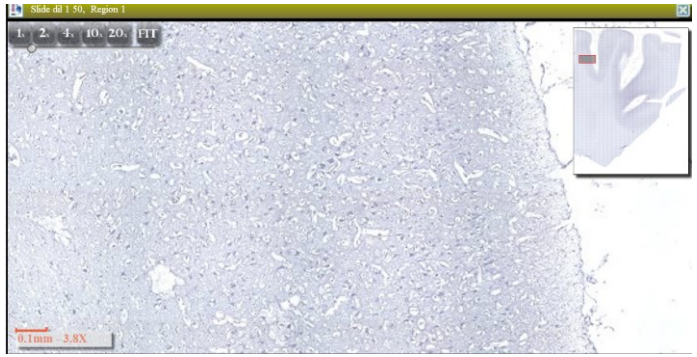

Pan-QKI

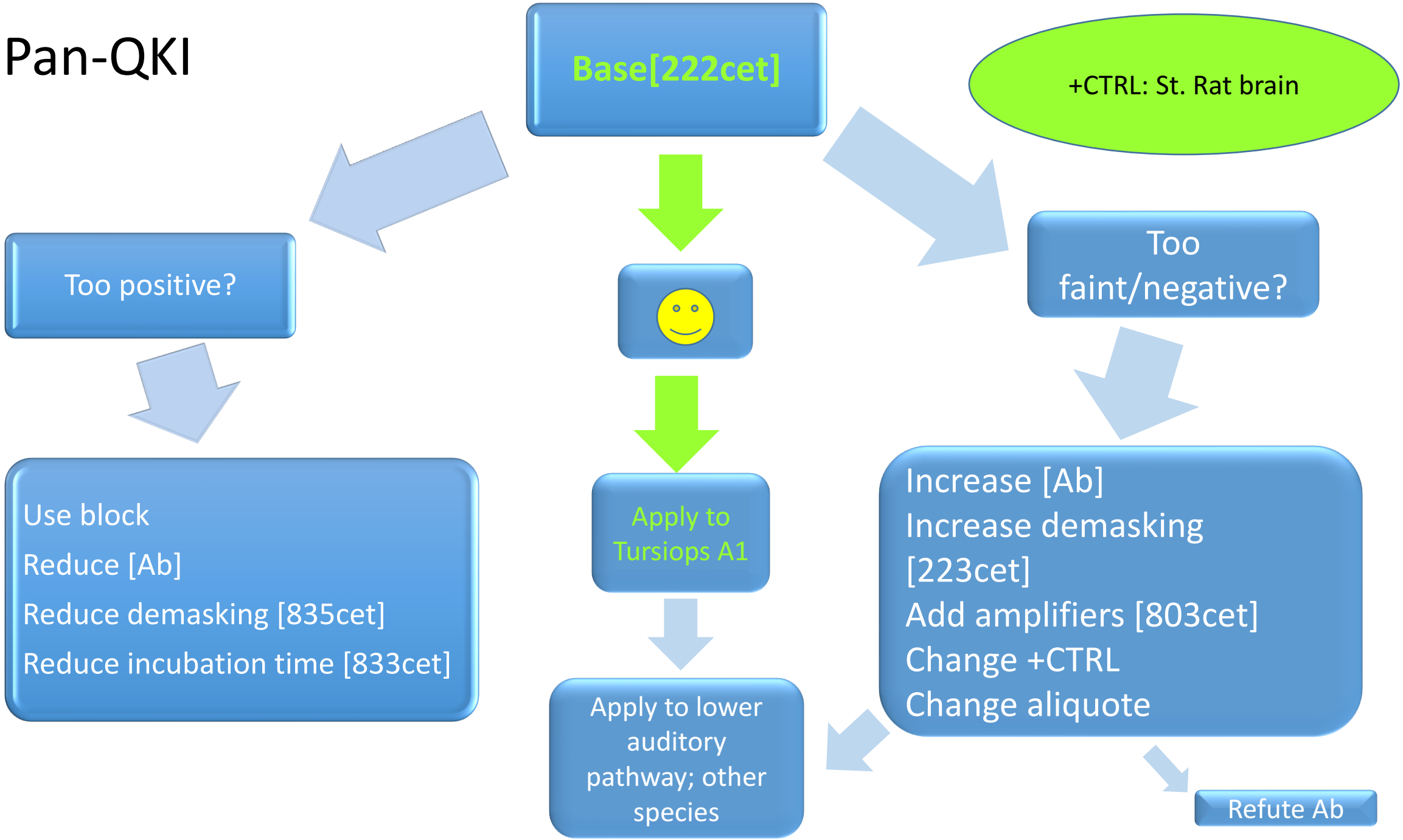
Base[222cet]
+CTRL: St. Rat brain
Too positive?
Too faint/negative?
Use block
Reduce [Ab]
Reduce demasking [835cet]
Reduce incubation time [833cet]
Apply to Tursiops A1
Increase [Ab]
Increase demasking [223cet]
Add amplifiers [803cet]
Change +CTRL
Change aliquote
Apply to lower auditory pathway; other species
Refute Ab

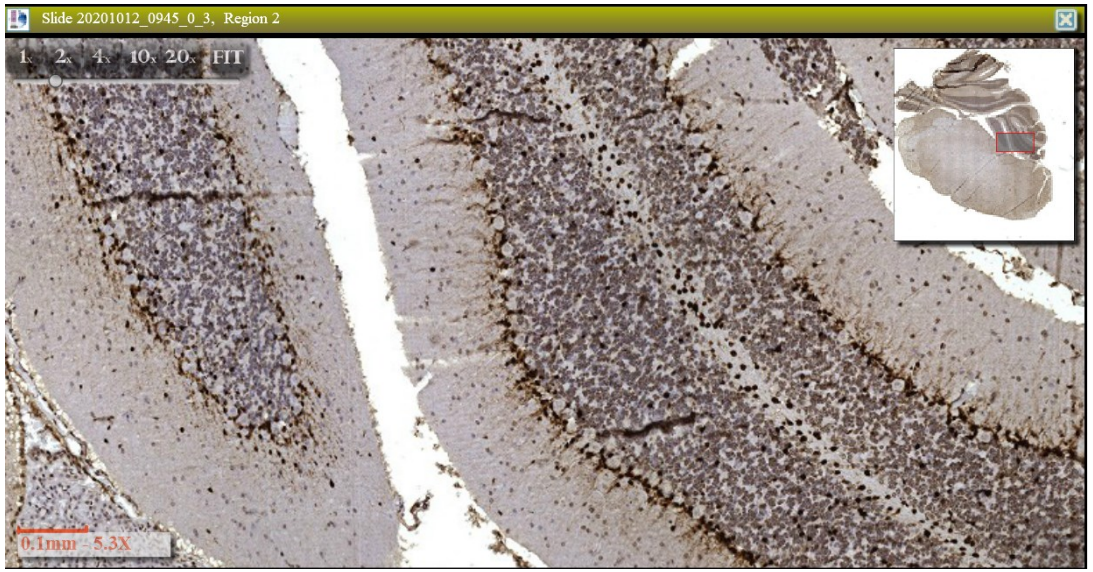

Pan-QKI: 1:50
dil; 222cet

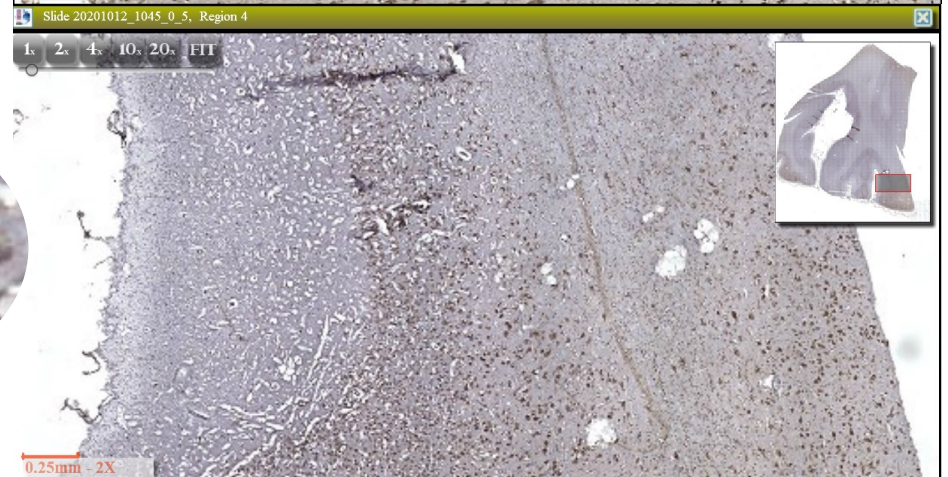

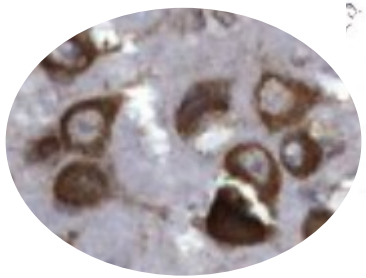

QKI-7

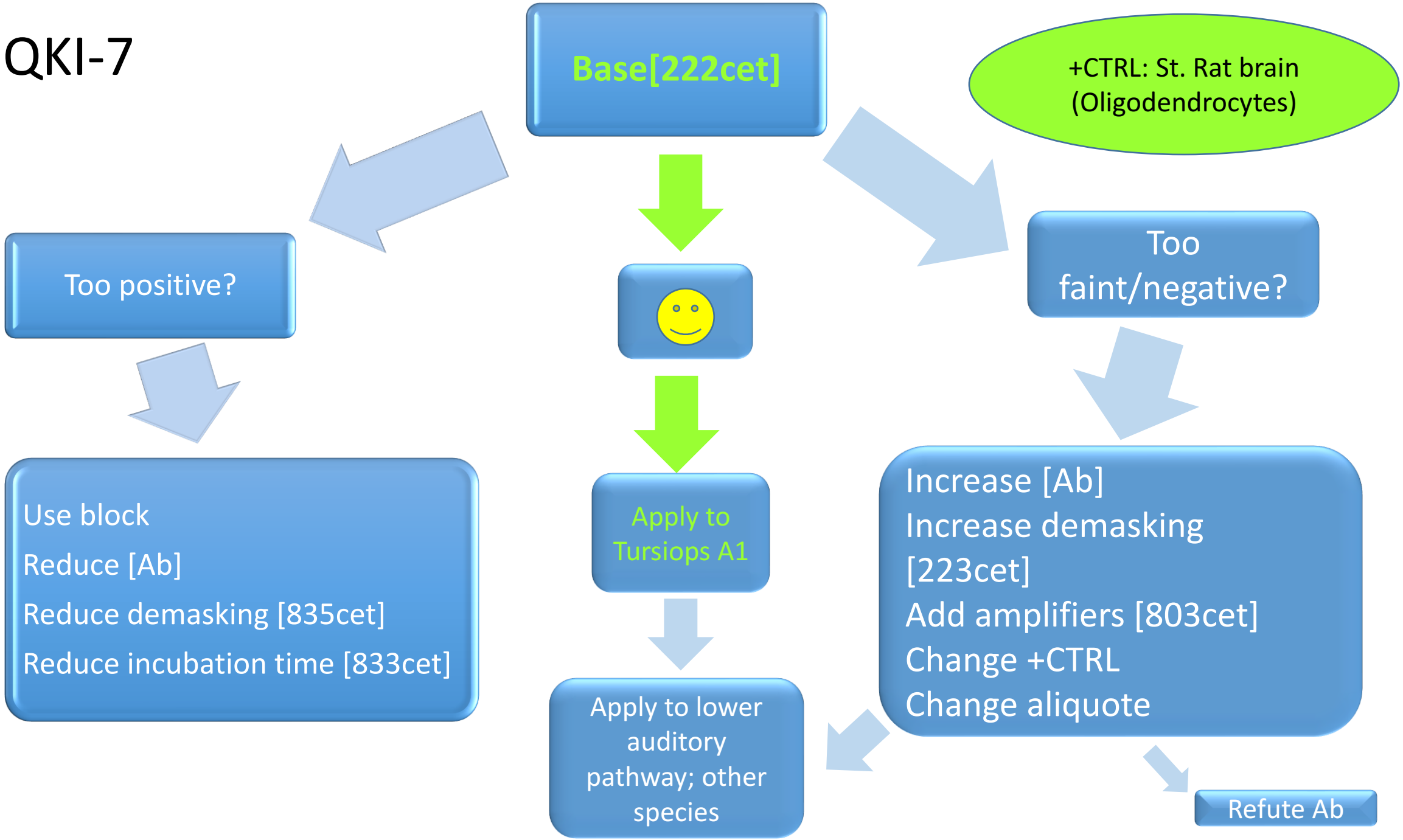
Base[222cet]
+CTRL: St. Rat brain (Oligodendrocytes)
Too positive?
Too faint/negative?
Use block
Reduce [Ab]
Reduce demasking [835cet]
Reduce incubation time [833cet]
Apply to Tursiops A1
Increase [Ab]
Increase demasking [223cet]
Add amplifiers [803cet]
Change +CTRL
Change aliquote
Apply to lower auditory pathway; other species
Refute Ab

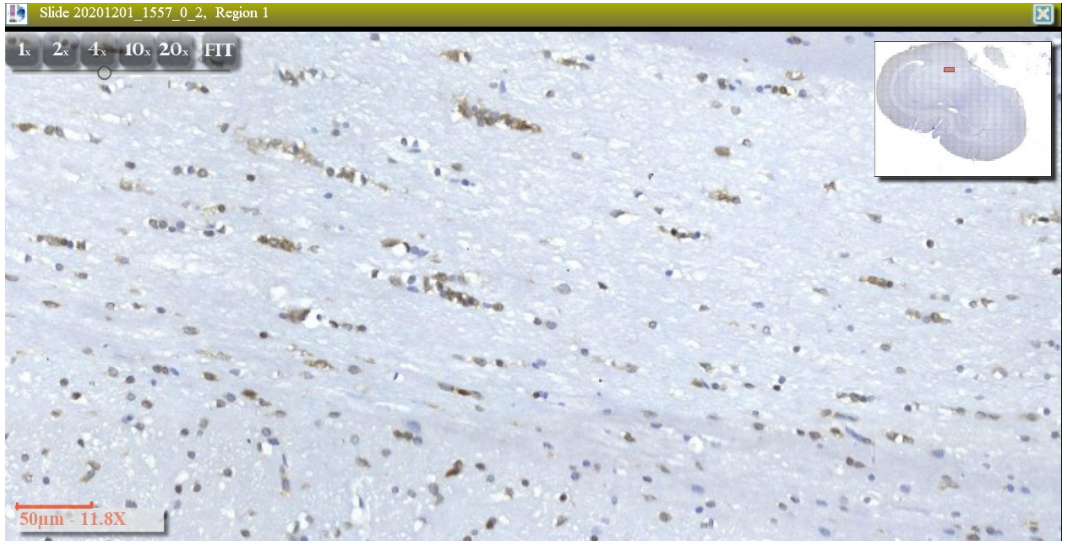

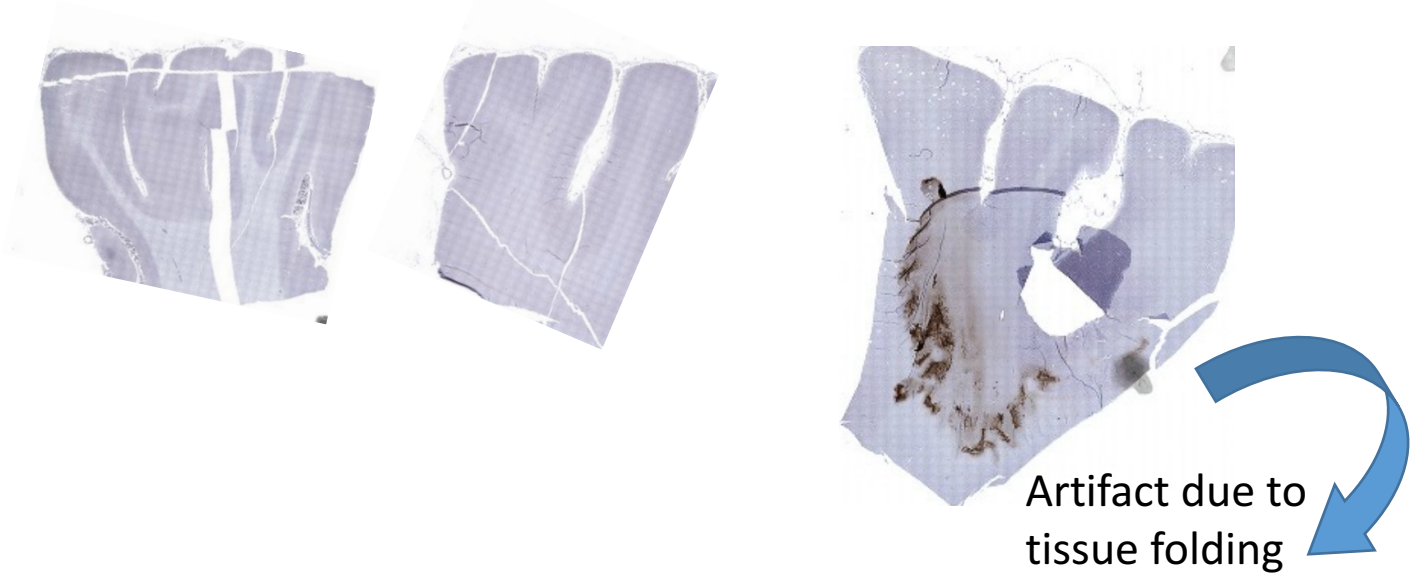

QKI-7: 1:100
dil; 222cet

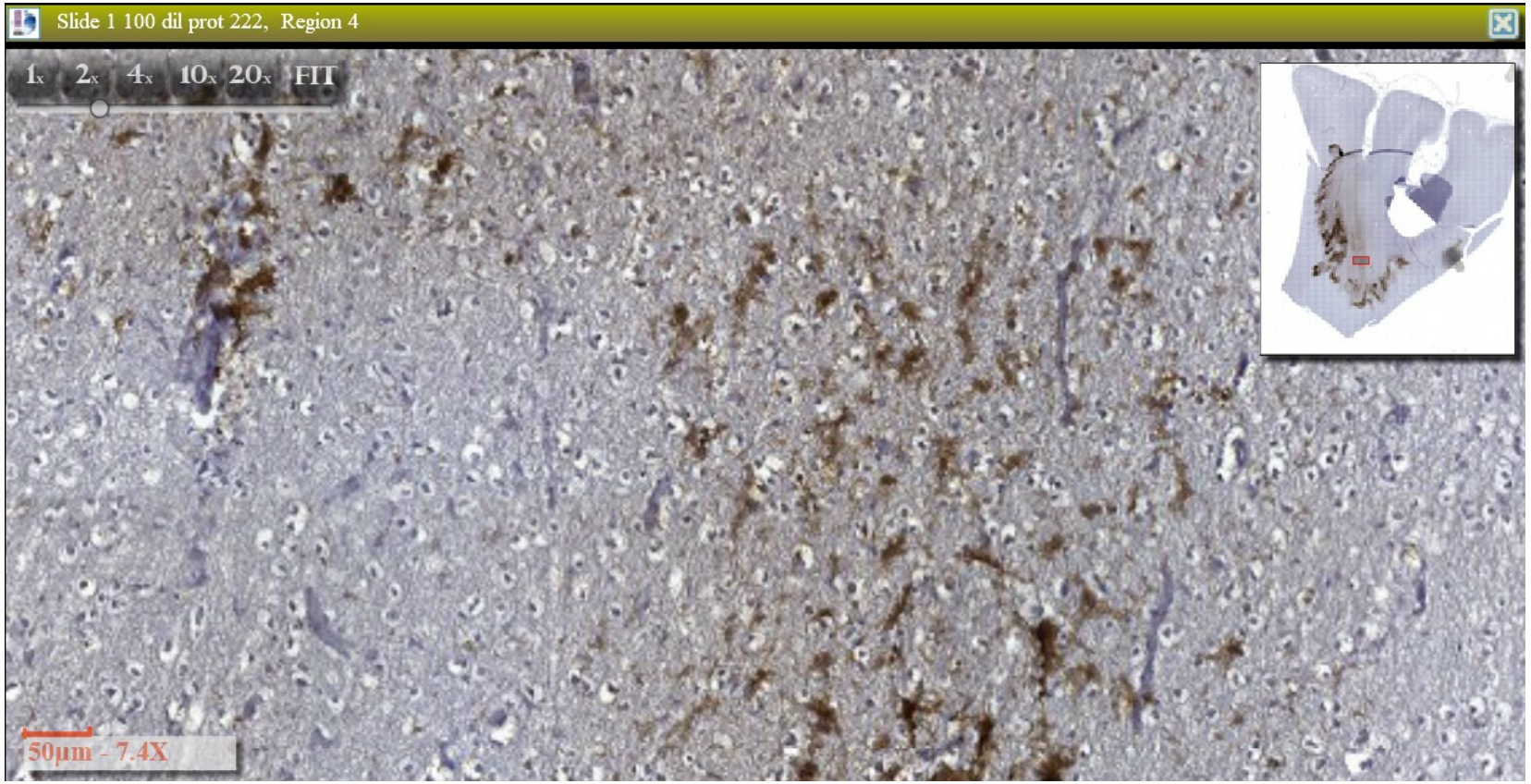

NF200

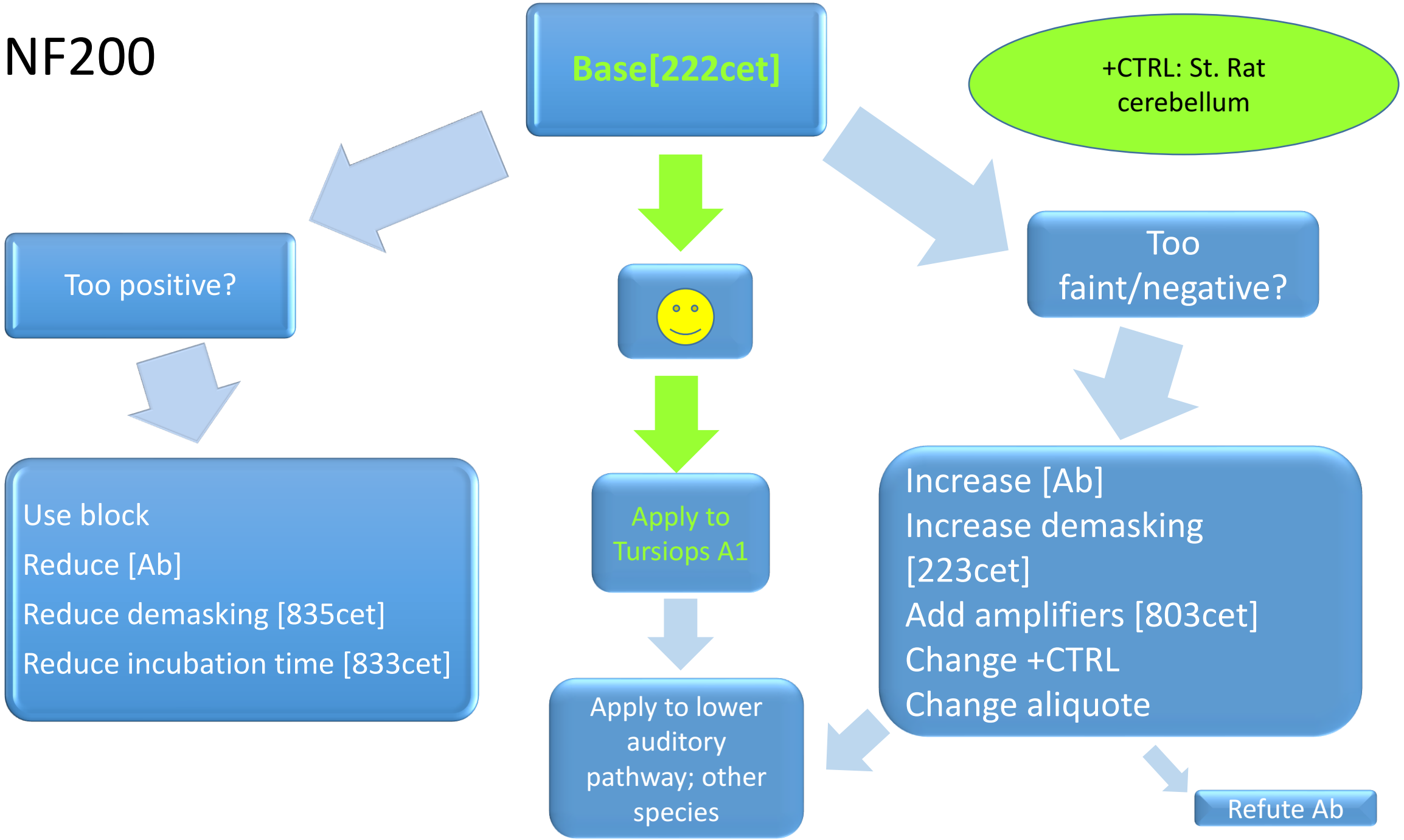
Base[222cet]
+CTRL: St. Rat cerebellum
Too positive?
Too faint/negative?
Use block
Reduce [Ab]
Reduce demasking [835cet]
Reduce incubation time [833cet]
Apply to Tursiops A1
Increase [Ab]
Increase demasking [223cet]
Add amplifiers [803cet]
Change +CTRL
Change aliquote
Apply to lower auditory pathway; other species
Refute Ab

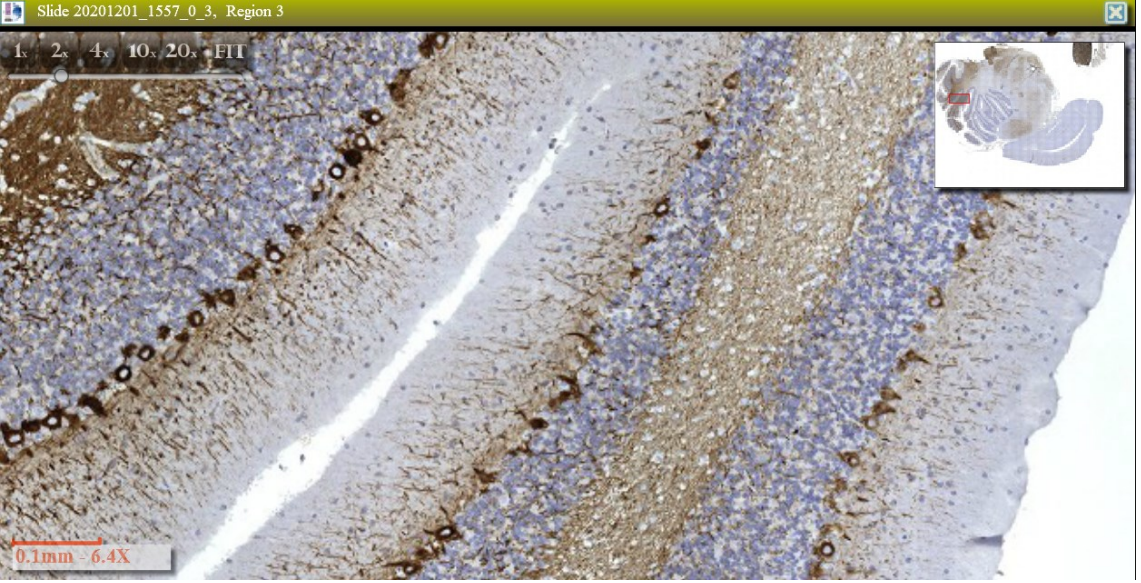

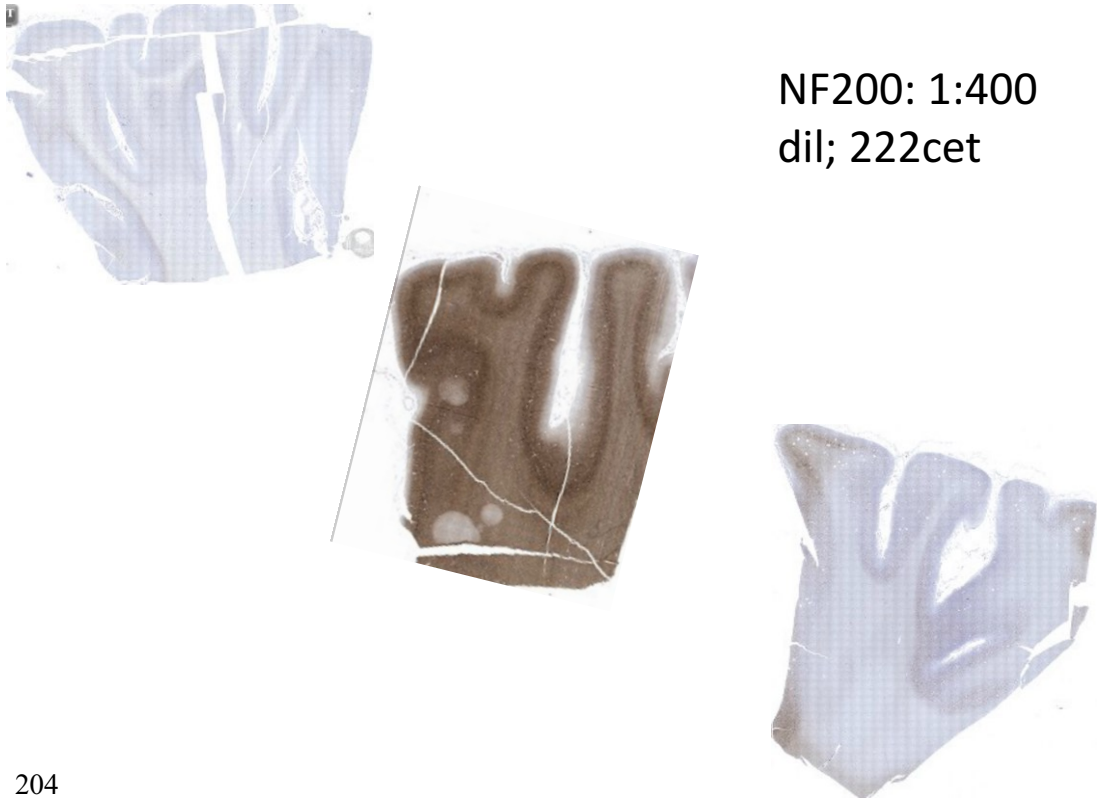

NF200: 1:400 dil; 222cet

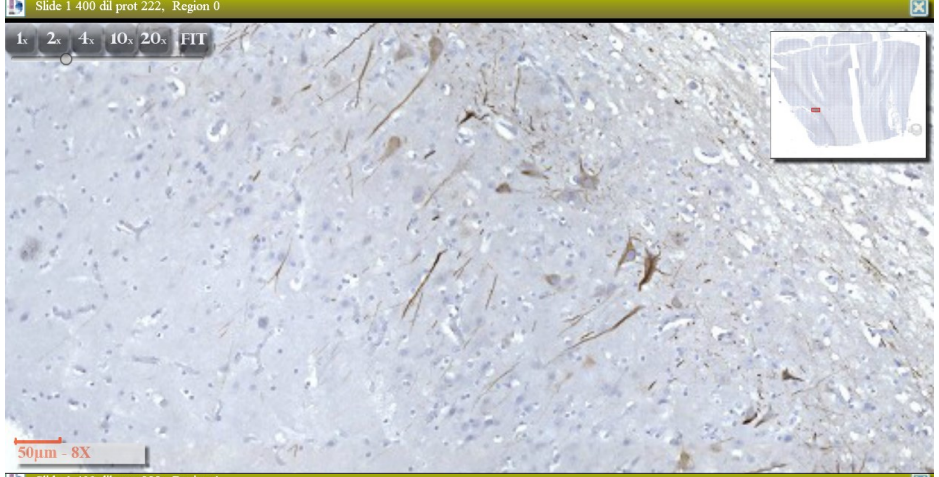

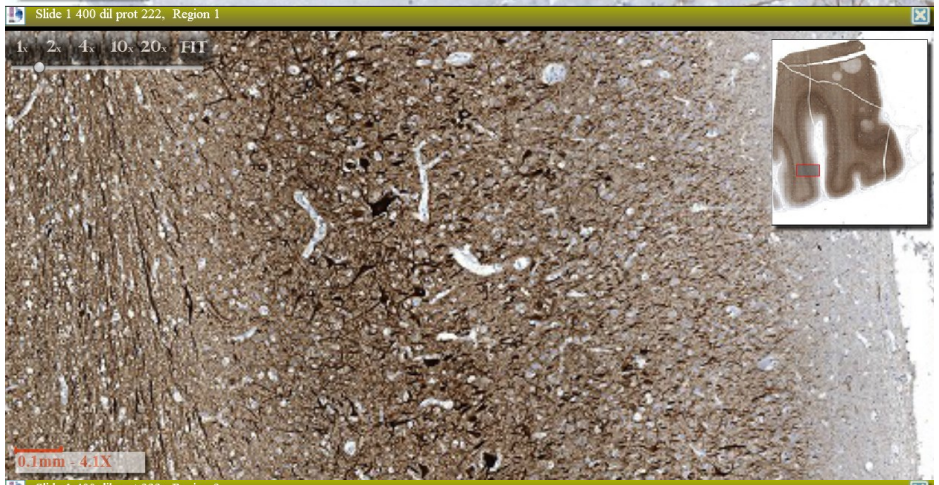

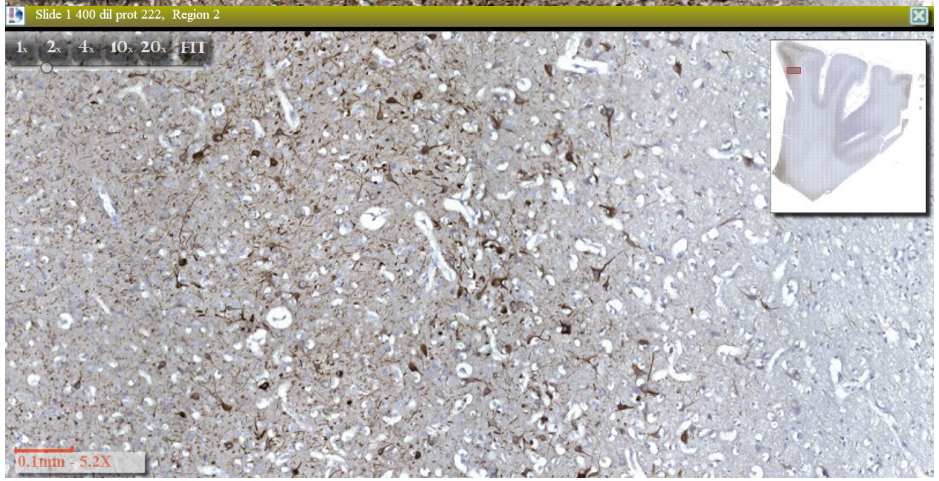

Excitatory/Inhibitory

- GAD^{67}
- GlyRs

GAD^{67}

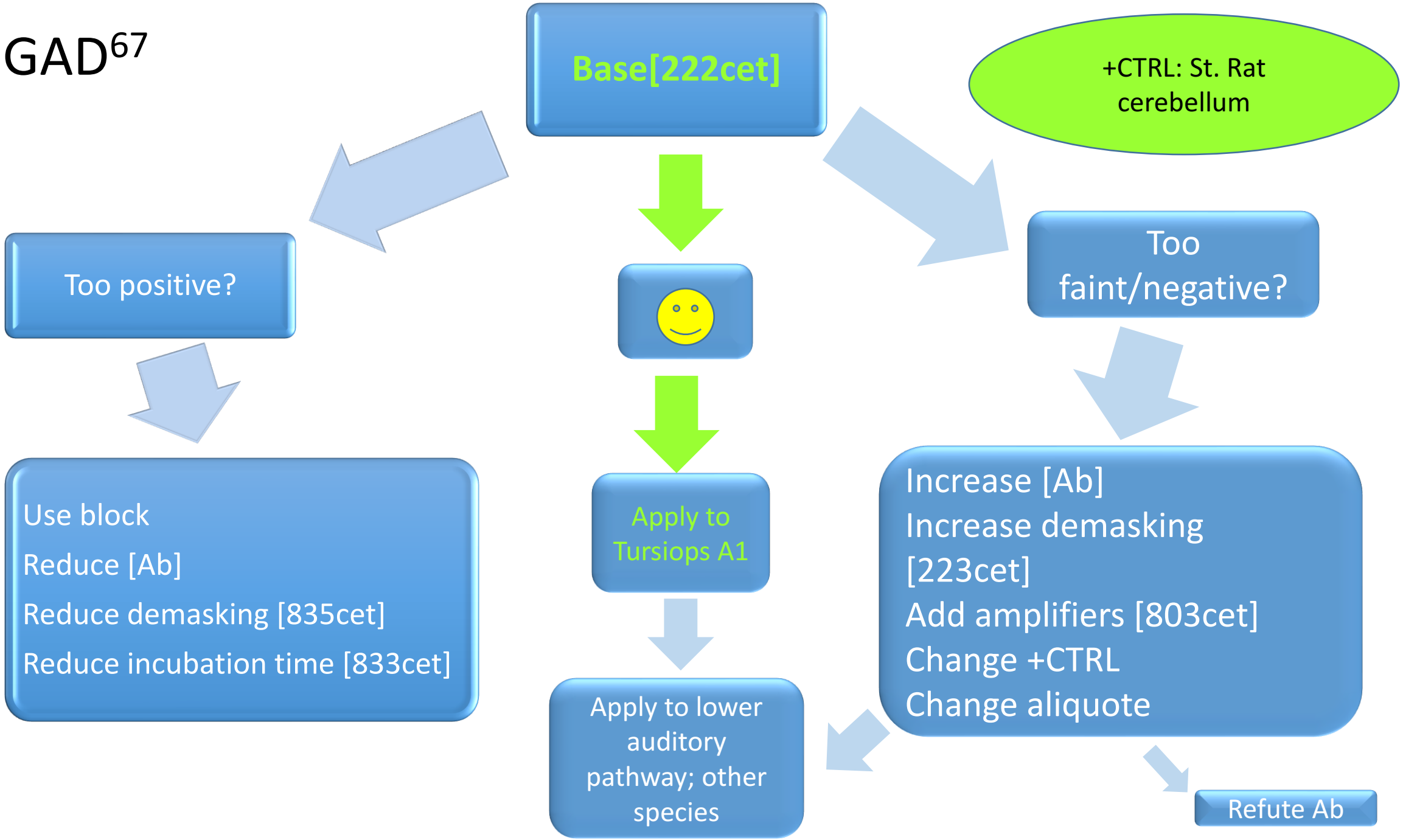
Base[222cet]
+CTRL: St. Rat cerebellum
Too positive?
Too faint/negative?
Use block
Reduce [Ab]
Reduce demasking [835cet]
Reduce incubation time [833cet]
Apply to Tursiops A1
Increase [Ab]
Increase demasking [223cet]
Add amplifiers [803cet]
Change +CTRL
Change aliquote
Apply to lower auditory pathway; other species
Refute Ab

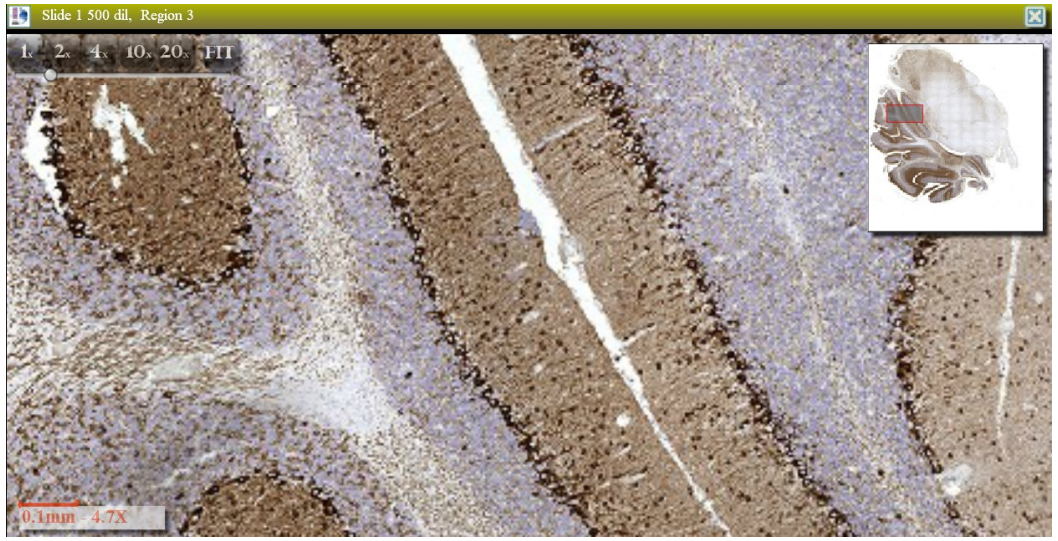

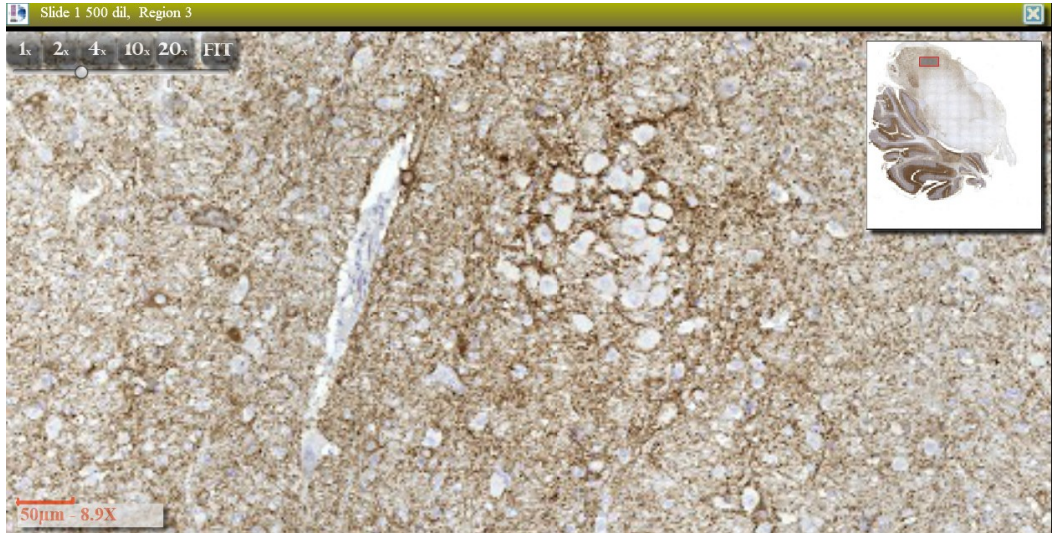

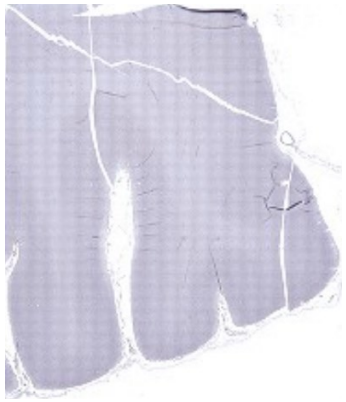

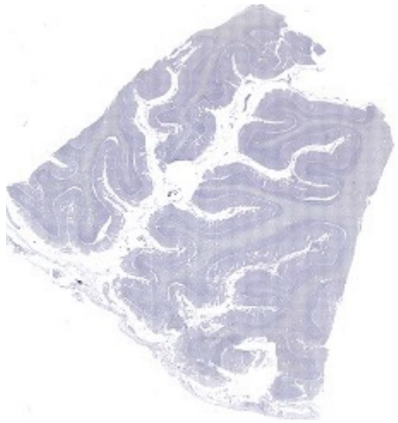

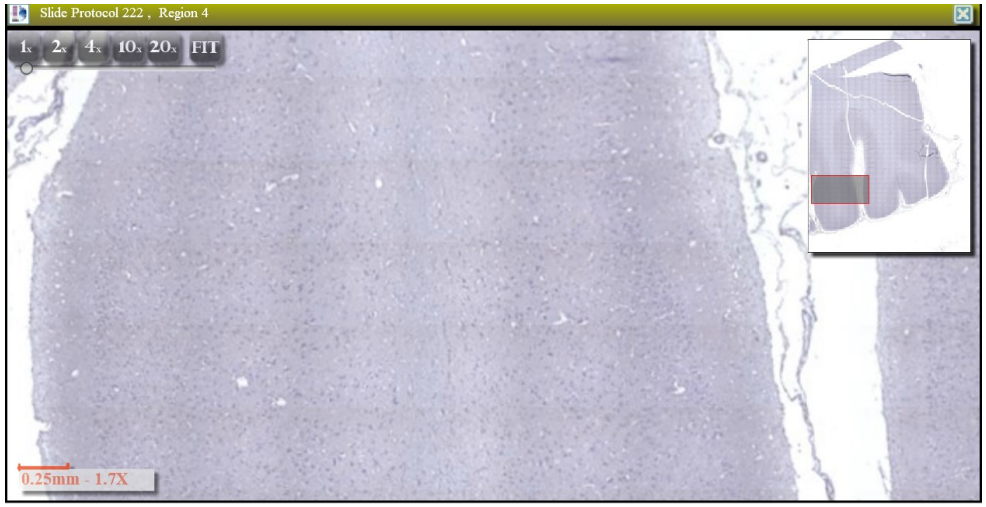

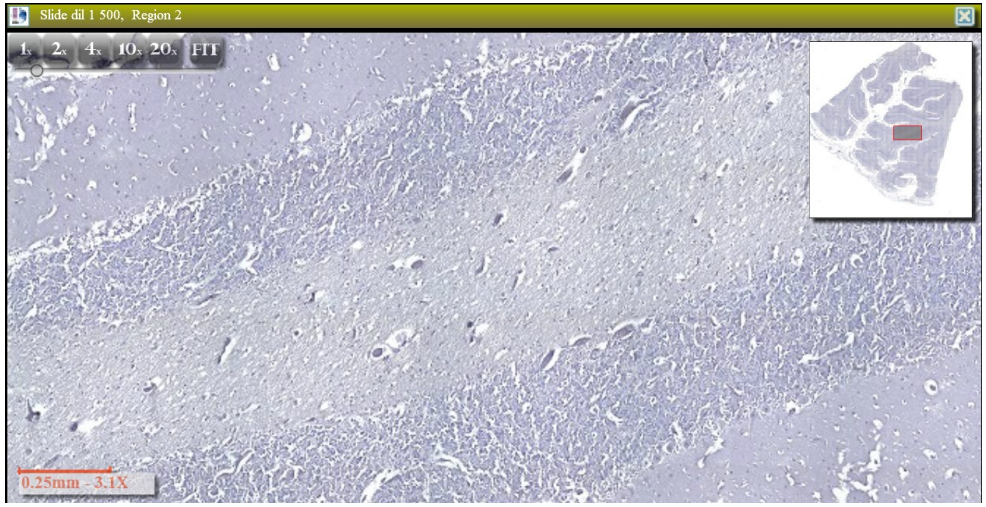

GAD67: 1:500
dil; 222cet

GlyRs

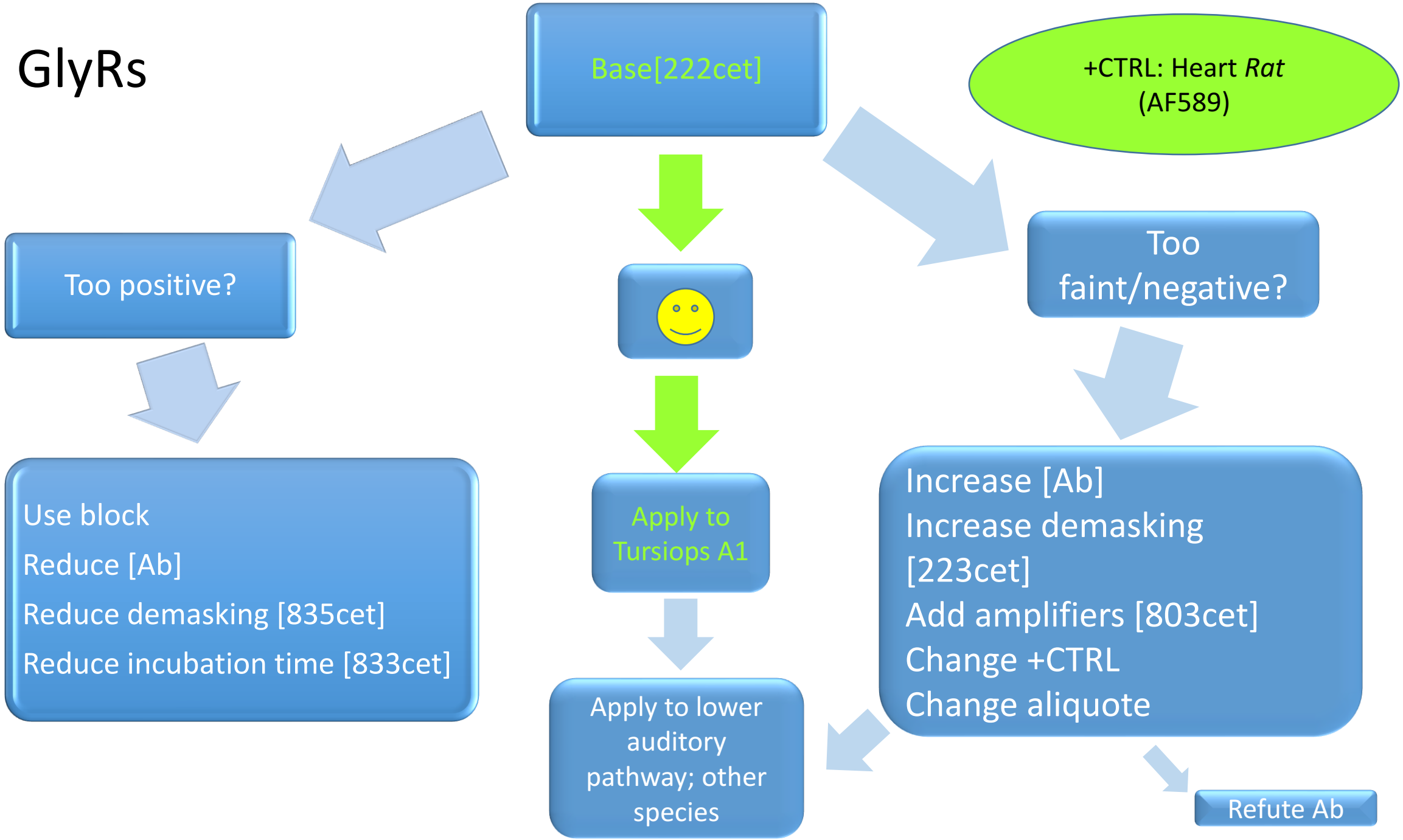
Base[222cet]
+CTRL: Heart *Rat* (AF589)
Too positive?
Too faint/negative?
Use block
Reduce [Ab]
Reduce demasking [835cet]
Reduce incubation time [833cet]
Apply to Tursiops A1
Increase [Ab]
Increase demasking [223cet]
Add amplifiers [803cet]
Change +CTRL
Change aliquote
Apply to lower auditory pathway; other species
Refute Ab

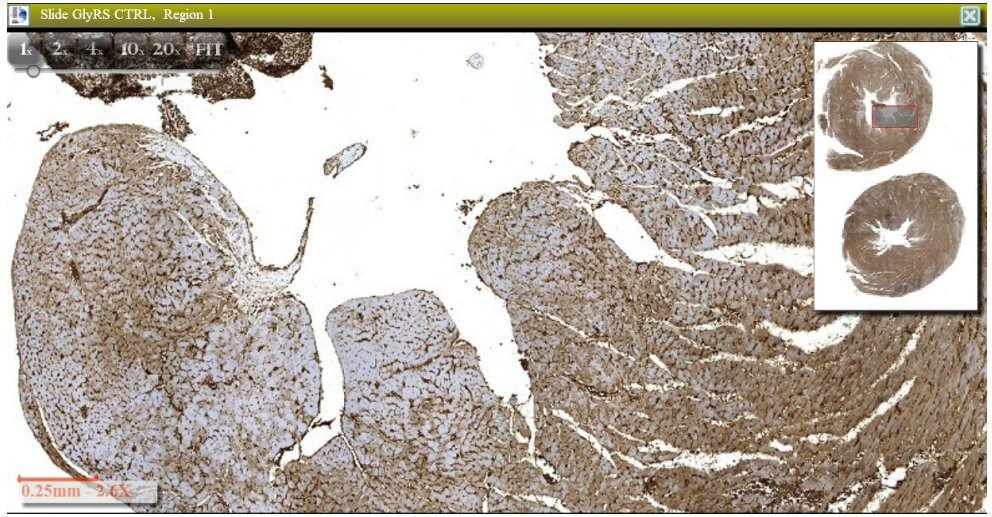

GlyRs: 1:100 dil;
222cet